TAMPEREEN TEKNILLINEN YLIOPISTO
TAMPERE UNIVERSITY OF TECHNOLOGY

Elina Laitinen

Physical Layer Challenges and Solutions in Seamless Positioning via GNSS, Cellular and WLAN Systems

Julkaisu 1470 • Publication 1470

Tampere 2017

Tampereen teknillinen yliopisto. Julkaisu 1470
Tampere University of Technology. Publication 1470

Elina Laitinen

Physical Layer Challenges and Solutions in Seamless Positioning via GNSS, Cellular and WLAN Systems

Thesis for the degree of Doctor of Science in Technology to be presented with due permission for public examination and criticism in Tietotalo Building, Auditorium TB109, at Tampere University of Technology, on the 5th of May 2017, at 12 noon.

Tampereen teknillinen yliopisto - Tampere University of Technology
Tampere 2017

Supervisor

Elena Simona Lohan, Associate Prof., Dr. Tech
Department of Electronics and Communications Engineering
Tampere University of Technology
Tampere, Finland

Pre-examiner

Wu Chen, Prof., Dr. Tech
Department of Land Surveying and Geo-Informatics
The Hong Kong Polytechnic University
Hong Kong

Pre-examiner and opponent

Jari Iinatti, Prof., Dr. Tech
Faculty of Information Technology and Electrical Engineering
University of Oulu
Oulu, Finland

Opponent

Joaquín Torres-Sospedra, Dr. Tech
Institute of New Imaging Technologies
Universitat Jaume I
Castellón, Spain

ISBN 978-952-15-3937-4 (printed)
ISBN 978-952-15-3942-8 (PDF)
ISSN 1459-2045

ABSTRACT

As different positioning applications have started to be a common part of our lives, positioning methods have to cope with increasing demands. Global Navigation Satellite System (GNSS) can offer accurate location estimate outdoors, but achieving seamless large-scale indoor localization remains still a challenging topic. The requirements for simple and cost-effective indoor positioning system have led to the utilization of wireless systems already available, such as cellular networks and Wireless Local Area Network (WLAN). One common approach with the advantage of a large-scale standard-independent implementation is based on the Received Signal Strength (RSS) measurements.

This thesis addresses both GNSS and non-GNSS positioning algorithms and aims to offer a compact overview of the wireless localization issues, concentrating on some of the major challenges and solutions in GNSS and RSS-based positioning. The GNSS-related challenges addressed here refer to the channel modelling part for indoor GNSS and to the acquisition part in High Sensitivity (HS)-GNSS. The RSS-related challenges addressed here refer to the data collection and calibration, channel effects such as path loss and shadowing, and three-dimensional indoor positioning estimation.

This thesis presents a measurement-based analysis of indoor channel models for GNSS signals and of path loss and shadowing models for WLAN and cellular signals. Novel low-complexity acquisition algorithms are developed for HS-GNSS. In addition, a solution to transmitter topology evaluation and database reduction solutions for large-scale mobile-centric RSS-based positioning are proposed. This thesis also studies the effect of RSS offsets in the calibration phase and various floor estimators, and offers an extensive comparison of different RSS-based positioning algorithms.

PREFACE

The research work for this dissertation has been carried out at the Department of Electronics and Communications Engineering, Tampere University of Technology (TUT), Finland, during the years 2006-2016. Due to maternity and family leaves, the accumulated length of my studies is approximately five years and nine months. I gratefully appreciate the financial support provided by Tampere Doctoral Programme in Information Science and Engineering (TISE), Doctoral training network in Electronics, Telecommunications and Automation (DELTA), Tuula and Yrjö Neuvo Fund (2015) and Doctoral Programme in Computing and Electrical Engineering (2016).

First and foremost, I would like to thank my supervisor Associate Prof., Dr. Elena Simona Lohan, for her guidance, support and encouragement throughout the years. She has always been available when needed, helping with any request or question I had. Secondly, my gratitude extends to Prof. Markku Renfors for offering me a position as a research assistant and later as a researcher in various wireless positioning projects. His positive and peaceful attitude has had an important role in making the department to a pleasant and inspiring working environment.

I am very grateful to the pre-examiners of this dissertation, Prof. Wu Chen, The Hong Kong Polytechnic University, and Prof. Jari Iinatti, University of Oulu, for their feedback and constructive comments regarding the manuscript. I am also very thankful for both Prof. Jari Iinatti and Dr. Joaquín Torres-Sospedra, Universitat Jaume I, for agreeing to act as opponents in the public defense of my dissertation.

I have had a privilege to work with many great persons and researchers during my years at the department. Therefore, I would like to thank all my colleagues, co-authors, office mates and members of our positioning-group during the years, especially Adina Burian, Abdelmonaem Lakhzouri, Toni Huovinen, Tero Isotalo, Danai Skournetou, Mohammad Zahidul H. Bhuiyan, Alexandru Rusu Casandra, Jukka Talvitie, Shweta Shrestha, Diego Alonso de Diego, Jari Nurmi, Ondrej Daniel, Pedro

Figueiredo e Silva, Giorgia Ferrara, and Tommi Paakki. In particular, I would like to mention my friend and former colleague Jie ”Cookie” Zhang, who passed away suddenly at too young age in August 2016. She was a bright and positive person, who will always be remembered. I am also thankful for Tarja Erälaukko, Daria Ilina, Sari Kinnari, Soile Lönnqvist, Heli Ahlfors, and Elina Orava for their valuable assistance in practical matters.

In addition to colleagues, I wish to extend my thanks to all my friends. To mention few, I would like to thank Marjo Lähteenmäki for the countless walks in the forests with the dogs during the last 12 years, and Katri Alavalkama and Jan Egeland-Jensen for the nice evenings with board games and good food. Special thanks also to our friends and best ever neighbors, Elina and Pasi Kivimäki with their children, for the joint trips and great time spent together.

It is obvious that this thesis would not been possible without all the support I have received from the people closest to me. Therefore, I would like to express my deepest gratitude to my parents, Hannele and Esa Pajala, who have always appreciated education and encouraged us to reach for the stars. I know that you have always believed in me. In addition, I would like to thank my sister Emilia, her husband Matti and their children Emma, Elli and Elmo, and my brother Antti and his wife Noora, for the encouragement and understanding. Besides my childhood family, I would like to thank my father-in-law Jorma Laitinen, his wife Pirjo Laitinen, and Jarmo Annala. Special thanks belong to my mother-in-love, Ulla Laitinen, for the numerous times she has taken care of the children, especially during the last two months of writing the thesis.

Combining the family with a research career is not an easy task. Having three children during the doctoral studies is even more difficult. The breaks at home in the middle of the research surely affected the length of my studies and the consistency of this dissertation, but I would definitely make still the same decision. Our three beautiful, clever girls are - and always will be - my biggest achievement. So, finally I would like to thank my family: my husband Ismo for loving me, supporting me, and being always there for me, and our daughters Venla, Senni and Alisa, for all the joy and happiness you bring to my life. This thesis is dedicated to you.

Nokia, March 2017

Elina Laitinen

TABLE OF CONTENTS

LIST OF FIGURES

LIST OF TABLES

LIST OF ABBREVIATIONS

A-GNSS Assisted GNSS

A-GPS Assisted GPS

aBOC Ambiguous BOC

ADOA Angle-Difference-Of-Arrival

AltBOC Alternative BOC

AOA Angle-Of-Arrival

AP Access Point

API Application Programming Interface

BDS BeiDou Navigation Satellite System

BOC Binary Offset Carrier

BPSK Binary Phase Shift Keying

BS Base Station

BSSID Basic Service Set Identifier

BW Bandwidth

CCK Complementary Code Keying

CDBOC Complex Double BOC

CDF Cumulative Distribution Function

CDMA Code Division Multiple Access

Cen Centroid

CFAR Constant False Alarm Rate

CID Cell Identity

CIR Channel Impulse Response

CNR Carrier-to-Noise Ratio

CosBOC Cosine BOC

CRLB Cramér-Rao Lower Bound

CWI Continuous Wave Interference

DGPS Differential GPS

DLL Delay Lock Loop

DME Distance Measuring Equipment

DN Differential Non-coherent correlation

DN2 Enhanced Differential Non-coherent correlation

DOA Direction-Of-Arrival

DSSS Direct Sequence Spread Spectrum

ECID Enhanced CID

E-OTD Enhanced Observed Time Difference

eNodeB Evolved Node B

ESA European Space Agency

ETSI European Telecommunications Standards Institute

EU European Union

eNodeB Evolved Node B

FDMA Frequency Division Multiple Access

FFT Fast Fourier Transform

FLL Frequency Lock Loop

FP Fingerprinting

G Generation

GLRT Generalized Likelihood Ratio Test

GNSS Global Navigation Satellite System

GPDI Generalized Post-Detection Integration

GPS Global Positioning System

GSM Global System for Mobile Communications

GST GNSS System Time

HS-GNSS High Sensitivity GNSS

HSPA High Speed Packet Access

HSPA+ Evolved HSPA

IEEE The Institute of Electrical and Electronics Engineers

INS Inertial Navigation System

IOT Internet of Things

IPDL Idle Period Down Link

IPS Indoor Positioning System

KL Kullback-Leibler

KNN *K* Nearest Neighbor

LTE Long-Term Evolution

LOS Line-Of-Sight

LS Least Squares

LSB Lower SideBand

MA Multiple Access

MAC Medium Access Control

maxRSS Maximum RSS-based selection criterion

MBOC Multiplexed BOC

MCMC Monte Carlo Markov Chain

MIMO Multiple Input Multiple Output

MS Mobile Station

MuRVaP Multivariate Random Variable Patterns

NC Conventional Non-coherent integration

NLOS Non-Line-Of-Sight

NN Nearest Neighbor

OFDM Orthogonal Frequency Division Multiplexing

OTDOA Observed-Time-Difference-Of-Arrival

PDF Probability Density Function

PDOA Phase-Difference-Of-Arrival

PL Path Loss

PLL Phase Lock Loop

PRN Pseudorandom

PRS Positioning Reference Signal

QAM Quadrature Amplitude Modulation

QPSK Quadrature Phase Shift Keying

RFID radio-frequency identification

RTT Round Trip Time

RSS Received Signal Strength

RSSD Received Signal Strength Difference

RSSI Received Signal Strength Indicator

SCM Sidelobe Cancellation Method

SCPC Sub-Carrier Phase Cancellation

SinBOC Sine BOC

SISO Single Input Single Output

SMP Smallest M-vertex Polygon

SOO Signals-Of-Opportunity

std standard deviation

SVM Support Vector Machine

TA Timing Advance

TACAN Tactical Air Navigation

TDMA Time Division Multiple Access

TDOA Time-Difference-Of-Arrival

TK Teager-Kaiser

TOA Time-Of-Arrival

TTFF Time-To-First-Fix

UAL Unsuppressed Adjacent Lobes

UHF Ultra High Frequency

UMTS Universal Mobile Telecommunications System

USB Upper SideBand

U-TDOA Uplink TDOA

UWB Ultra Wideband

VHF Very High Frequency

WCDMA Wideband Code Division Multiple Access

WeiC Weighted Centroid

WLAN Wireless Local Area Networks

WKNN Weighted KNN

LIST OF SYMBOLS

a	Signal amplitude
$[a_1, a_2, a_3, b_1, b_2]$	Beaulieu's approximation coefficients
b	RSS bias
$b_{data}(n)$	nth complex data symbol
BW_{GNSS}	BW of the GNSS system
BW_{int}	BW of the interference
$c_{j,n}$	jth chip corresponding to the nth symbol
C	Correlation output
$d_{i,k}$	Range between the estimated location of kth transmitter and ith FP
E_b	Data bit energy
$\mathbf{E}(\cdot)$	Expectation operation
f_c	Carrier frequency
f_{chip}	Chip rate
f_D	Doppler frequency shift
$\widehat{f_D}$	Tentative Doppler frequency shift
f_{sc}	Subcarrier frequency
K	KNN parameter
L	Number of channel paths
m_B,n_B	Indices for BOC modulation
m	Nakagami fading parameter
n_k	PL exponent for kth transmitter
$\hat{n}_{TX}$	Estimated PL exponent
$\mathbf{n}$	Noise vector
N_{AP}	Total number of detected APs in the radio map
N_{bins}	Number of search bins in the search window
N_{BOC}	BOC modulation order
N_{cbins}	Number of correct search bins in the search window
N_C	Coherent integration length
N_{DC}	Differential integration length

N_{floors}	Number of floors
N_{fp}	Total number of FPs in the radiomap
$N_{fp(k)}$	Number of FPs, where the transmitter k is detected
N_h	Number of heard transmitters in the user measurement
N_{NC}	Non-coherent integration length
N_{path}	Estimated number of channel paths
N_{TX}	Number of transmitters
N_u	Number of data samples in the used user track
N_z	Number of commonly heard transmitters in the FP and in the user measurement
O_z	Observed RSS levels in the user measurement
$p_{T_B}(\cdot)$	Pulse shaping filter
P_d	Detection probability
P_{fa}	False alarm probability
$P_{i,k}$	Measured RSS of the kth transmitter in the ith FP
P_{T_k}	Apparent transmit power for the kth transmitter
$\hat{P}_{T_{TX}}$	Estimated apparent transmit power
$\mathbf{P_k}$	RSS vector for kth transmitter
$Q(\cdot)$	Generalized Marcum Q-function
r_k	Distance to transmitter k
R	Random variable
$s(\cdot)$	Modulating waveform
$s_{CosBOC}(\cdot)$	SinBOC subcarrier as a modulating waveform
$s_{SinBOC}(\cdot)$	SinBOC subcarrier as a modulating waveform
s_{ref}	Reference PRN code at the receiver
S_F	Spreading factor
$sign(\cdot)$	Signum operator
T_c	Chip period
T_{sym}	Code symbol period
$\mathbf{T}$	Transpose operator
w_k	Weighting factor for kth transmitter
$x(\cdot)$	Transmitted signal (from one satellite)
x_{data}	Data sequence (after spreading)
$[x_i, y_i, z_i]$	3D location coordinates of the FP i
$[x_{MS}, y_{MS}, z_{MS}]$	3D location coordinates of receiver
$[\hat{x}_{MS}, \hat{y}_{MS}, \hat{z}_{MS}]$	Estimated 3D location coordinates of receiver
$[x_{TX_k}, y_{TX_k}, z_{TX_k}]$	3D location coordinates of kth transmitter
$[\hat{x}_{TX_k}, \hat{y}_{TX_k}, \hat{z}_{TX_k}]$	Estimated 3D location coordinates of kth transmitter

$x_{PRN,n}(\cdot)$	PRN code sequence for nth data symbol
X	Test statistic (i.e., decision variable)
$\mathbf{x_{MS}}$	User position (x_{MS}, y_{MS}, z_{MS}) in vector form
$y(\cdot)$	Received signal
Z	Output after correlation and integration (whole correlation block)
α_l	Time-varying complex fading coefficient of lth path
γ	Decision threshold
$\Gamma(\cdot)$	Gamma function
$\delta(\cdot)$	Dirac pulse
$(\Delta f)_{bin}$	Frequency bin length
$(\Delta f)_{max}$	Search uncertainty in frequency domain
$(\Delta t)_{bin}$	Time bin length
$(\Delta t)_{coh}$	Coherence time
$(\Delta t)_{max}$	Search uncertainty in time domain
Δ_{grid}	Horizontal grid resolution
Δ_{path}	Estimated channel path spacing
$\eta(\cdot)$	Additive Gaussian noise with zero mean and double-sided power spectral density N_0
Θ_k	Unknown PL parameters for kth transmitter excluding the coordinates
λ	Non-centrality parameter
τ	Code delay
$\widehat{\tau}$	Tentative code delay
τ_l	Delay of lth multipath
$\circledast$	Convolution operator

1. INTRODUCTION

1.1 Background and motivation

In July 2016, Niantic released Pokémon GO, a location-based reality game for smart phones [5]. The game became rapidly a global phenomenon and got downloaded hundreds of millions times within the first months after its release. Since Pokémon GO relies heavily on Global Positioning System (GPS) for most of the game's behaviors, is works accurately outdoors, but gets into trouble in urban canyons and indoors, due to multipaths and signal attenuation. As people spend a majority of their time (over 80%) indoors [6], it is obvious that many players have wished the game to work accurately also indoor environments, such as inside shopping centers and universities.

Location-based services is one of the fastest growing segments in mobile applications, Pokémon GO being only one example of the various possibilities in leisure, sports, navigation, asset tracking and many more. The size of indoor localization market is estimated to grow with annual growth rate of 37.5 % from 2016 to 2021 [4]. Thus, it is easy to understand the urgent need for accurate localization in any place at any time. Although satellite-based localization via Global Navigation Satellite System (GNSS) can offer positioning outdoors at global scale, the indoor localization remains challenging. GNSS signals are easily blocked indoors, and even those signals, that are strong enough to enter indoors, are still received at a very weak power due to severe attenuation. Therefore, many different indoor positioning systems have been proposed within the last decade.

The increasing demand for simple and cost-effective global indoor positioning system has led to the utilization of different wireless systems already available, such as cellular networks and Wireless Local Area Networks (WLAN) [52, 123, 130, 228, 238, 265, 275, 306, 313, 315, 328, 333, 334, 336, 356]. Other possibilities are, e.g.,

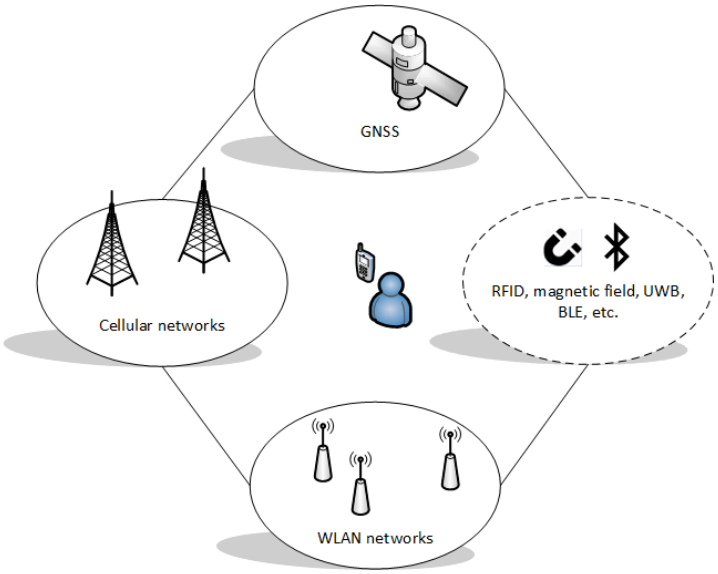

Fig. 1.1: *Different positioning systems as a hybrid solution.*

based on Bluetooth [59, 272, 321], magnetic fields [255, 314] or Ultra Wideband (UWB) [78, 113]. By combining different localization techniques as hybrid solutions as illustrated in Fig. 1.1, highest benefit in terms of positioning accuracy and cost-effectiveness can be obtained. Since many wireless communication networks offer an easy access to Received Signal Strength (RSS) measures without additional hardware, RSS-based positioning approaches are an attractive alternative for positioning purposes. However, there are still challenges to overcome. For GNSS-based positioning algorithms, the main challenges appear in indoor and urban canyon cases and they refer to No-Line-of-Sight (NLOS), low signal-to-noise ratios and multipath propagation. In addition, the new ambiguous modulation types, such as Binary Offset Carrier (BOC) modulation with its variants, create new challenges to the signal synchronization process. In RSS-based positioning techniques, most of the challenges are caused by unknown statistical characteristics of the propagation channel, suitability of the existing transmitter configuration for positioning purposes, storage and transmission requirements for large databases, RSS biases in training and estimation phases and the choice of appropriate positioning methods. Thus, current positioning algorithms have to be improved and new solutions have to be developed in order to cope with these challenges and to achieve seamless and accurate position estimates in all environments.

1.2 Objective and scope of research

The main target in this thesis work has been to research and develop new signal processing algorithms for wireless localization. The focus has been both on satellite-based positioning and on RSS-based positioning techniques in cellular and WLAN networks. Several of the challenges in wireless positioning techniques today have been addressed in this thesis, taking into account especially the high need for accurate indoor positioning and floor detection.

This thesis presents a comprehensive survey of different positioning methods, together with their challenges and state-of-the-art solutions. GNSS related challenges at physical layer are studied, to overcome the difficulties caused by multipath propagation and low signal levels. RSS-based methods have been investigated, both in cellular and in WLAN-based positioning, with unknown transmitter location and based on real measurements. The focus is on the two-stage localization approaches, where the process is divided into the training phase (i.e., data collection phase) and the estimation phase (i.e., user localization phase).

Parts of the results in this thesis are also based on the knowledge and measurement equipment obtained from participation in the following research projects:

1. ”Rx Positioning (RxPos)”, funded by HERE, 2010-2012.
2. ”Digital Signal Processing Algorithms for Indoor Positioning Systems (ACAPO)”, funded by the Academy of Finland, 2008.
3. ”Advanced Techniques for Personal Navigation (ATENA)”, funded by Tekes, the Finnish funding agency for Innovation, 2006-2007.
4. ”Mobile Positioning Techniques (MOT)”, funded by Tekes, 2003-2006.

1.3 Main contributions

The main contributions of this thesis are summarized below:

- An extensive state-of-the-art overview of GNSS, cellular and WLAN-based positioning is written.

- An analysis of the indoor fading channel model in GPS frequency bands is performed, based on indoor GPS measurements. The obtained fading channel characteristics are compared to typical fading distributions and Nakagami-*m* distribution is found to be the best fit.

- An efficient but simple simulation model is created for Nakagami-*m* distributed fading channels, as this type of fading proved to model the best the real-life channels. A previously proposed method, called the Beaulieu &al. method, is extended to a wider range of *m*-values, while keeping a low computational effort.

- Three Constant False Alarm Rate (CFAR) detectors are proposed for GNSS acquisition and analyzed in terms of detection probability and dependence on the channel conditions. The analysis is done for different channel conditions to show which of the proposed CFAR detectors is the most robust to noise.

- A novel enhanced differential non-coherent integration method is proposed for the acquisition stage in High Sensitivity (HS)-GNSS or GNSS receiver operating at low Carrier-to-Noise Ratio (CNR). A comparative analysis between the differential correlations and the conventional non-coherent integration method is carried out in multipath fading channels, taking into account both ambiguous Binary Offset Carrier (BOC) modulation and sideband based unambiguous technique.

- A Cramér-Rao Lower Bound (CRLB)-based criterion for RSS-based positioning is presented. This thesis shows how the derived CRLB-based criterion can be used either to calculate the expected accuracy bound in WLAN-networks with predefined topology or to choose the optimal Access Point (AP) density and AP topology for a certain target of positioning accuracy, in a network that is designed for positioning purposes. The proposed approach is verified with measurements.

- An analysis of path loss and shadowing models and of the relevant parameters for WLAN and cellular signals is presented. The analysis is based on extensive measurement campaigns. The similarities and differences between cellular and WLAN wireless propagation models are also discussed.

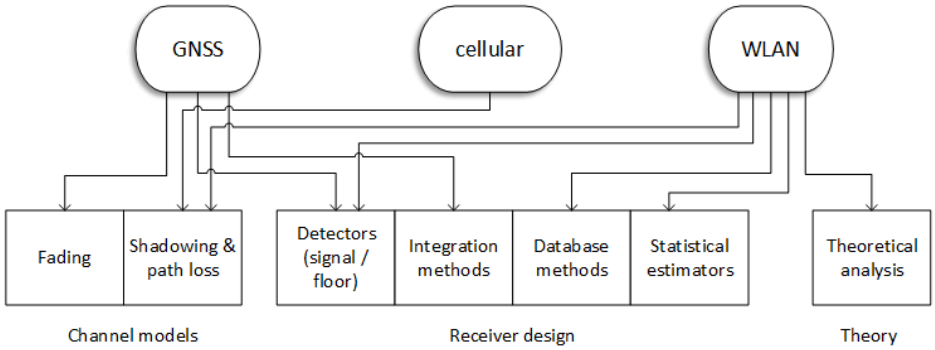

Fig. 1.2: *Block diagram of the contributions of this thesis in the field of wireless positioning.*

- A novel study of AP significance measures as database reduction solution for RSS-based positioning system is performed. AP significance is taken into account both at the training phase and at the estimation phase. AP reduction is examined with several choices for appropriate selection criterion. The effect of AP reduction to different methods (fingerprinting, path loss and weighted centroid based algorithms) is studied.

- The effect of a RSS bias or offset in the training and estimation phases of the RSS-based positioning system is studied extensively. Different offset types and offset values are studied on a large scale, in terms of 3D positioning accuracy and floor detection probability.

- Different RSS-based positioning methods (fingerprinting, path loss and weighted centroid based algorithms) are analyzed, in terms of complexity and performance, based on real measurements. Also, the effects of grid size for each method is studied.

- A novel low-complexity floor detection algorithm is presented. The proposed algorithm is compared with other floor detectors, in terms of performance and complexity.

The contributions of this thesis are also summarized as a block diagram in Fig. 1.2.

1.4 Thesis outline

This thesis is organized as follows. The thesis starts with an introductory overview of wireless positioning in Chapter 2. In Chapter 3, the structure of a GNSS receiver is described first, concentrating to the baseband processing and especially to the signal acquisition part. The chapter continues with a discussion of the main challenges. In Chapter 4, the focus is in RSS-based localization. The chapter starts with describing the system fundamentals of two-stage RSS-based positioning approaches and continues with discussion of the typical physical layer challenges in RSS-based localization. Thus, chapters 2-4 provide an extensive survey of GNSS and RSS-based positioning and their typical challenges, that will be completed with solution proposals in Chapters 5-11.

Chapters 5-6 offer solution proposals to GNSS challenges. In Chapter 5, the focus is on GNSS channel modeling. Indoor fading channel models are analyzed, and based on the results, an efficient Nakagami-*m* fading channel simulator is built. The challenges of multipath propagation, interference and ambiguous modulations are taken into account in Chapter 6, where improvements to the acquisition algorithms are proposed as solutions to the mentioned challenges.

Chapters 7-10 focus on solution proposals to the challenges in two-phase RSS-based localization. Since a significant part of the proposed solutions are based on or validated via real data measurements, this part of the thesis starts with describing the measurement set-ups and relevant information in Chapter 7. In Chapter 8, the positioning architecture design is addressed and a CRLB-based criterion is calculated to evaluate the AP topology in a building for positioning purposes. In Chapter 9, the challenges related to the training phase and data transferring is tackled. This chapter starts with shadowing modeling and path loss models, and continues with solutions to the large databases, namely with the choice of an appropriate grid interval and data removal solutions. In Chapter 10, solutions related to the estimation phase are proposed. A novel study of the effect of biases is presented and suitable positioning methods are discussed. A novel low-complexity floor detector is also proposed.

Finally, Chapter 11 offers a comparative analysis and summary of the discussed positioning approaches (namely GNSS, cellular and WLAN based positioning) and the proposed solutions to various challenges. This chapter also discusses the need of hybrid approaches to guarantee the availability, continuity and integrity. The conclu-

sions are drawn and future directions are discussed in Chapter 12.

2. STATE-OF-THE-ART IN WIRELESS POSITIONING

This chapter presents an overview of current and future positioning techniques. The chapter starts with a discussion about the differences in indoor and outdoor localization. System aspects and positioning algorithms are described shortly for satellite-based (Section 2.2), cellular-based (Section 2.3), and Wireless Local Area Networks (WLAN)-based positioning (Section 2.4) techniques. Few other indoor positioning systems are introduced in Section 2.5. Finally, the main challenges and differences between the positioning systems are discussed in Section 2.6.

2.1 Indoor versus outdoor: challenges, constraints, limitations

Positioning and navigation are taken nowadays for granted. Easy navigation solutions, offered by Global Navigation Satellite Systems (GNSS), have increased the safety and control, and have made many challenges in everyday life easier to handle. Global Positioning System (GPS) is familiar for everyone and works well outdoors, but the system has limitations as well. One limitation is its operation in urban areas with high buildings, that can block or attenuate the satellite signals or cause multipath propagation. In these situations, GPS does not work in a trustable manner in stand-alone mode, but needs some assistance, e.g., from mobile networks. Another very important limitation to satellite-based positioning is indoors. Wall materials attenuate the satellite signals remarkably, and the weak signal powers make the signal detection more challenging. Even with assistance data, satellite-based solutions are not able to provide exact positioning estimates indoors.

Due to the fact that people spend most of their time indoors (at home, at work, at school, in stores etc.), accurate localization indoors is as important than outdoors, or arguably, even more important. Numerous applications, varying from commercial and industrial to public safety and everyday life, get benefits of accurate indoor

localization. Old people's homes need indoor localization systems to track the elderly, hospitals need to track people with special needs and locate currently needed equipment, warehouses need to find specific items, and policemen and fire fighters need to be located fast inside buildings in emergency situations [303]. Since the GNSS generally fail to offer an accurate location estimate indoors mainly due to low visibility of satellites, weak signal powers and multipath propagation [99, 268, 285], many different indoor positioning solutions have been proposed and developed during the last decade. The explosion of smart-phones with built-in sensors and WLAN technologies has made several different indoor positioning techniques attractive and possible, varying from WLAN [173, 228, 230, 238, 328] or Bluetooth [59, 272, 321] to ultrasound [138] or magnetic fields [192, 255, 314] -based systems. In general, positioning indoors is more challenging than outdoors also with other techniques than GNSS. Changes in the building (or room) layouts and the number of people may affect the positioning results. Besides the position estimate, also floor detection and venue tracking (i.e., to provide smooth transition from outdoor to indoor positioning) are important, and indoor maps are needed to make the solutions meaningful. Indeed, the building infrastructure in the future is also changing, with bigger sizes of public buildings (such as hospitals, shopping malls or offices) and underground parking areas.

One big challenge nowadays is faced in the increasing number of different Indoor Positioning Systems (IPS) to choose from. There is not any standard way to build an IPS, and therefore, the number of different methods and systems is increasing. Due to the complexity of the indoor environment, a cost-effective but accurate positioning system is not easy task to achieve, and many existing systems require a lot of resources to implement a specific positioning infrastructure or demand a data collection phase with big databases to be saved and maintained. An ideal positioning system would be able to locate the user anywhere, both outdoors and indoors, seamlessly and accurately. Since no position solution works perfectly in every environment, the best option for a continuous positioning may be a combination of two or more techniques. This means that receivers support several positioning solutions, and switch between them when needed. Research is however still needed to achieve this goal.

2.2 GNSS positioning

In general, a GNSS refers to a satellite constellation based positioning system that provides global coverage within the system limitations. The Navstar GPS is the first and the most famous of the two universal satellite navigation system providing continuous real-time three-dimensional position (latitude, longitude, altitude), velocity and time with appropriate receivers. Its development started in the USA in the early 1960s with an original name Transit, when several U.S. government organizations were interested to develop satellite systems for positioning [161]. The GPS achieved full operational satellite constellation in 1995 and it is implemented and developed by U.S. Department of Defense. From the beginning, the target was to allocate navigation services for military purposes only, but soon the civil applications became available as well.

The growing demands for improved performance and the need to stay competitive with other international satellite positioning systems have led to the long-term modernization program of the GPS. The GPS modernization program is on-going project, that will provide many new capabilities, such as a new frequency band L5, new signals for civilian use, and new modulation types. The new signals are related to the new generations of navigation satellites, but the modernization involves some improvements to the GPS control segment as well. The baseline GPS was specified to consist of 24 satellites [161], but as a result of the modernization process, the GPS constellation consists of 32 Block II/IIA/IIR/IIR-M/IIF satellites at the time of writing, most recent one launched successfully on July 15th 2015 [7]. Fig. 2.1 shows an example of the sky plot with the movement of GPS satellites in terms of elevation (inclination) and azimuth (North, South, East, West), for one hour at TUT location at the time of writing the thesis. The current almanac information can be found in [3].

Right after the announcement of the GPS project in the mid-1970s, the former Soviet Union (later Russia) started to develop their own GNSS system, namely GLONASS. Similarly with GPS, also GLONASS was designed primarily for military purposes. GLONASS was fully operational in 1995, but due to the economic crisis caused by the collapse of the Soviet Union, the system was not maintained for several years and the number of operational satellites decreased significantly. In 2000, the repair and modernization process was started again with high effort, and since 2011, GLONASS has been fully operational with worldwide coverage and providing acceptable accur-

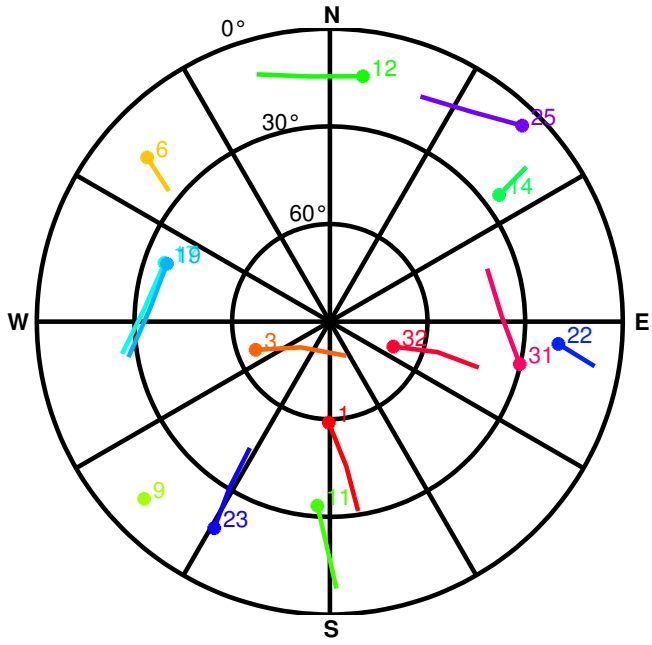

Fig. 2.1: *An example of a sky plot at TUT location at the time of writing the thesis.*

acy for most users. Also the restrictions have been removed, and the military-only signals are nowadays freely available to public use as well. GLONASS has been using since its inception the Frequency Division Multiple Access (FDMA) technique, in which the satellite transmissions are separated in frequencies and not in codes, as in Code Division Multiple Access (CDMA) technique used by GPS [161].

Besides the fully operational navigation systems GPS and GLONASS, two more worldwide satellite-based positioning systems are under development: an European Galileo and a Chinese BeiDou. China has been developing BeiDou Navigation Satellite System (BDS), that has been providing initial navigation services for the Asia-Pacific region since December 2012 (BeiDou Phase 2) [68]. At the time of writing, according to [1], 22nd BeiDou satellite has been launched and the system is expected to achieve global coverage around 2020 (BeiDou Phase 3). Galileo is a joint project of the European Space Agency (ESA) and the European Union (EU), another independent system with political and economical motivations, and the only system being developed by a consortium of nations. Despite of the independence of the new-coming system, Galileo will nevertheless be interoperable with both GPS and

GLONASS, and supposedly with BeiDou as well. This means that the user will be able to estimate the location using the same receiver for any combination of satellites of the above systems. The big difference between Galileo and other satellite-based positioning systems is that Galileo is developed and maintained from the beginning by civil, not military authorities. Thus, Galileo will be available to both civil users and military with the same full precision. Galileo has been developed already more than a decade; it was supposed to be operational in 2008, but financial and technical problems have delayed the commissioning with several years. At the time of writing, 18 Galileo satellites have been launched to their orbits [2]. The current estimate is that the system will be fully operational in 2020.

2.2.1 GNSS system aspects

Within the next five years, the number of operational GNSS satellites will be more than 100, transmitting a variety of signals on multiple frequencies. Different GNSSs have many things in common, e.g., signal spreading technique (i.e., Direct Sequence Spread Spectrum, DSSS), partially overlapping frequency bands, central frequencies and modulation types. The frequency allocation for each system is presented in Fig. 2.2, and as it can be seen, many carrier frequencies for different GNSSs are overlapping with each others allowing interoperability between the systems. E.g., GPS, Galileo, GLONASS and Compass all operate (or plan to operate) on L1 band centered at 1575.42 MHz. At the same time with the possibility for interoperability, GNSSs need to be compatible as well, meaning that the systems do not interfere each others. New modulation techniques (e.g., Binary Offset Carrier, BOC, with its variants) will help in this, by keeping the interference between the signals on the same frequency band as small as possible with spectral separation [33]. It has been however noticed, that more than three GNSSs operating on the same frequency band can increase the noise floor and cause more challenges to the signal reception [114].

Besides the common characteristics, the desire of independence for each GNSS leads to many differences as well. Table 2.1 shows both satellite constellation details and signal structures for all GNSSs, including the maximum number of planned satellites (svs) and orbital information (number of planes, orbital altitude, inclination and period), frequency bands, signal spreading technique, Multiple Access (MA) scheme, signals, used modulation types (abbreviations for modulation types of this

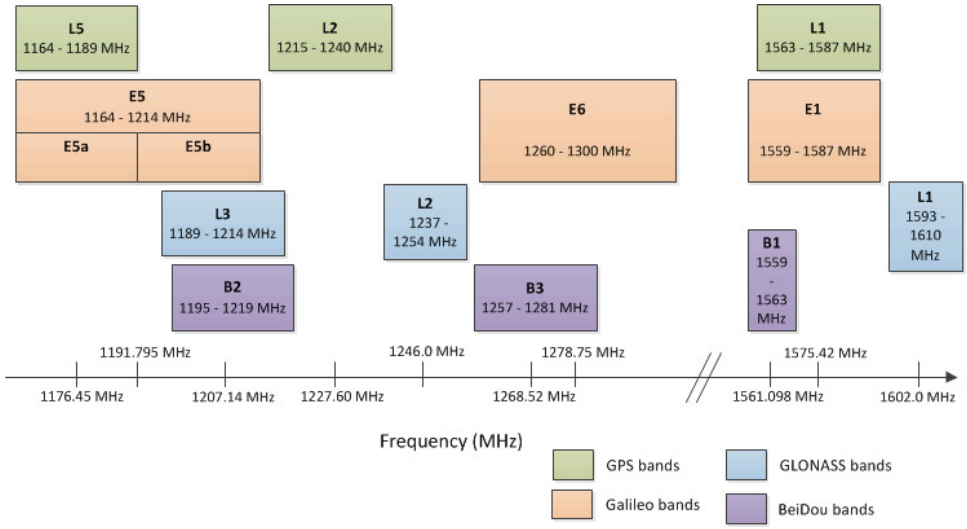

Fig. 2.2: *Frequency bands for GPS, Galileo, GLONASS and BeiDou.*

table will be described later on in Section 3.2.2) and pseudorandom (PRN) code lengths. BeiDou signals have different characteristics in different phases of BeiDou (Phase 1, Phase 2, Phase 3), and even some signals are added while some other are eliminated. Therefore, Galileo and BeiDou systems are described as they will be when fully operational ability is achieved.

2.2.2 GNSS positioning algorithms

Time-Of-Arrival

The satellite-based positioning technology is based on an accurate Time-Of-Arrival (TOA) measurement of the received time-stamped signal, by estimating the propagation delay it takes for a signal to arrive at the receiver from the satellite. This is calculated as the difference between receiving and transmission moments, being the basic measurement in GNSS. The propagation delay is then multiplied with the speed of the signal (i.e., speed of light) in order to calculate the distance between the transmitter and the receiver. In satellite based positioning, this satellite-receiver range is usually called pseudorange. [161, 278]

In order to be able to measure the pseudoranges and calculate the position, a GNSS receiver has to first find and acquire the signal from each visible satellite. After find-

Table 2.1: *Comparison of GNSS system characteristics [69, 196, 240, 278].*

	GPS	Galileo	GLONASS	BeiDou
Max. no of planned svs	31	30	27	35
No. of orbital planes	6	3	3	3 (MEO) 3 (IGSO) 1 (GEO)
Orbital altitude (km)	20200	23222	19100	21500 (MEO) 35800 (IGSO) 35800 (GEO)
Orbital inclination (degrees)	55	56	64.8	55 (MEO & IGSO)
Orbital period (MEO orbits)	11h58m2s	14h4m41s	11h15m44s	12h52m4s
Frequency bands	L1, L2 L5	E1, E6, E5, E5a, E5b	L1, L2 L3	B1, B2, B3
Signal spreading	DS-SS	DS-SS	DS-SS	DS-SS
MA	CDMA	CDMA	FDMA, CDMA [a]	CDMA
Signals	C/A, L1C, M-code, P/Y-code, L2C, L5	E1 OS, E1 PRS, E6 CS, E6 PRS, E5, E5a, E5b	L1OF, L2OF, L1SF, L2SF, L3OC, L1OC, L1SC, L2OC L2SC	B1-C, B1-A, B3, B3-A, B2, B2b, B2a
Used modulation	BPSK(1) BPSK(10) SinBOC(10,5) TMBOC(6,1,4/33) SinBOC(1,1) QPSK(10)	BPSK(5) CosBOC(10,5) CosBOC(15,2.5) AltBOC(15,10) CBOC(6,1,1/11) QPSK(10)	BPSK(1) BPSK(0.5) BPSK(5) SinBOC(1,1) SinBOC(5,2.5) SinBOC(4,4) QPSK(10)	BPSK(2) QPSK(10) BPSK(10) MBOC(6,1,1/11) SinBOC(15,2.5) AltBOC(15,10)
PRN code lengths for open signals	1023 10230	4092 5115 10230	511 10230	2046

[a] CDMA is now studied for future GLONASS.

ing the signals and measuring the pseudoranges, the receiver computes the satellite positions using the ephemeris data (or navigation data) decoded from the satellite signals. When the pseudoranges have been measured and the satellite positions are known, the position of the receiver can be finally calculated. Each GNSS system has its own GNSS System Time (GST), and the satellites of the same system are synchronized and have highly accurate atomic clocks on board. If the receiver was perfectly synchronized to the GST, it would be enough to have the pseudoranges and positions for three satellites in order to be able to calculate the three-dimensional receiver position. However, in reality, the receiver clock is not as accurate as the atomic clocks in satellites. Therefore, also the time difference between the satellites and the receiver clocks have to been taken into account as a one more unknown parameter in the non-linear equations, and the three-dimensional position estimate actually demands measurements from four satellites instead of three. [85, 161]

Since the focus on this thesis related to the GNSS receiver functions is on the signal acquiring and especially on acquisition algorithms, the latter two tasks of the GNSS receiver are not described here in details. More details about data demodulation and the position calculation can be found in many GNSS related books, e.g., in [161, 240, 278, 318]. Acquisition and tracking functions will be discussed more in Chapter 3.

Assisted GNSS

The main point with assisted GNSS (A-GNSS) or assisted GPS (A-GPS) is to provide information to the receiver. The aim of the assistance process is two-hold: first, to make the positioning task faster to the receiver (i.e., to decrease the time-to-first-fix, TTFF) and secondly, to make it possible to detect also signals with weaker power than it could be possible without any additional information [85]. The information is the same that the receiver could obtain also from the satellites, and the receiver still has to receive and process the satellite signals.

Even though every GNSS satellite uses the same frequencies, the satellite speeds cause some variation to the frequency, i.e. Doppler shift. Therefore, each satellite appears in reality on a different frequency. While a standard GNSS receiver has to look for all possible frequencies to find the satellites in view, in A-GNSS the idea is to provide some information to the GNSS receiver about the possible frequencies and also the satellite positions. Thus, all the receiver has to do is to measure the

pseudoranges and compute the position estimate. This decreases the TTFF remarkably. Indeed, if the receiver knows in advance the possible frequencies for the search process, it is possible to use longer dwell times [85]. This means that the sensitivity increases as well, and signals with lower signal strengths can be acquired. Thus, A-GNSS significantly improves the performance of the receiver. Besides A-GNSS, other improvements for the GNSS positioning exist. One example is the High Sensitivity (HS)-GNSS, where the position fix can be obtained with very weak signals (indoors, urban canyons) by utilizing a large number of correlators and with improved correlation and integration methods [85]. The accuracy and TTFF are however not as good as in ideal conditions.

2.3 Cellular (2G, 3G, 4G, 5G) positioning

Though GNSS provides very high accuracy positioning outdoors, it has also limitations, especially in urban areas and indoors, where the satellite signals are blocked and/or attenuated. Therefore, also other positioning methods are needed. One of the most attractive alternatives is to utilize the available radio networks and signals for localization. Besides the backup or assistance for GNSS, other localization methods are justified also with economical and operational reasons, such as implementation costs and energy-efficiency. Positioning accuracy is an important criteria, and is critical in emergency cases, but it is not always the most important one. One example is the location-based marketing, that requires a location application to run continuously as a background process in the cell phone. In this case, GNSS could offer a high-accuracy solution, but at the cost of energy-inefficiency. With non-GNSS techniques feasible accuracy can be obtained together with longer battery duration.

Mobile networks were from the beginning meant only for communication purposes. Thus, cellular positioning has been based on existing signals only, being an add-on feature in the current and previous network generations. When the need for more accurate location later came obvious, a position specific signal and positioning protocols to the specifications were added to the next generations of mobile networks. These are, e.g., Idle Period Down Link (IPDL) utilization in 3rd Generation (3G) cellular systems of Universal Mobile Telecommunications System (UMTS) [264, 300, 357] and the Positioning Reference signal (PRS) in 4G Long-Term Evolution (LTE) [274, 300]. Currently, the discussions and planning towards 5G commu-

nication networks is going on, and some insights can be found, e.g., in [17, 107, 245]. With new technologies aiming to provide 10-100 x higher user data rate, 1000 x higher mobile data volume per area, 10-100x higher number of connected devices and 10x longer battery lifetime [246], the upcoming dense 5G network infrastructure is perfectly suitable for accurate user positioning [312]. Indeed, it has been stated in [8] that 5G positioning technologies should be cooperatively with other techniques and the positioning accuracy in 5G should be from 10 m to < 1 m at 80% of occasions and better than 1 m indoors. It is stated also in [10, 235, 312] that the user should be able to be localized with sub-meter accuracy in 5G networks.

2.3.1 Cellular system aspects

Table 2.2 shows the differences and evolution of different mobile network generations, starting from 2G, i.e., Global System for Mobile Communications (GSM) network. The focus is on the system aspects related to positioning capabilities. Since many parameters, such as carrier frequencies, are area- or country-dependent, Table 2.2 concentrates on Europe only. Indeed, 3G refers here to UMTS only, i.e., the enhancements such as the development of Evolved High Speed Packet Access (Evolved HSPA or HSPA+) is not taken into account. The current status of the 5G technology for cellular systems is still in the early development stages, and hence, the parameters in Table 2.2 for 5G are more like current suggestions found in 5G white papers than specifications.

2.3.2 Cellular positioning algorithms

Localization in wireless networks has been studied widely [42–44, 52, 123, 130, 256, 306, 332–334, 336] and besides GNSS/A-GNSS, several different algorithms or algorithm combinations have been standardized and proposed for each mobile network generations. Cellular network based positioning methods can be divided roughly into three categories: coverage-area based, ranging based, or Angle-Of-Arrival (AOA) based methods. A short introduction to different methods can be found, e.g., in [276]. These methods are all based on measurements, that the Mobile Station (MS) has, can measure, or can obtain from the network. Besides these three categories, also other techniques have been proposed, e.g., GSM fingerprinting [247].

Table 2.2: *Comparison of cellular system characteristics [9,10,95,96,231,235,274,300,357, 366].*

	2G	3G	4G	5G
Modulation types	GMSK	QPSK	QPSK, 16QAM, 64QAM	adaptive, under definitions
MA	TDMA/ FDMA	WCDMA	OFDMA / SC-FDMA	OFDMA, NOMA, SCMA, under definitions
Positioning specific signal	–	–	Yes (PRS)	Most likely
Main carrier frequencies	900 MHz, 1800 MHz	1900 MHz / 2100 MHz	700, 800, 900, 1800, 2600 MHz	$1-100$ GHz
BW	200 kHz	5 MHz	1.4, 3, 5, 10, 15, 20 MHz	N/A (hundreds of MHz)
Standardized positioning methods	A-GPS, CID, RSS/TA-assisted CID/ECID, E-OTD, U-TDOA	A-GPS, CID, RSS/RTT-assisted CID/ECID, OTDOA-IPDL, U-TDOA	A-GPS, CID, RSS/TA/AOA-assisted CID/ECID, TDOA	under definitions

Table 2.2 summarizes also the standardized positioning methods by European Telecommunications Standards Institute (ETSI) for each existing network generation [9, 95, 96, 274, 300, 357]. A-GPS is still the primary positioning technology, and the network-based methods are seen as backups. For 5G, no standardization exists at the time of writing the thesis. In what follows, different positioning methods mentioned in Table 2.2 are introduced shortly.

Coverage-area based methods

Coverage-area based positioning methods are pure network-based methods. This means that the MS only assists the positioning process by providing information or measurements to the corresponding network element. One example of coverage-area based methods is the Cell Identity (CID) method [317], that can determine the mobile position at the network based on the coverage area of the serving communication node (i.e., Base Station (BS) in GSM network, Node B in UMTS or Evolved Node B (eNodeB) in LTE). In the simplest case, when there is not any additional information on the sectorization or beam width of the node antenna, the location of the MS is estimated as the location of the node itself or as the cell origin. Typically however, more than one node is heard, and the MS can be located in the intersection of the heard node's coverage areas. This is the case, e.g., in soft handover.

The CID method is very simple and fast [288] and available in all existing network generations, but its accuracy is totally dependent on the size of the serving cell or sector. In dense networks and small cells, such as pico- and femtocells, the accuracy may be even tens of meters, but in rural areas with wider cell radius, the performance decreases remarkably [9, 317]. Another problem is the cell breathing, where the cell size is reduced according to the traffic load. However, these simple methods are very good to provide approximate information on mobile position to the network. CID can be further improved by combining it with some ranging-based measurements, e.g., Timing Advance in 2G networks [302], Round Trip Time (RTT) in 3G networks [42, 43], AOA [274] or RSS [130]. This combined technique is called Enhanced CID (ECID).

Ranging-based methods

Ranging-based methods mean techniques, where the distance (range) between the transmitter (node) and receiver (MS) is estimated with either time delay or path loss measurements. If the distance can be determined to several nodes, the MS location can be estimated using standard trilateration or multilateration similarly to GNSS.

As described earlier in Section 2.2.1, GNSS is based on TOA. In principle, time-delay based distance estimation is as straightforward in cellular positioning as well. If a node sends a time-stamped transmission, the MS can calculate the distance between

the node and the MS, based on the time delay (i.e., the difference between the transmission and reception times). However, in order to be able to calculate the MS location, the node locations have to be known. Indeed, the method demands perfect synchronization between all the nodes in the network and the MS clock. One example of the available time-delay measurements is Timing Advance (TA) delay in 2G networks [9, 301]. GSM transmissions are Time Division Multiple Access (TDMA)-based, where all MSs connect to the BS using the same frequency, but different time slots. Since MSs are located with different distances from the BS, the propagation delay can still cause overlaps between the adjacent users. In order to avoid the interference, the BS has to measure propagation delays, i.e., the time it takes between the transmission of the beginning of a packet frame to the MS and the reception of the beginning of the corresponding respond packet from the MS. Based on the time delay, the MS can then adjust the allowed transmission time slots for the MS with a TA-parameter [278]. The TA-parameter can further be used to estimate the distance between the BS and the MS, though the resolution to the distance estimation is typically one bit, that corresponds to 550 m. Typically, as already mentioned, TA is combined together with CID method for assistance, resulting as a ECID (CID + TA) [302]. RTT in 3G/4G networks corresponds to the TA-parameter in GSM network. The positioning accuracy with CID + RTT in 3G/4G networks is typically better due to the better timing resolution of RTT, but depends still on the network topology [44]. Again, in the case of soft or softer handover, the measurements can be obtained from several BSs, and thus, the accuracy can increase remarkably [42].

Time-Difference-Of-Arrival (TDOA) or Observed-Time-Difference-Of-Arrival (OTDOA) methods are used, when the transmissions are not time-stamped and there is not time synchronization between the network nodes and the MS. In this kind of case, when there is no information about the exact transmission time, TOA can not be used to determine the time delay. The idea in TDOA method is to measure the time difference of arriving signals from two or more transmitters at the receiver, i.e., the relative arrival times. The transmitter locations have to be known, but the possible time bias between the node and the MS can be eliminated algebraically. With two transmitters, the position of the receiver can be seen as a hyperboloid. With three or more transmitters, the position of the MS can be found as an intersection of two or more hyperboloids, respectively. In GSM, this hyperbolic positioning, based on the existing OTD feature in GSM network, is called Enhanced Observed Time Difference

(E-OTD) [300, 357]. In 3G, IPDL is utilized to avoid the hearability problem, resulting as a method called OTDOA-IPDL [264, 300, 357]. Uplink TDOA (U-TDOA) is an uplink alternative to TDOA. It is a network based method and basically identical to OTDOA, the difference being that the timing measurements are made from signals coming from the mobile and received at neighboring nodes.

When in time delay-based methods the idea is to estimate the range between the receiver and the transmitter based on the travelling time of the the transmitted signal, in Path Loss (PL) based methods the range is estimated based on the signal attenuation due to the travelled distance. The attenuation can be seen by measuring the strength of the received signal, i.e., RSS. Assuming that transmitter's location and transmission power are known, the range between the transmitter and receiver can be calculated by using an appropriate propagation model to estimate the dependence between the RSS and the propagation distance. Again, RSS measurements are needed from three or more nodes with known locations, in order to be able to calculate the MS position in 3D via trilateration [97, 219, 338]. The basic PL model is free-space loss, but in practise, this model is way too simple to model reliable the PL in realistic environment. Besides the propagation distance, also other phenomena affects the RSS. E.g., different obstacles in the environment can cause reflections or diffraction. Since the environments are different (rural or urban areas, outdoors or indoors, etc.), several different PL models have been presented within the past years [11, 90, 242, 305]. Many models require knowledge of different parameters, that are not always available and are difficult (or impossible) to estimate. Therefore, the most suitable PL model for the particular environment is not always feasible due to the number of required parameters. In general, time-delay based distance estimation is more precise, and thus, the location estimation is more accurate, but the big drawback is that the devices need to be finely synchronized. The advantage of PL based location estimation is that no synchronization is needed between the transmitters and the receiver. Another advantage is the availability of RSS measurements for more than one node. In radio resource management of cellular networks, RSS measurements are needed for monitoring the signal levels, that is further used to make decisions of handovers. Thus, in addition to the serving cell, RSS measurements are typically available also for neighboring nodes as well. PL-based methods for cellular networks have been studied, e.g., in [11, 90, 170, 242, 305]. PL based positioning approaches are further discussed in Chapter 4.

Angle-Of-Arrival

While both time-delay based or ranging based methods provide distance estimation, AOA or Direction-Of-Arrival (DOA) is a method that estimates the direction of the incoming signal instead. AOA is network-based method, defined as the estimated angle of uplink transmission with respect to a reference direction. The basic principle of AOA is to use antenna arrays and measure the phase differences of the received signal between several antenna elements. The degree of the phase shift is a function of the AOA, the antenna element spacing, and the carrier frequency [300]. If the node characteristics are known, the AOA can be estimated by comparing the phase differences [300]. AOA measurements at two BSs are sufficient to provide a unique location in 2D. The major error source in AOA method is multipath propagation, due to the reflected signal, that may not be coming from the direction of the MS [52]. Indeed, AOA requires sophisticated antenna arrays on the nodes, and thus, it has not been standardized for positioning in the current networks, though it has been proposed in many papers [80, 331]. Since very dense networks and equipped antenna arrays are expected to be included in the future 5G networks, AOA is a very good alternative for positioning in future 5G networks. In [330], it has been shown that even a sub-meter positioning accuracy can be achieved with joint AOA/TOA method. One modification of AOA is Angle-Difference-Of-Arrival (ADOA), that is studied, e.g., in [189]. Also Phase-Difference-of-Arrival (PDOA) techniques exist, but they have not yet been much studied in the context of current cellular systems [119].

2.4 WLAN positioning

Though the primary purpose of WLAN networks (also called WiFi or IEEE 802.11) is in communications, the widespread infrastructure offers the possibility to locate mobile devices in an economical way. The main advantage of position determination using WLAN technology is that it can perform both indoors and outdoors, due to the very dense AP network, especially indoors and outdoor urban areas. Another advantage are relatively small signal coverage ranges, leading to better positioning accuracy. The main challenge is that an existing Access Point (AP) infrastructure may not be suitable for positioning. Indeed, AP topology may be changed relatively often, and that may affect also the positioning results. Many technologies and measurements

that are used, e.g., for cellular-based positioning, can be adopted for other access networks as well. This holds for coverage area-based, ranging-based and AOA-based methods, that were described in Section 2.3. One difference between outdoor and indoor positioning is that the indoor area is more limited, and thus, some positioning technologies may be more suitable indoors than outdoors. On the other hand, as a different aspect compared to outdoor positioning, floor detection has to be taken into account indoors.

2.4.1 WLAN system aspects

Table 2.3 shows some basic characteristics of the most important 802.11 standards, developed by The Institute of Electrical and Electronics Engineers (IEEE) [145–148]. The characteristics are bandwidth (BW), carrier frequencies, possible modulation types, MA schemes, possible multi-antenna support and cognitive spectrum use. The evolution of the 802.11-family started in 1997, and is still increasing while new specifications are continuously developed. The next generation wireless transmission standard is IEEE 802.11ay at 60 GHz. It is expected to be completed in 2017.

2.4.2 WLAN positioning algorithms

WLAN networks have not originally been designed for positioning, and hence, there are no extra protocols or suitable frame types for this purpose. Since the widespread networks with appropriate standards however have very good potential, WLAN-based positioning has gained considerable attention and become a huge research field over the last decade. Many different positioning approaches have been developed, varying from coverage-based methods [173] to fingerprinting [16, 23, 157, 174, 193, 228, 230, 238, 265, 275, 303, 313–315, 322, 323, 328], both for outdoor [127, 193, 197, 322, 356] and indoor situations [83, 173, 183, 241, 291, 316, 325, 328]. The main difference between coverage-area based methods between cellular and WLAN-networks is that the transmitter positions (i.e., BSs for cellular and APs for WLAN) are generally known in cellular networks, but this is usually not the case with WLAN networks. Thus, in order to be able to use, e.g., CID-based method for WLAN network, AP locations should be first estimated or alternatively use some coverage area estimates, like in [173]. AP locations are needed for distance-based estimation methods as well.

Table 2.3: *Comparison of most recent WLAN standards in terms of system characteristics [145–148].*

	802.11g	802.11n	802.11ac	802.11ad	802.11af
BW	20 MHz	20, 40 MHz	20, 40, 80 160 MHz	2.16 GHz	6, 7, 8 MHz
Carrier freq.	2.4 GHz	2.4, GHz 5.8 GHz	5 GHz	60 GHz	470 – 790 MHz
Modulation	BPSK, QPSK, 16QAM, 64QAM	BPSK, QPSK, 16QAM, 64QAM	BPSK, QPSK, 16QAM, 64QAM, 256QAM	SQPSK, QPSK, 16QAM, 64QAM, BPSK	BPSK, QPSK, 16QAM, 64QAM, 256QAM
MA	CCK, DSSS, or OFDM	CCK, DSSS, or OFDM	OFDM	OFDM, single carrier	OFDM
Multiple antenna support	No	Yes	Yes	No	Yes
Cognitive spectrum	No	No	No	No	Yes
Positioning methods	RSS	RSS	RSS	RSS, RTT TDOA, AOA	RSS, RTT, TDOA, AOA

As it was shown in Table 2.3, the underlying MA schemes for WLANs are either Complementary Code Keying (CCK), DSSS, or Orthogonal Frequency Division Multiplexing (OFDM) techniques. Also the underlying modulations range from Binary Phase Shift Keying (BPSK) and Quadrature Phase Shift Keying (QPSK) to higher order Quadrature Amplitude Modulation (QAM). Therefore, TOA or RTT based positioning approaches for WLAN positioning are still not widespread, due to the various underlying physical layer features of WLANs on the market. Another challenge is that an exact signal propagation delay is still difficult to measure, since a high-precision timer is not included in today's standard WLAN components [281]. This may however change in the future. As an alternative to TOA-based methods, most of the WLAN positioning methods are based on the RSS measurements extracted from the APs and identified by unique Medium Access Control (MAC) addresses [177, 181, 183, 225, 241, 265, 275, 303, 325]. As in cellular networks, RSS-based positioning methods have the advantage of easy accessibility and availability

in almost every user device, that makes the measurement both practical and cost effective. Besides different PL models (described in 2.3.2), RSS measurements are very suitable to be used in so-called fingerprinting (FP) methods, also called pattern recognition or pattern matching. Fingerprinting techniques are many times preferred, since they neither require the AP location nor attempt to model the signal strength via any path loss models. Some low-complexity methods are an alternative, such as Weighted Centroid (WeiC) -based algorithms. As already mentioned, many of the cellular-based positioning approaches described in 2.3.2 can be used similarly with other networks, including WLANs. Besides WLAN and cellular networks, RSS-based positioning can also be applied with radio-frequency identification (RFID) [57, 236], Bluetooth [59, 321], or ZigBee [40, 239] signals.

Fingerprinting

In general, RSS-based positioning methods have two stages: an initial off-line training phase and an on-line estimation phase [99,225,344]. In the training phase, models and/or databases are created based on collected information. Usually this collected information (also called training data or radiomap) means location dependent data samples (i.e., the fingerprints), such as RSS measurements with known locations. In the estimation phase, that involves real-time processing, the unknown position of a MS is calculated based on the observed RSSs of the hearable transmitters (or APs, in the case of WLAN network) and the radiomap database saved in the training phase. The radiomap consists of (x,y,z)-coordinates for each fingerprint or grid point in the building (or in the area of interest), together with the MAC-addresses for each hearable AP and the corresponding RSSs in the particular grid point. The RSS radiomap can be used for the localization purposes via several ways: by matching the measured RSSs by the MS with the radiomap (i.e., fingerprinting method) [16, 23, 157, 174, 193, 228, 230, 238, 265, 275, 303, 313–315, 322, 328, 334], by trilateration methods using some signal-to-distance mapping derived from the radiomap (PL based method) [241, 291], or by some low-complexity methods, such as WeiC [40, 88, 200]. Other possible methods are, e.g., clustering [60, 63, 76, 143, 175, 232, 269, 344] and spectral compression [311] based methods. All methods do not need the full radiomap information in the positioning phase, but only parts of it. E.g., in PL based method, the radiomap is used to calculate the path loss parameters in training phase, but after this, the collected data is not needed anymore, and the calculated paramet-

ers are the only data needed to be saved and transmitted to the mobile. This will be discussed more in Chapter 4.

Fingerprinting is a database correlation technique, where no distance measures are needed between a transmitter and a receiver. Most common data used for FP method is RSS, but any other location dependent signal characteristic is also possible. In the estimation phase, only the database of fingerprints and the current real-time measurements are used to calculate the position estimate online, by comparing the measured signal characteristics (e.g., RSS levels) by the MS to the measurements saved in the database. Further on, the position of the MS is estimated as the best match among the fingerprints. Several different fingerprinting-based positioning algorithms using pattern recognition technique have been presented in the literature: K Nearest Neighbor (KNN) [22, 122, 233, 258, 313, 315, 316], probabilistic methods (e.g., Gaussian likelihood) [16, 197, 224, 230, 275], neural networks, Support Vector Machine (SVM), and Smallest M-vertex Polygon (SMP). Fingerprinting is discussed more in Section 4.1.2.

Fingerprinting has the potential to use any existing radio signals in positioning. In addition to indoors, FP positioning method can be used outdoors, e.g., by utilizing cellular networks. The main drawback with all positioning methods based on RSS measurements is the need for training phase. The process to form the radiomap is not only slow and costly, but also very sensitive to changes in the environment. Indeed, RSSs can be affected by reflection, diffraction and scattering in the propagation environments, especially indoors. Besides the radiomap forming process, the size of the database causes challenges. Due to the high deployment of APs in many buildings, many indoor positioning methods suffer from having to deal with a huge amount of data. The memory requirements to store the radiomap database in large areas or buildings may become overwhelming, and also data transmission may become a bottleneck for the localization system, especially for fingerprinting. Thus, especially outdoors, where the target area is usually bigger, some methods with data compression may be more suitable. These challenges and how to address them are discussed more in Chapters 4, 9 and 10, respectively.

2.5 Other positioning systems

Due to the complexity of the indoor environment, a low-cost and accurate positioning system is not easy task to achieve. An ideal IPS would provide sub-meter accuracy and be cost-effective, but also be universal in that sense that it would work anywhere with any device, preferably also outdoors. Though several IPSs already exist, they all make some trade-offs with these requirements. Also the accuracy requirements change according to the use - finding a specific store in a multi-floor shopping center needs different application and accuracy than locating a specific item in a supermarket. It should also be remarked that locating a MS indoors is in many cases only half of the solution. For the location to be meaningful for navigation purposes, accurate indoor maps are needed. An Inertial Navigation System (INS) means some navigation aid, that includes motion and rotation sensors (accelerometers and gyroscopes) to the positioning, in order to be able to estimate also orientation and velocity of the MS. Venue tracking and floor detection bring their own challenges to the end solution.

Besides WLAN networks, positioning can be based on other radio frequency signals as well, e.g., on Bluetooth [59, 272, 321], ZigBee [40, 239] or digital television signals [58]. The main advantage with these Signals-Of-Opportunity (SOO) based methods is the low cost and wide coverage. Some methods require a deployment of a new specific infrastructure, such as Ultra Wideband (UWB) based positioning methods [78, 113]. Deploying a new network is expensive, but the advantage is seen as better positioning accuracy, when the new infrastructure is planned especially for positioning purposes. Other IPS technologies are based, e.g., on magnetic fields [192, 255, 314] or infrared [340]. Table 2.4 describes shortly some of the most known IPS today in addition to GNSS, cellular and WLAN.

Many of the systems presented in Table 2.4 can obtain very good indoor positioning accuracy. However, their implementation usually requires resources to form some specific infrastructure, e.g., beacons or tags meant only for positioning purposes. Therefore, these systems are used many times in relatively small areas, such as in one building only, and many of these do not achieve seamless outdoor-indoor positioning in large scale. As widespread and cost effective general solutions, WLAN and cellular network based positioning approaches are still offering most viable alternatives for mass-market large scale positioning solutions indoors.

Table 2.4: *Some existing IPS based on different technologies.*

Company	Technology	Positioning algorithm	Reported accuracy
Indoor Atlas	magnetic field, other sensors (proprietary solutions)	FP	1-3 m
Ekahau	WLAN, infrared (optional)	FP (RSSI)	1-3 m (sub-meter with infrared)
UbiSense	UWB	TDOA, AOA	$<$ 15 cm
Ambiplex	infrared	AOA	20-30 cm
Nimble Devices (Steerpath)	Bluetooth	N/A	2 m
Quuppa	Bluetooth	AOA, RTT	$<$ 1 m
Sensewhere	hybrid (Bluetooth, WLAN, GNSS, INS)	triangulation	5-10 m
Spreo	Bluetooth, INS	FP	sub-1 m
GloPos	Cellular networks, WLAN	N/A	sub-10 m (2G,3G), sub-3 m (WLAN)

2.6 Comparison of methods

Table 2.5 summarizes the main discussion of GNSS, cellular and WLAN-based positioning methods. Accuracies are rough estimates, since they naturally depend a lot on the used network and algorithms. Indoor/outdoor usage means here if the method can be used independently in these circumstances, like indoors, such that the accuracy is considerable. E.g., cellular network based methods can of course be used also indoors, but the accuracy is meaningful only if they are combined with some other methods (as a hybrid solution). DGPS in Table 2.5 stands for Differential GPS, that is an enhancement to a primary GNSS system consisting of reference stations enabling corrections to the positioning estimate.

The main weaknesses of GNSS (or A-GNSS) are the receiver complexity and power consumption, and the unsuitability to positioning indoors. On the other hand, GNSS is very accurate in most outdoor situations, and can be used also to augment or enable other positioning methods. Cellular methods can provide a coarse location estimate really fast, and can be used to improve the position estimates offered by GNSS,

Table 2.5: *Comparison of different positioning methods.*

	Methods	Accuracy	Outdoor usage	Indoor usage	Complexity	Power consumption
GNSS	TOA	10-15 m	Yes	No	High	High
	DGPS	3-10 m	Yes	No		
	A-GNSS	1-3 m	Yes	Partial		
cellular	TDOA	50-125 m	Yes	No	Low	Low
	RSS	100-200 m	Yes	Yes	Low	
	AOA	< 1	Yes	Yes (5G)	Moderate	
WLAN	RSS RTT	1-5 m (indoors)	Partial (urban areas)	Yes	Low	Low to moderate

e.g., in urban areas with low satellite visibility. The main drawbacks stay in lower accuracy, when compared to GNSS, and in the positioning techniques that may require synchronization to the network. WLAN based methods can be very accurate indoors and in urban areas. It is also a low-cost and low-complexity method, that does not require synchronization and can utilize the exiting AP infrastructure, but many algorithms need a database to be collected and maintained. Indeed, in low AP environments (outdoor suburban areas) the positioning accuracy is decreased.

Challenges for GNSS are naturally partly different than challenges for WLAN or cellular based techniques. While multipath is the main error sources in GNSS, it affects WLAN or cellular based methods directly only if TDOA or AOA positioning techniques are used. Same holds for No-Line-Of-Sight (NLOS). In RSS, the effect of multipath and NLOS is seen only as RSS fluctuations. Thus, all these effects can be lumped together and they do not have as high effect as on GNSS. Path losses affect the RSS of all systems, but not necessarily to the positioning accuracy, e.g., in WLAN fingerprinting. Narrowband interference (e.g., jamming) is a problem with GNSS but not with other systems, that are more affected by multiuser interference. GNSS does not require any databases, but for fingerprinting with any network these are a challenge: not only the collection and maintaining, but also the data transfer, that easily becomes a bottleneck of a system. The challenges typical to WLAN and cellular positioning, such as database size, may also become a challenge in the new studies and solutions of cloud GNSS [211]. Table 2.6 lists the main challenges for each positioning methods. Physical layer challenges in GNSS are discussed with

Table 2.6: *Most common challenges for different positioning methods.*

	Multipath	Path loss	Narrowband interference	Multiuser interference	NLOS	Database size
GNSS	Yes	Yes	Yes	-	Yes	only for cloud GNSS
cellular	For TDOA and AOA	For PL	Yes	Yes	For TDOA and AOA	For FP
WLAN (RSS)	- [a]	For PL	Yes Yes	In some range	- [b]	For FP

[a] Not directly, but can be seen as RSS fluctuations.
[b] Body impact is more significant than NLOS.

more details in Chapter 3, and in cellular and WLAN-positioning in Chapter 4.

2.7 Summary

This chapter has provided an introductory overview of wireless positioning. System aspects and most typical positioning algorithms have been described for GNSS, cellular and WLAN-based positioning approaches. Several comparative tables have been included. This survey and summary of methods provided in this chapter is a contribution towards the state-of-the-art. The discussion of GNSS and RSS-based localization approaches and their challenges will be continued in Chapters 3 and 4, respectively.

3. GNSS POSITIONING - SYSTEM OVERVIEW AND CHALLENGES

About half of the work in this thesis has been focused on improving the GNSS receiver design, concentrating especially in the acquisition part of baseband processing functions. In this chapter, the main tasks and the structure of GNSS receiver are discussed shortly before going into more details of GNSS challenges and possible solutions.

3.1 GNSS receiver fundamentals

As it was already mentioned in Section 2.2.2, satellite-based positioning is based on TOA measurements and trilateration principle. In order to be able to calculate its position, a GNSS receiver has to first find and acquire the signal from each visible satellite, and further on, decode the ephemeris data from the signals to find the position of the satellites and to be able to measure pseudoranges. Thus, the receiver has several important tasks starting from signal acquiring (acquisition and tracking functions) and continuing to data extraction and finally position calculation.

Fig. 3.1 shows the structure of a typical GNSS receiver. Each receiver consists of three main blocks, namely radio front-end, baseband processing unit and navigation unit [240]. After the signal is captured through the antenna, the radio front-end unit takes care of constructing the signals for baseband block. The main tasks for the front-end-block includes several functions, such as amplification, filtering, frequency conversation and signal digitization [240]. More detailed information about the radio front-end and its functions can be found, e.g., in [161, 240, 318]. After digitization, the signal arrives to the baseband processing unit, where it undergoes several signal processing operations. The first phase is signal acquisition, where the purpose is to identify the visible satellites in the sky and to get some coarse estimates of the code

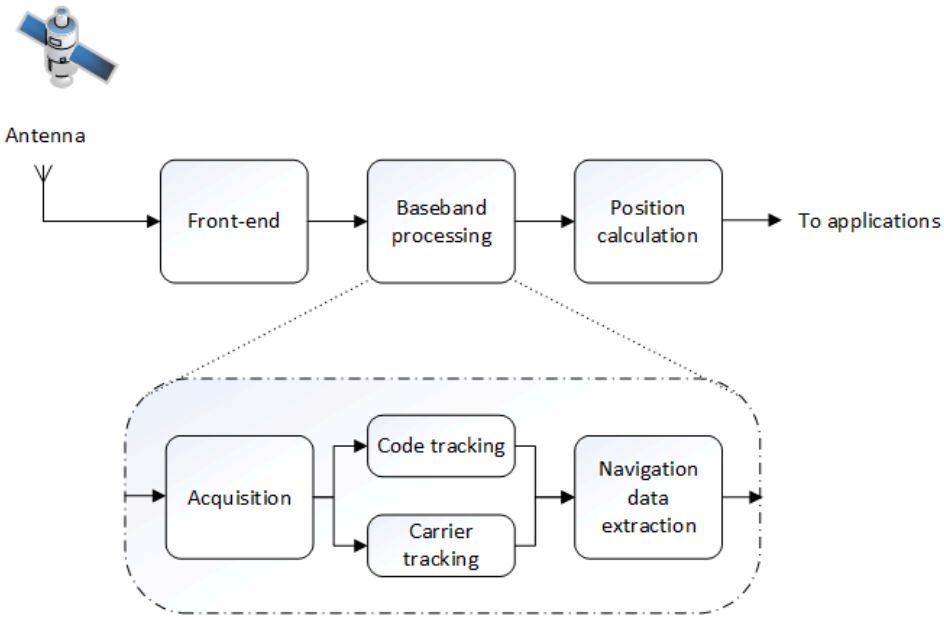

Fig. 3.1: *Simplified block diagram of a typical GNSS receiver.*

phase and carrier frequency. Signal acquisition is followed by tracking, where the produced coarse estimates are enhanced to get fine estimates. After navigation data extraction, a separate navigation unit takes care of the position solution calculation.

Since the focus of this thesis is in the baseband processing part and especially the signal acquisition, we will concentrate in this chapter mainly on signal acquisition phase. The reason for this is that code acquisition is typically considered as one of the most challenging and crucial tasks in a spread spectrum system [109]. More details of GNSS receiver functions concerning data extraction and position calculation can be found for example in [161, 240, 278, 318].

3.1.1 Signal acquisition

In spread spectrum systems, the PRN code sequence $x_{PRN,n}$ without pulse shaping can be modeled as

$$x_{PRN,n}(t) = \sum_{j=1}^{S_F} c_{j,n}\,\delta(t - nT_{sym} - jT_c), \tag{3.1}$$

where j is the chip index, n is the data symbol index, S_F is the spreading factor (i.e., $S_F = T_{sym}/T_c$), T_{sym} is the symbol period, $T_c = 1/f_{chip}$ is the chip period, $c_{j,n}$ is the jth

chip corresponding to the nth symbol, and $\delta(t)$ is the Dirac pulse. After spreading, the data sequence x_{data} can be expressed as

$$x_{data}(t) = \sum_{n=-\infty}^{\infty} \sqrt{E_b}\, b_{data}(n)\, x_{PRN,n}(t), \tag{3.2}$$

Here, E_b is the data bit energy and $b_{data}(n)$ is the nth complex data symbol (in the case of a pilot channel, $b_{data}(n) = 1$). The transmitted signal $x(t)$ can be expressed as the convolution between the PRN code with data modulation $x_{data}(t)$, the modulating waveform $s(t)$, and the pulse shaping filter $p_{T_B}(t)$ [205]:

$$x(t) = \sqrt{E_b} s(t) \circledast \sum_{n=-\infty}^{+\infty} \sum_{j=1}^{S_F} b_{data}(n) c_{j,n} \delta(t - nT_{sym} - jT_c) \circledast p_{T_B}(t), \tag{3.3}$$

where, $\circledast$ is the convolution operator. The modulating waveform $s(t)$ can be either BPSK [135] or BOC modulated. BOC modulation waveforms are further presented in Section 3.2.2. Detailed expressions for different modulations can also be found in [205].

Further on, if a discrete tap channel model is adopted, the received signal $y(t)$ in fading multipath channel can be expressed as

$$y(t) = \sum_{l=1}^{L} \alpha_l x(t - \tau_l) e^{-j2\pi f_D t} + \eta(t). \tag{3.4}$$

Here, L denotes the number of channel paths, l is the multipath index, α_l is time-varying complex fading coefficient for lth path, τ_l is the multipath delay, $x(\cdot)$ is the transmitted signal, and $\eta(t)$ is additive Gaussian noise with zero mean and double-sided power spectral density N_0 including all possible interference except multipath. White noise assumption is based on central limit theorem [298]. Frequency shift, namely Doppler shift f_D, is caused by the speed of the satellite and receiver with respect to each other, resulting as deviation to the carrier frequency f_c. Estimates for the timing and the correct frequency of the received signal are necessary, in order to be able to remove the carrier frequency and to despread the received signal to obtain the original data. Since each satellite transmits an unique PRN code in CDMA-based GNSS, the satellite can be detected through correlation between the received signal $y(t)$ and the reference PRN code s_{ref} with certain tentative delay $\widehat{\tau}$ and Doppler frequency $\widehat{f_D}$:

$$C(\widehat{\tau}, \widehat{f_D}, i) = \mathbf{E}\Big(\frac{1}{T_{sym}} \int_{(i-1)T_{sym}}^{iT_{sym}} y(t) s_{ref}(\widehat{\tau}, \widehat{f_D}, t) dt \Big), \tag{3.5}$$

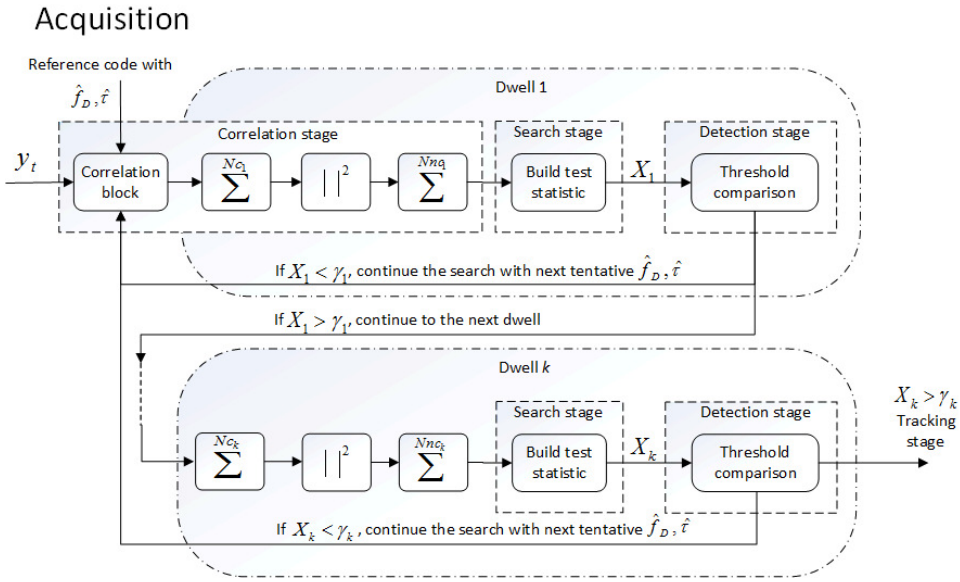

Fig. 3.2: *Simplified block diagram of the acquisition process with k dwells.*

where i is the index for code epoch, $\mathbf{E}(\cdot)$ means the expectation operation with respect to the PRN code, and

$$s_{ref}(\widehat{\tau}, \widehat{f_D}, t) = e^{-j2\pi\widehat{f_D}t} \sum_{j=1}^{S_F} c_{j,n}\, \delta(t - nT_{sym} - jT_c - \widehat{\tau}) \circledast p_{T_B}(t). \tag{3.6}$$

Since PRN codes have high correlations close to zero delay error, the high peak in the correlation output indicates that the satellite with this certain PRN code is available. Indeed, the correlation output also provides estimates for the code delay and frequency offset. Thus, the acquisition can be seen as three-dimensional search process.

Fig. 3.2 shows a block diagram of the acquisition, that consists of multiple dwells and three stages per dwell. A dwell refers to the time to reach a first decision, which can be further fine-tuned by sub-sequent dwells. Each dwell has a correlator block, a search stage and a detection stage, but the parameters of each of these 3 blocks differ from one dwell to another [240]. Single-dwell structures are the most used in GNSS, but also multi-dwell approaches have been studied for example in [53, 73, 204]. In the correlation phase, a two-dimensional correlation output is formed by correlating the received signal with the locally generated reference code s_{ref} with different tentative Doppler frequencies and delays. By examining the resulting correlation

output and looking for a correlation peak which appears for correct delay-frequency combination, it can be determined whether the signal is detected or not. Correlation can be accomplished either in time domain [161] or in frequency domain using Fast Fourier Transform (FFT) [13]. Wavelet-based acquisition structures have also been studied in [56, 191], but FFT-based correlators are nowadays the most widespread in software-defined radio implementations [45].

After the correlation is performed, the process is typically continued with both coherent and non-coherent integrations in order to reduce the noise from the received signal [75,85]. In coherent integration, the correlator outputs are coherently averaged over N_C chips (i.e., coherent integration length). However, the coherent integration length N_C is limited due to the channel fading, presence of data bits, residual Doppler error and the instability of the oscillator clocks [153, 178, 240, 318, 319]. Thus, N_C should be less than the coherence time $(\Delta t)_{coh}$ and less than the bit duration for non-pilot channels, in order to avoid the fading spectrum to be distorted. On the other hand, N_C also defines the frequency resolution in the frequency uncertainty. Naturally, the higher the N_C is, better frequency resolution is obtained, as it can be seen in Fig. 3.3. Due to the limitations in the coherent integration time, coherent integration can be followed by non-coherent averaging (or integration) over N_{NC} blocks (i.e, non-coherent integration length) [85, 161]:

$$Z(\widehat{\tau}, \widehat{f_D}) = \frac{1}{N_{NC}} \sum_{N_{NC}} \left| \frac{1}{N_C} \sum_{i=1}^{N_C} C(\widehat{\tau}, \widehat{f_D}, j) \right|^2. \tag{3.7}$$

It is also possible to use other types of post-correlation combination instead of non-coherent integration. These methods have been studied also in this thesis, and are presented in detail in Chapter 6.

Search stage

The search uncertainty in time domain $(\Delta t)_{max}$ is typically the PRN code length, e.g., 4092 chips for Galileo E1 signal and 1023 chips for GPS C/A signal. Frequency uncertainty is defined as $+/-$ maximum possible Doppler shift caused by the satellite's and receiver's relative speed. Thus, the search interval in frequency domain $(\Delta f)_{max}$ may be even tens of kHz, usually $+/-10$ kHz for Galileo signal [54]. If it is possible to estimate the Doppler shift in some range in advance, e.g., with A-GNSS, the search space can be reduced and the acquisition time decreased [85].

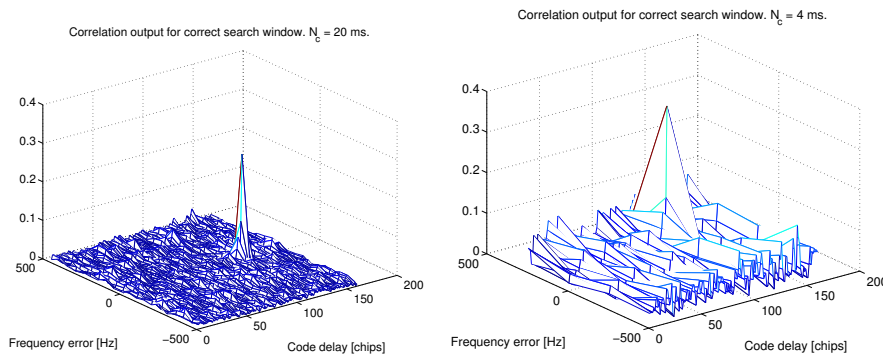

(a) ***(b)***

Fig. 3.3: *Examples of frequency resolution of FFT-based correlation output for (a) $N_C = 20$ ms and (b) $N_C = 4$ ms. Correct time-frequency window.*

In the search process, the search uncertainty area is divided into search windows, who define the decision region and whose number depends on the chosen search strategy. Each search window is divided into search bins, $(\Delta t)_{bin} \times (\Delta f)_{bin}$, where $(\Delta t)_{bin}$ is time bin, and $(\Delta f)_{bin}$ is frequency bin. For GPS, common values for the search bins are $(\Delta t)_{bin} = 0.5$ chip and $(\Delta f)_{bin} = 1$ kHz. For other GNSS signals, such as Galileo signals, smaller time bin steps are usually needed in order to avoid ambiguities in the correlation function. The problem of the acquisition ambiguities and solutions to it are discussed more in Section 3.2.2 and Chapter 6. Different search strategies can be roughly divided into serial [263], parallel [297] or hybrid search [159,161,204]. The serial and parallel search are also included as two extreme cases in hybrid search [204]. The choices of the best search algorithm and the suitable window and bin sizes are discussed more, e.g., by us in [251]. After the correlation output Z is formed for the search window as a grid of correlation values (see Fig. 3.4 with examples of correlation output for both correct and incorrect search window), a test statistic (or decision variable) X is computed. The choice of the decision variable has also been studied in this thesis and will be discussed in more detail in Chapter 6.

Detection stage

In the detection stage, the aim is to decide whether the signal is present or not in the current test window by comparing the test statistic X to a pre-determined threshold γ.

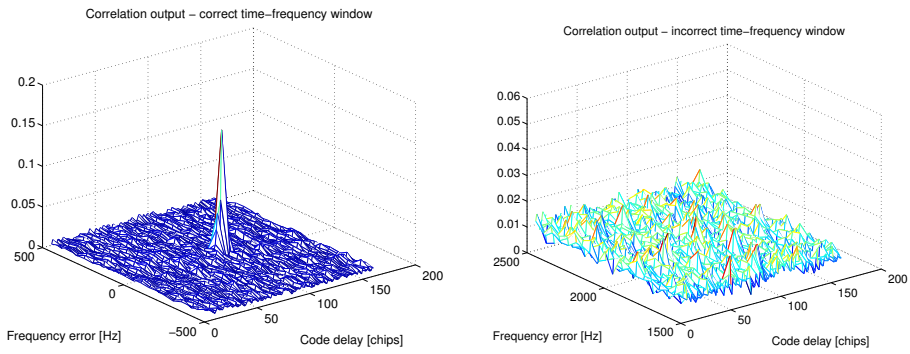

(a) ***(b)***

Fig. 3.4: *Examples of correlation output for (a) correct and (b) incorrect search windows.*

This is the classical detection problem [164]:

$$\begin{aligned} &\mathcal{H}_0 : signal absent \\ &\mathcal{H}_1 : signal present. \end{aligned} \tag{3.8}$$

With the assumption that there are no false alarms in the correct search window, the detection and false alarm probabilities (P_d and P_{fa}, respectively) can be calculated as the probability that at least one variable is higher than threshold γ [53, 164]

$$\begin{aligned} P_{fa} &= p(X \geq \gamma | \mathcal{H}_0) \\ P_d &= p(X \geq \gamma | \mathcal{H}_1). \end{aligned} \tag{3.9}$$

Under the assumption of an Additive White Gaussian Noise (AWGN) channel, in has been proven for example in [201] that the correlation output after the non-coherent integration is distributed according to either a central χ^2-distributed variable with a Cumulative Distribution Function (CDF) $F_c(\gamma)$ ($\mathcal{H}_0$), or according to a non-central χ^2-distributed variable with a CDF $F_{nc}(\gamma,\lambda)$ ($\mathcal{H}_1$). Thus, the formulas in Eq. (3.9) can be extended to [204]

$$\begin{aligned} P_{fa} &= 1 - (F_c(\gamma))^{N_{bins}} \\ P_d &= \mathbf{E}_\lambda\Big(1 - (F_c(\gamma))^{N_{bins}-N_{cbins}} \Pi_{i=1}^{N_{cbins}} F_{nc}(\gamma,\lambda_i)\Big), \end{aligned} \tag{3.10}$$

where λ is the non-centrality parameter depending on channel path energies, N_{bins} is the number of search bins in the search window, and N_{cbins} is the number of correct search bins. Due to the width of the main lobe of the ACF, there might be several $\mathcal{H}_1$ bins even in single-path channels. For multipath channels, there is always more than

one correct bin. The definitions for CDFs $F_{nc}(\gamma,\lambda)$ and $F_c(\gamma)$ are [294]

$$\begin{cases} F_c(\gamma) &= 1-\sum_{j=0}^{N_{NC}-1} e^{\left(-\frac{\gamma N_C N_{NC}}{2N_0}\right)}\left(\frac{\gamma N_C N_{NC}}{2N_0}\right)^j \frac{1}{j!} \\ F_{nc}(\gamma,\lambda) &= 1-Q_{N_{NC}}\left(\sqrt{\frac{\lambda N_C N_{NC}}{N_0}},\sqrt{\frac{\gamma N_C N_{NC}}{N_0}}\right) \end{cases} \tag{3.11}$$

where N_0 is the noise power spectral density and $Q_{N_{NC}}(\cdot)$ is generalized Marcum Q-function of order N_{NC}. If the threshold is set too high, false alarm probability decreases, but miss detection probability increases. Therefore, the choice of a proper threshold value is very important for the whole acquisition process. The chosen threshold can be either fixed to a constant value, or it can be adapted, e.g., according to estimated Carrier-to-Noise Ratio (CNR). Also the decision stage has been studied in this thesis and some results are shown in Chapter 6.

One advantage in signal detection would be to adapt the threshold γ according to desired P_{fa}. In decision theory for known signals, in a theorem called Neyman-Pearson criterion, P_d can be maximized for a given $P_{fa}=\alpha$, when deciding $\mathcal{H}_1$ if likelihood ratio $L(\mathrm{x})$ [164]

$$L(\mathrm{x}) = \frac{p(\mathrm{x};\mathcal{H}_1)}{p(\mathrm{x};\mathcal{H}_0)} > \gamma. \tag{3.12}$$

Here, the threshold γ is found from

$$P_{fa} = \int_{\{\mathrm{x}:L(\mathrm{x})>\gamma\}} p(\mathrm{x};\mathcal{H}_0)d\mathrm{x} = \alpha. \tag{3.13}$$

This can be seen as the optimal (and simplest) detector with known signals [164]. In practice however, unknown parameters, such as the noise characteristics, exist and the Probability Density Functions (PDF) under $\mathcal{H}_0$ and $\mathcal{H}_1$ are not completely known. Therefore, the likelihood ratio test of Eq. (3.12) would offer unrealistic results as such. One common approach in this kind of situation is Generalized Likelihood Ratio Test (GLRT) detector, that utilizes Maximum Likelihood estimates for the unknown parameters [164]. Constant False Alarm Rate (CFAR) detector is a variant of GLRT with the assumption that the asymptotic PDF under $\mathcal{H}_0$ does not depend on any unknown parameters. In CFAR detector, a threshold γ to maintain a constant P_{fa} can be found [150, 151, 164].

3.1.2 Signal tracking

Once the signal is detected, the coarse estimates for the code delay and frequency offset are passed to the tracking stage, as can be seen in Fig. 3.1. Tracking can be seen as a fine synchronization process, where the main target is to improve the coarse delay and frequency offset estimates achieved in the acquisition stage and also continuously keep track on them, since they tend to change over time. Besides the code delay and the carrier frequency estimations, also carrier phase estimation is included in the tracking stage. These three tracking processes are inter-operating feedback loops. One very common feedback loop for code tracking in GNSS is Delay Lock Loop (DLL) [161]. Carrier tracking is needed, since an exact carrier signal replica is necessary for successful navigation data demodulation. Carrier tracking loops that provide a phase estimate are called Phase Lock Loops (PLL). The phase of the incoming signal may differ from the original one broadcasted by the satellite, due to various errors. Frequency Lock Loops (FLL) are similarly used for carrier frequency tracking, since also the frequency changes due to the user and the satellite movements. If the frequency changes are small, PLL may be enough [45]. The FLL and PLL can also be used together as a FLL-assisted-PLL configuration [327]. Good comparisons between various tracking structures can be found, e.g., in [37, 38, 45, 240].

3.2 GNSS related challenges at physical layer

The errors in GNSS can be divided into three main categories:

1. Satellite-based, such as clock drifts or orbital errors [39]; these are not addressed in this thesis.
2. Channel-based, which are the ones addressed in this thesis and are described in Section 3.2.1.
3. Receiver-based, such as receiver clock errors, receiver noise and antenna error; these are not addressed in this thesis.

One of the challenges for the new GNSS signals is also the new modulation type BOC or its variants, that introduce ambiguities and side lobe peaks to the envelope

of the autocorrelation function. This challenge with possible solutions is described in Section 3.2.2. In order to compensate for such errors, good acquisition and tracking algorithms are needed at the receiver. The trade-off is always between complexity or power consumption and performance. Typical performance metrics in acquisition are P_d and the mean acquisition time. Typical performance metrics in tracking are the mean, the variance and the Root Mean Square Error (RMSE) of the tracking estimate and the multipath capability of the algorithm, measured often via multipath error envelopes.

3.2.1 Channel effects

Propagation channel related errors include everything that the signal faces on its way through the wireless communication channel. The signal travels through atmosphere, whose effects are divided into ionospheric and tropospheric. Among these, ionospheric effect is frequency dependent, i.e., signals that are transmitted at different frequencies have different delays and phase advances. This fact can be utilized in dual-frequency receivers, where the first order ionospheric delay can be removed by a linear combination of the available pseudorange measurements [93]. In single-frequency approaches, some ionospheric correction models are however needed. Indeed, also tropospheric models are needed to mitigate frequency independent tropospheric delay. Besides these delays caused by the atmosphere, the GNSS signal is also affected by reflections, scattering and diffraction together with possible other interferences before reaching the receiver.

Multipath effect

Multipath is a cause of reflections of the direct Line-Of-Sight (LOS) signal, where the transmitted signal arrives at the receiver through several paths from a number of different directions. Reflections are caused by surfaces surrounding the receiver, such as trees or building walls. As a result, the received signal is a combination of several copies of the transmitted signal, with different amplitude attenuation, phases, delays and arriving angles, that can cause the receiver to calculate an incorrect position.

In the acquisition stage, multipath propagation can be seen in the correlation output as multiple incoming versions of the transmitted signal, resulting as several correl-

ation peaks in the search uncertainty area. This is illustrated also in Fig. 3.5, that shows an example of three multipaths in the correct time-frequency window. However, the delays of the multipath signals can be also so small in comparison to the actual LOS signal, that they distort the phase and the amplitude of the LOS signal leading to a compounded signal in the correlation output. This kind of deformed correlation shape may be attenuated, and thus, more difficult to detect, especially in the case of low CNR. It is also possible that the maximum correlation value of the compounded signal is delayed more than the actual LOS signal, leading to errors in the pseudorange measurements. In severe multipath scenarios like indoors or dense urban canyons, it may also be that there are only reflected NLOS signal components available, and the multipath error can be even few tens of meters [116].

Despite the fact that some multipath effects may cause challenges already in acquisition stage, multipath mitigation is typically left for the tracking process and is handled in the acquisition stage only as several correct bins [240]. Indeed, according to [91], multipath effect is not seen as severe in the acquisition process than in the tracking, since in many multipath cases the signal can still be acquired within 1 chip interval, especially in the case of closely located channel paths. Many tracking algorithms have some kind of ability to deal with with multipath scenarios, and the trade-off between different tracking algorithms is usually between performance and complexity. Some comparisons can be found in [36, 38, 206].

However, in some acquisition algorithms the presence of multipaths needs to take into account. One example is forming the decision statistic, as will be discussed more in Chapter 6. Indeed, there are some proposed methods, that try to mitigate the multipaths already in the acquisition stage. In [46], so-called Monte Carlo Markov Chain (MCMC) method for multipath identification and elimination is suggested. Differential correlation ideas to deal better with multipaths are proposed in [282] and by us in [249]. These will be presented in more details in Chapter 6.

Wideband and narrowband interference

Besides multipath propagation, also different types of interference may degrade the receiver performance. Though certain frequency bands are reserved legally protected for GNSS, radio frequency spectrum is more and more crowded and unintentional interference is possible, especially since GNSS signal powers are rather weak after

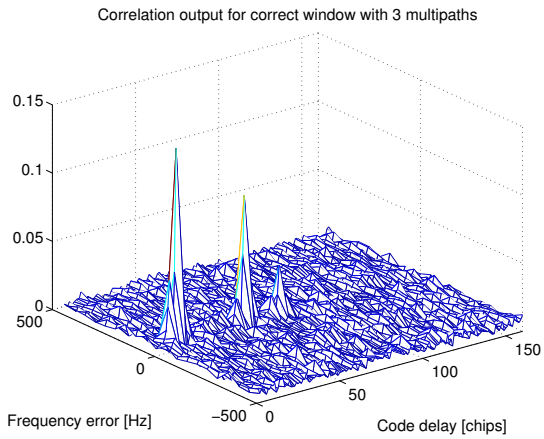

Fig. 3.5: *An example of a correlation output for a correct time-frequency window, in the presence of three multipaths.*

transmitted from great distance (20000 km). Also intentional interference, that can be divided into spoofing, meaconing and jamming, is possible [279]. While jamming is only blocking or interfering the GNSS signals from the receiver, spoofing and meaconing replace the true GNSS signals with false signals, without the receiver recognizing anything [279].

Depending on the BW of the interfering signal, unintentional interference can be either wideband or narrowband. In wideband interference, the BW of the interference BW_{int} is higher than the BW of the GNSS system BW_{GNSS} (i.e., $BW_{int} >> BW_{GNSS}$). One example of wideband interference is UWB technology with very wide BWs but low transmission powers [115, 125]. In narrowband interference, where $BW_{int} << BW_{GNSS}$, one class of disturbing signals is called Continuous Wave Interferences (CWIs). CWI includes narrowband signals that can be represented as pure sinusoids, such as Very High Frequency (VHF) and Ultra High Frequency (UHF) TV signals [41]. Another example of systems causing narrowband interference is radio-navigation aids offering support for airplanes to navigate and land. These systems, namely Distance Measuring Equipment (DME) and Tactical Air Navigation (TACAN), share the spectrum with L5 GNSS signal band, and their high-power radio pulses can severely disturb GNSS signals in the same frequency band [287]. The effect of narrowband interference on GPS has been studied, e.g., in [25, 35, 172] and on Galileo in [352, 353]. Several interference mitigation methods have been proposed in the literature, such as time-domain based blanking method [111] and

filtering methods based on convolution operations [67], or frequency-domain based zeroing technique [352] and cyclostationary approach [277]. Some interference mitigation methods are also compared in [279]. Interference mitigation remains still one of the main challenges in GNSS, especially in the new-coming Galileo, and in the case of intentional attacks [240].

In this thesis, the interference effect is also taken into account as we propose an enhanced differential correlation technique in Chapter 6. Our proposed method exploits the signal correlation in longer time intervals, and this reduces the interference effects that are coming from noise and other temporally uncorrelated sources. In CDMA systems, also multiple access interference is inherently very weakly time-correlated.

Low CNR

One very important challenge in all GNSS is also the low CNR. Typically low CNR is due to NLOS cases, especially in heavy urban areas and indoors. One possible solution is the HS-GNSS technology, that is able to obtain a position fix with weaker signals using some advanced detection algorithms. Increasing the coherent integration time would be one optimal strategy for improve the acquisition sensitivity in harsh environments, but as discussed in Section 3.1.1, coherent integration time has limitations as well. Thus, a wide variety of detection algorithms for weak signal acquisition have been proposed within the last few years. With these methods, the receiver sensitivity can be increased, but typically at the cost of complexity. Indeed, though the position estimate is possible to do with more challenging environments, the accuracy and TTFF are many times still not as good as in ideal conditions [349].

One solution studied in this thesis is different post-correlation combination algorithms, e.g., differential correlations or generalized post detection integration (GDPI) schemes [75, 207, 260] that are discussed more in Chapter 6. Since many new GNSS signals (e.g., E1 OS, E5, E6 signals of Galileo and L5, L2C, L1C signals of GPS) are composed of two channels (data and pilot), it is also possible to use channel combining acquisition to improve the sensitivity [112, 223, 308]. Other possible methods to mention are, e.g., a INS aided acquisition algorithm [213], a Block Acquisition Method [267] or a new peak finding algorithm [220].

3.2.2 Challenges related to GNSS modulation types

As mentioned in Chapter 2, in current standards the BOC modulation or its variants are introduced to be used for modernized GPS and Galileo signals. The reason for these new modulations is in their split spectrum ability, that makes interference between the signals on the same frequency band as small as possible [33]. BOC modulation was first introduced in [33], and since then, several variants are developed, such as Sine BOC (SinBOC) [33], Cosine BOC (CosBOC) [33], Alternative BOC (AltBOC) [134], Complex Double BOC (CDBOC) and Multiplexed BOC (MBOC) [133]. Many of these different variants are used (or proposed) to GNSS signals, as was shown in Table 2.1.

BOC modulation consists of modulating the chip level PRN code with a synchronized square wave subcarrier. As a result, most of the signal power heads near to the edges of the allocated frequency bands [27]. A BOC-modulated signal can be notated as BOC(f_{chip},f_{sc}), where f_{chip} is the chip rate in MHz and f_{sc} is the subcarrier frequency in MHz [33]. More common notation is however BOC(m_B,n_B), where m_B and n_B represent two indices computed from f_{chip} and f_{sc}, respectively, with respect to a reference frequency 1.023 MHz: $m_B = \frac{f_{chip}}{1.023MHz}$ and $n_B = \frac{f_{sc}}{1.023MHz}$. The BOC modulation order N_{BOC} is a positive integer showing the ratio $N_{BOC} = 2 \times \frac{m}{n} = 2 \times \frac{f_{sc}}{f_{chip}}$ [205]. Thus, e.g., $N_{BOC} = 2$ would represent, e.g., BOC(1,1) and BOC(2,2) and $N_{BOC} = 12$ would represent, e.g., BOC(15,2.5). The BPSK modulation is a special case of the BOC modulation with $N_{BOC} = 1$ [205].

The SinBOC subcarrier as a modulating waveform $s(t)$ (see Eq. (3.3)) is defined as [33, 240]:

$$s_{SinBOC}(t) = sign\left(sin\left(\frac{N_{BOC}\pi t}{T_c}\right)\right), 0 \leq t \leq T_c \tag{3.14}$$

where $sign(\cdot)$ is the signum operator. Similarly, the CosBOC subcarrier is expressed as

$$s_{CosBOC}(t) = sign\left(cos\left(\frac{N_{BOC}\pi t}{T_c}\right)\right), 0 \leq t \leq T_c. \tag{3.15}$$

Since $s_{SinBOC}(t)$ and $s_{CosBOC}(t)$ are sequences of -1 and $+1$, Eqs. (3.15) and (3.14) can be formed also as [205, 240]

$$s_{SinBOC}(t) = p_{T_B}(t) \circledast \sum_{i=0}^{N_{BOC}-1} (-1)^i \delta\left(t - i\frac{T_c}{N_{BOC}}\right) \tag{3.16}$$

and

$$s_{CosBOC}(t) = p_{T_B}(t) \circledast \sum_{j=0}^{1} \sum_{i=0}^{N_{BOC}-1} (-1)^{i+j} \delta\left(t - i\frac{T_c}{N_{BOC}} - j\frac{T_c}{2N_{BOC}}\right) \tag{3.17}$$

Further on, by combining Eq. (3.3) with Eqs. (3.16)-(3.17), the transmitted BOC modulated signal can be denoted as

$$x_{BOC}(t) = \begin{cases} p_{T_B}(t) \circledast \sum_{n=-\infty}^{\infty} \sum_{j=1}^{S_F} \sum_{i=0}^{N_{BOC}-1} \sqrt{E_b}(-1)^i b_{data}(n) \times \\ \qquad c_{j,n}\,\delta\left(t - nT_{sym} - jT_c - i\frac{T_c}{N_{BOC}}\right) \quad \text{for SinBOC} \\ p_{T_B}(t) \circledast \sum_{n=-\infty}^{\infty} \sum_{j=1}^{S_F} \sum_{i=0}^{N_{BOC}-1} \sum_{j=0}^{1} \sqrt{E_b}(-1)^{i+j} b_{data}(n) \times \\ \qquad c_{j,n}\,\delta\left(t - nT_{sym} - jT_c - i\frac{T_c}{N_{BOC}} - j\frac{T_c}{2N_{BOC}}\right) \quad \text{for CosBOC} \end{cases} \tag{3.18}$$

Since in the studies for this thesis the focus was on SinBOC(1,1) modulation, the other BOC waveforms are not presented here in details. Waveforms for other variants of BOC-modulation can be found in [133, 134, 205, 240].

Besides the ability to split the spectrum and decrease the interference within the signals operating at the same frequency band, another benefit of BOC modulation is the sharp shape of the main correlation peak enabling tracking with high accuracy [34]. The main challenge introduced by the BOC-modulated signals is however to deal with the ambiguities and side lobe peaks in the envelope of the ACF when compared to BPSK-modulated signal. This is illustrated in Fig. 3.6, that shows an ideal non-coherent squared ACF for BPSK, SinBOC(1,1) and CosBOC(15,2.5) modulated signals. These side lobe peaks will affect both acquisition process and tracking process. In signal acquisition, the time-bin step Δt_{bin} and other relevant parameters have to be chosen more carefully in order to be able to detect the signal. In tracking, the side lobe peaks may result as false lock points, and thus, cause inaccuracies in the delay estimation.

One way to handle narrower main peak and the side peaks in the acquisition function is to decrease the length of the search step in time domain, i.e., time-bin length Δt_{bin}. In order to be able to detect the main peak correctly, Δt_{bin} has to be smaller than $0.5\times$ the width of the main peak, preferably even smaller. Since the width is dependent on the BOC modulation order, as can be seen also in Fig. 3.6, the

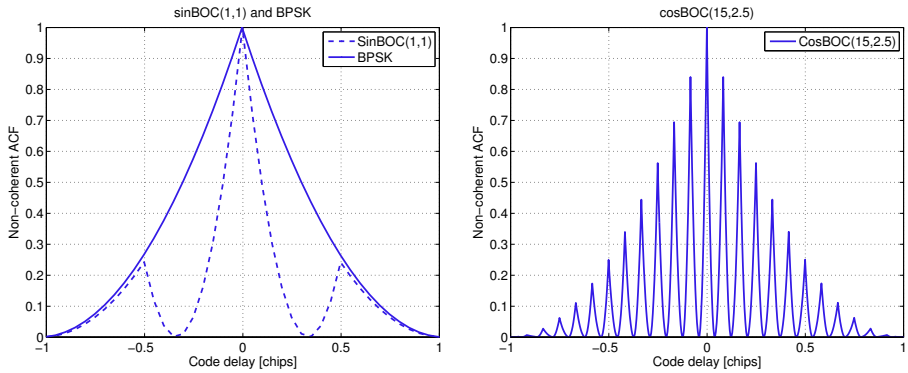

(a) ***(b)***

Fig. 3.6: *Ideal non-coherent squared ACF for (a) SinBOC(1,1) and BPSK, and (b) CosBOC(15,2.5) modulated signal.*

search process can become very time consuming task for higher BOC modulation orders. Therefore, other solutions have been searched for faster acquisition and to deal with the side lobe peaks. Some proposed methods methods, typically called as unambiguous acquisition methods, are the following: Betz and Fishman (B&F) algorithm [27, 32, 108], modified B&F algorithm [203], Martin and Heiries (M&H) algorithm [136, 137, 222], modified M&H algorithm [203] and Unsuppressed Adjacent Lobes (UAL) algorithm [203]. In all of these, the primary goal is to shape the ACF into BPSK-like form by removing the side lobe peaks within 1 chip interval from the maximum correlation peak [240]. In the original B&F method, the spectral sidebands are handled individually via filtering. If single sideband (SSB) processing is used, only one of the main lobes is processed, but due to possible integration losses [108], usually dual sideband (DSB) processing is chosen instead. In DSB, both sidebands are kept, processed separately and added non-coherently. B&F method is the most typical method in the current GNSS literature [240], and used also in this thesis (see Chapter 6). In M&H algorithm, both main lobes and possible lobes between them are selected and correlated with shifted version of the PRN reference code. However, it is noticed that M&H method is unable to work correctly with odd N_{BOC} orders [49,50,203]. Both modified B&F and modified M&H algorithms temp to decrease the correlation complexity and reduce the number of used filters [203]. The same holds for UAL, where the filtering part is removed totally to decrease the complexity, but at the cost of slightly reduced performance [203, 240]. Fig. 3.7 shows the effect of B&F and M&H methods for the ACF envelope, in the case of SinBOC(1,1)

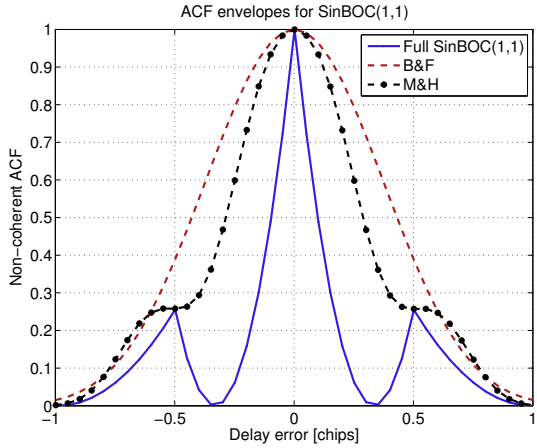

Fig. 3.7: *Normalized ACF envelopes for SinBOC(1,1) modulation, with B&F and M&H unambiguous methods.*

modulation. It can be seen, that the side lobe peaks are cancelled and higher Δt_{bin} can be used, if some unambiguous method is used. In this thesis, unambiguous methods are considered together with differential correlations in Chapter 6.

In tracking accuracy point of view, there is however one drawback in the unambiguous methods, namely in the width of the main correlation peak. In the ambiguous BPSK modulated signal, the sharp main peak would allow very precise delay estimation in tracking function, but after unambiguous methods, the main peak is as wide as with BPSK modulation. One solution for this is to remove the side lobe peaks, but still keep the main correlation peak untouched. There are few variations of these type of methods, such as Sub-Carrier Phase Cancellation (SCPC) method [136] and Sidelobe Cancellation Method (SCM) [48, 50, 51].

3.3 Conclusions

In the first part of this chapter, a closer look to GNSS receiver fundamentals has been taken, concentrating on baseband processing and especially on signal acquisition part. This part of the chapter has provided a compact overview of acquisition function and its main tasks. In the second part, the possible error sources and challenges in GNSS have been listed and discussed, to form a survey that will be completed with solution proposals in Chapters 5 and 6.

4. RSS-BASED POSITIONING APPROACHES - SYSTEM OVERVIEW AND CHALLENGES

As described in Chapter 2, there are several possible positioning technologies based on cellular and WLAN networks. One possibility is to utilize time delays to determine the distance between transmitter and receiver. Time delay -based techniques, such as TOA, RTT or OTDOA, however require very exact clocks and also fine synchronization in the network, in order to be able to estimate the propagation delays with high precision. Since the current network generations do not fulfill these requirements, expensive investments would be needed to the network structures. Therefore, other positioning techniques are preferred. Another challenge is the amount of different modulation and MA technologies, that may vary a lot in different networks and also between the transmitters in the same network, that is the case especially with WLAN transmitters. Besides time delays, the distance between transmitter and receiver can be estimated using RSS or RSS Indicator (RSSI). Many communication networks monitor the network status automatically using RSS measurements. The measurements define the signal quality, that is important in order to be able to make, e.g., handover decisions in cellular networks. Since the RSS measurements are easily available and due to their accessibility in Application Programming Interfaces (API) of many networks, they offer a very attractive and economical alternative for positioning.

Many different approaches for RSS-based localization have been presented in the literature, such as fingerprinting [16, 23, 157, 174, 193, 228, 230, 238, 265, 275, 303, 313, 315, 322, 328, 334], triangulation approaches [241, 291], weighted centroid -based [40, 88, 200, 304, 326] or clustering approaches [60, 63, 76, 143, 175, 232, 269, 344]. While about half of the work in this thesis has been focusing on improving the GNSS receiver design, the other half concentrates on improving RSS-based positioning algorithms. The focus has been on FP, PL and WeiC methods, that are the three most widespread approaches, but also clustering is shortly introduced in this

chapter. After the fundamentals of different RSS-based positioning approaches have been described, this chapter continues with discussion concerning the challenges.

4.1 Fundamentals of RSS-based localization

4.1.1 Training phase and database structure

RSS-based positioning approaches have typically two stages: an initial off-line training or learning phase, where the data is collected and models and databases are created, and an online estimation phase, where the actual position calculation is performed [99, 225, 344]. An alternative is to use some method that does not require training phase, e.g., SLAM method presented in [14, 24, 89], but in this thesis, we concentrate on the two-phase positioning approaches.

Typically, the radiomap target area is divided into a grid, where each grid point contains coordinates together with the actual data. The radiomap grid can be created with either uniform grid resolution [167, 238, 292, 323] or non-uniform grid resolution [124, 127, 139]. The uniform grid resolution means that all grid points have the same regular size, usually a square box a m $\times$ a m, with $a = 1, 5, 10$, etc. If the grid is non-uniform, the grid point locations can be adjusted, e.g., according to the building floor plan or according to the distance from the grid points to the transmitter, as proposed in [127]. Since the building floor plans and transmitter locations are however often unavailable, non-uniform grids would be difficult to utilize efficiently. For this reason together with the fact that uniform grids are many times simpler to implement in the database and in some of the positioning algorithms as well, only uniform grids are considered in this thesis. Grid size effect is discussed more in Section 4.2 and Chapter 9.

In this thesis, x_i, y_i, z_i are the 3D coordinates of the grid point i ($i = 1, ..., N_{fp}$), N_{fp} represents the total number of grid points (or fingerprints (FPs), as they are called for now on in this thesis), and the measured RSS of the kth transmitter in the ith FP is denoted by $P_{i,k}$. Thus, the data in FP i can be formed as

$$\left\{ x_i, y_i, z_i, \{k, P_{i,k}\} \right\}, k \in 1 : N_{TX}, i \in 1 : N_{fp}, \tag{4.1}$$

where N_{TX} is the total number of transmitters (or APs in the WLAN case) in the database. We remark that also the indexes (here, k) are needed together with the RSS

values for each transmitter, since pure RSS value does not indicate the transmitter it comes from. We also remark that the number of heard transmitters in each FP may vary.

Parameter estimation

Radiomap database can be used in the localization phase as such, or it can be used to estimate the required parameters for other positioning approaches than FP, such as PL or WeiC (see Section 4.1.2). Typically, the needed parameters are transmitter-related. Thus, it makes sense to organize the needed database also in transmitter-based order, where all FPs where the particular transmitter k is heard and corresponding RSS are included in a form of

$$\left\{x_{j,k}, y_{j,k}, z_{j,k}, P_{j,k}\right\}, j = 1 : N_{fp(k)}, k \in 1 : N_{TX}. \tag{4.2}$$

Here, $N_{fp(k)}$ is the number of FPs, where the transmitter k is detected.

One of the most common PL model is the one-slope log-distance model [21,128,155, 241,335], where the observed RSS for transmitter k in fingerprint i is

$$P_{i,k} = P_{T_k} - 10\, n_k\, log_{10}\, d_{i,k} + \eta_{i,k}. \tag{4.3}$$

Here, n_k stands for the PL exponent and P_{T_k} is the apparent transmit power for the kth transmitter, that are also the two unknown PL parameters together with the transmitter location $(x_{TX_k}, y_{TX_k}, z_{TX_k})$. $\eta_{i,k}$ is a noise factor with Gaussian distribution, standard deviation (std) σ_k and zero mean. $\eta_{i,k}$ is assumed to include not only measurement noise, but also shadowing or other random RSS fluctuations. Indeed, $d_{i,k}$ denotes the range between the estimated location of kth transmitter $(\hat{x}_{TX_k}, \hat{y}_{TX_k}, \hat{z}_{TX_k})$ and the ith FP

$$d_{i,k} = \sqrt{(x_i - \hat{x}_{TX_k})^2 + (y_i - \hat{y}_{TX_k})^2 + (z_i - \hat{z}_{TX_k})^2}. \tag{4.4}$$

Naturally, one-slope log-distance model may not be as accurate as multi-slope models to form the signal propagation and RSS variations. Due to the walls and other obstacles that affect the propagation path especially in indoor situations, the propagation parameters may change a lot even in relatively short distance. The parameters may also be different for different directions from the transmitter, and for different floors, due to floor losses. Multi-slope PL models have been proposed, e.g.,

in [55, 291, 355]. The advantage of one-slope log-distance model is however in the low number of parameters to be estimated. Since the type of the propagation environment may vary and many parameters are not known beforehand, it is important that the number of estimated parameters is kept as minimum. Therefore, the one-slope log-distance model is considered also in this thesis.

In matrix form, the one-slope PL model for kth transmitter can be presented as [291]

$$\mathbf{P_k} = \mathbf{H_k}\,\Theta_\mathbf{k}^\mathbf{T} + \mathbf{n}. \tag{4.5}$$

Above, $\mathbf{n}$ is a Gaussian distributed noise vector of size $N_{fp(k)} \times 1$. Θ_k includes the unknown PL parameters for kth transmitter excluding the coordinates (i.e., $\Theta_k = [n_k\, P_{T_k}]$), $\mathbf{P_k}$ contains RSSs for kth transmitter (i.e., $\mathbf{P_k} = [P_{1,k}\, P_{2,k} \ldots P_{N_{fp(k)},k}]$), $\mathbf{T}$ is transpose operator, and

$$\mathbf{H_k} = \begin{bmatrix} 1 & -10log_{10}d_{1,k} \\ & \ldots \\ 1 & -10log_{10}d_{N_{fp(k)},k} \end{bmatrix}. \tag{4.6}$$

Now, Eq. (4.6) is possible to be solved by linear regression [164] or by using classical deconvolution approaches, for example Least Squares (LS) [291, 309]. Further on, transmitter positions can be estimated, e.g., through brute-force approach [70], or by weighted centroid based techniques, as presented in [31]. Another possibility is to use deconvolution-based approach, where all unknown parameters (i.e., n_{TX}, $P_{T_{TX}}$, $\mathbf{x_{TX}}$) are estimated jointly [291, 309]. Here, $\mathbf{x_{TX_k}}$ represents the transmitter location $(x_{TX_k}, y_{TX_k}, z_{TX_k})$ in vector form.

4.1.2 Localization phase

Many different positioning methods can be employed in the localization phase. The most known ones are over-viewed in what follows.

Conventional fingerprinting

Fingerprinting is based on the assumption that each position has a unique RSS signature, where certain transmitters are heard with certain RSS levels. This unique RSS signature is used in the positioning, where the RSSs (or other location-dependent parameter, equivalently) measured by the receiver is compared to the measurements

Table 4.1: *Typical metrics in fingerprinting.*

Metric	Formula	References
Euclidean	$\frac{1}{2}\big(\sum_{z=1}^{N_z} \|\|O_z - P_{i,z}\|\|^2\big)^{\frac{1}{2}}$	[23, 265, 303, 328]
Square of Euclidean (Spearman distance)	$\sum_{z=1}^{N_z} \|\|O_z - P_{i,z}\|\|^2$	[72, 216]
Manhattan distance	$\sum_{z=1}^{N_z} \|\|O_z - P_{i,z}\|\|$	[139, 156, 303]
Mahalanobis distance	$\sqrt{(O_z - P_{i,z})^T \sum^{-1} (O_z - P_{i,z})}$	[139, 156, 303]
Logarithmic Gaussian likelihood	$\sum_{z=1}^{N_z} \log\left(\frac{1}{\sqrt{2\pi\sigma_z^2}} e^{\left(-\frac{(O_z - P_{i,z})^2}{2\sigma_z^2}\right)}\right)$	[124, 139, 303, 358] [76, 79, 120]
Number of commonly heard transmitters	N_z	[216]

in the training database. Among all the FPs in the training data, the best match is searched and the coordinates of the best-match-fingerprint are returned as the estimated location of the receiver. Therefore, fingerprinting is also called pattern matching [303] or map matching technique. Fingerprinting based user positioning can be either distance-based or probabilistic approach [139, 276, 303]. Probabilistic fingerprinting is studied, e.g., in [16, 121, 124, 176, 230, 275, 303, 344]. Some typical metrics are presented in Table 4.1. Other possible metrics can be found, e.g., in [139, 216, 303], and a comprehensive analysis of various distance and similarity measures is presented in [315].

In the equations in Table 4.1, observed RSS levels by the user is denoted with O_z (i.e., $O = [O_1\, O_2 \ldots O_{N_z}]$ dBm, the range for O_z is typically between -100 dBm and 0 dBm), and N_z is the number of commonly heard transmitters in the FP and in the user measurement. Since the number of heard transmitters is changing from one FP to another, one possible metric is to take into account in the comparison the number of commonly heard transmitters. Also combinations of the metrics shown in Table 4.1 are possible, e.g., the number of commonly heard transmitters and Euclidean.

The positioning approach, where the user location is estimated as the location of the best-match-FP, is called Nearest Neighbor (NN) method [23, 275, 276]. It is also possible to choose several FPs with smallest values of distance metric S; a method called K Nearest Neighbor (KNN) [22, 23, 66, 121, 122, 158, 184, 228, 238, 258, 265, 313, 315, 328], where the estimated receiver location $[\hat{x}_{MS}, \hat{y}_{MS}, \hat{z}_{MS}]$ is computed as an average over the locations of the chosen K FPs

$$[\hat{x}_{MS}, \hat{y}_{MS}, \hat{z}_{MS}] = \frac{1}{K}\left(\left[\sum_{n=1}^{K}\tilde{x}_n\,,\ \sum_{n=1}^{K}\tilde{y}_n\,,\ \sum_{n=1}^{K}\tilde{z}_n\right]\right). \tag{4.7}$$

Here, $[\tilde{x}, \tilde{y}, \tilde{z}]$ represents the group of K FPs, that are chosen to be the best matches among all FPs according to the current metric. The assumption in KNN is that by using averaging a position estimate is probably closer to the user's true location than any individual neighbor. In Weighted KNN (WKNN) method, averaging is similar to KNN method, but also weighting factor is included [238].

Path-loss based positioning

Since the training stage in PL approaches includes the calculation of the transmitter position and the PL parameter estimates $\hat{n}_{TX}$ and $\hat{P}_{T_{TX}}$, in the estimation phase the receiver location is computed using only these obtained parameters and the observed RSS. One way to do this is to use standard trilateration method [97, 219, 338], where the receiver location is estimated based on the distance to the transmitter locations. This distance r_k can be solved from the one-slope path loss model of Eq. (4.3) for kth transmitter as

$$r_k = 10^{\frac{\hat{P}_{T_k} - O_k}{10\hat{n}_k}}. \tag{4.8}$$

Since the transmitter positions are also estimated and if the distance r can be obtained for at least three transmitter, the receiver location can further be calculated using non-linear LS methods. Another way to calculate the user position is to utilize the PL models to re-create the original FP data by estimating the RSS for each transmitter in every fingerprint. Further on, the user position can be estimated equivalently as in conventional FP approach. The advantage of this method is that the FP database does not have to be saved and transmitted, since it can be easily regenerated based on the PL parameters.

Weighted centroid based positioning

In the WeiC-based positioning, the user position is estimated as a weighted average over the locations of the heard transmitters (e.g., APs), with certain weighting factors [40, 88, 200, 208, 304, 326]. Since the aim is to give more weight to those transmitters which are closer to the unknown receiver location, the measured RSS by the receiver can be here selected as an appropriate quantifier. Thus, all that is needed in the estimation phase is the observed RSS O_k and the estimated transmitter positions $(\hat{x}_{TX_k}, \hat{y}_{TX_k}, \hat{z}_{TX_k})$ for the kth transmitter, that are computed in the training phase. The user position (x_{MS}, y_{MS}, z_{MS}) is marked as $\mathbf{x_{MS}}$ in vector form, and is calculated as

$$\mathbf{x_{MS}} = \sum_{k=1}^{N_h} w_k \, \hat{\mathbf{x}}_{\mathbf{TX_k}} \tag{4.9}$$

Here, N_h is the number of heard transmitters and w_k is the weighting factor, that is calculated in this thesis as

$$w_k = \frac{10^{\frac{O_k}{10}}}{\sum_{k=1}^{N_h} 10^{\frac{O_k}{10}}}. \tag{4.10}$$

In other words, the weights are just the RSS measurements obtained by the receiver in linear scale. Obviously, several variants for defining the weights can be found in the literature, e.g., based on the inverse of the estimated distance between the transmitter and the receiver [304]. Other possible weighting variants can be found also in [190, 221].

Clustering

Clustering is a modification of the conventional fingerprinting, where the main point is to try to reduce the amount of data to be transferred between the database server and the receiver and to minimize the databases to be saved in the receiver by choosing only a subset of all available data in the positioning phase. Clustering can be performed either based on the the coordinates (also called 3D clustering [76]), as studied in [60, 214, 269, 364], or based on the RSS vectors, as studied in [86, 142, 280, 344]. 3D clustering can be performed, e.g., by using well-known K-means with Euclidean distances and a predetermined number of clusters [19, 76]. Hence, for some particular set of FP coordinates $\mathbf{x}$ and clusters $\mathbf{c}$, K-means clustering algorithm attempts to

divide M vectors $\{\mathbf{x_1}, \ldots \mathbf{x_i}\}$ into $M_c < M$ clusters c by minimizing the within-cluster sum of squares [76, 269]:

$$\sum_{d=1}^{M_c} \sum_{\mathbf{x} \in c_d} ||\mathbf{x_i} - \mu_d||^2 \tag{4.11}$$

Here, c_d represents the dth cluster and μ_d is the mean of the points in the cluster c_d. Further on, only the FPs that belong to the chosen clusters (e.g., the closest ones according to the initial positioning estimate [76]) will be used in the positioning, e.g., using KNN. Several novel clustering methods have been proposed within the last few years, and e.g., in [63, 142] the authors suggest a clustering based on AP similarity. Clustering can also be used in floor detection, as proposed in [269].

4.2 Physical layer challenges in RSS-based cellular and WLAN-positioning

While the most encountered challenges in GNSS include especially NLOS and multipath propagation, the challenges for WLAN and cellular positioning are somewhat different, as it was shown in Table 2.6. Since the work in this thesis has focused on the RSS-based localization, the challenges regarding the methods that are based on RSS data, are of utmost interest. The main difference in WLAN and cellular RSS-based approaches is in the number of heard transmitters. In WLAN, basically all near-by APs are considered and the RSS is measured for every heard AP, resulting even tens of APs in each scan. In cellular networks, the process is different, and RSS measurements are not necessarily performed for all neighboring BSs. This happens, e.g., if the RSS from the serving BS is very good.

Fig. 4.1 presents the challenges related to certain stages (positioning architecture design, training phase, data transferring and estimation phase) in the RSS-based positioning, together with the corresponding solutions. The solutions for challenges in stages B and C have to be often treated jointly, since for example the choice of grid interval affects both the database forming and the data transferring. In this section, we go through the main challenges in RSS-based localization system. The structure of Fig. 4.1 is followed in the upcoming chapters, where the proposed solutions to the challenges are presented in detail.

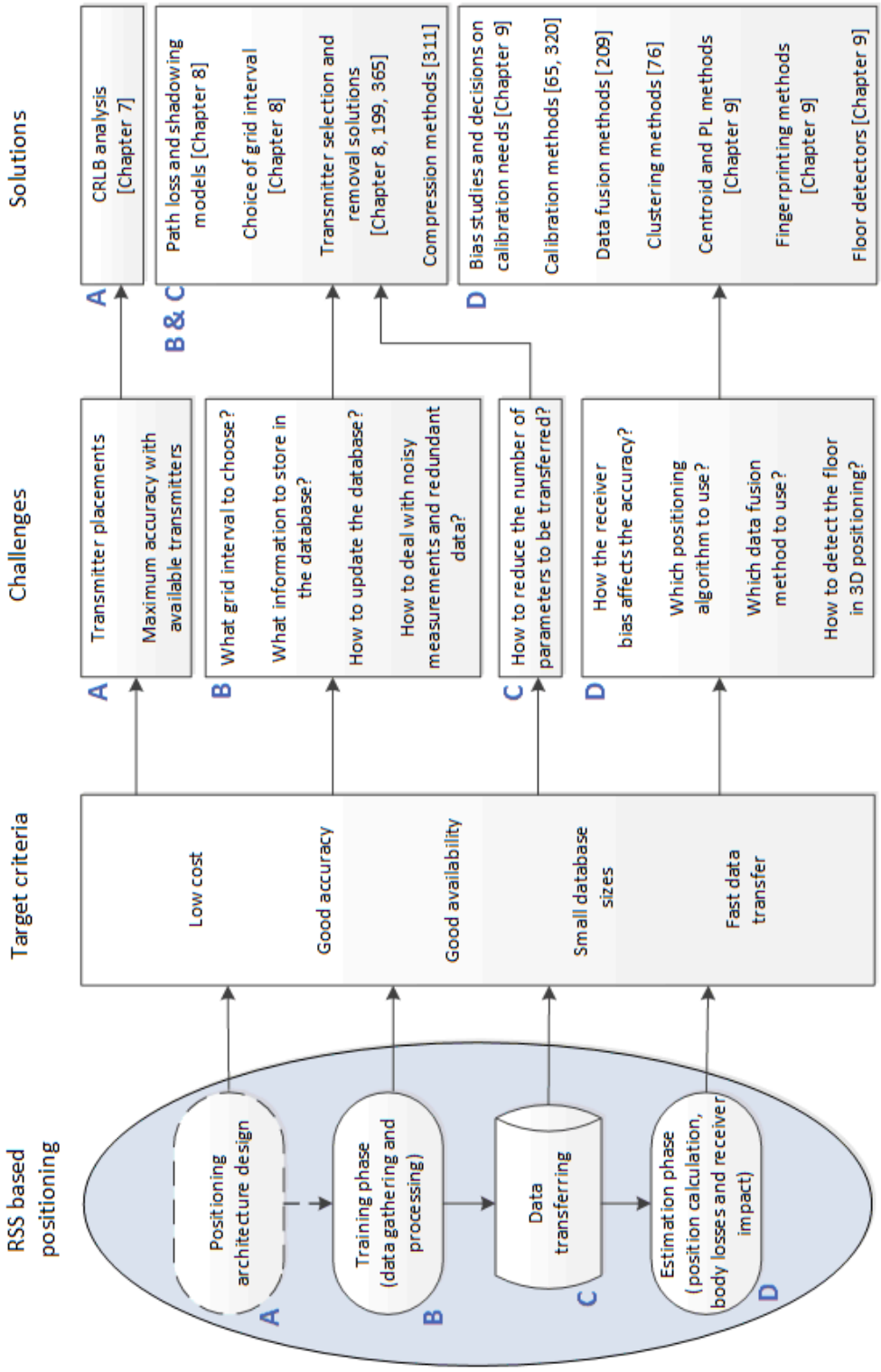

Fig. 4.1: *Challenges and solutions in RSS-based positioning.*

4.2.1 Challenges related to the positioning architecture design

One possible challenge or error source in any positioning system using existing networks is the network infrastructure. Both in cellular and WLAN networks, the transmitters are placed according to communication needs. Therefore, the existing transmitter configuration may not be suitable for positioning purposes at all. This challenge is considered more in Chapter 8, where we present a criterion to estimate the expected accuracy bound in WLAN networks with certain topology.

4.2.2 Challenges related to the training phase and data transfer

In two-stage positioning approaches, the first stage covers the measurement gathering process, and possibly also forming the models, if path loss models or other signal-to-distance mapping based methods are used. The data samples to the training radiomap can be collected either beforehand as manual data collection, or continuously using crowd-sourcing [60, 94, 143, 160, 226, 238, 337, 360, 361]. In manual data collection, the main challenge is how to maintain the fresh database. One solution is to repeat the collection process continuously, but this is usually too expensive and time-consuming. Regardless of the chosen data collection method, one challenge in data collection is that the measurement collection process can result as incomplete, where more measurements are gathered from one part of the town or building, while another part remains partly or totally uncovered [310]. The reason for these coverage gaps in the radiomap can be that the people collecting the measurements are not allowed to enter some parts of the building (e.g., personal offices etc.), or that the measurements are collected only with a car, leaving pedestrian streets uncovered. Naturally, coverage gaps affect the localization performance [310].

Another challenge in the data collection is caused by the uncontrolled measurement collection, that can easily lead to errors in the database. One possible situation is that the location for a collected data sample is incorrect for some reason (e.g., due to the incorrect coordinates offered by a reference system, or due to human mistakes), resulting as an outlier in the radiomap. In outdoor environments for cellular networks, GNSS location can be utilized as a reference location in the data collection process, but in indoor cases, some other methods are needed. Same holds for urban canyons, where GNSS location estimates may be erroneous. It should be remarked that in two-stage positioning approaches, the accuracy of the data sample locations in the training

radiomap plays an important role, since the inaccuracies affect directly the positioning performance of the location approach to be used. Since the reference position is not an easy task to achieve indoors, especially in crowd-sourced mode, the measurement collection process often becomes very complex. One solution is to collect the data and insert the reference locations for each measurement point manually, using indoor maps installed in the collection device. This is however quite exhausting process, and rarely possible for crowd-sourcing based solutions. Another possibility is passive crowd-sourcing, where the collection is performed using inertial sensors. In this case, some control is still needed to find the outliers and to observe the data quality, especially because the positioning error tends to cumulate in pure sensor-based positioning [84, 289].

Besides the possible error sources caused by data collection, many important questions are also related to the database structures and updates. Two examples are the grid density and the resolution type (uniform or non-uniform). Naturally, the grid density affects the number of FPs in the radiomap, but when the FP area increases, also the number of saved transmitters for each FP increases. Indeed, when the grid interval increases, the positioning accuracy may be decreased. The grid size impact is discussed more in Chapter 9. In the radiomap grid, the location information for each grid point (or FP) is typically defined as the center coordinates instead of the real position of the collected data sample [232]. Thus, all gathered measurements in the synthetic or server-defined grid point area belong to the same FP. Several measurements can be collected in exactly the same location, as it is the case, e.g., with crowd-sourcing. Hence, the questions related to database updates need to be taken into account also in the collection phase, when a data sample is collected in a FP that already has a saved sample. Also the questions related to FP data updates are discussed more in Chapter 9.

When thinking of indoor positioning and of an average size office building with several floors and plenty of offices, or a multifloor shopping mall with tens of small stores and boutiques, it is clear that the transmitter infrastructure can be very dense. A huge number of transmitters, e.g., APs, naturally means a lot of transmitters to be detected in each measurement scan (i.e., in the training phase), leading into a huge amount of data to be handled and transferred. Thus, one addressed challenge in this thesis is how such huge amount of data can be reduced. In the two-stage positioning approaches, the pre-collected RSS radiomap database can be used in many

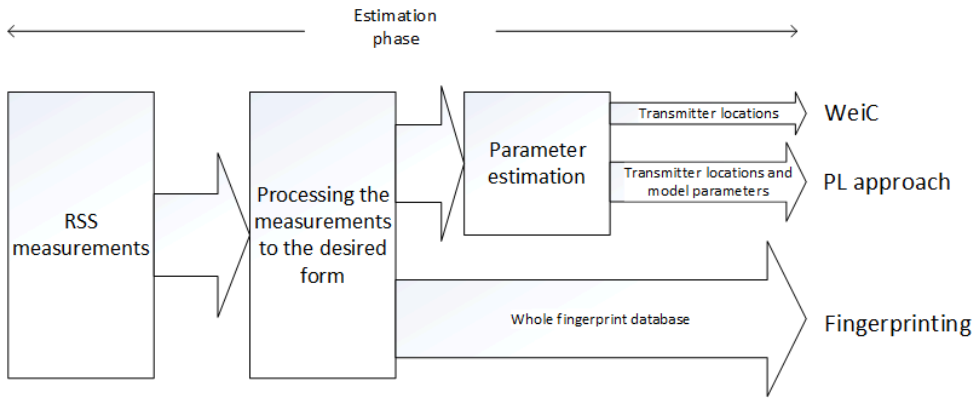

Fig. 4.2: *A simplified illustration of the database use for three positioning methods, when the transmitter locations are unknown. Arrow thickness represents the amount of data to be transferred.*

different ways. In fingerprinting, where the positioning estimate is calculated using some pattern matching algorithm, the whole database is needed in the positioning phase [174, 322, 334]. One way to reduce the amount of transmitted data is to use some other positioning methods, that do not necessarily need the whole radiomap in the positioning phase, but use it only to estimate certain parameters or models needed in the position calculation, as was discussed in Section 4.1. These kind of methods are the PL based positioning, that utilizes the radiomap information to estimate PL models [241, 291], or the WeiC method, that requires only transmitter locations in the localization phase [40, 88, 200]. This is also illustrated in Fig. 4.2, that shows the block diagram for database use for FP, PL and WeiC methods, when the transmitter locations are unknown. We remark that if the transmitter locations are known, WeiC method does not need the whole database at all. The three methods are further compared and analyzed in Chapter 10.

Though the amount of data needed to be transferred is clearly less for some other methods, it should be noticed, that in two-stage positioning approaches with training database, all methods need the radiomap in a way or another - either they utilize directly the collected fingerprints or use the fingerprints to estimate models and/or parameters to be used in the positioning phase. Thus, the memory requirements are the same for every method, at least in the training phase. Data removal solutions can help in this, by reducing the unnecessary data to be stored. Data removal solutions naturally also decrease the amount of transmitted data, but serve more in the

FP method, where the whole database needs to be transferred, than in PL or WeiC methods.

Besides the memory and data transmission requirements, the dense transmitter network may also cause other challenges. When a mobile hears tens of transmitters in one RSS measurement, it is clear that some of the heard transmitters are more important than others from the positioning point of view. As it was noticed, e.g. in [342] and in our results in [182], too many transmitters in the positioning calculation may even decrease the positioning accuracy. While the primary goal for the WLAN network is still in communications to guarantee the coverage and to efficiently serve plenty of users at the same time, the system infrastructure may have several APs physically in the same location or very close to each others. Indeed, since the APs are usually separated only by their MAC-addresses, the special WLAN transmitters that support multiple BSSIDs will also be seen as several transmitters in an exactly same location. Since these kind of APs and also other closely located ones surely transfer at least partly correlated data, not all of these are needed in the positioning calculation. The unnecessary and redundant data can be seen as noise, that increases the complexity of the localization process [100, 177]. The challenge of large databases and unnecessary data together with possible solutions is studied extensively in Chapter 9.

Another challenge in any RSS-based positioning method comes from the RSS fluctuations, caused e.g. by shadowing. In many existing PL propagation models, shadowing is included in the models, but the fluctuations affect in every method. RSS values may variate due to many reasons, such as device placement, user orientation and body shape. The observed RSS is different, if the device is hold in hand, when compared to the case where the device is in a pocket or backpack, or stands still in a table. The RSS fluctuations may also be caused by the changes in the environment, especially indoors, e.g. when people are passing by, or doors are opened and closed [64]. The LOS is easily disturbed, when the user turns and blocks the LOS connection with his/her body. In general, signal shadowing is very difficult to model accurately indoors not only due to the changes in the environment, but also because of multipaths, reflections and scattering. The situation is better outdoors, especially in rural areas with more LOS situations, but dense city centres with high buildings are almost as challenging than indoor cases.

Due to the RSS variations, the measurement collection process in the training phase has to be carefully planned. If the data samples are collected in the absence of other

people in the building, the RSS values may not be realistic. For the same reason, several measurement samples should be collected for every fingerprint. Since basically everything affects the RSS, one sample in each location is not enough. Thus, despite of the possible uncertainties, continuous crowd-sourcing is a very good option to obtain realistic data measurements. Channel effects are studied in more detail in Chapter 9.

4.2.3 Challenges related to the estimation phase

One of the main challenges in the estimation phase is that the device used in the data gathering may be different than the device used in the positioning phase. The main parameters in the radiomap FPs are RSS/RSSI values and transmitter (e.g., AP or BS) detection. Since the chipsets on the devices are different, the value of observed RSS in the same location may vary between different devices, resulting as RSS biases. These problems lead to the use of complex calibration or mitigation methods [87, 92, 124, 216, 254, 325], in order to compensate the effect of more or less constant RSS variations to the positioning accuracy. The offset can be also partial, meaning that one device is used for the data collection in one part of the building, but some other device is used for the rest of the building. Fig. 4.3 illustrates this effect showing the relation between RSS values in dB and RSSI for three different chipsets (Atheros, Symbol, Cisco) [26]. As it can be seen in this figure, both the RSS scale and the steps differ between the chipset manufacturers remarkably. Different offsets due to lack of calibration are studied extensively by us in [183] and in Chapter 10.

Another challenge in the estimation phase is the choice of an appropriate positioning algorithm and the questions of how to detect the floor in indoor positioning. Different methods require different amount of data to be transferred to the receiver, but on the other hand, the accuracy is still the key question, and low-complexity methods with decreased data transferring needs do not necessarily offer as good performance as the more complex algorithms. The challenges and solutions related to positioning algorithms and floor detectors are discussed more in Chapter 10.

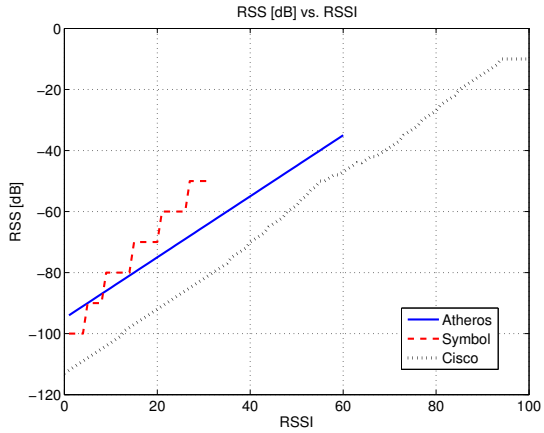

Fig. 4.3: *An illustrative example for the relation between RSS values (in dB) and RSSI for three different chipsets.*

4.3 Conclusions

In this chapter, the fundamentals of two-stage RSS-based localization approaches have been first described, concentrating on the most widespread methods (fingerprinting, path loss and weighted centroid). Secondly, this chapter has included an extensive overview of the typical physical layer challenges in RSS-based positioning. The discussion related to challenges will be completed with solution proposals in Chapters 8, 9 and 10.

5. PROPOSED SOLUTIONS FOR GNSS CHANNEL MODELING

As stated in Chapter 3, one of the biggest challenges for GNSS is indoors. The solutions to address this challenge can be divided into

- Indoor propagation modeling for GNSS signals. This challenge is taken into account in this chapter by proposing indoor fading channel models for GPS-like signals, based on indoor measurements. The results are also published by us in [152].
- Improved integration schemes at the receiver side, such as HS-GNSS. This challenge is studied more in Chapter 6.

A related challenge to the GNSS channel effects is how to build suitable channel simulators for wireless GNSS channel to be used further to develop acquisition and tracking algorithms in different environments. A simple and efficient simulator for Nakagami-*m* distributed fading channels is presented in this chapter, and the results are also published by us in [250].

5.1 Indoor fading distributions for GPS signals

Indoor channel models are one important part of learning the GNSS signal propagation in indoor environment, and very useful for positioning algorithms developed for indoor GNSS and pseudolite GNSS. Pseudolites can be used as independent indoor positioning systems or alternatively as augmentation to GNSS [262, 324]. The more realistic indoor fading channels can improve tracking performance by helping to enhance interference mitigation and multipath mitigation methods, and by increasing integration times for HS-GNSS. In this section, the indoor channel propagation is analyzed based on data measurements. The purpose is to give further insight on the

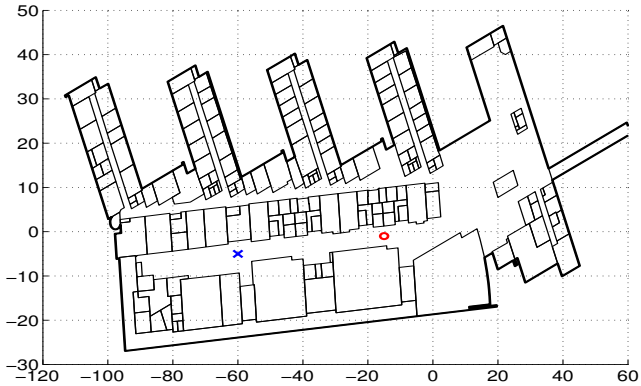

Fig. 5.1: *Illustration of the measurement environment. Blue cross represents the transmitter location, and red circle the receivers location.*

GNSS-like signal propagation indoors by studying the indoor signal fading characteristics. The fading distributions of the measured channel peaks are also compared to several theoretical distributions.

5.1.1 Measurements set-up description

The measurement campaign was carried in the main corridor, lower floor of one of the buildings of Tampere University of Technology, as it is shown in Fig. 5.1. In the signal reception, one transmitter of GPS-like signals (with different codes than the actual GPS) and two synchronized GPS receivers were used: one receiver was a reference receiver, that was used to capture the data from the transmitter via cable, and the another receiver was used to capture the wireless signal and obtain the channel characteristics. The transmit antenna is placed in a fixed position as shown in Fig. 5.2. The measurement scenarios were divided into two different sets, where the receiver was moving towards the transmitter (Set 1) or away from the transmitter (Set 2).

The block diagram of the measurement set-up is shown in Fig. 5.3, where CIR refers to Channel Impulse Response. Initial estimates for Doppler frequency and delay were obtained based on the strong cable signal (i.e., the reference signal) shown in Fig. 5.3, by scanning the whole delay-frequency space. Indeed, the frequency and code drifts and navigation data were estimated based on the reference signal and then removed from the wireless signal [186–188]. Further on, the wireless signal was correlated with the replica spreading code, by taking into account the estimates for the delay

Fig. 5.2: *Transmitter position in the measurement set-ups.*

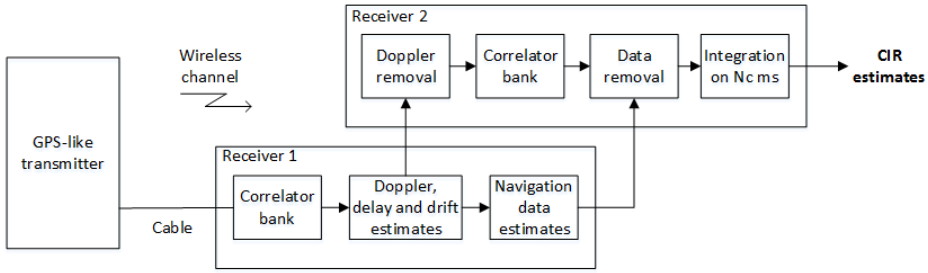

Fig. 5.3: *Block diagram of the measurement set-up.*

and frequency and including the possible drifts. In the indoor environment, N_C has to be high enough, i.e., more than 20 ms, in order to decrease the noise level. Therefore, navigation data removal had to be done before the coherent integration [186–188].

5.1.2 Data analysis - Fading distributions

The fading distributions have been analyzed for the averaged amplitudes after $N_C = 200$ ms integration. This integration length has been chosen in here as a relevant case for HS-GNSS, where large integration periods are used. The LOS delay was computed in two ways: either as the delay corresponding to the peak of the reference signal $\widehat{\tau}_{LOS,ref}$ (using the fact that the two receivers are synchronized), or as the delay of the global peak in the wireless signal $\widehat{\tau}_{peak,air}$. The measurement data Probability Density Function (PDF) and Cumulative Distribution Function (CDF) were compared to several theoretical distributions, such as Rayleigh [164, 293, 329], Rice [171, 234, 329], Nakagami-*m* [186, 234, 293, 345], Log Normal [74, 117], and

Loo [210, 329] distributions, respectively. These distributions are the most common distributions reported in literature especially in satellite communications (see, e.g., [74, 293, 329]).

In the case of at least one strong LOS signal combined with possibly several weaker NLOS signals, the fading channel distribution is typically assumed to be Rician [293]. In Rayleigh fading, the fading fluctuations are deeper, i.e., Rayleigh distributed fading is more severe than Rician fading [243]. Thus, Rayleigh distribution is likely to fit quite well the measured data, when only NLOS propagation paths are available [185,266,293]. With Nakagami-*m* distribution, that is also called *m*-distribution, a wider class of fading channel conditions can be modeled than with Rayleigh or Rician distributions only [234]. In [186, 187] it was also shown that Nakagami-*m* provides the best fit for satellite-to-indoor channel propagation. The PDF of a Nakagami-*m* fading amplitude is [29, 187, 234, 293, 345]:

$$f_{Naka}(a) = \frac{2}{\Gamma(a)} \left(\frac{m}{\mu_{Naka}} \right)^m a^{2m-1} \exp\left(- \frac{ma^2}{\mu_{Naka}} \right), \tag{5.1}$$

where a stands for the signal amplitude, $\Gamma(\cdot)$ denotes the gamma function and μ_{Naka} is the average path power ($\mu_{Naka} = \mathbf{E}(a^2)$). m represents the Nakagami fading parameter [293] and is equal to the inverse of the normalized variance of the squared envelope [187, 266]:

$$m = \frac{\left(\mathbf{E}(a^2)\right)^2}{var(a^2)}. \tag{5.2}$$

Above, $var(a^2)$ means the variance of a^2. The value for m-parameter can range between $1/2 - \infty$. The channel converges to a static channel, when the $m \to \infty$. As special cases, Nakagami-*m* distribution covers Rayleigh distribution when $m = 1$, and one-sided Gaussian when $m = 1/2$ [234, 266]. Besides Nakagami-*m*, other distributions considered in this section are Rician [171,234,329], Rayleigh [164,293], log-normal power distribution [117, 329] and Loo's distribution [210].

The best theoretical distribution for the averaged amplitude distributions ($N_C = 200$ ms) was searched by minimizing the Mean Square Error (MSE) between the CDF of the measurement data and the CDF of the theoretical distribution. MSE as a similarity measure is used, e.g., in [18, 286]. Other possibilities to measure the goodness of fit are, e.g., Kullback-Leibler (KL) divergence [18, 162, 286] or maximum likelihood estimation [296].

Table 5.1: *Best amplitude distribution fit.*

$\widehat{\tau}_{LOS,ref}$		$\widehat{\tau}_{peak,air}$	
Set 1	Set 2	Set 1	Set 2
Naka ($m = 0.67$)	Naka ($m = 0.623$)	Naka ($m = 0.68$)	Naka ($m = 0.619$)

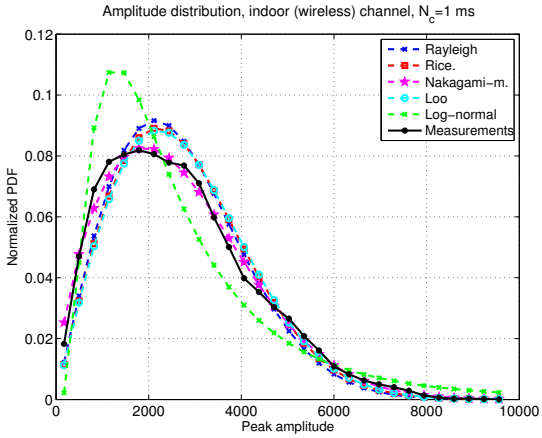

Fig. 5.4: *PDFs for theoretical distributions and wireless signal instantaneous amplitude measurements at $\widehat{\tau}_{LOS,ref}$ (Set 2, $N_C = 1$ ms).*

According to the chosen minimization criterion, the results are shown in Table 5.1 as the best fit distribution. The best choice seems clearly to be Nakagami-*m* distribution with relatively low *m*, i.e., $m = 0.6 - 0.7$. This finding is equivalent with earlier studies in [186–188], where Nakagami-*m* was noticed to be the best fit both in outdoor-to-outdoor and outdoor-to-indoor environments, with smaller *m*-parameter values in indoor case. The results were also checked visually, and an example of the PDFs of measurements and theoretical distributions is shown in Fig. 5.4.

5.1.3 Data analysis - Average number of paths and path spacings

The number of channel paths was examined using the wireless CIR estimates. In order to decrease the noise level, $N_C = 200$ ms was used. The normalized CIR amplitudes were studied and all detected peaks higher than a threshold (here, the threshold was chosen to be $2.5 \times \mathbf{E}(CIR)$, according to [299]) were considered as true channel

Table 5.2: *Estimated number of channel paths N_{path} and path spacings Δ_{path}. Both mean and standard deviation (std) included. Wireless channel.*

		Set 1	Set 2
N_{path}	mean	1.14	1.07
	std	0.41	0.43
	max	4	6
Δ_{path}	mean [chips]	0.12	0.03
	std [chips]	0.36	0.19

paths. A window of 200 correlators (i.e., about ± 6.25 chips around the global peak) was used with oversampling factor $16.367/1.023 \approx 16$ samples per chip. Table 5.2 shows the mean, maximum and std of the number of detected peaks and the average and std of the path spacings (in chips) for both scenarios. Clearly, if more than one path is present, they are located very close to the first one.

5.2 An improved simulation model for Nakagami-*m* fading channels

Since the Nakagami-*m* distribution has been noticed to provide the best fit for the fading amplitudes of realistic satellite-to-outdoor, satellite-to-indoor and indoor-to-indoor channels [152, 187, 188, 250], it is very important to find a simple and feasible simulation model for Nakagami-*m* distribution for studying and developing positioning algorithms. However, the existing simulation models for Nakagami-*m* distributed fading channels include only the values of m between $0.5 - 10$ [29, 343], and the modelling for $0.5 < m < 0.65$ is noticed to be computationally quite expensive [343]. In [29], Beaulieu &al. suggested one of the simplest model, based on a simplified approximation of the inverse of the CDF of the Nakagami distribution, for simulating Nakagami-*m* fading channels. Although any arbitrary value of m between the values 0.65 and 10 were supposed to be covered in the Beaulieu &al. model in [29], only 12 values in this interval were presented, and the procedure to obtain any other arbitrary value was not explicit or straightforward. Therefore, in this section, we introduce an efficient low-complexity method to generate a Nakagami-*m* distributed channel coefficients directly from Rayleigh-distributed variables, based on an accurate approximation function. Our method extends the Beaulieu &al. approach [29] to a wider range (i.e, $0.5 - 16$) of Nakagami m-parameters. Thus, our contribution in

this section is to present a fast simulation-based approach to model realistic channels using Nakagami-*m* fading model.

5.2.1 Beaulieu &al. method

In [29], Beaulieu &al. showed that with certain transforms, Rayleigh distributed random variables can be used to generate Nakagami-*m* distributed fading channel parameters. The principle of this method is illustrated in Fig. 5.5, i.e., the blocks except the additional interpolation stage (marked with dashed block and lines). Rayleigh distributed amplitudes from the channel model (here, we used the channel model of Schumacher &al. [259, 283, 284]) are transformed to Nakagami-*m* distributed by using Beaulieu's functions. The phases are assumed to remain uniformly distributed. This assumption is in [29] noticed to be reasonable for most of the wireless channels.

Beaulieu &al. method is based on the accurate approximation for the inverse of Nakagami-*m* CDF. The inverse CDF function $F_R(\cdot)$ for Nakagami-*m* fading can be defined as [29]

$$F_R(x) = \int_0^{x(u)} \frac{2m^m t^{2m-1}}{\Omega^m \Gamma(m)} e^{\left(-\frac{mt^2}{\Omega}\right)} dt. \tag{5.3}$$

where R represents a random variable and

$$u = 1 - e^{\frac{-R^2}{2\sigma^2}}. \tag{5.4}$$

Above, σ^2 means the second moment of random variable R (i.e., $\sigma^2 = E[R^2]$). Since the inverse $F_R^{-1}(u)$ can not be directly generated, Beaulieu &al. proposed the following approximation $F_R^{-1}(u) \approx G(\lambda(u))$, where

$$G(\lambda(u)) = \lambda(u) + \frac{a_1\lambda(u) + a_2\lambda(u)^2 + a_3\lambda(u)^3}{1 + b_1\lambda(u) + b_2\lambda(u)^2}. \tag{5.5}$$

Here, $\lambda(u)$ is defined as

$$\lambda(u) = \left(\sqrt{ln\frac{1}{1-u}}\right)^{\frac{1}{m}} \tag{5.6}$$

and the coefficients a_1, a_2, a_3, b_1, and b_2 are used to minimize the approximation error $\sum_{u\in[0,1)} \left|F_R^{-1}(u) - G(\lambda(u))\right|^2$. The coefficients are dependent on m and some example values for them are introduced in Table I of [29]. For other values of m than those shown in [29], the coefficients can be calculated by minimizing the mentioned approximation error, but at the expense of complexity.

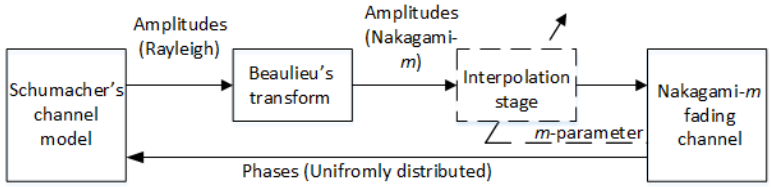

Fig. 5.5: *Implementing Beaulieu's transforms for Schumacher's channel model. Interpolation stage (dashed block) is included only in the proposed approach.*

5.2.2 Proposed approach

Since Beaulieu &al. presented in [29] the coefficients to minimize the approximation error only for finite values of m between 0.65 and 10, our purpose is to extend the method for a wider range of m-values with lower computational load. The fading channel model used here is based on the Multiple Input Multiple Output (MIMO) radio channel model of Schumacher &al. [259, 283, 284], where the multipath fading channel environment is created using specific channel coefficients. These Rician or Rayleigh-distributed coefficients are generated in frequency domain in order to achieve speed-dependent fading spectrum. The MIMO model of [259, 283, 284] is simplified to Single Input Single Output (SISO) channel model, since MIMO modelling is not necessary in our approach.

The block diagram for the Nakagami-m channel model is shown in Fig. 5.5, including also the additional interpolation stage (dashed block and lines). The coefficients, that were shown by Beaulieu &al. in [29], are kept as a starting point. The rest of the coefficients are selected according to two conditions: the minimum error between the simulated and theoretical Nakagami-m distributed PDFs (J_1), and the minimum error between the true m and the target m of the channel (J_2):

$$J_1 = \sum_{R=0}^{\infty} \mid p_{sim}(R, \underline{\alpha}) - p_{th}(R) \mid^2, \tag{5.7}$$

where $p_{sim}(R, \underline{\alpha})$ is the simulated PDF for the coefficients $\vec{\alpha}$, $p_{th}(R)$ is the theoretical PDF and $\underline{\alpha} = [a_1\, a_2\, a_3\, b_1\, b_2]$ represent the currently tested values for the coefficients.

$$J_2 = \mid m_{sim}(\underline{\alpha}) - m_{th} \mid^2, \tag{5.8}$$

where m_{th} is the target m (i.e., m of the theoretical PDF) and $m_{sim}(\underline{\alpha})$ is the true m of the simulated channel. The best coefficients $\widehat{\underline{\alpha}}$ were chosen to be the coefficients

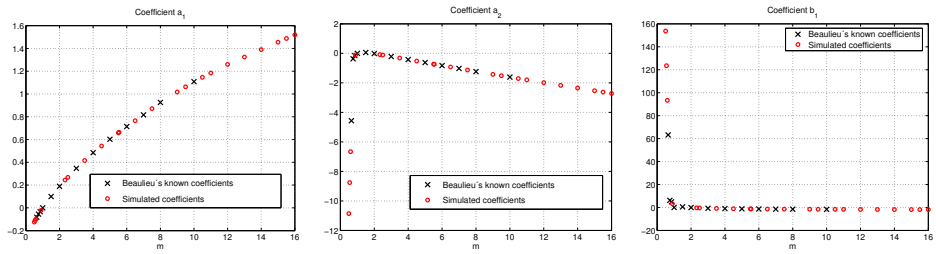

(a) *(b)* *(c)*

Fig. 5.6: *Examples of known and simulated approximation coefficients for: (a) coefficient a_1, (b) coefficient a_2, and (c) coefficient b_1. Similar figures for a_3 and b_2 are shown in [250].*

m	a_1	a_2	a_3	b_1	b_2
0.55	−0.1109	−8.7589	−29.3969	123.5136	35.4096
0.60	−0.0969	−6.6612	−22.6394	93.3546	29.3539
0.90	−0.0224	−0.1029	−0.3155	3.2833	0.8055
2.33	0.2444	−0.0834	0.2744	−0.2899	0.1006
3.5	0.4159	−0.3188	0.2634	−0.8254	0.2208
5.54	0.6637	−0.7375	0.3028	−1.2587	0.4186
9.5	1.0631	−1.5159	0.5651	−1.5753	0.6273
10.5	1.1464	−1.7039	0.6449	−1.6344	0.6722
11.0	1.1839	−1.7983	0.6883	−1.6642	0.6955
13.0	1.3247	−2.1692	0.8949	−1.7408	0.7608
15.0	1.4550	−2.5349	1.1083	−1.8082	0.8194
15.5	1.4874	−2.6264	1.1615	−1.8264	0.8353
16.0	1.5197	−2.7178	1.2147	−1.8446	0.8512

Table 5.3: *Some examples of the generated values for all approximation coefficients.*

minimizing the criterion $J_1 + J_2$:

$$\underline{\widehat{\alpha}} = argmin\,(J_1 + J_2). \tag{5.9}$$

The generation of the approximation coefficients included interpolation for $0.65 \leq m \leq 10$ (i.e., for those m-values which were not defined in [29]), and extrapolation for both $0.50 \leq m < 0.65$ and for $m > 10$. Some illustrative values of the generated coefficient values for Beaulieu's transforms are presented in Fig. 5.6 and in Table 5.3. More values are shown by us in Table 1 of [250]. Not all the generated coefficient values are introduced here nor in [250], but the missing ones between $0.5 \leq m \leq 16$ can be approximated using linear interpolation for the known coefficient values

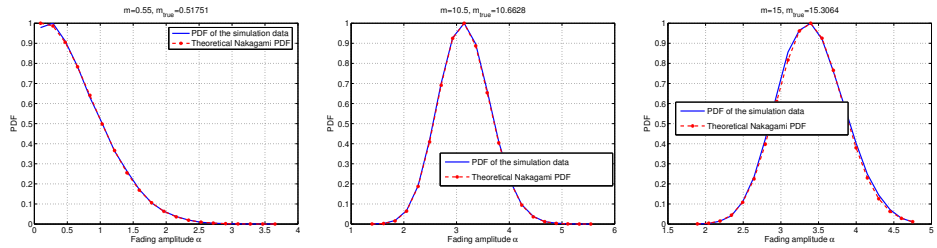

(a) *(b)* *(c)*

Fig. 5.7: *Examples of theoretical and simulated Nakagami-m PDFs for (a) $m = 0.55$, (b) $m = 10.5$, and (c) $m = 15$. The target value for m-parameter is denoted with m and the true m-value in the simulated channel is denoted with m_{true}.*

shown in [29, 250] and in Table 5.3.

Fig. 5.7 shows the PDFs of simulated and theoretical Nakagami-*m* distributed fading amplitudes. PDFs for all presented values of *m* match well to theoretical PDF; there is typically a slight mismatch, which also varies by the simulation round due to a limited number of generated random variables.

5.3 Conclusions

This chapter has concentrated on the challenge of GNSS signals indoors via channel modeling. Based on measured GPS-like data indoors, the indoor fading characteristics have been analyzed for the purpose of deriving appropriate indoor channel models for GNSS signals. In the analysis, it has been noticed that the amplitude variations indoors match the Nakagami-*m* distribution, typically with $m = 0.6 - 0.7$. It has also been observed that typical indoor channels have only few signal paths, and they are located at short distances (i.e., within less than one chip). Thus, an appropriate indoor channel model can consist of one or two closely-located paths, with the LOS signal obeying Nakagami-*m* distribution for amplitudes and uniform distribution for phases. Based on these indoor channel studies, an efficient and low-complexity simulation model has been introduced for Nakagami-*m* distributed fading channels, by extending the method proposed by Beaulieu &al. to a wider range of *m*-values. The approximation coefficients have been generated for *m*-parameter with a range $0.5 - 16$, and the PDFs for theoretical and simulated Nakagami-*m* channels have been compared.

The main contributions of this chapter can be summarized as follows:

- Indoor fading channel models are analyzed for GPS-like signals, based on real indoor measurements. Obtained fading channel characteristics are compared to typical fading distributions to find suitable channel model for GNSS indoor propagation.
- Based on the studied indoor channel models, a simple and efficient Nakagami-*m* fading channel simulator has been built with extended range of *m*-values for wireless GNSS signals. This channel model can be used further to develop acquisition algorithms in various fading environments.

Based on the work presented in this chapter, there have been also two publications:

1. **Elina Pajala**, Tero Isotalo, Abdelmonaem Lakhzouri and Elena Simona Lohan, "An improved simulation model for Nakagami-m fading channels for satellite positioning applications", in *Proc. of 3rd Workshop on Positioning Navigation and Communication (WPNC)*, Hannover, Germany, Mar 2006, pp. 81-89.
2. Najmul Islam, Elena Simona Lohan, Abdelmonaem Lakhzouri, **Elina Pajala**, Heikki Laitinen and Markku Renfors, "Indoor fading distributions for GPS-based pseudolite signals", in *Proc. of International Workshop on Satellite and Space Communications (IWSS)*, Salzburg, Austria, Sep 2007.

6. PROPOSED SOLUTIONS FOR HS-GNSS

One possible solution for the challenges in indoor positioning is the HS-GNSS technology, that is able to obtain a position fix with weaker signals using some advanced detection algorithms. However, besides the ability to work in a harsh indoor environment, another important challenge in GNSS low-complexity and fast acquisition, which works under multipath propagation and with ambiguous modulation types, such as BOC, which are specific to modern GNSS. For this, the solutions are:

- Good choice of decision variables and decision thresholds. In this chapter, three CFAR detectors are studied. The main goal is to build a simple and robust decision variable which eases the design process, in the sense that it allows to use a decision threshold which is independent of channel conditions. Our results are presented also in [252].
- Good choice of integration schemes. The solutions are the same as for dealing better with indoor GNSS. We show in this chapter and in [249] that the DC schemes also work with unambiguous acquisition techniques (i.e., Betz and Fishman (B&F)-method [27, 32, 108]).

In this chapter, we focus only on acquisition stage.

6.1 CFAR detectors

As was mentioned in Chapter 3, P_d and P_{fa} are highly dependent on the chosen threshold γ. Therefore, the choice of a proper threshold value is very important for the whole acquisition process. The chosen threshold can be either fixed to a constant value, or it can be adapted, e.g., according to estimated CNR. Since the channel conditions are typically chancing, a constant decision threshold may not be the best

Table 6.1: *Different decision statistics.*

X	Equation	Name	References
X_{ref}	$\max_{i=1}^{N_{bins}} Z_i$	The classical decision statistic	[28, 132, 150, 204, 267]
X_1	$\frac{\max_{i=1}^{N_{bins}} Z_i}{\mathbf{E}(Z_i)}$	The peak-to-mesh ratio	Proposed by us in [252]
X_2	$\frac{\max_{i=1}^{N_{bins}} Z_i}{Z_{m_2}}$	The ratio-of-peaks	[154, 252, 253]
X_3	$\frac{(\max_{i=1}^{N_{bins}} Z_i)^2}{Z_{m_2} Z_{m_3}}$	The modified ratio-of-peaks	Proposed by us in [252]

solution. It is also possible to find a threshold, that is independent on CNR and channel fading statistics, if the decision variable X is built in a suitable manner.

The CFAR detectors, that are the most used in practice [150, 151], were presented earlier in Chapter 3. In this section, three decision statistics for CFAR detectors and hybrid-search acquisition of a BOC modulated CDMA signal are proposed and analyzed. The comparison is done in terms of P_d and the dependence of the threshold on the channel conditions. We also show how to choose the threshold for each of these three situations, and which of the proposed ways to build the decision variable is the most robust to noise and channel conditions. As a benchmark, the classical decision statistic, where the decision variable is chosen as the maximum over the squared absolute value of the averaged correlation function, is kept in the analysis. The results are also published by us in [252].

Proposed decision variables

Different ways to build the test statistic X are shown in Table 6.1. X_{ref} is the classical one [28, 132, 150, 204, 267], but the drawback is that it requires that γ is adapted according to the current CNR level, as was shown in [28] and as we also noticed in [252]. Therefore, other choices, that would be independent on CNR, were searched. These proposed decision variables are denoted by X_j and the corresponding threshold by γ_j, $j = 1, 2, 3$. A decision statistic similar with X_2 (i.e., ratio-of-peaks) have previously been proposed also in [253]. However, the method in [253] was described only for single-path channels and the choice of the second largest peak was not detailed.

In the equations in Table 6.1, Z_i represents the correlation output in the search window i, $\mathbf{E}(\cdot)$ is the expectation operator (that can be approximated, e.g., via the mean over all Z_i values, $i = 1, \ldots, N_{bins}$), Z_{m_2} is the second local maximum and Z_{m_3} is the third local maximum in the time-frequency mesh. In the case of single-path channel, looking for the next local maximum is straightforward. However, since the occurrence of multipaths is very typical, this challenge needs to be taken into account for both X_2 and X_3 decision variables. E.g., for X_2, two first maxima are found from the correlation output and then compared. If the second local maximum was chosen as the next maximum of the residual correlation output without any limitations, it would very probably correspond to another channel path with relative high value. Naturally, comparing two multipath correlation peaks would lead to smaller value of the decision threshold, and hence, to lower detection probability P_d. Therefore, the multipaths have to be estimated and ignored when looking for the next maximum. Thus, in practice, e.g., Z_{m_2} = the second local maximum out of $Z_i - K$ variables, after removing from the time-frequency mesh the K values corresponding to the channel paths and to their closest neighbors (K is chosen in such a manner to account for the maximum delay spread of the channel and for the estimated maximum Doppler spread). More details of how to choose the second and third local maximum is presented by us in [248, 252].

Simulation results

The robustness of the detection threshold in the presence of various channel profiles and various steps of the time bins (Δt_{bin}) in the search stage was analyzed by us in [252]. For a fair comparison of between different decision variables, the false alarm probability P_{fa} was fixed from the beginning and the target corresponding threshold γ_j was then computed in order to meet this accurate P_{fa}. The best threshold will be chosen in such a way to exhibit a good P_d (when false alarm is fixed) and to be independent on CNR, the channel type and the time-bin step.

The coherent integration length N_C and the non-coherent integration length N_{NC} were fixed to some desired values in order to get realistic results for each channel cases. The simulations were done for two different Nakagami-m distributed fading channel profiles with multipath propagation. The first fading channel profile (denoted as "channel 1" for now on) is a 4-path fading channel with $m = 2.5$, $N_C = 20$ ms

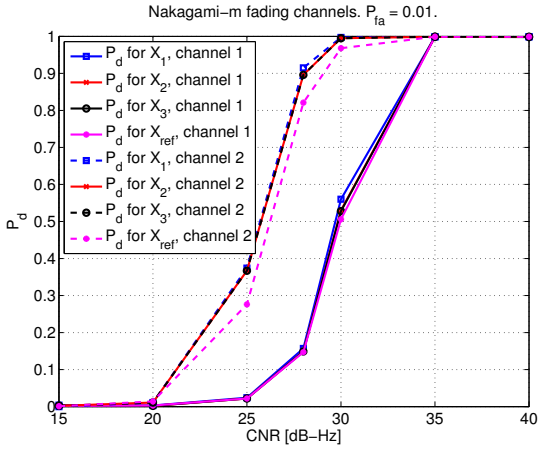

Fig. 6.1: *P_d for different decision variables X_j, $j = 1,2,3$, and X_{ref}, for various CNR. Channel 1 (solid lines) with $v = 45$ km/h and channel 2 (dashed lines) with $v = 3$ km/h.*

and $N_{NC} = 4$ blocks. The second fading channel profile (denoted as "channel 2" for now on) is a 2-path fading channel with $m = 0.75$, $N_C = 40$ ms and $N_{NC} = 2$ blocks. The sum of the channel path powers was normalized to 1. The time-bin step was $\Delta t_{bin} = 0.125$ chips. The test statistic was build over time-frequency windows of size 20 chips $\times 1$ kHz (i.e., hybrid search). The used modulation was SinBOC$(1,1)$.

The impact of the decision variable on the P_d, when P_{fa} is fixed to 0.01, is illustrated in Fig. 6.1. Both fading channel profiles are included, channel 1 with mobile speed $v = 45$ km/h and channel 2 with $v = 3$ km/h. As it can be noticed, the differences between the three studied decision variables X_1, X_2, and X_3 are very small. In the "channel 1" case, where the mobile speed is higher, P_d for the decision variable X_{ref} is slightly lower than P_d for the other three decision variables.

Fig. 6.2 shows the impact of the decision variable on P_d for two different mobile speeds with channel 2 profile. The distinction between the P_ds for the three decision variables X_1, X_2 and X_3 remain about at the same level but the P_d for X_{ref} is clearly affected by the mobile speed. With mobile speed 3 km/h the decision variable X_{ref} may give even 0.15 lower P_d than the other decision variables. The impact of different CNR values on γ_j is shown in Fig. 6.3 ((a) for X_1, X_2 and X_3 and in (b) for X_{ref}). According to the results, the detection threshold for the proposed three test statistics is totally independent on CNR. On the other hand, as expected [28], the detection threshold for X_{ref} is highly affected by CNR, and therefore it should be set adaptively.

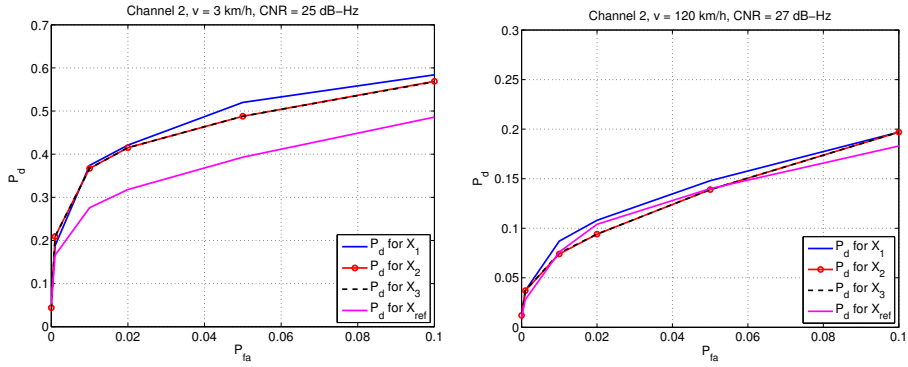

(a) ***(b)***

Fig. 6.2: *P_d versus P_{fa} for different decision variables X_j, $j = 1,2,3$, and X_{ref}, for different mobile speeds: (a) 3 km/h and (b) 120 km/h. Channel 2 scenario.*

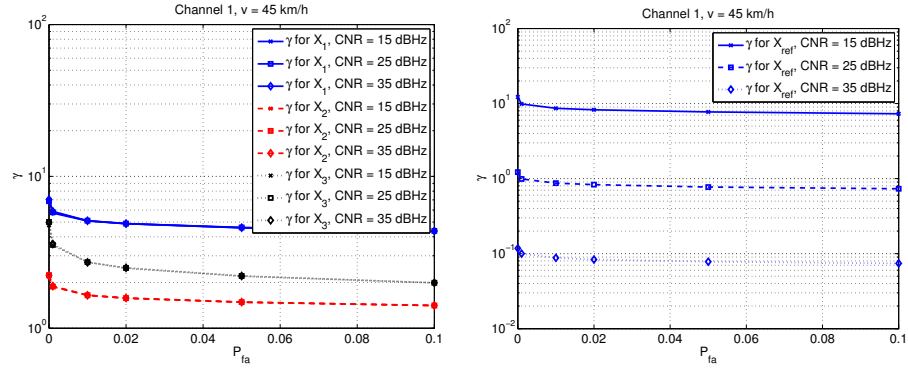

(a) ***(b)***

Fig. 6.3: *Impact of the CNR on γ_j values with different constant P_{fa}: (a) decision variables X_1, X_2 and X_3 and (b) X_{ref}. Channel 1 with $v = 45$ km/h.*

This follows that errors in the CNR estimation may affect the detection probability when the classical detection variable is used.

Furthermore, the impact of channel conditions on the detection threshold γ_j was examined for all three proposed test statistics. Fig. 6.4 shows the impact of the mentioned two channel profiles, 4-path and 2-path, on the γ_j value with different constant P_{fa} values. As it can be seen, γ_1 values for the decision variable X_1 are clearly dependent on the channel profile and the coherent and non-coherent integration lengths. The detection thresholds γ_2 and γ_3 remain almost at a constant level (i.e., they are independent of the channel profile and the integration lengths).

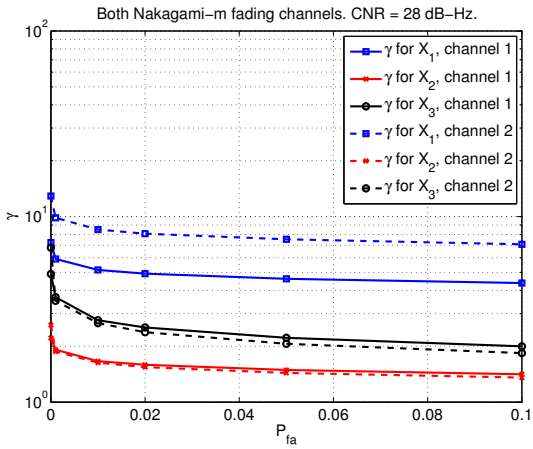

Fig. 6.4: *Detection threshold γ_j versus P_{fa} for both channel profiles: channel 1 with $v = 45$ km/h (solid lines) and channel 2 with $v = 3$ km/h (dashed lines).*

It is obvious that, if γ_j is independent of CNR, the channel type and the time-bin step, the threshold value is easier to choose, and therefore the acquisition design can be done in a simple way. Therefore, the simplest test statistic is that one for which the detection threshold is the least dependent on the channel and receiver parameters, such as CNR, integration times, channel type and time-bin step. When examining our results both in here and in [252], it can been concluded that

- P_d for X_{ref} is affected by the mobile speed. With low mobile speeds, the decision variable X_{ref} may give even 0.15 lower P_d than the other decision variables.
- The threshold γ for X_{ref} needs to be set adaptively according to current CNR in order to prevent decrease in P_d.
- The thresholds γ_j for all three studied decision variables X_1, X_2 and X_3 are independent on CNR.
- When studying the effect of channel profile and N_C and N_{NC} lengths to the γ_j of decision variables X_1, X_2 and X_3, X_2 was noticed to be the most robust choice, according to the above conditions.

Thus, by choosing the decision variable X_2 and by defining the threshold γ_2 according

to the values given in Table 1 in [252], the target P_{fa} under any channel conditions can be selected.

6.2 Enhanced differential correlation

Instead of the non-coherent integration, other types of post-correlation combination are also possible. These techniques include differential non-coherent correlation (DN) [273], enhanced differential non-coherent correlation (DN2) proposed by us in [249], Teager-Kaiser (TK) based scheme [126,206] and different generalized post-detection integration (GPDI) schemes, such as full GPDI [75, 260], Truncated GPDI and Fractional GPDI [207]. The non-coherent combination may cause some squaring loss [71], but due to its simplicity, it is suitable for conventional GNSS receivers. GPDI schemes are planned for harsh environments (such as indoors) to increase the sensitivity, but at the cost of complexity. Differential correlation methods instead can be seen as a trade-off between sensitivity and complexity [282, 350], to be used in HS-GNSS receivers. A comprehensive analysis of the mentioned post-detection integration techniques can be also found in [207].

Differential correlation methods have previously been proposed for CDMA-based wireless communication systems [149, 273, 350] and more recently in satellite navigation context [136, 144, 249, 282]. In [282], it was noticed that differential correlation methods have better resistance to noise and other temporally uncorrelated interference sources than the traditional non-coherent integration methods, with medium and low coherence times of the fading channel and in the absence of frequency errors. Thus, differential correlation methods can help to exploit the temporal correlation of fading signals and, consequently, to improve the acquisition process and the receiver sensitivity in challenging environments. The big advantage of the differential methods is that they do not, nonetheless, increase much the computational load of the acquisition stage, when compared to the conventional methods.

In this section, we present an enhanced differential correlation technique, which increases the signal detection probability in multipath fading channels. Since this enhanced method exploits the signal correlation in longer time intervals, the interference effects (coming from noise and other temporally uncorrelated sources) can be diminished. Indeed, since the analysis in [282] by Schmid et al. is limited to GPS signals with BPSK modulation only, it is important to make the analysis also for BOC

modulated signals currently used in modernized GPS, Galileo and Beidou systems, and soon to be used in Glonass CDMA signals. Therefore, we study the effect of differential correlations with and without unambiguous acquisition methods.

6.2.1 Enhanced differential non-coherent correlation method

Differential correlation with ambiguous acquisition

For the conventional non-coherent integration (NC), the correlation output $Z_{aBOC,NC}$ is given as in Eq. (3.7). In traditional differentially non-coherent correlation, denoted as DN for now on, the correlation is performed between two consecutive outputs of the coherent integration I_k. These correlation variables are then integrated (i.e., averaged) in order to obtain differential acquisition variable. Thus, the differential correlation output Z for ambiguous BOC (aBOC) method can be given as

$$Z_{aBOC,DN} = \left| \frac{1}{N_{DC}-1} \sum_{n=1}^{N_{DC}-1} I_n^* I_{n+1} \right|^2, \tag{6.1}$$

where I_n, $n = 1,\ldots,N_{DC}$, are the outputs of the coherent integration and N_{DC} stands for the differential integration length. For now on, it is assumed that $N_{DC} = N_{NC}$, in order to have a fair comparison between differential and conventional non-coherent approaches. Since differential coherent integration (where only real parts of the differential correlation outputs are integrated) has been noticed to be more sensitive to residual Doppler errors [144], only non-coherent differential methods are considered here.

Sometimes temporal correlations in a desired signal may occur in relatively long time intervals. If the coherent integration time, prior to taking the differential correlation, is small (i.e., clearly smaller than $(\Delta t)_{coh}$), long time correlations can be exploited as follows [273]:

$$Z = \left| \mathbf{E}\left(\sum_{i=1}^{P} I_n^* I_{n+i} \right) \right|^2, \tag{6.2}$$

in which $\mathbf{E}(\cdot)$ is the expectation operator (i.e., an average over n) and $P \in 1 \ldots N_{NC}$. This improves suppression of temporally uncorrelated interference. Here, under considerations is an enhanced DN method as a particular case of Eq. (6.2), denoted by

DN_2. This method has been found empirically, using simulations for Galileo signals. The acquisition variable of DN_2 for aBOC method is expressed as:

$$Z_{aBOC,DN_2} = \left| \frac{1}{N_{DC}-2} \sum_{n=1}^{N_{DC}-2} (I_n^* I_{n+1} + I_n^* I_{n+2}) \right|^2 . \tag{6.3}$$

As it will be seen later in this section, even this simplest particular case of Eq. (6.2) offers a clear gain in acquisition accuracy for both aBOC and unambiguous B&F-technique.

Differential correlation with unambiguous acquisition

For unambiguous acquisition techniques, such as B&F method, the NC, DN and DN_2 algorithms are applied separately on the lower sideband (LSB) and upper sideband (USB) correlation outputs, as illustrated in Fig. 6.5 and in Eqs. (6.4)-(6.5):

$$Z_{SS,DN_2} = \left| \frac{1}{N_{DC}-2} \sum_{n=1}^{N_{DC}-2} (\underline{I}_n{}^* \underline{I}_{n+1} + \underline{I}_n{}^* \underline{I}_{n+2}) \right|^2 \tag{6.4}$$

and

$$Z_{DS,DN_2} = \left| \frac{1}{N_{DC}-2} \sum_{n=1}^{N_{DC}-2} \left(\underline{I}_n{}^* \underline{I}_{n+1} + \underline{I}_n{}^* \underline{I}_{n+2} + \overline{I}_n{}^* \overline{I}_{n+1} + \overline{I}_n{}^* \overline{I}_{n+2} \right) \right|^2 , \tag{6.5}$$

where Z_{SS} is the acquisition variable for single sideband and Z_{DS} for dual sideband, and $\underline{I}_n$ and $\overline{I}_n$ are the coherent correlation outputs after LSB and USB filtering, respectively. Only DN_2 expression is shown here for clarity reasons, but the formulas for DN and NC are straightforward.

Fig. 6.5 shows the block diagram of the B&F unambiguous acquisition technique [27, 32, 108] with the additional differential correlation block. Here, DN/DN_2 block forms the differential products $I_n^* I_{n+i}$. Typically in dual sideband methods, the lower and upper sidebands are combined after non-coherent squaring [108]. Since the DN-methods were noticed to provide better detection probability P_d if the non-coherent squaring is performed after dual sideband combining, the upper and lower sidebands

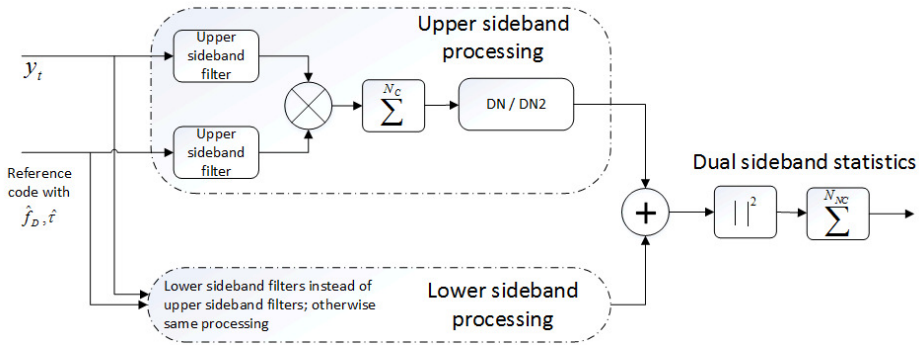

Fig. 6.5: *Block diagram of the B&F-method with differential correlation.*

are in our method combined before non-coherent squaring, for both DN and DN_2 -methods (see Fig. 6.5). Fig. 6.6 justifies this choice, by showing the P_d vs. CNR for DN and DN_2 -methods with both combination orders. Here, "order 1" means the order where the combination of the sidebands is done *after* non-coherent squaring, and "order 2" means the order where the combination is done *before* non-coherent squaring (as in Fig. 6.5). Also the NC-method is included in the figure as a reference. As it can be seen, P_d increases for DN and DN_2 methods, if the non-coherent squaring is performed after the sideband are combined. In the case of single sideband technique, there is obviously only one possible configuration (i.e., non-coherent squaring immediately after DN/DN_2 blocks).

Fig. 6.7 presents the correlation function envelopes for aBOC and dual sideband B&F, with both NC and DN_2 methods, respectively, in the case of SinBOC(1,1) modulation. As it can be seen, DN_2 processing decreases the sidelobe peaks clearly in the case of aBOC. Indeed, in the case of unambiguous BOC, DN_2 makes the main peak approximately 0.5 chips narrower, when compared to the aBOC with NC processing. This may also increase the tracking sensitivity in the receiver.

6.2.2 Simulation results for comparing different correlation methods

In what follows, the traditional conventional non-coherent integration (i.e., NC), DN method and the new DN_2 -method are compared in fading channels. Both aBOC and unambiguous B&F-technique (dual/single sideband) [27, 32, 108] are taken into account. In all simulations, we use a constant false alarm of $P_{fa} = 10^{-2}$ (see Section 6.1), SinBOC$(1,1)$ modulation [134, 135] and hybrid search. The decision variable

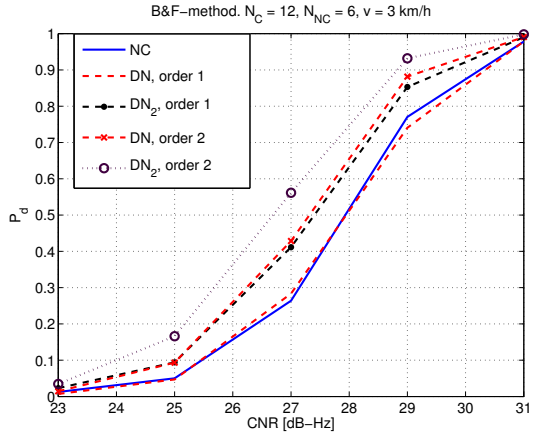

Fig. 6.6: *Effects of placing the squaring block before or after the dual sideband combining: in "order 1", the sidebands are combined after the non-coherent squaring; in "order 2", the sidebands are combined before the non-coherent squaring.*

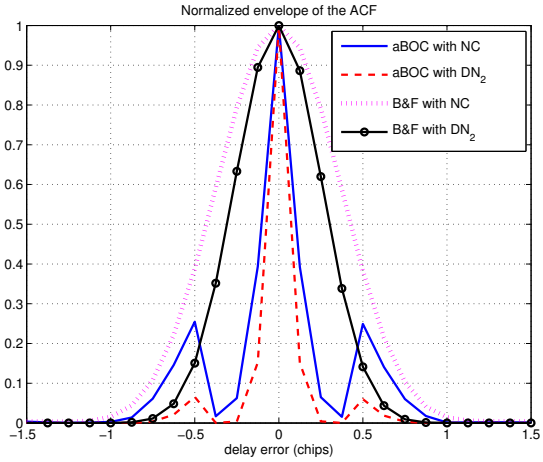

Fig. 6.7: *Envelope correlation functions for aBOC and dual sideband B&F and for NC and DN_2 methods, respectively. SinBOC(1,1), order 2.*

is chosen to be the ratio-of-peaks, according to the results shown in Section 6.1 and in [252]. In the case of multipath channels, the detection probability P_d is calculated as the probability that at least one channel path is detected with an error of less than or equal to 1 chip. As it was shown in Section 5.1 and in [187, 188, 250], both indoor and outdoor channels match to the Nakagami-*m* distribution with various values of *m*-parameter. Therefore, Nakagami-*m* distributed multipath fading channels were used

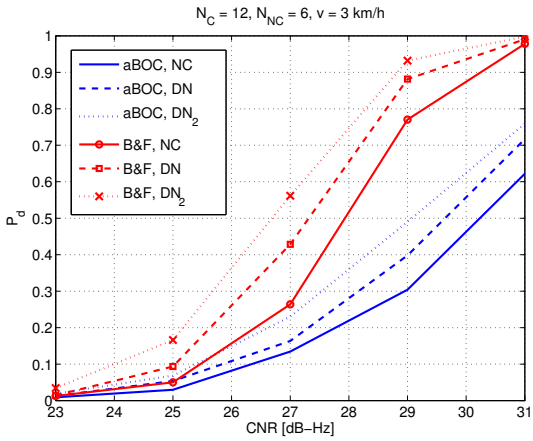

Fig. 6.8: *P_d vs. CNR for NC and DN_2 correlation methods. Ambiguous BOC and B&F -techniques, order 2. $P_{fa} = 0.01$ and $v = 3$ km/h.*

in the simulations.

Fig. 6.8 shows the impact of the different correlation methods (i.e., NC, DN and DN_2) on the P_d, for the aBOC and B&F -techniques. In both cases, the P_d is clearly increased with DN_2-method, when compared to NC or DN method. Fig. 6.9 presents the P_d versus mobile speed v for NC, DN and DN_2 correlation methods in Nakagami-m channel with (a) 1 path and B&F -technique and with (b) 3 paths and aBOC -technique. Based both on Fig. 6.9 and other results shown by us in [249], it is obvious that DN_2-method is offering the best P_d with low mobile speeds. However, if the mobile speed increases, DN-methods deteriorate quite fast when compared to the NC-method. This makes sense, since when the fading is faster, temporal correlation between consecutive outputs of coherent integrator gets weaker. Therefore, with high mobile speeds, the differential integration actually starts to suppress the desired signal.

Based on the results shown in here, for indoor environments, where the mobile speed is typically very low, DN_2-method is always the best choice. In outdoors, where the mobile speeds are higher, the best correlation method needs to be considered more carefully. Therefore, we proposed in [249] a combined correlation method, where the best correlation method can be chosen according to the estimated coherence time $(\Delta t)_{coh}$ of the channel. We also explain in [249] how $(\Delta t)_{coh}$ can be explicitly estimated.

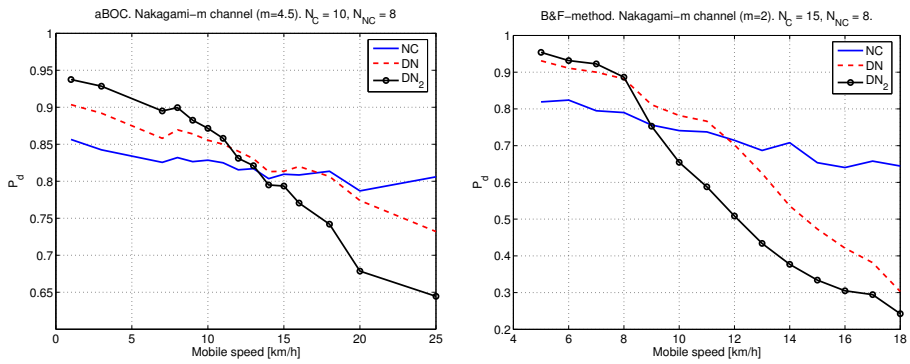

(a) ***(b)***

Fig. 6.9: *P_d vs. mobile speed v for NC, DN and DN_2 correlation methods. Nakagami-m channel with 1 path. (a) aBOC, $m = 4.5$ and $N_C = 10$ ms. (b) B&F-method, $m = 2$ and $N_C = 15$ ms.*

6.2.3 Possible extensions for DN2 method

GPDI can be divided into full GPDI [75, 260] and its variants, namely Truncated GPDI [207] and Fractional GPDI [207]. Full GPDI combines the traditional NC $Z_{aBOC,NC}$ with k-span cross-correlations as [207]

$$Z_{GPDI} = Z_{aBOC,NC} + 2\left|\sum_{n=1}^{N_{DC}-1}\sum_{k=n+1}^{N_{DC}} I_{k-1}^{*} I_k\right|^2 . \tag{6.6}$$

Formulas for Truncated and Fractional GPDI can be found in [207]. Differential correlation methods were noticed in this section to outperform the non-coherent one when the coherence time of the channel is low. In [207], GPDI schemes have been noticed to be more robust to the residual Doppler errors and to obtain the best performance in terms of P_d, when compared to differential and non-coherent methods. Thus, one idea for further research would be to combine the GPDI with DN_2 method. E.g., the inner correlation term $I_{k-1}^{*} I_k$ could be replaced with the enhanced differential correlation as

$$Z_{GPDI,DC_2} = Z_{aBOC,NC} + 2\left|\sum_{n=1}^{N_{DC}-2}\sum_{k=n+1}^{N_{DC}-1} I_{k-1}^{*} I_k + I_{k-1}^{*} I_{k+1}\right|^2 . \tag{6.7}$$

This would not increase the system complexity, but possibly increases the performance, when compared to the GPDI scheme as such.

6.3 Conclusions

In this chapter, we have focused on improving the acquisition algorithms to address the challenges of multipath propagation, interference and ambiguous modulation types. Our first goal was to build a simple and robust decision variable which eases the design process, in the sense that it allows to use a decision threshold which is independent of channel conditions. Three CFAR detectors were proposed and analyzed together with the classical decision statistic. We showed that the most suitable decision variable is the ratio of the first 2 significant peaks in the time-frequency mesh of a hybrid-search algorithm, since it is the most robust with respect to varying channel conditions.

Secondly, we paid attention to the post-detection correlation schemes, and proposed an enhanced differential non-coherent integration method for the acquisition of a BOC-modulated GNSS signal. We showed via simulations, that this enhanced differential correlation method increases the P_d performance in multipath fading channels, when compared to the conventional non-coherent integration and to the traditional differential non-coherent integration methods, especially indoors where the mobile speed is low. The results are valid for both unambiguous (i.e., B&F-method) and ambiguous acquisition techniques.

The main contributions of this chapter can be summarized as follows:

- A novel analysis of several CFAR detectors is presented, in terms of detection probability and dependence on the channel conditions.
- A novel enhanced differential non-coherent integration method is proposed. We also offer a comprehensive analysis of different correlation methods.

Based on the work presented in this chapter, there have been also two publications:

1. **Elina Pajala**, Elena Simona Lohan and Markku Renfors, "CFAR detectors for hybrid-search acquisition of Galileo signals", in *Proc. of European Navigation Conference (ENC-GNSS)*, Munich, Germany, Jul 2005.
2. **Elina Pajala**, Toni Huovinen and Tapani Ristaniemi, "Enhanced differential correlation method for acquisition of Galileo signals", in *Proc. of 10th In-*

ternational Conference on Communication Systems (ICCS), Singapore, Nov 2006.

7. DESCRIPTION OF THE WLAN AND CELLULAR RSS MEASUREMENTS

Real data measurements are used to create or validate most of the proposed solutions for RSS-based positioning in the following chapters (Chapters 8-10). Therefore, it is appropriate to describe the measurement set-ups before going into details of the different solution proposals. We describe also the database update method and performance metrics used in this thesis. The parameters described in this chapter are valid for the subsequent Chapters 8-10.

7.1 Cellular measurements

Cellular measurements consisted of outdoor and indoor measurements, for 2G and 3G networks. The measurements were collected using a Nokia C7 mobile phone, that had an incorporated GPS unit. Different outdoor scenarios are detailed in Table 7.1, showing the location, type of the measurement area and the number of detected BSs N_{BS} in the considered measurement set. District in Table 7.1 refers a part of a town, that is different from downtown. Since the measurement device was able to gather the data either for 2G or for 3G at a time, some areas have measurements only for one type of cellular network. Besides the outdoor measurements, cellular measurements were gathered also indoors. Since the measurement device had only GPS as a reference position, the map positions indoors could not be saved. Therefore, fixed point measurement approach was adopted. In the fixed point measurements, the mobile was kept stationary during the measurements, with a duration ranging between $1-10$ hours, and the data was captured continuously with 1 s time slots. A huge set of fixed point measurements from various indoor locations was collected, in same towns as outdoor measurements (i.e., Tampere and Rovaniemi (Finland), Bucharest (Romania) and Munich (Germany)), resulting as 15 different indoor data

Table 7.1: *Outdoor measurement scenarios for cellular data (2G and 3G).*

Set-up	Location	Area	Measurement device	Network	N_{BS}
$2G_1$	Tampere, Finland	Large district	Nokia C7	2G	47
$2G_2$	Bucharest, Romania	Park	Nokia C7	2G	21
$2G_3$	Bucharest, Romania	Downtown	Nokia C7	2G	77
$2G_4$	Bucharest, Romania	Large district	Nokia C7	2G	81
$3G_1$	Rovaniemi, Finland	Downtown	Nokia C7	3G	29
$3G_2$	Munich, Germany	Small district	Nokia C7	3G	7
$3G_3$	Tampere, Finland	Large district	Nokia C7	3G	77

scenarios for GSM data and 19 different scenarios for WCDMA data. Both outdoor and indoor cellular measurements are used for channel modeling in Section 9.1.

7.2 WLAN measurements

WLAN measurements were collected manually with two different tablets, a Windows Acer and an Asus Nexus 7 with Android 4.3.1 OS, that included proprietary software solutions and detailed HERE indoor maps. In the measurement collection, the same device was always used in one building. After the data samples used to form the training data were collected, the user tracks, that were used for the positioning analysis, were collected separately during different days and covering several floors in each building. All indoor measurement scenarios used in this thesis, with building descriptions and main characteristics, are detailed in Table 7.2, showing the building type, location, used measurement device, the number of floors N_{floors}, estimated building size, the number of data samples in the used user track N_u, number of FPs N_{fp} in the radiomap, the used horizontal grid resolution Δ_{grid} (typically, between $1-5$ m, though sometimes even higher resolution was used), the total number of detected APs saved in the radio map N_{AP}, and the AP density per m^2. One letter corresponds to one building. We remark that the number of FPs N_{fp} is not the same than number of gathered measurements in the building of interest, but the number of FPs with fixed grid resolution (thus, N_{fp} is dependent on the chosen resolution). The number of APs N_{AP} in Table 7.2 shows the number of individual MAC addresses

detected during the measurement collection, but due to the multiple BSSID support, some APs may have several MAC addresses. Thus, some APs here may be physically at the same location.

Altogether, indoor WLAN measurements included 10 different buildings (university buildings, office buildings and shopping malls) located either in Tampere (Finland), Klaukkala (Finland) or in Berlin, Germany. In some buildings, the measurement process was performed more than once, and new measurements were clumped together with the older measurements. Thus, each building may have several measurement set-ups with different measurements, or only different forming of the same measurements, where, e.g., only grid resolution is changed. Examples with two different uniform grid resolution Δ_{grid} in one floor of building A, with set-ups A4 ($\Delta_{grid} = 1$ m) and A5 ($\Delta_{grid} = 5$ m), are shown in Fig. 7.1.

7.3 Database updates

The number of measurements in one building as a result of collection process, e.g., crowd-sourcing, may be huge. Several measurements may occur in the same location, or very close to each other, and saving all of them in the radiomap can increase the amount of data remarkably. Too many measurements can also slow down the estimation phase, or even decrease the positioning performance. For this reason, the radiomap is typically divided into a synthetic grid, where the location information for each grid point (i.e., FP) is defined as the center coordinates instead of the real positions of the collected data samples [139, 232]. If the same transmitter is detected in several measurements collected in the same grid point area, alternatively all RSS values can be saved as in [275] or only one parameter, such as the mean over the RSS measurements, is saved for each transmitter [265].

In this thesis, when a collected data sample appears in a FP that already has a saved sample, all transmitters in both samples are examined. If a new transmitter has been detected in the incoming sample, this new transmitter with its RSS is saved to the FP data. If some transmitter is detected both in the old and incoming measurement, the arithmetic mean between the old and new RSS values is calculated. If all samples are wanted to be kept equally weighted, only a counter is needed to keep track of the number of samples to be used in the average calculation. By using this kind of incremental updating via the arithmetic mean, similar measurements can be combined and

Table 7.2: *WLAN measurement scenarios indoors.*

	Building	Location	Measurement device	N_{floors}	Building size [m]	**Set-up**	N_{fp}	N_u	Δ_{grid} [m]	N_{AP}[a]	AP density per m^2
A	University building 1	Tampere, Finland	Windows	4	163×58	**A1**	1479	158	1	309	0.0082
			Nexus			**A2**	505	181	1	238	0.0063
						A3	4417	606	1	556	0.015
						A4	6168	9638	1	509	0.014
						A5	1046	250	5	509	0.014
B	University building 2	Tampere, Finland	Windows	3	152×93	**B1**	584	176	1	354	0.0083
						B2	4086	2301	1	489	0.012
						B3	705	2301	5	489	0.012
C	Office building 1	Berlin, Germany	Nexus	9	75×65	**C1**	624	850	5	573	0.013
						C2	14611	250	1	727	0.017
						C3	1446	250	5	727	0.017
						C4	516	250	10	727	0.017
						C5	14611	2611	1	727	0.017
D	Office building 2	Tampere, Finland	Nexus	7	59×61	**D1**	844	143	1	995	0.040
						D2	8201	250	1	1213	0.050
						D3	1082	250	5	1213	0.050
						D4	398	250	10	1213	0.050
						D5	8201	3873	1	1213	0.050
E	Shopping mall 1	Berlin, Germany	Nexus	6	205×235	**E1**	1633	520	5	468	0.0016
						E2	14596	196	1	878	0.0030
						E3	3093	196	5	878	0.0030
						E4	1201	196	10	878	0.0030
F	Shopping mall 2	Tampere, Finland	Windows	6	160×139	**F1**	1887	205	1	326	0.0024
G	Shopping mall 3	Berlin, Germany	Nexus	3	175×160	**G1**	306	776	5	574	0.0068
						G2	3405	776	1	631	0.0075
						G3	796	776	5	631	0.0075
						G4	388	776	10	631	0.0075
H	Shopping mall 4	Tampere, Finland	Windows	3	152×123	**H1**	358	215	1	69	0.0012
						H2	512	11846	5	147	0.0026
I	Shopping mall 5	Tampere, Finland	Nexus	3	53×126	**I1**	1988	250	1	162	0.0081
						I2	373	250	5	162	0.0081
						I3	141	250	10	162	0.0081
J	Shopping mall 6	Klaukkala, Finland	Windows	1	96×50	**J1**	75	283	(not synthetic)	31	0.0065

[a] Each AP is identified by an individual MAC-address, but since some WLAN transmitters may have multiple MAC-addresses, some of the APs here can be at the same physical location.

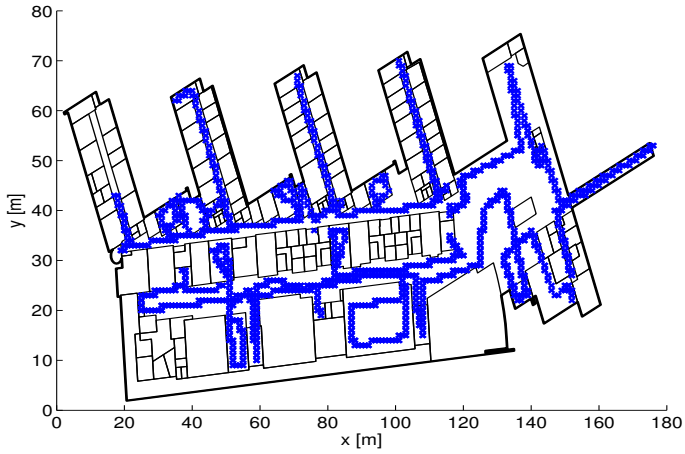

(a)

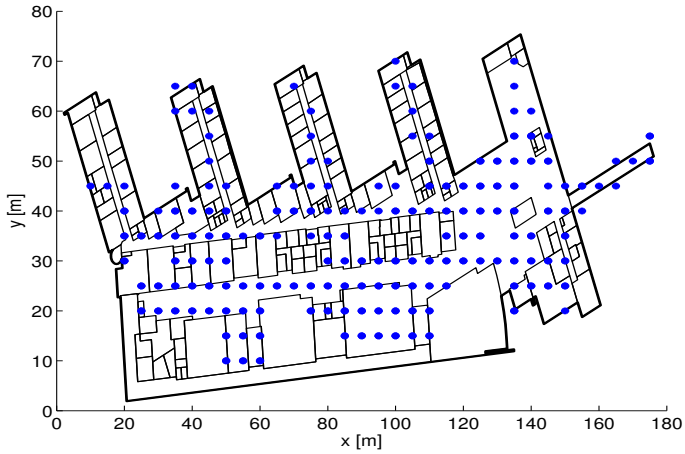

(b)

Fig. 7.1: *Examples of uniform grid intervals in building A with (a) $\Delta_{grid} = 1$ m (set-up A4) and (b) $\Delta_{grid} = 5$ m (set-up A5).*

the database size decreased, when compared to a case where all RSS values are saved as such. Another possibility would be to save only the latest measurement sample for each FP, but in this way the risk of saving an outlier would increase.

7.4 Performance measures

In this thesis, we use several performance metrics when comparing the results. The most used metric is mean distance error ε (see, e.g., [40, 57, 63, 86, 88, 104, 194, 241,

275,280,310,311,314,316,326,348]), that is calculated as the mean of Euclidean distances between the user location estimates $(\hat{x}_{MS}, \hat{y}_{MS}, \hat{z}_{MS})$ and the true user locations (x_{MS}, y_{MS}, z_{MS}) in three dimensional Cartesian coordinate system as

$$\varepsilon = \frac{1}{N_u} \sum_{u=1}^{N_u} \left(\sqrt{(x_{MS_u} - \hat{x}_{MS_u})^2 + (y_{MS_u} - \hat{y}_{MS_u})^2 + (z_{MS_u} - \hat{z}_{MS_u})^2} \right). \tag{7.1}$$

Besides this mean distance error, in some results it is more convenient to use other performance measure, such as standard deviation (std) of the distance error [102, 348]. In addition, median distance error [66, 241], Root Mean Square Error (RMSE) [83, 173] and percentage of distance errors of less than 5 meters are included in some results. One important metric is also floor detection probability (also called floor identification accuracy), that is calculated as the probability of correct floor estimation in the 3D position estimation and used as a performance metric, e.g., in [15, 208, 217, 218, 307, 310, 311]. The floor is chosen in this thesis according to the estimated z-coordinate of the position estimate, and choosing the closest floor to it.

7.5 Conclusions

In this chapter, we have presented the used cellular and WLAN measurement set-ups. We have also described the database update method and performance measures used in this thesis.

8. PROPOSED THEORETICAL BOUNDS IN WLAN-BASED POSITIONING

As it was discussed in Chapter 4, the existing transmitter configurations may not be suitable for positioning purposes, even if the number of transmitters is large, since the AP deployment inside a building is primarily optimized for communication and not for navigation purposes. In this chapter, we concentrate on the challenges and solutions related to the phase A presented in Fig. 4.1, namely the positioning architecture design. We tackle these challenges by calculating a CRLB-based criterion for RSS-based positioning. The proposed criterion can be used

- to choose the optimal AP density and the optimal AP topology in a WLAN network that is designed for localization needs or
- to estimate the expected accuracy bound in an existing WLAN network, based on its underlying AP topology or density.

Our results were also published in [180].

8.1 Proposed CRLB-based analysis

The number of transmitters (here, APs) in a building may be huge. Several APs located next to each others may carry redundant information for positioning purposes, while in some other parts of the building there may be lack of APs. Therefore, it is necessary to clarify the constraints of localization accuracy under a certain given AP configuration and to be able to make guidelines for the deployment planning if the AP topology can be revised for the navigation needs.

CRLB has previously been computed for the RSS-based PL positioning method in [351] and Received Signal Strength Difference (RSSD) based fingerprinting in [141].

In [257], the CRLB has been derived for the RSS-based localization in sensor networks, and further used to optimize the locations of anchor nodes in [270], but only in theory without real measurements. The effect of quantity and geometry of APs is studied shortly in [303], based on the computed CRLB for RSS measurements in WLAN network, but again, the studies are based on simulations and restricted number of APs only.

The difference to the studies of [141, 257, 270, 303, 351] and other studies of AP topology for positioning purposes found in the literature, e.g., [20, 61, 98, 103, 363], is that in our studies, the target is to determine a theoretical limit, that can be used both as a tool to understand the restrictions of an existing AP configuration and to provide guidelines for AP placing if the network can be primarily set up for localization needs. The presented criterion can show what is the best possible localization accuracy with the current AP deployment, and it can also predict what the positioning accuracy can be with increased number of APs. The results in this chapter are based both on measurements and theoretical derivations. We address both FP and PL methods.

The CRLB defines a lower bound on the variance of any unbiased estimator of an unknown parameter [163]. If the estimated receiver location is $\hat{\phi} = (\hat{x}_{MS}\ \hat{y}_{MS}\ \hat{z}_{MS})^T$, its covariance matrix is given by

$$Cov_{\phi}(\hat{\phi}) = \begin{bmatrix} \sigma^2_{\hat{x}} & \sigma_{\hat{x}\hat{y}} & \sigma_{\hat{x}\hat{z}} \\ \sigma_{\hat{y}\hat{x}} & \sigma^2_{\hat{y}} & \sigma_{\hat{y}\hat{z}} \\ \sigma_{\hat{z}\hat{x}} & \sigma_{\hat{z}\hat{y}} & \sigma^2_{\hat{z}} \end{bmatrix}. \tag{8.1}$$

We know that $Cov_{\phi}(\hat{\phi}) \geq \{I(\phi)\}^{-1}$ [163], where $I(\phi)$ denotes the Fisher matrix [163]:

$$I(\phi) = E\left[\left(\frac{\partial ln\, p(x;\phi)}{\partial \phi}\right)^2\right] = -E\left[\left(\frac{\partial^2 ln\, p(x;\theta)}{\partial^2 \theta}\right)\right]. \tag{8.2}$$

Here, the expectation operation E is calculated with respect to the likelihood function $p(x;\phi)$ and $p(x;\phi)$ stands for the PDF of observations $x;\phi$. By using Eqs. 8.1 and 8.2, the Fisher information matrix $I(\phi)$ can be computed as

$$I(\phi) = -\begin{bmatrix} \frac{\partial^2 p(x;\phi)}{\partial^2 x} & \frac{\partial^2 p(x;\phi)}{\partial x \partial y} & \frac{\partial^2 p(x;\phi)}{\partial x \partial z} \\ \frac{\partial^2 p(x;\phi)}{\partial y \partial x} & \frac{\partial^2 p(x;\phi)}{\partial^2 y} & \frac{\partial^2 p(x;\phi)}{\partial y \partial z} \\ \frac{\partial^2 p(x;\phi)}{\partial z \partial x} & \frac{\partial^2 p(x;\phi)}{\partial z \partial y} & \frac{\partial^2 p(x;\phi)}{\partial^2 z} \end{bmatrix}. \tag{8.3}$$

The used pdf in this paper is the Gaussian one, and we take into account the joint power (i.e., sum over all hearable APs):

$$p(x;\phi) = \sum_{r=1}^{N_r} \frac{1}{\sqrt{2\pi\sigma_r^2}} e^{\left(\frac{(O_r(x_{MS},y_{MS},z_{MS}) - P_{i,r}(x_i,y_i,z_i))^2}{2\sigma^2}\right)}. \tag{8.4}$$

PL model is chosen to be the one-slope log-distance model in Eq. (4.3). Thus, neglecting the noise terms, the observed power for the transmitter r (detected both in the FP and in the user measurement) by the receiver is $O_r(x,y,z) = P_{T_r} - 10n_r \log_{10} d$, where d is the distance between the unknown MS location (x_{MS}, y_{MS}, z_{MS}) and transmitter r location $(x_{TX_r}, y_{TX_r}, z_{TX_r})$ and $d_{i,r}$ is the distance between the fingerprint i (x_i, y_i, z_i) and the transmitter r location. Since

$$\begin{aligned} O_r - P_{i,r} &= P_{T_r} - 10n_r \log_{10} d - (P_{T_r} - 10n_r \log_{10} d_{i,r}) \\ &= -10n_r \log_{10}\left(\frac{d}{d_{i,r}}\right), \end{aligned} \tag{8.5}$$

the pdf is

$$p(x;\phi) = \sum_{r=1}^{N_r} \frac{1}{\sqrt{2\pi\sigma_r^2}} e^{\left(-\frac{\left(10n_r \log_{10}\left(\frac{d}{d_{i,r}}\right)\right)^2}{2\sigma_r^2}\right)}. \tag{8.6}$$

Using Eq. (8.6), the first derivative (derivatives marked with D for now on) of the diagonal elements of Eq. (8.3) with respect to x is

$$\begin{aligned} \frac{\partial\, ln\ p(x;\phi)}{\partial x} &= \mathrm{D}\left[\ln\left[\frac{1}{\sqrt{2\pi\sigma_r^2}} e^{\sum_{r=1}^{N_r} \frac{\left(-10n_r \log_{10}\left(\frac{d}{d_{i,r}}\right)\right)^2}{2\sigma_r^2}}\right]\right] \\ &= \mathrm{D}\left[ln\ 1 - ln(\sqrt{2\pi\sigma_r^2}) + \sum_{r=1}^{N_r} \frac{\left(-10n_r \log_{10}\left(\frac{d}{d_{i,r}}\right)\right)^2}{2\sigma_r^2}\right] \\ &= \mathrm{D}\left[\sum_{r=1}^{N_r} \frac{\left(-10n_{ap} \log_{10}\left(\frac{d}{d_{i,r}}\right)\right)^2}{2\sigma_r^2}\right] \\ &= \sum_{r=1}^{N_r} \mathrm{D}\left[\frac{\left(-10n_r \log_{10}\left(\frac{d}{d_{i,r}}\right)\right)^2}{2\sigma_r^2}\right] \\ &= \frac{1}{2\sigma_r^2} \sum_{r=1}^{N_r} \mathrm{D}\left[\left(-10n_r \log_{10}\left(\frac{d}{d_{i,r}}\right)\right)^2\right] \\ &= \frac{1}{2\sigma_r^2} \sum_{r=1}^{N_r} \mathrm{D}\left[\left(-10n_r \log_{10}\left(\frac{d}{d_{i,r}}\right)\right)^2\right] \end{aligned}$$

$$= \frac{1}{2\sigma_r^2}\sum_{r=1}^{N_r} 2\cdot(-10n_r)^2\cdot\log_{10}\left(\frac{d}{d_i}\right)\cdot \mathrm{D}\left[\log_{10}\left(\frac{d}{d_{i,r}}\right)\right]$$

According to the derivation rule for logarithm function and knowing that $d_{i,r}$ is not dependent on x, we get

$$\begin{aligned}\frac{\partial\, ln\; p(x;\phi)}{\partial x} &= \frac{1}{2\sigma_r^2}\sum_{r=1}^{N_r} 2\cdot(-10n_r)^2\cdot\log_{10}\left(\frac{d}{d_i}\right)\cdot\frac{1}{ln10}\cdot\frac{(x-x_{TX_r})}{d^2}\\ &= \frac{1}{\sigma_r^2\ln 10}\sum_{r=1}^{N_r}(-10n_r)^2\;\log_{10}\left(\frac{d}{d_{i,r}}\right)\frac{(x-x_{TX_r})}{d^2}\\ &= \sum_{r=1}^{N_r}\rho\;\log_{10}\left(\frac{d}{d_{i,r}}\right)\frac{(x-x_{TX_r})}{d^2},\end{aligned}$$

where $\rho = \frac{(-10n_r)^2}{\sigma_r^2\ln 10}$. Further on, the second derivative with respect to x is

$$\begin{aligned}\frac{\partial^2\, ln\;(x;\phi)}{\partial^2 x} &= \mathrm{D}\Big[\sum_{r=1}^{N_r}\rho\;\log_{10}\left(\frac{d}{d_{i,r}}\right)\frac{(x-x_{TX_r})}{d^2}\Big]\\ &= \sum_{r=1}^{N_r}\rho\cdot\left(D\left[\log_{10}\left(\frac{d}{d_{i,r}}\right)\right]\cdot\frac{(x-x_{TX_r})}{d^2}+\log_{10}\left(\frac{d}{d_{i,r}}\right)\cdot D\Big[\frac{(x-x_{TX_r})}{d^2}\Big]\right)\\ &= \sum_{r=1}^{N_r}\rho\cdot\left(\frac{1}{ln10}\;\frac{(x-x_{TX_r})}{d^2}\cdot\frac{(x-x_{TX_r})}{d^2}+\right.\\ &\quad\left.\log_{10}\left(\frac{d}{d_{i,r}}\right)\cdot\frac{(y-y_{TX_r})^2+(z-z_{TX_r})^2-(x-x_{TX_r})^2}{d^4}\right)\\ &= \sum_{r=1}^{N_r}\rho\cdot\left(\frac{1}{ln10}\;\frac{(x-x_{TX_r})^2}{d^4}+\right.\\ &\quad\left.\log_{10}\left(\frac{d}{d_{i,r}}\right)\cdot\frac{(y-y_{TX_r})^2+(z-z_{TX_r})^2-(x-x_{TX_r})^2}{d^4}\right)\end{aligned}$$

Since the expectation value for $\log_{10}\left(\frac{d}{d_{i,r}}\right)=0$, the latter part of the Eq. 24 equals 0 and thus, we get

$$\frac{\partial^2\, ln\; p(\xi;\phi)}{\partial^2\xi} = \sum_{r=1}^{N_r}\frac{\rho}{ln10}\;\frac{(\xi-\xi_{TX_r})^2}{d^4}, \tag{8.7}$$

where ξ is any of the x, y, z coordinates.

Further on, the computed CRLB can be utilized to calculate an optimal AP density in a building, when the AP deployment is adaptive. The following steps to this process are proposed:

1. Generate AP locations inside a 3D building, according to specific rules (e.g., uniform, rectangular, circular, or according to desired topology).

2. Generate the radiomap for training phase with randomly allocated measurement positions and the involved RSS according to the PL model in Eq. (4.3).

3. Generate random receiver positions or user tracks within the considered 3D building, e.g., via random walk model.

4. Based on the training data generated at Steps 1-3, compute the achievable CRLB for each desired scenario using Eq. (8.7).

5. Choose the configuration (e.g., number of APs per building area) that gives the lowest average CRLB, under a sufficient number of Monte Carlo simulations (in our simulations, we used 10000).

8.2 Measurement-based verification of the proposed CRLB-based criterion

In this section, we use measurement-based results to verify that the CRLB can be used to estimate the expected RSS-based positioning accuracy according to the AP deployment and density in a building. Both FP and PL approaches are addressed in the verification. For the FP method, we use probabilistic approach and the logarithmic Gaussian as the distance metric (see Section 4.1.2 and Table 4.1), since it offers the best results according to [139,241,291]. For FP method, also KNN-method of Eq. (4.7) is used, with $K = 5$, according to our results presented in [184] (see more in Section 4.1.2 and in [22,23,66,121,122,158,184,228,238,258,265,313,315,328]). For PL approach, we use one-slope path loss model of Eq. (4.3), and assume that the PL coefficient n_k for the kth AP remains constant within the distance between the transmitter and receiver. The noise std σ_k for each AP can be obtained from the measurements. Different WLAN measurement scenarios used here were described in detail in Chapter 7 and in Table 7.2.

Table 8.1: *Measurement results (see Table 7.2 for building details). For FP and PL, the results are calculated as std of the distance error.*

Building	CRLB [m]	FP (std) [m]	PL (std) [m]	AP density per m^2
A3	1.18	7.94	15.78	0.0082
B1	1.49	17.04	17.41	0.0083
C1	1.45	7.22	10.37	0.0131
D1	0.66	6.49	5.75	0.0395
E1	1.86	12.36	17.47	0.0016
F1	2.32	18.08	28.17	0.0024
G1	2.83	15.30	29.65	0.0068
H1	10.03	31.23	32.93	0.0012

Table 8.1 shows the CRLB, std of the distance error (see Section 7.4) for both FP and PL method and the AP density for several buildings. Based on Table 8.1, the following observations can be made:

- In general, the FP approach performs better than the PL method, and FP is also closer to the CRLB limit, as expected.
- In buildings with high AP density (e.g., A3, B1, C1 and D1), the CRLB is at most 1.5 meters.
- The smaller AP density (in buildings E1, F1, G1 and H1) results both as increased CRLB and higher positioning errors.
- In a multi-floor building with incomplete data (e.g., building H1), even the CRLB with unfiltered data rarely obtains sub 3 m accuracy. Additional filtering and sensor integration may indeed decrease the error.

8.3 Choice of AP density in flexible network topologies

In this section, we will show an example of how to use the CRLB as a benchmark to find out a sufficient AP density for the best achievable localization results, using a 2D simulation model (i.e., only one floor). The size of the simulated building is defined as x m $\times$ y m, where both x and y are varied randomly between 50-150. AP

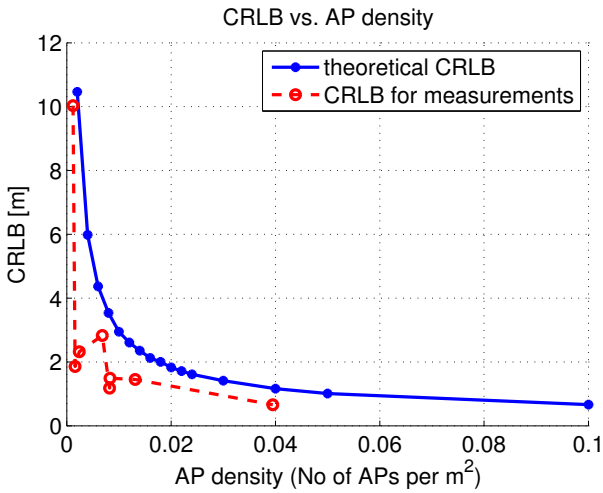

Fig. 8.1: *CRLB vs. AP density both for a simulated building (i.e., theoretical CRLB) and real measurements (same buildings included as in Table 8.1).*

density is fixed to desired value, but AP placings and receiver positions are defined randomly inside the simulated building according to uniform distribution. Fig. 8.1 illustrates the CRLB vs. AP density both for the measurements and for a simulated building. The results for simulated building are computed over 100 receiver locations and 10000 iterations, due to the randomizing. In the case of real measurements, the AP density is calculated as an average over all floors in the particular building. As it can be noticed in Fig. 8.1, the curves for CRLB vs. AP density for the measurements and for the simulations are close to each other. It can be also examined in Fig. 8.1 that exactly two meter positioning accuracy can be obtained with AP density of $0.018/m^2$ (i.e., by placing an AP for about every 7.5 m). Indeed, we can obtain sub-meter accuracy by placing an AP for every $\sqrt{10} \approx 3$ m, but placing them closer than this will not bring much benefit.

Besides the AP density, naturally also the AP deployment (i.e., AP placements) is important from the localization accuracy point of view. Therefore, an average Voronoi area is calculated between the estimated AP positions to show the impact of AP configuration. Fig. 8.2 shows one example of the Voronoi polygons for 4th floor of building C1. The polygons in Fig. 8.2 are drawn only inside the outer walls of the building, i.e., the polygons outside the building area are not taken into account. The AP locations are marked with red circles, Voronoi vertices with black dots, and the area of the polygon specified by the Voronoi vertices is determined with blue lines.

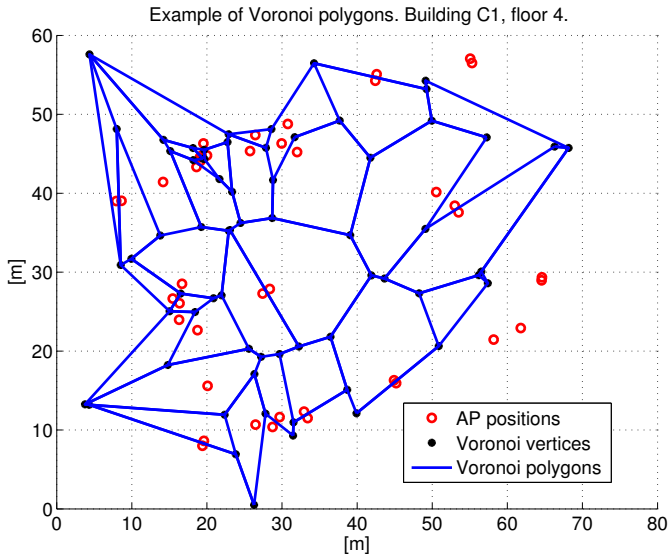

Fig. 8.2: *Illustration of the Voronoi polygon areas between the estimated AP locations. Building C1, 4th floor.*

The average area of blue polygons represent the average Voronoi area.

Fig. 8.3 shows an average Voronoi area (within the building limits) between the estimated AP positions for both the real measurements and for simulated building. As it can be noticed, both real measurements and theoretical (i.e., simulated) case are following the same trend: higher Voronoi area corresponds to to higher CRLB and small Voronoi area to small CRLB. The results in Fig. 8.3 verify that the CRLB-based criterion takes into account also the AP placements, not only AP density. The conclusion is that CRLB-based criterion is a powerful tool to predict the best possible localization results for a given AP configuration.

8.4 Conclusions

In this chapter, we have studied the challenge of the transmitter topology in indoor environment. We have presented a CRLB-based criterion, that can be used either to estimate the expected positioning accuracy limit in WLAN-networks with predefined topology or to find out the best AP density for a certain goal of positioning accuracy, in a network designed for localization. We have verified with measurement-based results the suitability of the presented CRLB criterion, addressing both FP and PL

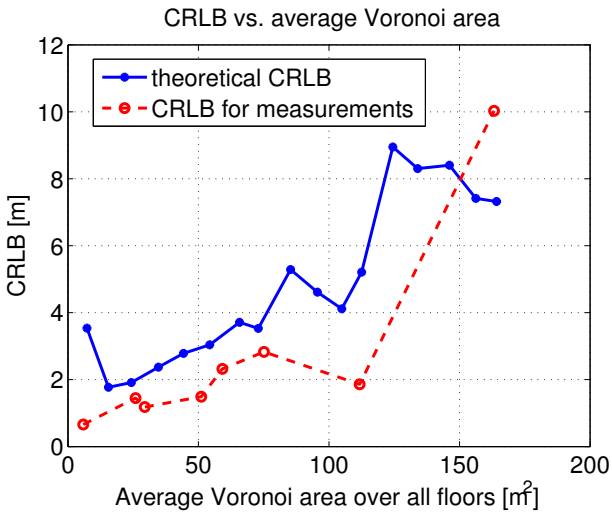

Fig. 8.3: *CRLB vs. average Voronoi area over all floors both for a simulated building and real measurements (same buildings included as in Table 8.1).*

positioning methods. We have explained how to use the CRLB and we have also shown that that the CRLB-based criterion considers not only AP density, but also the AP positions. The results we have shown here can provide more insight for designing an efficient WLAN-based localization environment and for evaluating existing WLAN AP deployments in the context of positioning accuracy.

The main contributions of this chapter can be summarized as follows:

- A CRLB-based criterion is presented, to be used as a benchmark to evaluate the AP topology in a building for positioning purposes.

The work in this chapter has also resulted in the following publication:

1. **Elina Laitinen** and Elena Simona Lohan, "Access Point topology evaluation and optimization based on Cramér-Rao Lower Bound for WLAN indoor positioning", in *Proc. of International Conference on Localization and GNSS (ICL GNSS)*, Barcelona, Spain, Jun 2016.

9. PROPOSED SOLUTIONS FOR TRAINING PHASE AND DATA TRANSFER IN WLAN AND CELLULAR POSITIONING

In this chapter, we propose solutions for the challenges related to the phases B and C presented in Fig. 4.1, namely the training phase and data transferring related challenges. As it was discussed in Chapter 4, many challenges in the training phase and in the data transferring have to be handled jointly, since, e.g., choice of the grid density and large databases affect both phases. As a reminder from Fig. 4.1, the solutions to address the challenges related to the phases B and C are:

- Propagation modeling for WLAN and cellular signals, both indoors and outdoors. This challenge is considered in this chapter, by proposing suitable path loss models for RSS-based localization systems with adequate shadowing modeling. The results were also published by us in [290].
- Appropriate choice of grid density. This challenge is discussed in this chapter, by illustrating the effect of grid density both to the positioning performance and database size, with three most widespread RSS-based positioning algorithms (FP, PL, WeiC).
- Data removal solutions to decrease the memory and bandwidth requirements for data transfer. In this chapter, the impact of AP selection on FP, PL and WeiC methods is studied with a variety of different removal criteria. We show that even 50% of the APs can be safely removed from the radiomap with a properly chosen removal criterion without increasing much the localization error. Our results were also published in [179, 181, 182].
- Compression methods [311]. This solution is not discussed in this thesis.

This chapter is organized as follows: in Section 9.1, we study the path loss and shadowing models and their parameters, for both cellular and WLAN signals. In

Section 9.2, we continue with a discussion of the database updates and choice of the grid interval, and in Section 9.3.1, we concentrate on database reduction solutions.

9.1 WLAN and cellular channel models

In this section, wireless propagation effects are studied for WLAN and cellular signals. The focus is especially in indoor environments, but also outdoor cases are considered. Our purpose is to analyze the path loss and shadowing models and their parameters, and clarify the differences and similarities between WLAN and cellular wireless propagation models, such as whether RSS fluctuations (e.g., shadowing and fading effects) are system dependent or can be modeled with similar path-loss models for all the envisaged systems.

9.1.1 Path loss parameter estimation

The results shown in this section are based on measurements with both WLAN and cellular signals described in Chapter 7. The path loss coefficient $\hat{n}$ and the apparent transmit power $\hat{P}_T$ (mean and std) are estimated using first-order polynomial regression and omni-directional one-slope path loss model of Eq. 4.3. An example of the linear regression is shown in Fig. 9.1. Since the transmitter positions are not known beforehand, they were estimated in the analysis using WeiC based techniques (see Eq. (4.9) and [31]).

Tables 9.1, 9.2, 9.3 and 9.4 show the approximated path loss coefficient $\hat{n}$ (mean, std and maximum) and the apparent transmit power $\hat{P}_T$ (mean and std), for different measurement scenarios and for WLAN signals indoors (for floorwise measurements in Table 9.1 and for 3D measurements in Table 9.2) and 2G and 3G signals outdoors, respectively. In the beginning of these studies, we had the measurements only separately for different floors, and therefore, the parameters were estimated in the first place for the floorwise case only in 2D (Table 9.1). These floorwise results, that we have presented in [290], are here completed with 3D measurements (Table 9.2). WLAN signals outdoors were noticed to be generally too weak to draw any conclusions, and therefore, they were left out from the comparison here. Only those transmitters that were detected in at least 10 measurement points were considered in the

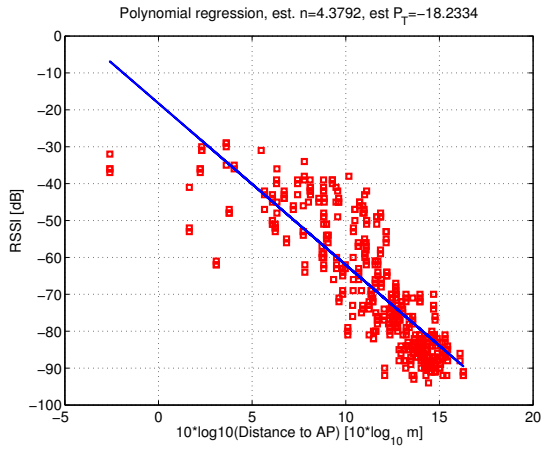

Fig. 9.1: *An example of linear regression for estimating $\hat{n}$ and $\hat{P}_T$.*

Table 9.1: *Estimated path loss parameters for WLAN signals indoors. Floorwise measurements only. Std stands for standard deviation.*

Set-up	Mean $\hat{n}$	Std $\hat{n}$	Max $\hat{n}$	Mean $\hat{P}_T$ [dBm]	Std $\hat{P}_T$ [dB]	N_{AP} / floor (detected)
A1, 1st floor	2.49	1.89	10.3	-50.13	25.36	190
A1, 2nd floor	2.50	2.02	11.8	-49.73	29.84	205
B1, 1st floor	1.38	1.02	4.5	-62.88	19.43	244
B1, 2nd floor	1.43	1.08	5.4	-64.14	18.89	331
F1, 2nd floor	1.42	1.27	4.7	-66.35	24.20	158
F1, 3rd floor	1.25	1.42	7.6	-69.63	24.79	188
H1, 1st floor	1.61	1.03	4.2	-59.01	23.25	64
J1, 1st floor	1.94	1.28	4.0	-52.73	25.57	31
mean	1.75	1.38	6.6	-59.33	23.92	176

analysis. According to our results shown in [290], where the AP location estimates were compared to the true locations, such approximation is reasonable.

In the case of floorwise WLAN measurements (Table 9.1), the estimates for $\hat{n}$ were computed floor-by-floor, and $\hat{n}$ represents the two-dimensional path loss exponent. Due to the floor losses, the $\hat{n}$ may be different in 3D environment, i.e., when examining the RSS values also in z-direction. Therefore, also the 3D case was taken into account (Table 9.2). When comparing the results of WLAN indoor signals (Tables 9.1 and 9.2), it can be seen that the averages of estimated $\hat{n}$ and $\hat{P}_T$ are very sim-

Table 9.2: *Estimated path loss parameters for WLAN signals indoors. 3D measurements.*

Set-up	Mean $\hat{n}$	Std $\hat{n}$	Max $\hat{n}$	Mean $\hat{P}_T$ [dBm]	Std $\hat{P}_T$ [dB]	N_{AP} / building (detected)
A5	1.67	0.77	3.1	-56.25	12.44	509
B3	2.25	1.01	4.3	-46.40	16.14	489
C3	2.11	1.16	5.4	-53.36	16.19	727
D3	1.63	0.88	4.2	-58.88	11.74	1213
G3	1.20	0.85	4.2	-59.22	15.78	631
H2	1.70	1.02	4.2	-52.87	19.95	147
I2	1.33	0.84	3.4	-63.81	14.09	162
mean	1.70	0.93	4.1	-55.83	15.19	554

Table 9.3: *Estimated path loss parameters for 2G signals indoors.*

Set-up	Mean $\hat{n}$	Std $\hat{n}$	Max $\hat{n}$	Mean $\hat{P}_T$ [dBm]	Std $\hat{P}_T$ [dB]	N_{BS}
$2G_1$	1.73	0.85	4.82	-28.81	23.37	47
$2G_2$	0.79	0.81	3.26	-65.05	19.26	21
$2G_3$	2.19	1.91	8.71	-19.04	51.17	77
$2G_4$	1.73	1.51	10.08	-26.67	49.76	81
mean	1.61	1.27	6.72	-34.89	35.89	57

Table 9.4: *Estimated path loss parameters for 3G signals indoors.*

Set-up	Mean $\hat{n}$	Std $\hat{n}$	Max $\hat{n}$	Mean $\hat{P}_T$ [dBm]	Std $\hat{P}_T$ [dB]	N_{BS}
$3G_1$	1.25	0.76	2.98	-51.76	26.56	29
$3G_2$	1.03	1.11	3.14	-60.83	33.18	7
$3G_3$	1.37	0.76	3.88	-46.73	22.77	77
mean	1.22	0.88	3.33	-53.11	27.50	38

ilar in both cases, but the estimates for $\hat{n}$ vary more between different measurement scenarios in the case of floorwise measurements. Also, the estimated $\hat{P}_T$ in the floorwise case is slightly lower. This is expected, since when the estimations were done floor-by-floor, some of the detected APs may be located in some other floor, resulting as lower estimated value for the apparent transmit power. Fig. 9.2 illustrates

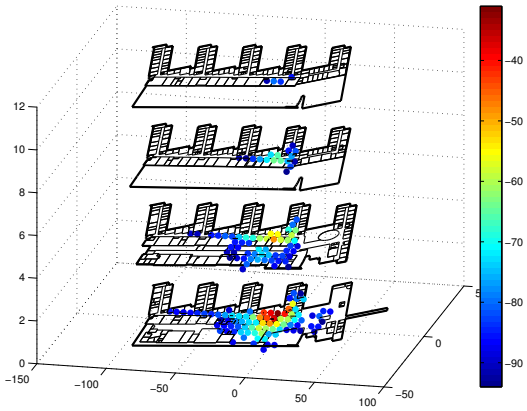

Fig. 9.2: *An example of RSS values for one AP in different floors. Measurement set-up A1.*

this, by showing the RSS values for one AP in building A in different floors (set-up A1). However, as an interesting conclusion, it seems clear that PL models can be calculated as 3D omnidirectional models in multi-floor buildings, and additional floor losses are not needed. For outdoor cellular cases (Tables 9.3 and 9.4), the average for $\hat{n}$ is close to the estimate for WLAN signals in the case of 2G, and slightly lower for 3G case. The estimated $\hat{P}_T$ is on average higher for 2G than for 3G and WLAN cases. The number of transmitters in total is clearly smaller for the cellular networks when compared to the WLAN cases, and this may affect the statistics.

9.1.2 Shadowing modeling

Shadowing effect was studied with two different approaches: fixed point measurements and path loss-based. Assuming that the measurement errors remain the same, the shadowing effect can be seen in fixed point measurements as the fluctuations in the observed RSS values. Thus, for kth transmitter, shadowing part Ψ_k (in dB) can be modeled as

$$\Psi_k = P_k - \mathbf{E}(P_k), k = 1 : N_{TX} \tag{9.1}$$

where $\mathbf{E}(\cdot)$ is the expectation operator, estimated here as the mean. The mean RSS values versus the std of the shadowing part (std(Ψ_k) in indoor environment are illustrated in Fig. 9.3, for WLAN, 2G, and 3G signals, respectively. As it was detailed in Chapter 7, the fixed point measurements were gathered in various indoor locations in several different towns, and the number of scenarios was 43 for WLAN signals, 15

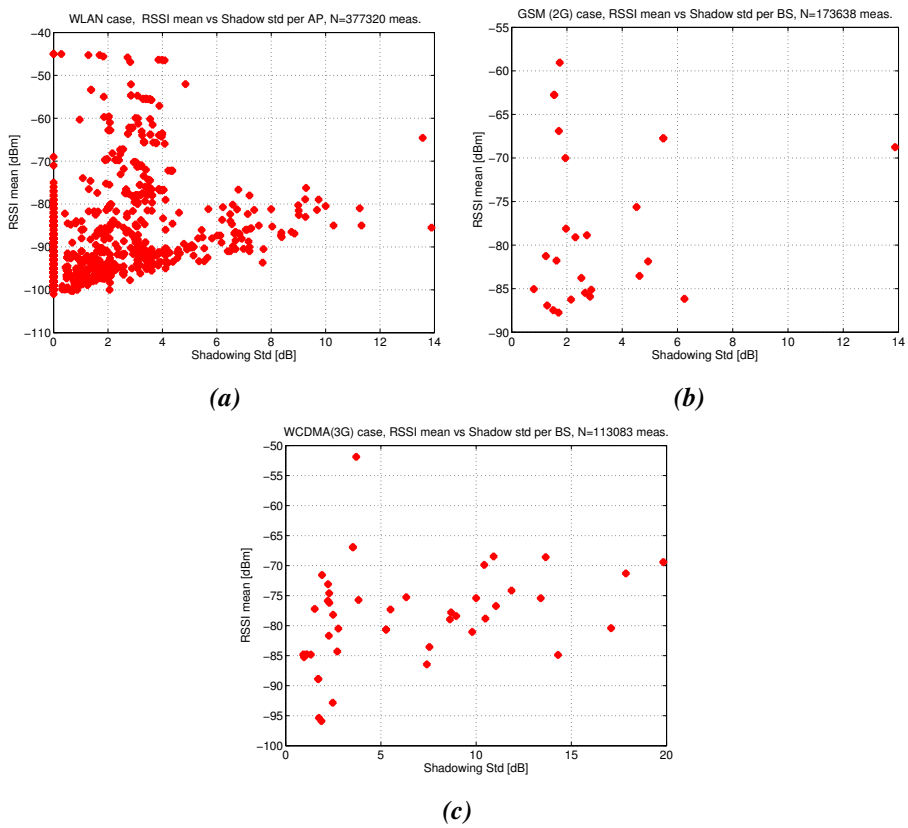

Fig. 9.3: *Mean RSS versus the std of the shadowing, with fixed point measurements indoors. (a) WLAN, (b) 2G and (c) 3G signals.*

for 2G cellular signals, and 19 for 3G signals. Each point in the figures corresponds to one transmitter in a measurement scenario. Since the amount of measurements for WLAN case is higher, and since the number of detected 2G or 3G BSs indoors is lower than the number of detected WLAN APs, Fig. 9.3 (c) has more points. Based on the Fig. 9.3, it can be noticed that the shadowing std is not dependent on the signal strength. In other words, a signal received closer to the transmitter and a signal received further away from the transmitter are likely to be affected similar shadowing fluctuations. We also noticed that shadowing fluctuations in 2G and WLAN networks had a std always below 14 dB, while for the 3G case the shadowing std can be as high as 20 dB. The mean values are presented in Table 9.5.

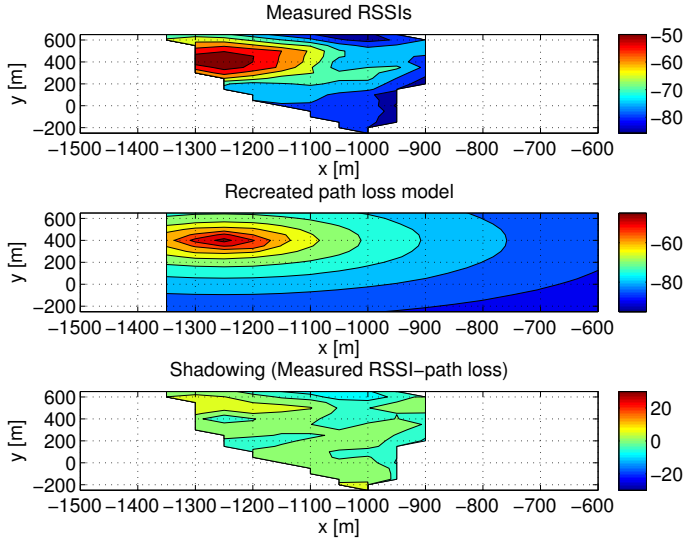

Fig. 9.4: *An example of the three steps in shadowing analysis. 2G data, outdoors.*

Besides fixed point measurements, shadowing effect was studied also based on the following methodology:

1. Path loss parameters and transmitter location were estimated as in Section 9.1.1.

2. Based on the estimated parameters and the path loss model in Eq. (4.3), the power map was re-created.

3. The re-created power map was subtracted from the original power map, to form the shadowing part. The mean and std are further calculated from the residual shadowing part.

The three steps are illustrated in Fig. 9.4.

Table 9.5 presents results for the shadowing analysis, for both fixed point and path loss based approach. The analysis was performed for WLAN signals indoors and cellular signals both indoors and outdoors. In the case of path loss based approach and floorwise WLAN measurements, the average is calculated over the scenarios A1 (first and second floors), B1 (first and second floors), F1 (second and third floors), H1 (first floor) and J1 (first floor). In the case of path loss based approach and 3D WLAN measurements, the the average is calculated over the scenarios A5, B3, C3, D3, G3,

Table 9.5: *Average std of shadowing [dB] for WLAN and cellular signals. Both fixed point measurements and path loss based approach.*

	Fixed point approach		Path loss based approach	
	Indoor	Outdoor	Indoor	Outdoor
WLAN (floorwise)	1.94	-	6.40	-
WLAN (3D)	-	-	4.47	-
2G	3.15	-	-	5.14
3G	6.08	1.53	-	6.42

H2 and I2. In the case of 2G and 3G measurements, the averages are calculated over all 2G/3G scenarios (see Table 7.1).

When examining Table 9.5, it can be seen that the average std of shadowing with path loss based approach is $4.47 - 6.42$ dB. In fixed point measurements, the values are slightly smaller. One explanation for this is that there is not enough spatial variability in the fixed point measurements data, as the number of measurement locations is remarkably less when compared to hundreds of spatial positions in the path loss based approach. The results for path loss based approach also include the std of model mismatch and not only shadowing part. In other words, in path loss based approach, the shadowing value shown in Table 9.5 consists of both the true shadowing std and std of the path loss modeling errors.

9.2 The choice of the grid interval

Another relevant questions related to database forming concerns the grid density. As it was mentioned in Section 4.2, increasing the grid interval Δ_{grid} will decrease the number of FPs in the database, but too loose FP density may decrease the positioning results. Higher FP density can improve the positioning accuracy, but only up to certain limits. Unnecessarily dense grid results as highly correlating FPs and increased amount of data to be saved. Fig. 9.5 shows the mean distance error (see Section 7.4) versus Δ_{grid} for four different buildings, when fingerprinting approach is used. As it can be seen, in some buildings (e.g., buildings D and G) the best results are achieved with $\Delta_{grid} = 1$ m, while for some other (e.g., buildings C and I), 5 m grid

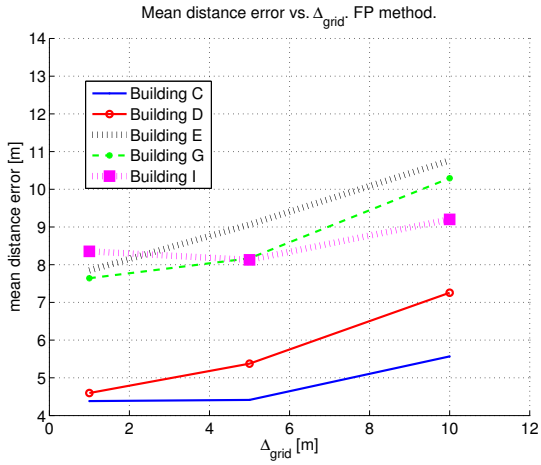

Fig. 9.5: *Mean distance error vs. Δ_{grid}, for 5 different buildings. Fingerprinting approach with logarithmic Gaussian likelihood.*

interval gives as good results as 1 m grid interval. This may be caused, e.g., by the AP configuration in the building or by the measurement collection process.

Fig. 9.6 illustrates the number of FPs for different grid resolutions for the same buildings. Based on Figs. 9.5 and 9.6, it is clear that the grid density has to be carefully planned, since the difference between the amount of stored data may be huge, but the improvement in the mean distance error for smaller Δ_{grid} very small, if any. The discussion of the grid interval effect in different positioning approaches is continued also in the next section, because the grid interval is also related to data reduction solutions. Some other studies on the grid size can be found, e.g., in [328].

9.3 Database reduction solutions

As it can be seen in Table 7.2 and as it will be discussed more in Chapter 10, the APs infrastructure is very dense in many buildings. For example, we can have hundreds or even more than one thousand MAC-addresses detected in buildings of up to only 0.048 km^2 area. Both the number of transmitters and the number of FPs can be significant, and this leads to big amount of data for the localization approaches to deal with. The memory requirements for the database in large areas or with many buildings may become overwhelming, and also data transmission may become a bottleneck for the positioning system, especially for FP method. In addition, not all

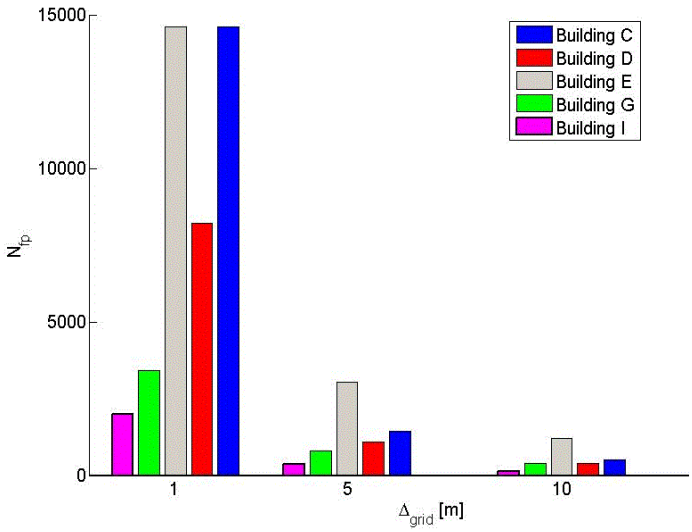

Fig. 9.6: *Illustration of the N_{fp} vs. Δ_{grid}, for 5 different buildings.*

available information is needed in localization. With such high density of APs in many buildings, some APs are more significant than others and the irrelevant APs can be simply seen as noise [99, 177]. This holds for, e.g., WLAN transmitters supporting multiple Basic Service Set Identifiers (BSSID), meaning that several MAC addresses can be heard from exactly the same transmitter. Typically, the AP infrastructure inside a building is optimized primarily for communication targets, such as serving many users in the best possible way. For this reason, multiple APs can be placed next to each other, and since RSS is dependent on the distance between the mobile and an AP, as well as on the environment, these closely located APs may transmit heavily correlated RSSs. Thus, all APs do not carry relevant information for localization needs, and the unnecessary and redundant APs can be dropped from the estimation process, in order to decrease the storage demands and computational complexity of the localization system [100]. Besides with AP selection and reduction, the size of the training database can be decreased by increasing the Δ_{grid}, as was illustrated in Section 9.2.

In this section, we study the impact of AP selection and removal, on three different positioning algorithms (FP, PL, WeiC), taking into account also the effect of chosen Δ_{grid}. The positioning approaches for FP and PL are the same than described in Section 8.2. For WeiC method, the position estimate is calculated as Eq. (4.9) and

Eq. (4.10). AP selection has been previously studied, e.g., in [62, 101, 104, 176, 199, 229, 344, 359, 365], but the AP selection together with the grid interval and with several positioning approaches has not been addressed before. AP selection can be done in the online positioning phase [104, 176, 365], in the offline training phase [62, 344, 359], or by taking into account both phases [182, 229]. In this section, we describe the used selection methods and we continue with AP selection, first in the training phase and secondly in the estimation phase.

9.3.1 AP selection criteria

In what follows, we investigate seven different criteria to choose the most relevant APs in the offline training phase for all three positioning algorithms. Both traditional selection methods, i.e., max-mean [344] and InfoGain [62], are taken into account. With all selection criteria presented in-what-follows, excluding MIMO selection, any reduction percentage is possible: e.g., 5%, 10%, or 55% out of all detected APs can be removed from the training database, i.e., the removal percentage is chosen adaptively. In MIMO selection, however, the number of APs located next to each others is building dependent: we use the AP deployment as it is, and therefore, it varies between the buildings how many APs are co-located and removed with the MIMO removal criterion. The studied criteria are:

1. No selection

   - In this criterion no selection is performed, but all APs are stored in the radiomap. The results obtained with no selection are used in the comparison as a benchmark to understand better the effect of AP selection.

2. Maximum RSS (maxRSS)

   - In this criterion, APs with maximum RSS value are chosen to form the AP subset. This method is similar with max-mean of Youssef et al. in [344], but the difference is that only the maximum RSS instead of the average RSS is considered when sorting the APs. The reason for this is that we have noticed maxRSS to have similar or slightly better performance than max-mean algorithm [182].

3. Entropy / InfoGain

   - In this criterion, so-called entropy of RSS is computed for ever AP, and the APs with maximum entropy are selected to form the AP subset. This criterion is based on Info gain in [62], with only slight modifications. The entropy used in this paper is defined in the following manner, by using an analogy with the definition of the classical entropy [341]:

$$E_k = max\left(\mathbf{P_k} log_2\left(\mathbf{P_k}\right)\right), \tag{9.2}$$

   where $\mathbf{P_k}$ includes the RSSs of kth AP in vector form, i.e.,

$$\mathbf{P_k} = [P_{1,k} P_{2,k} \ldots P_{N_{fp(k)},k}]. \tag{9.3}$$

4. MIMO (or multiple BSSID) selection

   - As already discussed, it is possible that one WLAN AP has several BSSIDs (i.e., transmissions with multiple MACs coming from the same physical location). The target of this selection criterion is to avoid to use correlated data, that the closely located or similar APs may provide. In our research, these kind of MIMO APs (or any other APs containing several MACs) are identified only based on their estimated location: if more than one AP are estimated to be located within maximum one meter range, only one among them is chosen. One meter was chosen to allow also estimation errors in AP location estimation. The unknown AP positions are estimated as in Eq. (4.9). Three different selection options are examined here: only one (according to the maximum average RSS), two or three APs among the co-located ones will be kept. Removal percentage is naturally the highest in the first case, where only one AP is chosen. We remark that the total number of APs located at the same place depends on the AP infrastructure of the building.

5. FFT

   - FFT transform can extract the information about spectral content of a image. If AP patterns are considered as a image, FFT can be used to show the the most relevant APs. In a FFT-based criterion, the AP subset is selected according to the spectral content calculated in FFT domain. The

FFT is computed over a matrix, that contains a RSS-dependent information of every AP in each FP (i.e., size of the matrix is $N_{TX} \times N_{fp}$). If an AP is heard in a FP i, the RSS-dependent information is computed as $P_{i,k} + P_{th}$. P_{th} is a threshold, that is selected here based on an assumption that the lowest expected RSS is -100 dB, and thus, $P_{th} = 100$ (in order to have positive values at the FFT input). If an AP is not detected in the particular fingerprint, the RSS input is set to 0. After the FFT is performed over the information matrix, the APs are sorted in a descending order, according to their maximum value in the FFT-matrix.

6. KL

   - Kullback-Leibler (KL) criterion is chosen to one selection criterion, due to its ability to measure the difference between two probability distributions. In this criterion, we calculate a divergence value for each AP based on the RSS levels, by using the Kullback-Leibler (KL) criterion for divergence. By KL analogy, we define a D_{KL} matrix; $D_{KL} = [d_{a,b}]_{a,b=1..N_{TX}}$, where

$$d_{a,b} = \sum_a \sum_b |P_a - P_b| \, log(|P_a - P_b|). \tag{9.4}$$

   The APs with highest KL divergence value are chosen to form the AP subset.

7. Dissimilarities

   - Another possible criterion is based on dissimilarities between APs. In this criterion, we build a dissimilarity matrix according to the RSS differences between any pair of APs, as below:

$$\mathbf{D_{Diss}} = \begin{bmatrix} 0 & |\bar{P}_1 - \bar{P}_2| & ... & |\bar{P}_1 - \bar{P}_{N_{TX}}| \\ |\bar{P}_2 - \bar{P}_1| & 0 & ... & |\bar{P}_2 - \bar{P}_{N_{TX}}| \\ & ... & ... & \\ |\bar{P}_{N_{TX}} - \bar{P}_1| & |\bar{P}_{N_{TX}} - \bar{P}_2| & ... & 0 \end{bmatrix} \tag{9.5}$$

   where $\bar{P}_k$ is the average RSS detected from kth AP. Further on, we compute an independent dissimilarity value for each AP as a sum over the dissimilarities between the particular AP and all other APs. AP subset is then formed based on the maximum dissimilarity value.

Besides the criteria listed in here, we tested also average RSS, variance of RSS, number of points (where the target was to emphasize more those APs with higher coverage area by sorting APs in descending order based on the number of fingerprints where an AP is detected) and random AP selection (used only as a benchmark). Some results were published by us in [182]. Since none of these additional criteria provided very promising results, they were left out from the comparison here.

9.3.2 AP selection in the training phase

The positioning results for AP selection are presented in this section as mean distance error (see Section 7.4). For FP method, also KNN-method is used, with $K = 5$, according to our results presented in [184]. Fig. 9.7 shows the mean distance error for the seven studied AP selection criteria for buildings C3, D3 and I2, with $\Delta_{grid} = 5$ m and with all three positioning methods. The percentage of removed APs from the training database varies between $10\% - 80\%$, excluding the MIMO selection. For MIMO criterion, the number of removed APs is varied so that either one (with the maximum average RSS value), two or three APs were kept out of the closely located APs (within 1 m range). When we keep only one AP, the removal percentage is the highest compared to the case when we remove two or three APs.

According to the results shown in Fig. 9.7, the main observations are:

- For FP method, APs can be removed up to $50 - 60\%$, but after that, the performance starts to decrease faster.
- PL method is very robust to AP selection and also to removals with high percentage.
- WeiC method is very sensitive to AP selection and only 20% of the APs can be removed safely without deteriorating the results.
- Removing APs using MIMO AP selection criteria and and keeping only one AP among the subset of co-located APs does not increase the positioning error in the case of FP and PL methods. However, the number of MIMO APs is clearly building dependent, and therefore the percentage of removed APs may vary between only few percent and even 60%.
- The best AP selection criteria for PL and WeiC methods are maxRSS and KL.

- In the case of FP method, the best criterion is more building-dependent. Up to 50% removal, the differences in the results between different removal criteria are very small. If more than 50% of the APs are removed, maxRSS seems to be the most consistent among different buildings. This conclusion is based on Fig. 9.7, the results obtained for other buildings and our studies presented in [179, 182].

It was also noticed based on Fig. 9.7 that in the case of the PL approach, removing APs may be better than keeping all. The reason for this is probably in the parameter estimation process. For example, by considering maxRSS criterion, the transmitters with high RSS values probably have the parameter estimates closer to the true ones, when compared to the transmitters for which the maxRSS values are clearly lower. Thus, the positioning performance can be increased, when only these "good" APs are saved in the radiomap and used in the estimation process.

Figs. 9.8 illustrate the effects of both AP removal and grid interval Δ_{grid} as mean distance errors, again for all three positioning approaches and choosing maxRSS-selection criterion. Δ_{grid} is varied between $1-20$ m and the removal percentage between $10-80\%$. We remark that the color bars are different for each figure. The reason for this is that the results variate in the case of WeiC so widely (between $10-55$ m), that the much smaller variation for FP (between $5-15$ m) would not be visible anymore if the same color bar was used for all figures. In addition, Table 9.6 shows the mean and median distance errors and RMSE in meters for several buildings, both without any AP selection and with a 50% removal using maxRSS criterion. Based on Figs. 9.8 and Table 9.6, the following conclusions can be drawn:

- As was noticed already in Fig. 9.7, FP and PL methods are more robust to AP removal also with higher removal percentages, but according to Fig. 9.8, the grid interval clearly affects more.

- Both FP and PL methods can handle the 50% data removals. Based on Table 9.6, the mean distance error for the FP approach is increased by only about 8% with the maxRSS-based removal criterion, when compared with the case without any removal. For PL method, the mean distance error is increased by about 6% with the maxRSS-method.

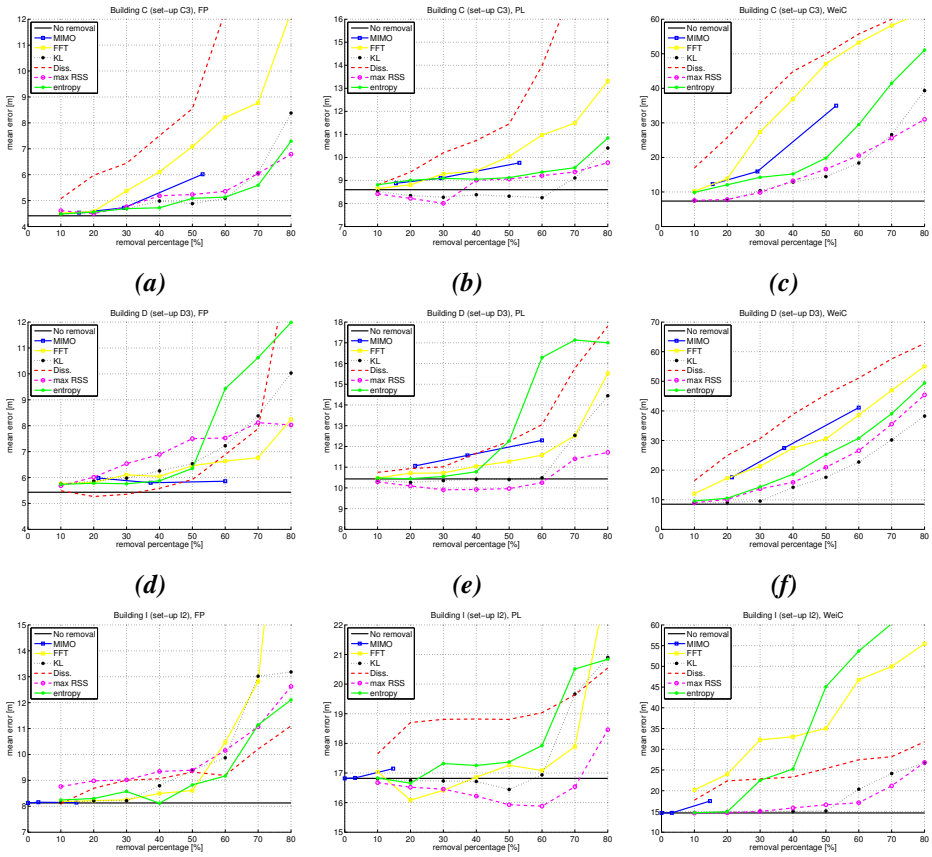

Fig. 9.7: *Mean distance error [m] for all AP selection criteria. FP, PL and WeiC positioning approaches. Building C3 (**a,b,c**), building D3 (**d,e,f**) and building I2 (**g,h,i**), all with* $\Delta_{grid} = 5$ *m.*

- WeiC method is very sensitive to AP selection, but grid interval affects only slightly to the accuracy.
- In general, the positioning accuracy for FP method is clearly better than for PL and WeiC.

Based on the results shown in this section, we cam make the following recommendations, in order to maintain the performance loss to less than 10% of the maximum achievable performance with no AP removal and $\Delta_{grid} = 1$ m:

- For FP method, we recommend $\Delta_{grid} = 5$ m and a maximum 50% AP removal

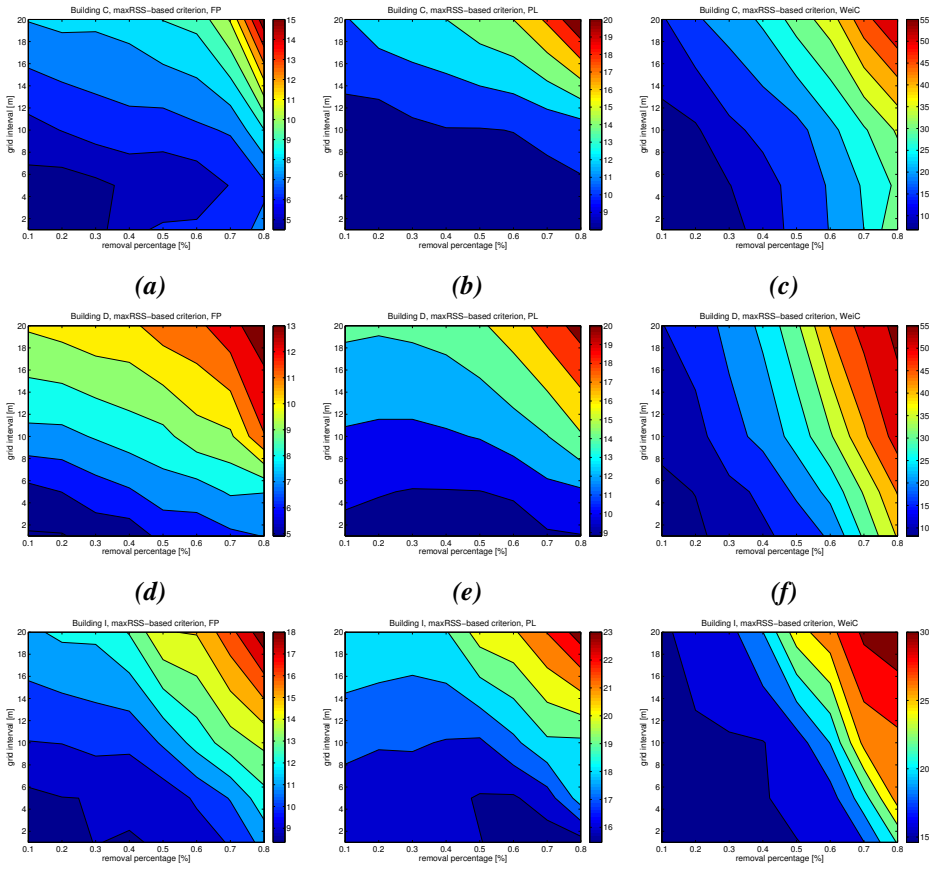

Fig. 9.8: *Effects of joint AP removal and grid size for building C3 (**a,b,c**), building D3 (**d,e,f**) and building I2 (**g,h,i**) in mean distance error. FP, PL and WeiC positioning approaches with maxRSS-selection criterion.*

with maxRSS-based criterion.

- For PL method, we recommend $\Delta_{grid} = 5$ m and a maximum 60% AP removal with maxRSS-based criterion.

- For WeiC method, we recommend $\Delta_{grid} = 10$ m and a maximum 20% AP removal with maxRSS-based criterion.

Table 9.6: *Results for several buildings and measurement set-ups,* 50% *removal. Mean and median distance errors and RMSE, all presented in meters.*

	Building	Criteria	mean error [m]	median error [m]	RMSE [m]
FP	A3	No removal	5.87	3.11	8.55
		maxRSS 50%	6.00	3.99	8.48
	B1	No removal	9.33	7.59	11.96
		maxRSS 50%	9.77	8.08	12.50
	C1	No removal	4.01	3.59	4.54
		maxRSS 50%	4.92	4.33	5.60
	E1	No removal	7.40	6.44	8.51
		maxRSS 50%	8.04	7.16	9.27
	H1	No removal	17.47	13.58	23.69
		maxRSS 50%	18.47	13.22	25.27
PL	A3	No removal	9.74	8.21	11.76
		maxRSS 50%	10.06	8.77	12.06
	B1	No removal	9.01	7.38	12.45
		maxRSS 50%	9.39	7.44	12.69
	C1	No removal	6.09	5.87	6.75
		maxRSS 50%	6.99	7.26	7.73
	E1	No removal	11.05	9.08	13.16
		maxRSS 50%	12.07	10.26	13.77
	H1	No removal	20.46	19.51	23.77
		maxRSS 50%	20.22	19.31	23.48
WeiC	A3	No removal	10.53	9.71	12.65
		maxRSS 50%	12.99	10.96	16.21
	B1	No removal	8.53	7.29	10.31
		maxRSS 50%	10.19	7.11	13.88
	C1	No removal	6.10	6.18	6.66
		maxRSS 50%	17.00	13.28	20.74
	E1	No removal	10.06	8.66	11.65
		maxRSS 50%	28.42	20.36	39.30
	H1	No removal	26.59	25.42	30.23
		maxRSS 50%	27.17	24.95	31.26

9.3.3 AP selection in the estimation phase

Since the amount of transmitters can be clearly limited in the training phase, it begs the question of whether it is advantageous to limit also the detected transmitters to be used in the position estimation phase. Fig. 9.9 presents the mean distance error

in different buildings (buildings C3, D3, G3 and I2, all with $\Delta_{grid} = 5$ m), when only the part of detected APs in the estimation phase are chosen, according to the highest RSSs. Based on Fig 9.9, the following observations can be drawn:

- For FP approach (Fig. 9.9 (a)), it can be concluded that minimum required number of transmitters is around 10. If only three transmitters are used instead of 10, the positioning error would increase approximately 37%.
- In the case of PL approach (Fig. 9.9 (b)), the differences between different number of used APs are smaller. In general, the results improve slightly when all detected APs are not used for the position calculation. According to results shown in Fig. 9.9 (b), the best choice is typically between $7-10$ APs. However, if only 3 APs are used in the estimation phase, the positioning accuracy deteriorates only 5% when compared to the results obtained with 7 APs. Thus, PL method performs very well also when APs are limited in the estimation phase. This would decrease the amount of transmitted data and save out the memory space needed to re-create the database.
- In WeiC approach (Fig. 9.9 (c)) the best results are achieved when at least 10 APs are considered in the estimation phase. Similarly with PL approach, also with WeiC, the differences are small between different number of used APs. In general, when compared to the the results obtained with 10 APs, we would get approximately 8% increase in the positioning error.
- As a conclusion, the number of used APs in the estimation phase can be limited to decrease the complexity without decreasing the performance with PL and WeiC approaches. With FP method, limiting in the estimation phase is possible, but only up to 10 APs, in order not to deteriorate the positioning results.

9.4 Conclusions

In this chapter, we have concentrated on the challenges and solutions related to phases B and C in Fig. 4.1. We have studied the the path loss and shadowing effects in cellular and WLAN wireless channels both outdoor and indoor environments. We have

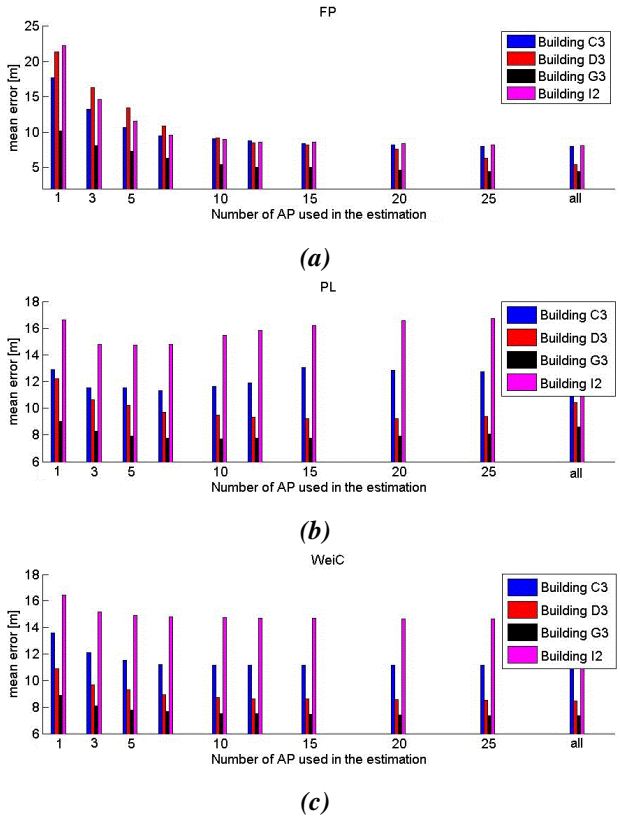

Fig. 9.9: *AP selection in the estimation phase. (a) FP, (b) PL and (c) WeiC approaches. Buildings C3, D3, G3 and I2.*

shown that WLAN and GSM have similar RSS shadowing fluctuations, but for 3G case, standard deviations of shadowing are typically larger. The obtained results are useful for wireless positioning algorithms, especially for PL based approaches. Indeed, we try to solve the challenge of large databases by studying the effects of grid interval and AP selection to different methods. We have compared several different AP removal criteria and concluded that the maxRSS-based criterion provides consistently the best results in the majority of indoor scenarios. We have also shown that in the case of FP method, 50% of the APs can be removed safely from the radiomap with a properly chosen selection criterion without increasing much the positioning error, but decreasing the database size remarkably (database sizes are discussed more in Chapter 10). The expression 'safely' means here that the performance deterioration after 50% AP removal is no more than 8% from the performance where all AP are kept. In addition, we have shown that the studied low-complexity method

WeiC is very sensitive to AP selection, while PL method is very robust also to high percentage reduction. If the grid size is increased to 5, the performance for every positioning method (with no removal) in general remains still less than 6% away from the performance with 1 m grid interval. In Chapter 10 we will show how the choice of an appropriate grid interval and data removal solutions can significantly decrease the number of parameters in the training database needed especially for FP method.

The main contributions of this chapter can be summarized as follows:

- An analysis of wireless propagation effects of WLAN and cellular signals, based on indoor and outdoor measurements.
- A discussion of the database updates and effect of grid interval.
- An extensive analysis of the effect of grid interval and AP selection, with various selection criteria, and for three positioning approaches (FP, PL and WeiC).

The work presented in this chapter has also resulted in the following four publications:

1. Shweta Shrestha, **Elina Laitinen**, Jukka Talvitie and Elena Simona Lohan, "RSSI Channel Effects in Cellular and WLAN positioning", in *Proc. of 9th Workshop on Positioning Navigation and Communication (WPNC)*, Dresden, Germany, Mar 2012, pp. 187-192.
2. **Elina Laitinen**, Elena Simona Lohan, Jukka Talvitie and Shweta Shrestha, "Access Point Significance Measures in WLAN-based Location", in *Proc. of 9th Workshop on Positioning Navigation and Communication (WPNC)*, Dresden, Germany, Mar 2012, pp. 24-29.
3. **Elina Laitinen** and Elena Simona Lohan, "Are all the Access Points necessary in WLAN-based indoor positioning?", in *Proc. of International Conference on Localization and GNSS (ICL GNSS) 2015*, Gothenburg, Sweden, Jun 2015.
4. **Elina Laitinen** and Elena Simona Lohan, "On the Choice of Access Point Selection Criterion and Other Position Estimation Characteristics for WLAN-Based Indoor Positioning", in *MDPI Sensors*, vol. 16 (5), May 2016.

10. PROPOSED RSS-BASED POSITIONING SOLUTIONS

In this chapter, we propose solutions for the challenges related to the phase D presented in Fig. 4.1, namely the estimation phase. The challenges include the decisions regarding which positioning method to use and how to detect the floor in 3D indoor positioning, but also how the possible RSS offsets between the training and estimation phases affect the positioning result. The solutions to address these challenges are:

- Study of bias effects and calibration needs. An extensive study different offsets due to lack of calibration is presented in this chapter. We show that certain amount of offsets can be easily tolerated without any calibration. Our results are published also in [183].
- Calibration methods [110, 168, 216, 325], data fusion methods [209] and clustering methods [60, 63, 76, 86, 142, 214, 269, 344]. These solutions are not studied in this thesis.
- Good choice of the positioning algorithm. This challenge is partly covered in this chapter, by comparing FP, PL and WeiC approaches in terms of database requirements and positioning accuracy. Parts of the results are also published by us in [181].
- Floor detectors. We propose in this chapter a low-complexity floor detection algorithm to decrease the amount of data to be transferred to the mobile. We show that this novel floor detection algorithm much less complex than FP approach, but offers 31% better floor detection probability than the traditional low-complexity approaches.

The chapter is organized as follows: in Section 10.1, the effect of an offset in the RSS values between the training and estimation phases is examined. In Section 10.2, we

continue with the comparison of different RSS-based positioning algorithms in terms of complexity. Finally, our proposal of a novel floor detector is presented in Section 10.3.

10.1 Resistance to biases and calibration methods

Several different phenomena may result as fluctuations or an offset in the RSS values. Naturally, if the RSS that is saved to the database in the training phase differs significantly from the RSS of the user device in the real-time localization phase, the positioning accuracy may be degraded. An offset can be caused for example, by different equipment type, which is especially true in crowd-sourced data collection and is most likely seen as a constant positive or negative bias. Indeed, temporal propagation dynamics such as user orientation, body losses in more or less crowded period during the training phase compared with the estimation phase can result as random bias. One possible reason for offsets is also environmental changes between the two phases, that can be seen as localized bias. A localized bias can be caused also by only partly updated FP database.

It is generally known, that a bias between the RSS values in the training and estimation phases caused by different equipment or environmental changes can decrease the positioning accuracy. For this reason, both calibration techniques and different calibration-free positioning algorithms have been proposed, e.g., in [110, 168, 169, 216, 325]. Indeed, some studies present how different equipment measures the RSSI, e.g., [157, 212]. This was illustrated also in Fig. 4.3. Even $25-30$ dBs differences in RSSs for different devices have been reported [83, 110, 157]. However, research on the offsets and their impact on the positioning accuracy exists in the literature only in some limited studies. In [64], the effect of three dynamic factors (relative humidity level, people presence and movements, and open/closed doors) to the WLAN positioning accuracy was studied shortly, but the research was limited into one corridor only with very few APs and the amount of the RSS offset is not specified or studied at all. Also in [320], where the positioning performance of different devices in the same environment was studied, the indoor environment was limited to two corridors of one-floor only.

In this section, we study extensively the effect of an offset between the RSS values in the training and estimation phases for WLAN-based positioning. We address fin-

gerprinting estimation method and show the effect of different bias types and values. Our results clarify how much a constant or a random bias affects the positioning results and what is the amount of bias that is still reasonable in terms of positioning accuracy. All the results are based on measurements in several multi-floor buildings (as detailed in Table 7.2). Solutions for calibration methods are not proposed in this thesis, but various calibration methods from the literature are discussed shortly in the end of this section.

10.1.1 The effect of a RSS offset

When studying the effect of a bias between the RSS values (in dBm) in the training and estimation phases, a bias b is artificially added to the original measured RSS $P_{i,k}$ (see Eq. (4.1)) in the FPs. Thus, the FPs are formed now as

$$\left\{ x_i, y_i, z_i, \{k, \tilde{P}_{i,k}\} \right\}, k \in 1 : N_{TX}, i \in 1 : N_{fp}, \tag{10.1}$$

where $\tilde{P}_{i,k} = P_{i,k} + b$. Three models of this artificially added bias are adopted: either a constant one, a random one or a localized constant bias, where a RSS offset occurs just for a certain part of the FPs for every floor. A localized bias is illustrated in Fig. 10.1, where all FPs are shown for three floors of building A (set-up A1). The blue crosses represent the positions of the FPs without a RSS bias and magenta dots represent the positions of the FPs with additional RSS bias. In this example, a bias occurs for 30% of the FPs. The areas with a bias are created by choosing first randomly one FP and then adding a bias to the RSS levels for all APs detected in this FP and every neighboring FP within 20 m range [310]. Then, the next FP is chosen randomly and a new area with the RSS bias is created. This is continued as long as the chosen percentage (e.g., 30%) of the FPs with a RSS bias is filled.

In what follows, the positioning results are presented as mean distance error, floor detection probability and percentage of distance errors of less than 5 m (see Section 7.4). Floor detection possibilities are discussed more in Section 10.3. In our analysis, both constant bias was analyzed by varying the amount of a bias between -30 dB and $+30$ dB and random bias was analyzed by varying the amount of a bias between -50 dB and $+50$ dB. In the position estimation, we used again the probabilistic fingerprinting with logarithmic Gaussian likelihood as the distance metric (see Section 4.1.2 and Table 4.1) together with KNN-method ($K = 5$) of Eq. (4.7). The noise

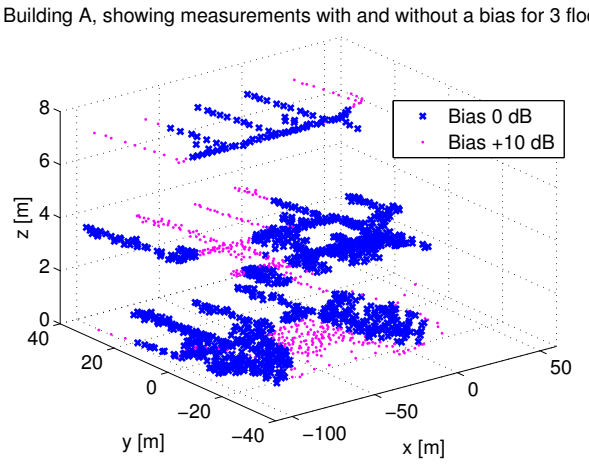

Fig. 10.1: *Illustration of a localized bias for 3-floors of the building A (set-up A1).*

variance σ_z (see Table 4.1), that represents both shadowing and measurement error effects, was assumed to be equal for all APs and was chosen to be $\sigma_z = 4.47$ dB, according to the average shadowing variance observed in WLAN indoor channels in Section 9.1. In addition, results for $\sigma_z = 10$ dB are presented by us in [183]. For the cases of random bias and localized bias, all of the results are averaged over 1000 random iterations.

The mean distance error, the floor detection probability and the percentage of distance errors are shown in Tables 10.1, 10.2 and 10.3, respectively. In each table, the first row (i.e., bias $b = 0$) shows the results without any offset and it is kept in the comparison as a reference. Several data scenarios from Table 7.2 are included, and the results are shown with various constant bias values, with two different scenarios of random bias and with two different scenarios of localized bias. For the random bias, the amount of bias was selected randomly according to uniform distribution, and the two cases are following:

1. The amount of a bias was varied between -10 dB and $+10$ dB (case 1).
2. The amount of a bias was varied between -50 dB and $+50$ dB (case 2).

For the localized bias, the cases are following:

1. The bias is set up to be -10 dB for 50% of the FP database and $+10$ dB for the rest 50% (case 1).

2. +10 dB bias occurs in 70% of the FPs, and 30% of the FPs are without any bias (case 2).

When studying the Tables 10.1-10.3, it can be seen that the negative constant bias $b = -10$ dB deteriorates the results less than the positive constant bias $b = +10$ dB. The averaged mean distance error over all of the data scenarios with $b = -10$ dB increases 17% in general, when compared to the reference case (bias $b = 0$). The effect for the averaged percentage of distance errors of less than 5 m is at the same level (i.e., decrease of 20%), but the floor detection probability decreases only slightly (-2.6% in general). With $b = +10$, the averaged mean distance error increases even more than 50%, and the averaged percentage of distance error and the averaged floor detection probability decrease with 35% and 9%, respectively. For constant bias of higher than $+/-10$ dB, the results start to deteriorate faster. The same conclusions can be drawn also based on Fig. 10.2, that shows the CDF of absolute distance error for measurement set-ups A1, E1, F1 and G1, for constant biases of $b = +/-10$ dB, $b = +/-20$ dB and $b = +/-30$ dB, random bias case 1 and localized bias case 1.

Similar results as for the constant bias of $+/-10$ dB are obtained also for the two localized bias cases, where either two different biases ($+/-10$ dB) are covering the whole building (i.e., localized bias, case 1) or a bias of 10 dB occurs in some part of the building only (i.e., localized bias, case 2). In the case of the random bias, a different uniformly distributed random bias either between -10 dB and $+10$ dB (case 1) or between -50 dB and $+50$ dB (case 2) was added for every heard AP in every FP. As it can be seen in Tables 10.1-10.3, the smaller random bias (i.e., case 1) affects the results very little, if any. Both the mean distance error and the floor detection probability are at the same level for every building, and also the percentage of distance errors is decreased only by about 4.7 meters on average. For case 2 of random bias, the results are deteriorated clearly more, being approximately at the same level than with constant bias $b = +/-30$ dB.

Based on the Tables 10.1-10.3, the following general observations can be made:

- A negative constant bias of -10 dB increases the mean distance error less than 20% in general, but a positive constant bias of $+10$ dB affects more (the averaged mean distance error increases more than 50%).

- The results seem to be building dependent, i.e., in buildings with high number

Table 10.1: *Mean distance error [m].*

Bias b [dB]	A1	A2	B1	C1	D1	E1	F1	G1	H1	mean
0	3.9	5.6	9.4	4.1	3.3	7.3	9.9	8.4	16.1	7.6
-10	5.7	7.0	8.9	5.9	3.3	10.3	11.2	10.9	16.9	8.9
$+10$	5.5	8.8	15.8	4.5	4.7	11.0	16.1	13.6	27.0	11.9
-20	16.0	17.9	20.8	12.3	6.5	23.7	19.4	18.8	35.4	19.0
$+20$	12.4	16.6	32.0	8.0	9.0	16.4	23.1	23.7	45.7	20.8
-30	25.8	36.8	47.9	15.9	12.1	76.1	36.3	62.3	46.4	40.0
$+30$	23.5	32.4	46.6	13.1	15.5	42.8	27.5	44.9	51.4	33.1
Random, case 1	4.1	5.9	9.7	4.3	3.4	7.4	10.4	9.0	17.3	7.9
Random, case 2	28.0	32.4	40.5	11.8	11.1	49.3	28.1	34.02	38.7	30.4
Localized, case 1	6.2	8.1	11.9	5.5	4.0	10.9	12.8	12.2	21.3	10.3
Localized, case 2	5.2	7.7	13.0	4.8	4.5	9.0	13.6	11.9	22.5	10.2

Table 10.2: *Floor detection probability [%].*

Bias b [dB]	A1	A2	B1	C1	D1	E1	F1	G1	H1	mean
0	94.9	97.8	90.3	91.1	87.4	88.1	89.3	87.9	91.6	90.9
-10	91.1	93.4	92.6	90.6	86.7	91.2	74.6	83.8	92.6	88.5
$+10$	86.1	88.4	74.4	88.0	81.8	86.9	67.3	78.0	97.2	83.1
-20	66.5	69.1	61.4	64.4	46.9	64.4	42.4	61.0	88.8	62.8
$+20$	67.7	62.4	44.9	69.4	51.0	82.9	47.3	53.9	94.0	63.7
-30	52.5	47.0	36.9	55.8	31.5	30.4	28.8	27.2	81.4	43.5
$+30$	60.8	42.5	56.8	39.4	37.1	57.1	37.1	27.3	65.1	47.0
Random, case 1	93.2	97.8	90.3	90.5	88.0	88.1	86.6	87.4	90.6	90.3
Random, case 2	54.0	29.7	43.8	30.9	22.7	26.6	32.9	39.3	92.1	41.3
Localized, case 1	87.0	91.0	82.1	86.3	81.6	85.4	72.6	79.8	93.0	84.3
Localized, case 2	87.8	92.0	78.9	86.2	81.0	86.3	76.5	79.8	90.2	84.3

Table 10.3: *Percentage of distance errors less than 5 m [%].*

Bias b [dB]	A1	A2	B1	C1	D1	E1	F1	G1	H1	mean
0	74.3	50.2	30.0	71.5	83.9	34.1	23.7	27.9	16.5	45.8
-10	59.3	42.1	33.8	42.3	77.9	23.4	18.9	22.9	10.4	36.8
$+10$	51.9	28.9	15.3	63.3	62.2	16.6	10.7	9.7	7.8	29.6
-20	11.8	8.1	16.9	6.9	44.0	3.4	4.1	9.6	1.3	11.8
$+20$	17.9	4.2	5.6	31.3	19.8	5.3	1.4	4.9	0.2	10.1
-30	0.0	0.1	0.6	4.1	8.4	0.0	1.0	0.4	0.5	1.7
$+30$	6.4	0.0	1.1	8.6	9.2	0.5	2.1	0.9	0.9	3.3
Random, case 1	71.6	47.5	24.9	69.7	83.0	31.7	16.2	18.4	6.7	41.1
Random, case 2	0.0	0.0	0.0	0.0	1.4	0.0	0.0	0.0	0.0	0.2
Localized, case 1	41.8	28.0	8.1	48.4	77.5	6.0	6.2	2.4	0.6	24.3
Localized, case 2	56.0	28.6	12.5	60.1	66.4	11.5	6.3	4.6	1.0	27.4

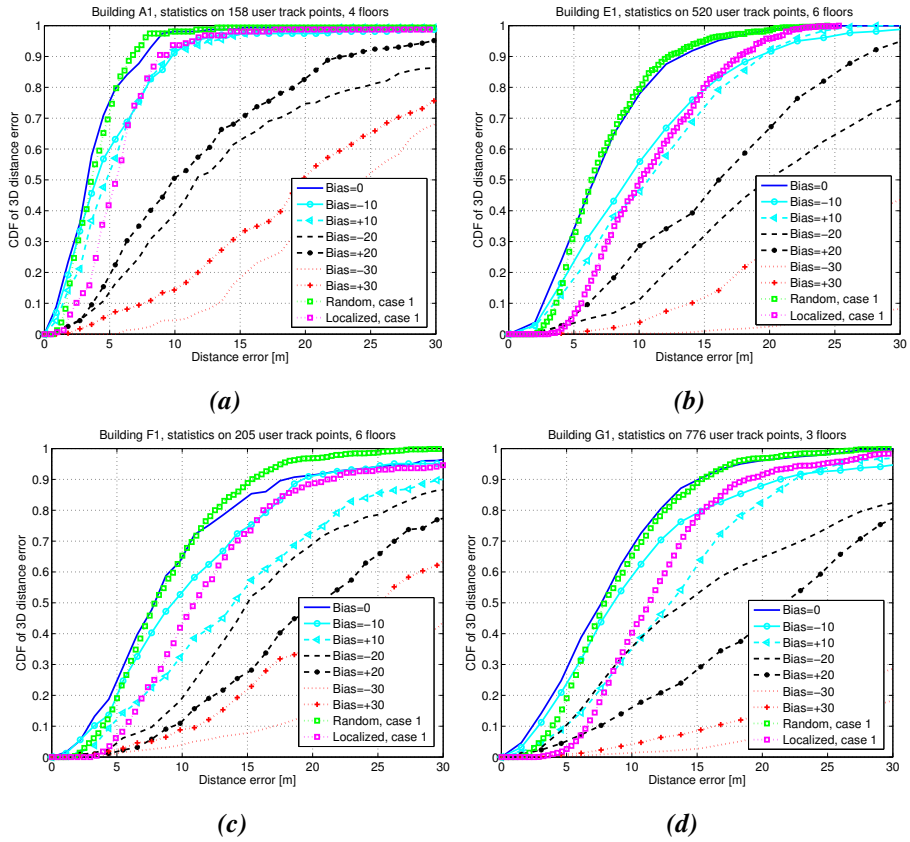

Fig. 10.2: *CDF of absolute distance error for buildings and set-ups (a) A1, (b) E1, (c) F1 and (d) G1.*

of APs and FPs, the positive bias may give as good results as negative bias (e.g., buildings A1 and C1).

- Random bias between -10 dB and $+10$ dB affects the results very little, if any (less than 4% deterioration in mean distance error in general).
- Both cases of localized bias increase the mean distance error with around 35%.

The results obtained in this section are partly different than the results for higher shadowing variation $\sigma_z = 10$ dB presented by us in [183], where we noticed that both constant or random biases between -20 dB to $+10$ dB covering either the whole building or only parts of it, can be easily tolerated in indoor environments. This is natural, since when the shadowing is smaller, the effects of the possible offsets become more visible.

10.1.2 Calibration methods

Though small RSS offsets (i.e., less than $-/+10$ dB) can be neglected, in some cases the offset is larger and calibration is needed in order to compensate the effect of more or less constant RSS variations to the positioning accuracy. Calibration or mitigation methods are widely studied in the literature, see for example [65, 87, 92, 124, 168, 169, 216, 254, 320, 325]. Different devices with different chipsets scale the measured RSS values to RSSIs with various equations and steps, as was shown in Fig. 4.3. In some cases the observed RSS values can be linear, as was noticed in [124, 131, 168], but due to chipset sensitivity, antenna spacings, antenna gains and operating systems, linearity is not a guarantee [110, 198, 325].

Calibration can be performed either in offline phase, as for example in [124, 168, 320] or in online phase, as for example in [65, 339]. In the offline calibration, measurements are collected from a variety of devices (e.g., using crowdsourcing) to find an appropriate signal mappings for each equipment type. The drawback with this is that a large dataset is required to able to calculate the mapping models. Alternatively, the measurement database can be based on only one device, and the mapping to another device types is performed before the localization phase, in an offline phase called a learning period [124, 168]. This learning period can be automatic or manual [124].

In online phase, the mapping or adaptation is done simultaneously with the estimation phase. [140] proposes to use the differences of signal strengths instead of absolute RSS values in the FP database. Another example is to use only RSSI ratios, where one transmitter and corresponding RSS in the measurement is selected and the rest RSSs in the data sample are divided by this chosen RSS. This type of RSS relation approach, that does not need a separate calibration phase, is used for example in [65, 169].

An interesting alternative to online adaptation is to use so-called test rank based method proposed in [216], where the detected transmitters in the measurement are sorted according to their RSS values. The order of the transmitters forms the so-called ranking vector, and in the positioning phase, only these ranking vectors of the FP and the mobile are compared. Similar approach is also presented in [339]. However, also in these approaches, it is assumed that the order of the sorted RSS values is the same between different devices. More discussion on different calibration schemes can be found, e.g., in [131].

10.2 Complexity comparison of FP, PL and WeiC approaches in WLAN networks

In this section, the comparison of different RSS-based positioning approaches is considered in terms of complexity, that is measured in terms of database size and simulation times in WLAN networks. Though database size and simulation time are not highly used as complexity measures, the number of needed parameters (i.e., the database size) as a complexity measure is adequate, when the idea is to compare the amount of data to be transferred between the server and the mobile with different algorithms. In addition, when it is difficult to calculate other computational complexity measures, simulation or computation time is used, as, e.g., in [215, 269]. Also more advanced computational complexity measures, such as number of operations (see, e.g., [347]), are possible.

Table 10.4 shows the total number of parameters needed to be stored for the training radiomap for all three positioning methods. Three different buildings with different Δ_{grid} are included as examples with numeric values, since the total number of parameters is naturally building dependent. Besides the building size and layout, also the measurement collection (i.e., if the whole building is covered or not) and the number of detected APs affects the total number of parameters. For FP, the number of parameters is the sum of parameters per fingerprint, i.e., the fingerprint coordinates (x_i, y_i, z_i), the AP index or identifier k and the measured power for the kth AP $P_{i,k}$ for each hearable AP in the particular fingerprint i. Since the number of heard APs may vary from one fingerprint to another, the number of parameters may be different for different fingerprints. Indeed, the number of parameters needed for FP positioning is remarkably decreased, if the grid interval is increased and thus, the number of fingerprints is smaller, as illustrated in Fig. 9.6 and as can be seen in Table 10.4 as well. In the case of PL and WeiC positioning approaches, the number of parameters is not dependent on grid size, but only on the amount of available transmitters. For PL, all we need is the AP positions (x_{TX}, y_{TX}, z_{TX}) for each AP, and an AP identifier together with AP dependent PL parameter estimates (here, transmit power P_{T_k} and path loss coefficient n_k). For WeiC, the number of parameters is even less, namely the AP identifier and positions only.

It can easily be noticed, that the motivation for using PL and WeiC approaches is in the amount of stored data and their ability to offer statistical solutions for large

Table 10.4: *Number of the parameters needed to be transmitted for different positioning methods. Examples for buildings C, D and I, with* 1 *m,* 5 *m and* 10 *m grid intervals.*

Building	FP	PL	WeiC
	$\sum_{i=1}^{N_{fp}}(3+\sum_{m=1}^{N_{TX}(i)}2)$	$N_{TX}\times 6$	$N_{TX}\times 4$
C2	$N_{C2}=1091029$	4362 ($\approx 0.4\%$ of N_{C2})	2908 ($\approx 0.3\%$ of N_{C2})
C3	$N_{C3}=171090$	4362 ($\approx 2.5\%$ of N_{C3})	2908 ($\approx 1.7\%$ of N_{C3})
C4	$N_{C4}=76074$	4362 ($\approx 5.7\%$ of N_{C4})	2908 ($\approx 3.8\%$ of N_{C4})
D2	$N_{D2}=1196629$	7278 ($\approx 0.6\%$ of N_{D2})	4852 ($\approx 0.4\%$ of N_{D2})
D3	$N_{D3}=225246$	7278 ($\approx 3.2\%$ of N_{D3})	4852 ($\approx 2.1\%$ of N_{D3})
D4	$N_{D4}=104682$	7278 ($\approx 7.0\%$ of N_{D4})	4852 ($\approx 4.6\%$ of N_{D4})
I1	$N_{I1}=90542$	972 ($\approx 1.1\%$ of N_{I1})	648 ($\approx 0.7\%$ of N_{I1})
I2	$N_{I2}=23025$	972 ($\approx 4.2\%$ of N_{I2})	648 ($\approx 2.8\%$ of N_{I2})
I3	$N_{I3}=10483$	972 ($\approx 9.3\%$ of N_{I3})	648 ($\approx 6.2\%$ of N_{I3})

areas. In FP method, the number of FPs may be very large and the data that we save for each FP usually contains more than ten variables. E.g., if in a certain FP i the number of heard APs is 18, we need to save 39 parameters for this one fingerprint only: 3 parameters for the FP coordinates, 18 for RSSs and 18 for the AP indexes. In the PL-based approach with one-slope model, we only need to store 5 parameters per transmitter. Thus, with PL approaches, it is possible to save even up to 11 times in the database size [291] when compared to the FP approach. Moreover, PL models can be easily used to predict the RSS values in areas where the data is missing with interpolations and extrapolations. The drawback of PL models is that, in general, these approaches have slightly worse positioning accuracy when compared to FP, due to the modeling inaccuracies, as we showed in Section 9.3.1 via WLAN measurements. In order to be able to calculate the AP positions and PL parameter estimates, the full radiomap is still needed for PL and WeiC approaches as well, though the amount of transmitted data is remarkably decreased.

Different positioning methods are also compared in terms of time consumption in Table 10.5 for buildings C and D, with two different Δ_{grid} lengths. The time is calculated over all user measurements (i.e., $N_u = 250$), with $\Delta_{grid} = 1$ m and $\Delta_{grid} = 5$ m. The idea is to compare the time consumption of different methods with all data included, and also if 50% of the database were removed. It can be seen that the FP

Table 10.5: *Performance comparison via algorithm time consumption [s] for* 250 *user measurements. All positioning methods included, with no AP selection and* 50% *AP removal. Buildings C and D, with both* 1 *m and* 5 *m grids.*

Building		FP	PL	WeiC
Building C2	No removal	$t_1 = 1483$ s	$0.10 \times t_1$	$1.1 \times 10^{-5} \times t_1$
	50% removal	$0.81 \times t_1$	$0.07 \times t_1$	$1.1 \times 10^{-5} \times t_1$
Building C3	No removal	$0.18 \times t_1$	$0.10 \times t_1$	$1.1 \times 10^{-5} \times t_1$
	50% removal	$0.17 \times t_1$	$0.06 \times t_1$	$1.1 \times 10^{-5} \times t_1$
Building D2	No removal	$t_2 = 2472$ s	$0.08 \times t_2$	$7.0 \times 10^{-6} \times t_2$
	50% removal	$0.82 \times t_2$	$0.06 \times t_2$	$7.0 \times 10^{-6} \times t_2$
Building D3	No removal	$0.23 \times t_2$	$0.08 \times t_2$	$7.0 \times 10^{-6} \times t_2$
	50% removal	$0.13 \times t_2$	$0.05 \times t_2$	$7.0 \times 10^{-6} \times t_2$

method is clearly slower than other methods, due to more complex pattern matching algorithm and big data matrices in the radiomap. When the grid size is increased to 5 m, the time consumption for FP is decreased remarkably, even more than 80%. We can also notice that the difference between FP and PL methods is clearly smaller with 5 m grid. For PL approach, 50% data removal slightly decreases the time consumption. WeiC algorithm, that uses only AP positions in the estimation and is very fast algorithm, is not basically affected by the decrease in the number of APs. Indeed, the grid interval affects the time consumption of the PL method only slightly, if any, and is not affecting the time consumption of WeiC at all, since the number of parameters for these methods remains the same for all grid intervals, as was seen in Table 10.4. Based on the results shown in Tables 10.4 and 10.5, it can be concluded that with an appropriate length of Δ_{grid} and AP selection methods presented in Chapter 9, the complexity of FP method can be decreased remarkably.

10.3 Floor detection

One important aspect in indoor positioning is the floor detection. The position estimation in a multi-floor building can be performed either directly in 3D mode, or alternatively estimate first the correct floor and then calculate the position estimate in 2D in the chosen floor. In this section, we propose a novel low-complexity floor detection algorithm. We show that the proposed algorithm outperforms the other low-

complexity methods in terms of floor detection probability, but is not as complex as FP approach.

10.3.1 Possible floor detection algorithms

Many positioning algorithms can be used to estimate the position directly in 3D. In these cases, e.g., in FP approach, the floor can further be decided according to the position estimate. If no KNN method is used, the best FP in the building tells also the floor estimate (or z-coordinate, respectively). If KNN is used, and the chosen FPs are located in different floors, the floor can be estimated by simply mapping to the closest one. The traditional low-complexity methods for positioning, and also for floor detection, are centroid (Cen) [47] and WeiC [40, 88, 200, 208, 304, 326] algorithms. In Cen, the idea is to use only the estimated (or known) transmitter locations, and calculate the user position only as a centroid over the detected transmitters. In WeiC, the idea is the same, but a weighting factor is included to emphasize more, e.g., the transmitters with higher RSS level. WeiC algorithm was presented earlier in Section 4.1.2. Both Cen and WeiC can be similarly be used to estimate the transmitter locations in the training phase. Other possible floor detection algorithms are, e.g., a low-complexity approach presented in [269], based on K-means clustering.

10.3.2 Novel floorwise radiomap matrix model

In this section, it is assumed that in the data gathering process the radiomap database is built floorwise, and N_{fp_f} measurements (or FPs) are available from floor f, with $f = 1, \ldots, N_{floors}$. For each floor f, a RSS matrix $\mathbf{R}^{(f)}$ is defined as

$$\mathbf{R}^{(f)} = \begin{bmatrix} r_{1,1}^{(f)} & r_{1,2}^{(f)} & \cdots & \cdots & r_{1,N_{fp_f}}^{(f)} \\ \cdots & \cdots & \cdots & \cdots & \cdots \\ \cdots & \cdots & r_{k,m}^{(f)} & \cdots & \cdots \\ \cdots & \cdots & \cdots & \cdots & \cdots \\ r_{N_{TX},1}^{(f)} & r_{N_{TX},2}^{(f)} & \cdots & \cdots & r_{N_{TX},N_{fp_f}}^{(f)} \end{bmatrix}. \tag{10.2}$$

where $r_{k,m}^{(f)}$ includes the information of both heard and non-heard transmitters, as follows:

$$r_{k,m}^{(f)} = \begin{cases} 0 & \text{if } k\text{th AP is not heard in } m\text{th FP} \\ & \text{in } f\text{th floor} \\ 10^{\frac{P_{m,k}}{10}} & \text{if } k\text{th AP is heard in } m\text{th FP} \\ & \text{in } f\text{th floor} \end{cases} \tag{10.3}$$

Further on, the $N_{TX} \times N_{fp_f}$ radiomap data can be modelled via the following *floorwise observation matrix* $\mathbf{U}^{(f)}$:

$$\mathbf{U}^{(f)} = \begin{bmatrix} u_{1,1}^{(f)} & u_{1,2}^{(f)} & \dots & \dots & u_{1,N_{fp_f}}^{(f)} \\ \dots & \dots & \dots & \dots & \dots \\ \dots & \dots & u_{a,m}^{(f)} & \dots & \dots \\ \dots & \dots & \dots & \dots & \dots \\ u_{N_{TX},1}^{(f)} & u_{N_{TX},2}^{(f)} & \dots & \dots & u_{N_{TX},N_{fp_f}}^{(f)} \end{bmatrix}. \tag{10.4}$$

with the column vectors $\mathbf{v}_m(f) = [u_{1,m}^{(f)}, u_{2,m}^{(f)} \dots u_{N_{TX},m}^{(f)}]^T$ having the elements equal to the normalized RSS values:

$$u_{k,m}^{(f)} = \frac{r_{k,m}^{(f)}}{\sum_{m=1}^{N_{fp_f}} r_{k,m}^{(f)}},\ m = 1,\dots,N_{fp_f},\ k = 1,\dots,N_{TX} \tag{10.5}$$

The floorwise observation matrix $\mathbf{U}^{(f)}$ can be therefore seen as a collection of vector observations at f-th floor:

$$\mathbf{U}^{(f)} = [\mathbf{v}_1(f)\, \mathbf{v}_2(f) \dots \mathbf{v}_{N_{fp_f}}(f)] \tag{10.6}$$

In other words, each vector $\mathbf{v}_m(f)$ of size $N_{TX} \times 1$ contains implicitly the information about which APs are heard and which are not heard in the mth FP. The floorwise matrix $\mathbf{U}^{(f)}$ can be thus seen as the realizations of a multivariate column random vector $\mathbf{v}^{(f)} \in R^{N_{TX} \times 1}$, with mean per floor ${\mu_\mathbf{v}}^{(f)}$:

$${\mu_\mathbf{v}}^{(f)} = \left[\sum_{k=1}^{N_{TX}} u_{k,1}^{(f)} \sum_{k=1}^{N_{TX}} u_{k,2}^{(f)} \dots \sum_{k=1}^{N_{TX}} u_{k,N_{fp_f}}^{(f)} \right]^T \tag{10.7}$$

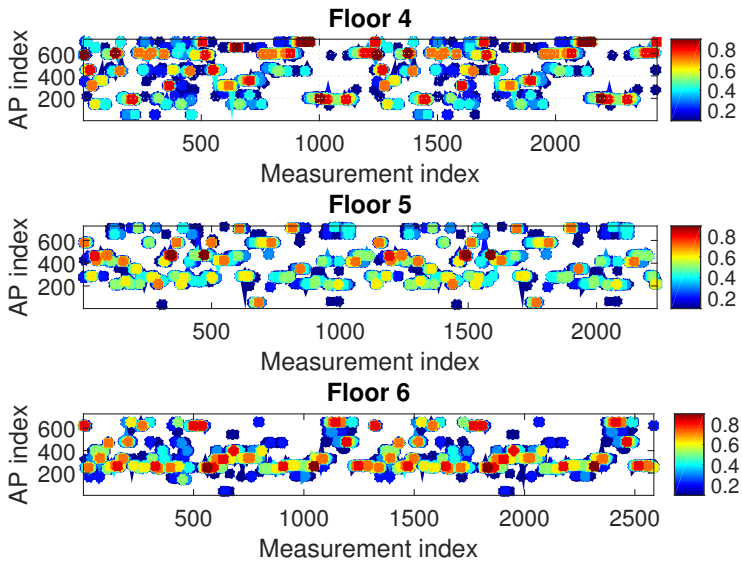

Fig. 10.3: *An example of AP patterns per floors for* 3 *successive floors in building C5 of* 9 *floors.*

Basically each floor has a different observation matrix $\mathbf{U}^{(f)}$ and a different pattern mean vector $\boldsymbol{\mu}_{\mathbf{v}}{}^{(f)}$. An example of the observation matrices for three successive floors in a 9-floor building is shown in Figure 10.3.

Due to the correlated measurements, the covariance matrix of the multivariate vector $\mathbf{v}^{(f)}$ does not have full rank, and therefore, the multivariate vector distribution probability distribution function is degenerate. Thus, in the floor detection algorithm presented here, we will use only the information stored in the floorwise mean vectors $\boldsymbol{\mu}_{\mathbf{v}}{}^{(f)}$. Thus, the floorwise mean vector information is the only information that needs to be transmitted to or stored at the mobile from the training dataset, in addition to the estimated AP location in 2D $(\hat{x}_{TX}, \hat{y}_{TX})$. With this way, the amount of data needed to be transferred to the receiver can be decreased remarkably, when compared to the whole FP database.

10.3.3 Novel positioning algorithm via multivariate random variable patterns

In this section, we present a novel Multivariate Random Variable Patterns (MuRVaP) floor detection algorithm. The main idea in our proposed algorithm is that the most likely floor is detected based only on the certain patterns of heard and non-heard APs,

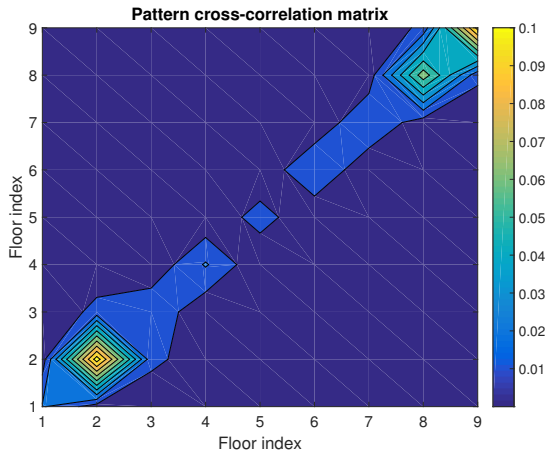

Fig. 10.4: *An example of the pattern cross-correlation matrix in building C5 of 9 floors.*

that are build separately for each floor. It can be assumed that the pattern mean vectors ${\mu_{\mathbf{v}}}^{(f)}$ are uncorrelated across different floors, as illustrated in Fig. 10.4, which shows the cross-correlation mean pattern values ${\mu_{\mathbf{v}}}^{(f_1)}{\mu_{\mathbf{v}}}^{(f_2)}$ for each pair of floors (f_1, f_2) in a 9-floor building.

In the estimation phase, the receiver detects a set of APs with certain RSSs O_k. Also in this phase, a vector $\mathbf{w}$ of heard and non-heard APs can be build as

$$\mathbf{w} = \left[\frac{r_1}{\sum_{k=1}^{N_{TX}} r_k} \cdots \frac{r_{N_{TX}}}{\sum_{k=1}^{N_{TX}} r_{N_{TX}}} \right]^T, \; k = 1, \ldots, N_{TX}, \tag{10.8}$$

where $r_k = 0$, if the kth transmitter is not detected, and $r_k = 10^{\frac{O_k}{10}}$, if the kth AP is detected by the receiver, with O_k [dB].

In order to decide which is the most likely floor $\widehat{f}$, the Euclidean distance between the vector observed by the transmitter $\mathbf{w}$ is compared with the floorwise mean pattern vectors ${\mu_{\mathbf{v}}}^{(f)}$;

$$\widehat{f} = argmin_f \left(\mathbf{w} - {\mu_{\mathbf{v}}}^{(f)} \right)^T \left(\mathbf{w} - {\mu_{\mathbf{v}}}^{(f)} \right) \tag{10.9}$$

Thus, the estimated $\hat{z}_{MS}$-coordinate of the transmitter location will be the height of the estimated floor $\widehat{f}$, while the estimated $\hat{x}_{MS}$- and $\hat{y}_{MS}$-coordinates can be calculated using, e.g., WeiC (see Section 4.1.2) or other low-complexity estimation approaches.

Table 10.6: *Floor detection probabilities [%].*

Building	Cen	WeiC	Floor of strongest AP	MuRVaP (new)	FP
A4	61.9	69.9	69.1	85.5	87.3
B2	68.9	90.3	86.4	90.8	97.7
C5	34.6	74.6	73.7	82.8	81.5
D5	54.7	80.4	81.5	86.5	94.5
G2	49.9	76.1	80.3	84.0	90.3
Average	54.3	78.3	78.2	85.9	90.3

10.3.4 Measurement-based results and complexity comparison

Table 10.6 presents the floor detection probabilities for 5 different multi-floor buildings, comparing several floor detection algorithms: the proposed MuRVaP, Cen, WeiC, a low-complexity estimator based only on the estimated floor of the strongest detected AP, and FP approach. It can be seen that the proposed low-complexity MuRVaP approach offers, on average, between 7.7% and 31.6% better floor detection probability than the other low-complexity estimators (Cen, WeiC and floor of strongest AP). Indeed, the proposed MuRVaP also has only 4.4% lower floor detection probability on average than the high-complexity FP approach, with the advantage of a much lower complexity.

Table 10.7 presents the simulations times for estimating one user track point of each considered building. As was noticed already in Section 10.2 and Table 10.5, FP approaches are not so good for mobile-centric real-time solutions, as an estimate per user track point requires $0.1-0.52$ seconds. On the other hand, the low-complexity approaches discussed in here are all offering very fast position estimates (less than 0.5×10^{-3} s per estimate) and are fully adequate for real-time mobile-centric solutions. When considering the number of parameters to be saved and transmitted to the mobile, the MuVRaP algorithm outperforms the FP approach clearly, even though the number of parameters is slightly higher than, e.g., in WeiC algorithm.

10.4 Conclusions

In this chapter, we have focused on the challenges related to estimation phase (phase D in Fig. 4.1). We have presented in this chapter a novel study of offsets between

Table 10.7: *Complexity comparison via algorithm time consumption (simulation times for one user track point) in milliseconds.*

Building	Cen [ms]	WeiC [ms]	Floor of strongest AP [ms]	MuRVaP (new) [ms]	FP [ms]
A4	0.047	0.063	0.039	0.079	164
B2	0.049	0.064	0.045	0.12	100
C5	0.050	0.079	0.061	0.23	501
D5	0.055	0.083	0.063	0.19	522
G2	0.065	0.087	0.070	0.23	107
Average	0.053	0.075	0.056	0.18	279

the RSS values in the training and estimation phases of fingerprinting. We have investigated both constant and random biases, covering either the whole building or only parts of it. We have shown in our analysis that if the shadowing is small, only small amounts of biases (i.e., less than $+/-10$ dB) can be tolerated without any calibration. This holds both for a bias in the whole building and for a localized bias. However, random bias between -10 to $+10$ dB does not increase the positioning errors. We have also presented an overview of the possible calibration methods found in the literature.

The challenge of the choice of appropriate positioning algorithm was taken into account in this chapter by continuing the analysis of FP, PL and WeiC approaches. The analysis was started in Section 9.3, where the three positioning methods were compared in terms of positioning accuracy together with AP reductions. In this chapter, the analysis is continued by comparing FP, PL and WeiC approaches in terms of complexity. The complexity was measured in terms of database size and simulation times for the actual positioning. We showed, that the database size and algorithm time consumption for FP method are multiple when compared to the PL and WeiC methods, but can be efficiently decreased with AP removal and good choice of the grid interval. In the last section in this chapter, we proposed a novel floor detection algorithm. The proposed algorithm called MuRVaP offers clearly better floor detection than the traditional low-complexity methods, while keeping low computational load and requiring only a fraction of the database size needed for the FP approach.

The main contributions of this chapter can be summarized as follows:

- A novel study of a various offsets in RSS-based localization, based on extensive WLAN measurements.
- A comprehensive comparison of three most widespread positioning approaches, in terms of positioning accuracy and complexity.
- A novel low-complexity floor detection algorithm.

Based on parts of the work presented in this chapter, there has been also one publication:

1. **Elina Laitinen**, Jukka Talvitie and Elena Simona Lohan, "On the RSS biases in WLAN-based indoor positioning", in *Proc. of IEEE International Communication Workshop (ICCW)*, London, UK, Jun 2015, pp. 797-802.

11. COMPARISON OF GNSS, CELLULAR AND WLAN POSITIONING SOLUTIONS

Regarding the different challenges and solutions presented in this thesis, the purpose in this chapter is to make a brief comparative analysis and summary of the discussed three positioning method, namely GNSS, cellular and WLAN-based. In addition, we will discuss the hybrid positioning solutions.

11.1 Comparative analysis of the different methods

In Section 2.6 and Table 2.5, the three different positioning approaches (GNSS, cellular and WLAN) were compared shortly. In addition, Table 2.6 presented the main challenges for these systems. Table 11.1 brings in new concepts, focusing especially to the solutions addressed in this thesis. Since the solutions in outdoor and indoor cases for each method can be different, both environments are taken into account separately. As it is presented in Table 11.1, some aspects are common for all methods, while some, for example PL models, are more relevant for RSS-based approaches (i.e., WLAN and cellular). As another example, fading models are important in GNSS, but in the case of RSS-based approaches, they are typically modelled jointly with path losses. As seen in Table 11.1, GNSS are highly suitable in outdoor environments, but have limited availability indoors. WLAN and cellular act as complementary to GNSS, through their indoor availability and floor detection capabilities.

11.2 Hybrid positioning solutions

An ideal positioning system would be able to provide accurate location estimates anywhere at any time, and guarantee the continuity of the serving, both outdoors and

Table 11.1: *Comparison of different positioning methods and solutions to various challenges addressed in this thesis. $N_{TX_{min}}$ represents the minimum number of transmitters.*

	Outdoor positioning			Indoor positioning		
	GNSS	WLAN RSS	cellular RSS	GNSS	WLAN RSS	cellular RSS
Availability	Very high	Low to moderate	High	Low	Very high	High
Most used PL models	-	single-slope PL [21, 155, 241]	Okumura-Hata [129, 244], COST Hata [12, 295]	-	single-slope PL [21, 155, 241]	single- & multi-slope PL [55, 355]
Most used fading models	Nakagami-*m* [186, 187]	Typically modelled jointly with path losses [Chapter 8]		Nakagami-*m* [Chapter 5]	Typically modelled jointly with path losses [Chapter 8]	
User privacy	Very high	Needs privacy-preserving mechanisms		Very high	Needs privacy-preserving mechanisms	
$N_{TX_{min}}$ for < 5 m error	4 (clear sky), 7 (urban canyons)	10 [Chapter 9]	10 [Chapter 9]	Needs assistance from other systems	10 [Chapter 9]	10 [Chapter 9]
Floor detection capability	-	-	-	Low	High [Chapter 9]	Moderate [81]
Impact of different receiver types	Receiver sensitivity	RSS biases [Chapter 9]	RSS biases	Receiver sensitivity	RSS biases [Chapter 9]	RSS biases
Methods to increase performance	Enhanced integration methods [Chapter 6]	Topology optimization [Chapter 7]	Hybridization with GNSS [354] or WLAN [166]	Enhanced integration methods [Chapter 6]	Topology optimization [Chapter 7]	Hybridization with GNSS [354] or WLAN [166]
Methods to decrease complexity	Cloud GNSS [211]	Statistical models [Chapter 9], AP significance & grid interval [Chapter 8]	Statistical models [Chapter 9], grid interval [Chapter 8]	Cloud GNSS [211]	Statistical models [Chapter 9], AP significance & grid interval [Chapter 8]	Statistical models [Chapter 9], grid interval [Chapter 8]

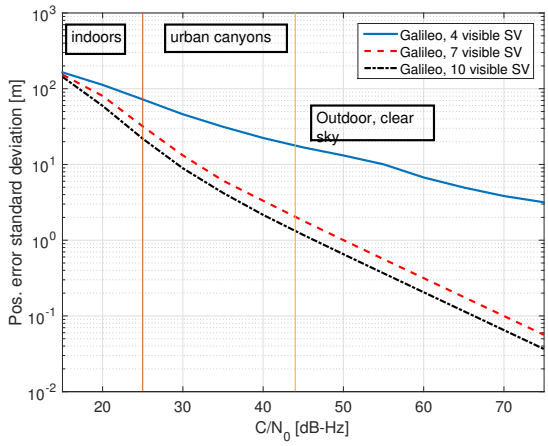

Fig. 11.1: *Galileo signal performance versus CNR.*

indoors. As it has been stated earlier in this thesis, GNSS as a stand-alone solution does not solve the challenge of an accurate indoor positioning. This can be shown by following the model of [202]. Assuming no multipath or ionospheric errors, a coarse estimate of Galileo signal performance versus CNR is shown in Fig. 11.1, assuming 4, 7 or 10 visible Galileo satellites, respectively. Clearly, at low CNR specific to indoor environments, Galileo (and similarly, other GNSS signals as well) cannot achieve good accuracy; the accuracy is of the order of tens to hundreds of meters. Clear sky at outdoor scenarios usually occurs above 44 dB-Hz [285]. Indoor scenarios typically have CNR below 20-25 dB-Hz, and in-between we may have deep urban canyons or signal severely affected by multipaths. Carrier and code tracking in GNSS are typically not working well below 24 dB-Hz [346], and thus, there is a certain CNR limit under which the GNSS-based positioning is no longer reliable.

The high need for global indoor positioning and the difficulty of utilizing GNSS indoors led to the development of A-GNSS and HS-GNSS receivers. In addition, several proposals for indoor positioning has been presented in the literature within the last decade. However, due to contradictory conditions for positioning in outdoor and indoor environments, none of the existing or proposed systems is able to provide global positioning in all conditions as a stand-alone solution. The most promising approach is a hybrid solution, where GNSS is supplemented, e.g., with WLAN or cellular based positioning or other types of sensors.

Lately, GNSS has been proposed to be combined with cellular networks [77, 227, 354], with WLAN [82, 105, 195, 237, 271, 362], with UWB [30, 106, 118], or with

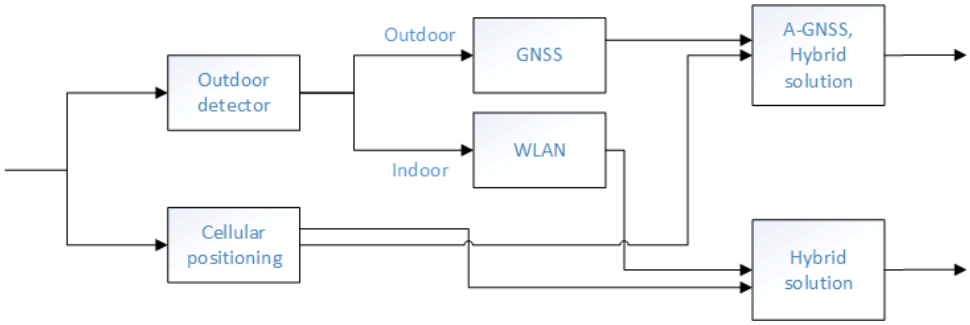

Fig. 11.2: *An example of a block diagram with a hybrid architecture.*

INS [165]. In [261], a ubiquitous solution with multiple techniques combined together, is presented. In [105,362], a hybrid solution combining GNSS and WLAN positioning was studied to overcome the challenges of GNSS in urban canyons. In [82], a hybrid solution was proposed for ubiquitous positioning both outdoors and indoors, by utilizing GNSS and WLAN measurements together with place detection method.

By utilizing the already existing signals that have widespread deployment and easy access to measurement data, such as cellular and WLAN networks, the hybrid approaches can result both as an accurate and as economical solution. One possible flowchart of a hybrid positioning solution using GNSS with cellular and WLAN data is presented in Fig. 11.2. The outdoor/indoor detection can be done based on the GNSS availability, as for example in [82]. If enough GNSS signals are not detected, the positioning is switched to WLAN-based approach. Cellular networks, that have wide coverage and that are typically always available on the mobile device, but that are not as accurate as a stand-alone solution with the current networks, can be used as an add-on to the GNSS or WLAN-based positioning.

11.3 Conclusions

This chapter has provided a short concluding overview of the studied challenges and solutions, concerning the three positioning approaches covered in this thesis. We presented a comparative table, and discussed also the hybrid approaches as future solutions.

12. CONCLUSIONS AND FUTURE ISSUES IN WIRELESS MOBILE LOCALIZATION

As stated in Chapter 11, none of the currently existing wireless positioning methods can solve the global positioning problem in every environment as a stand-alone solution but hybrid approaches are needed. Therefore, the focus in this thesis was on different positioning approaches, namely GNSS, cellular and WLAN-based localization. In the case of cellular and WLAN-based positioning, this thesis concentrated on the two-stage RSS-based localization, due to the easy availability and accessibility of RSS measurements in the mentioned networks. Positioning approaches based on existing wide-coverage networks can provide low-complexity and economical solutions.

This thesis started with GNSS related challenges, and analyzed indoor fading channel characteristics based on GPS-like signals. It was showed that the amplitude variations indoors match the Nakagami-*m* distribution, and based on these findings, a simple and efficient Nakagami-*m* fading channel simulator, that can be used to model various fading environments in developing acquisition and tracking algorithms, was built. GNSS acquisition algorithms were improved to address the challenges of GNSS in indoor environments, such as multipath propagation and low CNR. The ambiguous modulation types, that will be used in the new GNSS signals, were also taken into account. First, it was showed in this thesis that the ratio of the first two significant peaks in the time-frequency mesh is the most robust to varying channel conditions among several other studied CFAR detectors, and therefore, it is the best choice to be used as the decision variable. Secondly, an enhanced differential correlation method was proposed to be used as a post-detection correlation method in HS-GNSS receivers. In was showed in this theses that the proposed method outperforms the conventional non-coherent integration method and traditional differential correlation method in indoor environment, where the mobile speed is low.

The typical challenges in RSS-based positioning are related either to the positioning architecture design, training phase, data transferring and storage, or estimation phase. The architecture related challenges, such as transmitter density and placements, were considered by calculating a CRLB-based criterion, that was also confirmed via real measurements. This criterion can be used as an efficient tool to evaluate the existing or planned transmitter topology and density in a building, in terms of positioning accuracy. Shadowing effect was studied both in WLAN and cellular networks based on measurement data. One important conclusion was that based on the estimated path loss coefficients, 3D path loss models can model very well the signal propagation in multi-floor buildings and no separate floor losses are needed.

One important question is the choice of an appropriate positioning algorithm, that was studied continuously in the thesis. FP method provided consistently the best positioning performance, but it also requires larger database and more parameters to be transmitted to the mobile. Therefore, the effect of grid density and AP removals was studied for three positioning approaches (namely FP, PL and WeiC). It was showed that maxRSS-based criterion, where the transmitters were sorted according to their maximum RSS values and only the highest ones were kept, was the best choice in terms of positioning accuracy. It was also noticed that in FP method, even 50% of the training database can be reduced without deteriorating significantly the positioning results. This is an important finding, since the complexity of FP method can be reduced remarkably with AP reduction and with good choice of the grid interval. Related to the estimation phase, the possibility of RSS offset caused by different devices in the training phase than in the estimation phase was considered. Several different types of offsets were investigated, and it was noticed that if the shadowing is small, the small mounts of biases (i.e., between -10 dB and $+10$ dB) affect the localization results very little and no calibration is needed. In addition, a novel floor detector, that was noticed to outperform the other low-complexity floor detection methods without increasing the complexity, was proposed.

As discussed in Chapter 11, combining several positioning methods together will lead not only to more accurate location solutions but also better availability, continuity and integrity. In the future, an accurate estimate of the user position will not be dependent on whether the user is outdoors or indoors. The increasing number of networks and transmitters will result as improved communication resources, but also as improved performance and availability of various network-based positioning solutions.

The upcoming 5G networks with femtocells and dense transmitter infrastructure can allow more accurate positioning, and hyper-precision positioning is mentioned to be even a requirement for technology developments in 5G [10]. In addition, the new network architecture will also explode the number of possibilities offered by Internet of Things (IoT). IoT will require positioning solutions in many services, and especially accurate indoor positioning is essential. Thus, the convergence of communication and localization would be very beneficial in the future, e.g., as a design of joint signals for both communication and positioning purposes.

BIBLIOGRAPHY

[1] "China launches 22nd BeiDou satellite," http://gpsworld.com/china-launches-22nd-beidou-satellite/, referred 27.5.2016.

[2] "Four Galileos launched at once, speeding constellation completion," http://gpsworld.com/four-galileos-launched-at-once-speeding-constellation-completion/, referred 21.11.2016.

[3] "GPS NANUs, Almanacs, and Operational Advisories," http://www.navcen.uscg.gov/?pageName=gpsAlmanacs, referred 22.4.2016.

[4] "Indoor Location Market by Component (Technology, Software Tools, and Services), Application, End User (Transportation, Hospitality, Entertainment, Shopping, and Public Buildings), and Region - Global Forecast to 2021," http://www.researchandmarkets.com/, referred 13.11.2016.

[5] "Pokémon GO," http://www.pokemongo.com/, referred 13.11.2016.

[6] "Strategy Analytics," http://www.strategyanalytics.com, referred 10.10.2016.

[7] "U.S. Naval Observatory Home Page - Current GPS Constellation," http://tycho.usno.navy.mil/gpscurr.html, referred 22.4.2016.

[8] "5G White Paper, Next Generation Mobile Networks Alliance, Version 1.0, Final Executive Version." 2014.

[9] 3GPP, "Overview of 2G LCS Technnologies and Standards," in *3GPP TSG SA2 LCS Workshop*, London, Jan 2001.

[10] "5G new wave: towards future societies in the 2020s," 5G Forum, Mar 2015.

[11] M. Abdallah, W. Dyab, T. Sarkar, C. Misra, M. Prasad, A. Lamparez, and M. Salazar-Palma, "Electromagnetic macro model for analysis of propagation path loss in cellular networks," in *IEEE Antennas and Propagation Soc. Int. Symp.*, 2014, pp. 947–948.

[12] R. V. Akhpashev and A. V. Andreev, "COST 231 Hata adaptation model for urban conditions in LTE networks," in *Proc. of 17th International Conference of Young Specialists on Micro/Nanotechnologies and Electron Devices (EDM)*, Jul 2016.

[13] D. Akopian, "A Fast Satellite Acquisition Method," in *Proc. of the 14th International Technical Meeting of the Satellite Division of The Institute of Navigation (ION GPS)*, Sep 2001.

[14] P. F. Alcantarilla, J. J. Yebes, J. Almazan, and L. M. Bergasa, "On combining visual SLAM and dense scene flow to increase the robustness of localization and mapping in dynamic environments," in *Proc. of IEEE International Conference on Robotics and Automation (ICRA)*, May 2012, pp. 1290–1297.

[15] I. H. Alshami, N. A. Ahmad, and S. Sahibuddin, "A light WLAN radio map for floor detection in multi-floor environment localization," in *Proc. of 9th Malaysian Software Engineering Conference (MySEC)*, Dec 2015, pp. 135–139.

[16] N. Alsindi, Z. Chaloupka, N. AlKhanbashi, and J. Aweya, "An Empirical Evaluation of a Probabilistic RF Signature for WLAN Location Fingerprinting," in *IEEE Transactions on Wireless Communications*, vol. 13, no. 6, Jun 2014, pp. 3257–3268.

[17] J. Andrews, S. Buzzi, W. Choi, S. Hanly, A. Lozano, A. Soong, and J. Zhang, "What will 5G be?" in *IEEE Journal on Selected Areas in Communications*, vol. 32, no. 6, Jun 2014, pp. 1065–1082.

[18] S. Atapattu, C. Tellambura, and H. Jiang, "A Mixture Gamma Distribution to Model the SNR of Wireless Channels," in *IEEE Transactions on Wireless Communications*, vol. 10, no. 12, Dec 2011, pp. 4193–4203.

[19] A. B. Ayed, M. B. Halima, and A. M. Alimi, "Survey on clustering methods: Towards fuzzy clustering for big data," in *Proc. of 6th International Conference of Soft Computing and Pattern Recognition (SoCPaR)*, Tunis, 2014, pp. 331–336.

[20] O. Baala, Y. Zheng, and A. Caminada, "The Impact of AP Placement in WLAN-Based Indoor Positioning System," in *Proc. of 8th International Conference on Networks (ICN)*, Mar 2009, pp. 12–17.

[21] M. Babalou, S. Alirezaee, A. Soheili, A. Ahmadi, M. Ahmadi, and S. Erfani, "Microcell path loss estimation using Log-Normal model in GSM cellular network," in *Proc. of International Symposium on Signals, Circuits and Systems (ISSCS)*, Jul 2015.

[22] T. Bagosi and Z. Baruch, "Indoor localization by WiFi," in *Proc. of IEEE International Conference on Intelligent Computer Communication and Processing (ICCP)*, 2011, pp. 449–452.

[23] P. Bahl and V. N. Padmanabhan, "RADAR: an in-building RF-based user location and tracking system," in *Proc. of 19th Annual Joint Conference of the IEEE Computer and Communications Societies (INFOCOM)*, Mar 2000, pp. 775–784.

[24] T. Bailey and H. Durrant-Whyte, "Simultaneous localization and mapping (SLAM): part II," in *IEEE Robotics & Automation Magazine*, vol. 13, no. 3, Sep 2006, pp. 108–117.

[25] A. T. Balaei, A. G. Dempster, and J. Barnes, "A Novel Approach in Detection and Characterization of CW Interference of GPS Signal Using Receiver Estimation of C/No," in *Proc. of IEEE/ION Position, Location, And Navigation Symposium*, San Diego, CA, Apr 2006, pp. 1120–1126.

[26] J. Bardwell, "The Truth About 802.11 Signal And Noise Metrics," 2010.

[27] B. C. Barker, J. W. Betz, J. E. Clark, J. T. Correia, J. T. Gillis, S. Lazar, K. A. Rehborn, and J. R. Straton, "Overview of the GPS M Code Signal," in *Proc. of the 2000 National Technical Meeting of The Institute of Navigation*, 2000, pp. 542–549.

[28] F. Bastide, O. Julien, C. Macabiau, and B. Roturier, "Analysis of L5/E5 acquisition, tracking and data demodulation thresholds," in *Proc. of the 15th International Technical Meeting of the Satellite Division of The Institute of Navigation (ION GPS)*, Portland, OR, Sep 2002, pp. 2196–2207.

[29] N. C. Beaulieu and C. Cheng, "An Efficient Procedure for Nakagami-m Fading Simulation," in *Proc. of Global Telecommunications Conference (GLOBECOM)*, vol. 6, Nov 2001, pp. 3336–3342.

[30] A. Belakbir, M. Amghar, and N. Sbiti, "An Indoor-Outdoor Positioning System Based on the Combination of GPS and UWB Sensors," in *Journal of Theoretical and Applied Information Technology*, vol. 61, no. 1, Mar 2014.

[31] M. Bern, D. Eppstein, L. Guibas, J. Hershberger, S. Suri, and J. Wolter, "The Centroid of Points with Approximate Weights," in *Proc. of 3rd Annual European Symposium on Algorithms*, 1995, pp. 460–472.

[32] J. Betz, P. Capozza, and J. Fite, "System for direct acquisition of received signals," US Patent Application Publication 7447259 B2, Nov 2008.

[33] J. W. Betz, "The Offset Carrier Modulation for GPS Modernization," in *Proc. of National Technical Meeting of The Institute of Navigation*, San Diego, CA, Jan 1999, pp. 639–648.

[34] ——, "Design and Performance of Code Tracking for the GPS M Code Signal," in *Proc. of the 13th International Technical Meeting of the Satellite Division of The Institute of Navigation (ION GPS)*, Sep 2000, pp. 2140–2150.

[35] ——, "Effect of Narrowband Interference on GPS Code Tracking Accuracy," in *Proc. of 2000 National Technical Meeting of The Institute of Navigation*, Anaheim, CA, Jan 2000, pp. 16–27.

[36] M. Z. H. Bhuiyan and E. S. Lohan, "Advanced Multipath Mitigation Techniques for Satellite-Based Positioning Applications," in *International Journal of Navigation and Observation*, vol. 2010, 2010.

[37] M. Z. H. Bhuiyan, E. S. Lohan, and M. Renfors, "Code Tracking Algorithms for Mitigating Multipath Effects in Fading Channels for Satellite-Based Positioning," in *EURASIP Journal on Advances in Signal Processing*, vol. 2008, 2008.

[38] M. Z. H. Bhuiyan, "Analysis of Multipath Mitigation Techniques for Satellite-based Positioning Applications," Ph.D. dissertation, Department of Communications Engineering, Tampere University of Technology, Tampere, Finland, Sep 2011.

[39] B. Bidikar, G. S. Rao, L. Ganesh, and MNVS S. Kumar, "Satellite Clock Error and Orbital Solution Error Estimation for Precise Navigation Applications," in *Positioning*, vol. 5, no. 1, 2014, pp. 22–26.

[40] J. Blumenthal, R. Grossmann, F. Golatowski, and D. Timmermann, "Weighted Centroid Localization in Zigbee-based Sensor Networks," in *Proc. of International Symposium on Intelligent Signal Processing (WISP)*, Alcala de Henares, Spain, Oct 2007, pp. 1–6.

[41] D. Borio, "GNSS Acquisition in Presence of Continuous Wave Interference," in *IEEE Transactions on Aerospace and Electronic Systems*, vol. 46, no. 1, Jan 2010.

[42] J. Borkowski, J. Niemelä, and J. Lempiäinen, "Enhanced Performance of Cell ID+RTT by Implementing Forced Soft Handover Algorithm," in *Proc. of IEEE Vehicular Technology Conference*, vol. 5, Sep 2004, pp. 3545–3549.

[43] ——, "Location Techniques for UMTS Radio Networks," in *Proc. of the Mobile Venue Conference*, May 2004.

[44] ——, "Performance of Cell ID+RTT hybrid positioning method for UMTS radio networks," in *Proc. of 5th European Wireless Conference*, Feb 2004, pp. 487–492.

[45] K. Borre, D. M. Akos, N. Bertelsen, P. Rinder, and S. H. Jensen, *A Software-Defined GPS and Galileo Receiver - A Single-Frequency Approach*. Birkhauser Boston, 2007.

[46] F. Brahim, T. Chonavel, and O. Rabaste, "An MCMC Algorithm for BOC and AltBOC Signaling Acquisition in Multipath Environments," in *Proc. of IEEE/ION Position, Location and Navigation Symposium*, May 2008.

[47] N. Bulusu, J. Heidemann, and D. Estrin, "GPS-less low-cost outdoor localization for very small devices," in *IEEE Personal Communications*, vol. 7, no. 5, Oct 2000, pp. 28–34.

[48] A. Burian, E. Laitinen, E. S. Lohan, and M. Renfors, "Acquisition of BOC-modulated signals using enhanced sidelobes cancellation method," in *Proc. of The European Navigation Conference (ENC-GNSS)*, Toulouse, France, Apr 2008.

[49] A. Burian, E. S. Lohan, V. Lehtinen, and M. Renfors, "Complexity Considerations for Unambiguous Acquisition of Galileo Signals," in *Proc. of 3rd Workshop on Positioning, Navigation and Communication (WPNC)*, Hannover, Germany, Mar 2006, pp. 65–74.

[50] A. Burian, E. S. Lohan, and M. Renfors, "BPSK-like Methods for Hybrid-Search Acquisition of Galileo Signals," in *Proc. of IEEE International Conference on Communications (ICC)*, Jun 2006.

[51] ——, "Efficient Delay Tracking Methods with Sidelobes Cancellation for BOC-Modulated Signals," in *EURASIP Journal on Wireless Communications and Networking*, vol. 2007, no. 2, 2007.

[52] J. J. Caffery Jr. and G. L. Stuber, "Overview of Radiolocation in CDMA Cellular Systems," in *IEEE Communications Magazine*, vol. 36, no. 4, Aug 1998, pp. 38–45.

[53] C. Caini, G. E. Corazza, and A. Vanelli-Coralli, "Multi-dwell architectures for DS-CDMA code acquisition in fading channels," in *Proc. of IEEE International Symposium on Spread Spectrum Techniques and Applications*, vol. 1, Sep 2002, pp. 214–218.

[54] R. Campana, F. Gottifredi, V. Valle, and B. F. Lombardo, "Different Acquisition Algorithms for the GALILEO L1 Signal with BOC(1,1) Modulation," in *Satellite Communications and Navigation Systems - Signals and Communication Technology*, 2008, pp. 341–352.

[55] J. M. Castro-Arvizu, P. Closas, and J. A. Fernandez-Rubio, "Cramér-Rao lower bound for breakpoint distance estimation in a path-loss model," in *Proc. of IEEE International Conference on Communications Workshops (ICC)*, Jun 2014.

[56] C.-L. Chang, H.-N. Shou, and J.-C. Juang, "Wavelet-based method for signal acquisition in GNSS receivers," in *proc. of SICE Annual Conference*, Aug 2010.

[57] K. Chawla, C. McFarland, G. Robins, and C. Shope, "Real-time RFID localization using RSS," in *Proc. of International Conference on Localization and GNSS (ICL-GNSS)*, Turin, Italy, 2013, pp. 1–6.

[58] L. Chen, O. Julien, P. Thevenon, D. Serant, A. G. Pena, and H. Kuusniemi, "TOA Estimation for Positioning With DVB-T Signals in Outdoor Static Tests," in *IEEE Transactions on Broadcasting*, vol. 61, no. 4, Sep 2015, pp. 625–638.

[59] L. Chen, H. Kuusniemi, Y. Chen, L. Pei, T. Kroger, and R. Chen, "Information filter with speed detection for indoor Bluetooth positioning," in *Proc. of International Conference on Localization and GNSS (ICL-GNSS)*, Tampere, Finland, 2011, pp. 47–52.

[60] Q. Chen and B. Wang, "FinCCM: Fingerprint Crowdsourcing, Clustering and Matching for Indoor Subarea Localization," in *IEEE Wireless Communications Letters*, vol. 4, no. 6, Dec 2015.

[61] Q. Chen, B. Wang, X. Deng, Y. Mo, and L. T. Yang, "Placement of Access Points for Indoor Wireless Coverage and Fingerprint-based Localization," in *Proc. of 10th International Conference on High Performance Computing and Communications & 2013 IEEE International Conference on Embedded and Ubiquitous Computing (HPCC/EUC)*, Nov 2013, pp. 2253–2257.

[62] W. Chen, Q. Chang, H.-T. Hou, and W.-P. Wang, "Power-Efficient Access-Point Selection for Indoor Location Estimation," in *IEEE Transactions on Knowledge and Data Engineering*, vol. 18, no. 7, Jul 2006, pp. 877–888.

[63] ——, "A novel clustering and KWNN-based strategy for Wi-Fi fingerprint indoor localization," in *Proc. of International Conference on Computer Science and Network Technology (ICCSNT)*, Dec 2015.

[64] Y.-C. Chen, J.-R. Chiang, H.-H. Chu, P. Huang, and A. W. Tsui, "Sensor-assisted WiFi Indoor Location System for Adapting to Environmental Dynamics," in *Proc. of 8th ACM international symposium on Modeling, analysis and simulation of wireless and mobile systems*, 2005, pp. 118–125.

[65] W. Cheng, K. Tan, V. Omwando, J. Zhu, and P. Mohapatra, "RSS-Ratio for enhancing performance of RSS-based applications," in *Proc. of IEEE INFOCOM*, Apr 2013, pp. 3075–3083.

[66] Y.-C. Cheng, Y. Chawathe, and J. Krumm, "Accuracy Characterization for Metropolitan-scale Wi-Fi Localization," in *Proc. of the 3rd international conference on Mobile systems, applications, and services (MobiSys)*, 2005.

[67] Y.-R. Chien, Y.-C. Huang, D.-N. Yang, and H.-W. Tsao, "A Novel Continuous Wave Interference Detectable Adaptive Notch Filter for GPS Receivers," in *Proc. of Global Telecommunications Conference (GLOBECOM)*, Miami, Florida, Dec 2010, pp. 1–6.

[68] "BeiDou Navigation Satellite System, Open Service Performance Standard," Available via: http://en.beidou.gov.cn/, China Satellite Navigation Office, 2013, referred 17.4.2016.

[69] "BeiDou Navigation Satellite System, Signal In Space Interface Control Document - Open Service Signal (Version 2.0)," Available via: http://en.beidou.gov.cn/, China Satellite Navigation Office, 2013, referred 17.4.2016.

[70] Y. Cho, M. Ji, Y. Lee, J. Kim, and S. Park, "Improved Wi-Fi AP position estimation using regression based approach," in *Proc. of International Conference on Indoor Positioning and Indoor Navigation (IPIN)*, Nov 2012.

[71] I. H. Choi, S. H. Park, D. J. Cho, S. J. Yun, Y. B. Kim, and S. J. Lee, "A Novel Weak Signal Acquisition Scheme for Assisted GPS," in *Proc. of the 15th International Technical Meeting of the Satellite Division of The Institute of Navigation (ION GPS)*, Portland, OR, Sep 2002, pp. 117–183.

[72] I. Contreras, "Emphasizing the rank positions in a distance-based aggregation procedure," in *Decision Support Systems*, vol. 51, no. 1, Apr 2011, pp. 240–245.

[73] G. E. Corazza, C. Caini, A. Vanelli-Coralli, and A. Polydoros, "DS-CDMA code acquisition in the presence of correlated fading - Part I: theoretical aspects," in *IEEE Transactions on Communications*, vol. 52, no. 7, Jul 2004, pp. 1160–1168.

[74] G. E. Corazza, *Digital Satellite Communications*. Springer, 2007.

[75] G. E. Corazza and R. Pedone, "Generalized and Average Likelihood Ratio Testing for Post Detection Integration," in *IEEE Transactions on Communications*, vol. 55, no. 11, Nov 2007, pp. 2159–2171.

[76] A. Cramariuc, H. Huttunen, and E.-S. Lohan, "Clustering benefits in mobile-centric WiFi positioning in multi-floor buildings," in *International Conference on Localization and GNSS (ICL-GNSS)*, Jun 2016.

[77] G. De Angelis, G. Baruffa, and S. Cacopardi, "GNSS/Cellular Hybrid Positioning System for Mobile Users in Urban Scenarios," in *IEEE Transactions on Intelligent Transportation Systems*, vol. 14, no. 1, Mar 2013.

[78] G. De Angelis, A. Moschitta, and P. Carbone, "Positioning Techniques in Indoor Environments Based on Stochastic Modeling of UWB Round-Trip-Time Measurements," in *IEEE Transactions on Intelligent Transportation Systems*, vol. 17, no. 8, Aug 2016.

[79] L. F. M. de Moraes and B. A. A. Nunes, "Calibration-free wlan location system based on dynamic mapping of signal strength," in *Proc. of the 4th ACM international workshop on Mobility management and wireless access (MobiWac)*, 2006, pp. 92–99.

[80] N. Deblauwe and L. V. Biesen, "An Angle Of Arrival Location Estimation Technique for Existing GSM Networks," in *Proc. of IEEE International Conference on Signal Processing and Communications (ICSPC)*, Nov 2007, pp. 1527–1530.

[81] J. A. del Peral-Rosado, M. Bavaro, J. A. López-Salcedo, G. Seco-Granados, P. Chawdhry, J. Fortuny-Guasch, P. Crosta, F. Zanier, and M. Crisci, "Floor Detection with Indoor Vertical Positioning in LTE Femtocell Networks," in *Proc. of Globecom Workshops*, Dec 2015.

[82] G. Y. Delisle, "A Pervasive Indoor-Outdoor Positioning System," in *Journal of Networks*, Nov 2008.

[83] F. Della Rosa, T. Paakki, H. Leppäkoski, and J. Nurmi, "A Cooperative Framework for Path Loss Calibration and Indoor Mobile Positioning," in *Proc. of 7th Workshop on Positioning Navigation and Communication (WPNC)*, Dresden, Germany, Mar 2010.

[84] Z.-A. Deng, G. Wang, D. Qin, Z. Na, Y. Cui, and J. Chen, "Continuous Indoor Positioning Fusing WiFi, Smartphone Sensors and Landmarks," in *MDPI Sensors*, vol. 16, no. 9, Sep 2016.

[85] F. V. Diggelen, *A-GPS - Assisted GPS, GNSS, and SBAS*. Artech House, 2009.

[86] G. Ding, Z. Tan, J. Zhang, and L. Zhang, "Fingerprinting localization based on affinity propagation clustering and artificial neural networks," in *Proc. of Wireless Communications and Networking Conference (WCNC)*, Shanghai, 2013, pp. 2317–2322.

[87] F. Dong, Y. Chen, J. Liu, Q. Ning, and S. Piao, "A calibration-free localization solution for handling signal strength variance," in *Mobile Entity Localization and Tracking in GPS-less Environments - Lecture Notes in Computer Science*, vol. 5801, 2009, pp. 79–90.

[88] Q. Dong and X. Xu, "A Novel Weighted Centroid Localization Algorithm Based on RSSI for an Outdoor Environment," in *Journal of Communications*, vol. 9, no. 3, 2014, pp. 279–285.

[89] H. Durrant-Whyte and T. Bailey, "Simultaneous localization and mapping: part I," in *IEEE Robotics & Automation Magazine*, vol. 13, no. 2, Jun 2006, pp. 99–110.

[90] E. Ekiz and R. Sokullu, "Comparison of path loss prediction models and field measurements for cellular networks in Turkey," in *Proc. of International Conference on Selected Topics in Mobile and Wireless Networking (iCOST)*, 2011, pp. 48–53.

[91] H. A. El-Natour, A.-C. Escher, C. Macabiau, and M.-L. Boucheret, "Impact of Multipath and Cross-Correlation on GPS acquisition in Indoor Environments," in *Proc. of the National Technical Meeting of The Institute of Navigation*, San Diego, CA, Jan 2005, pp. 1062–1070.

[92] A. Eleryan, M. Elsabagh, and M. Youssef, "Synthetic Generation of Radio Maps for Device-Free Passive Localization," in *Proc. of Global Telecommunications Conference (GLOBECOM)*, Dec 2011, pp. 1–5.

[93] U. Engel, "A theoretical performance analysis of the modernized GPS signals," in *Proc. of IEEE/ION Position, Location and Navigation Symposium*, May 2008, pp. 1067–1078.

[94] L. M. Eslim, H. S. Hassanein, W. M. Ibrahim, and A. Alma'aitah, "A cooperative localization scheme using RFID crowdsourcing and time-shifted multilateration," in *Proc. of 39th Annual IEEE Conference on Local Computer Networks*, Sep 2014, pp. 185–192.

[95] *Universal Mobile Telecommunications System (UMTS); Stage 2 functional specification of User Equipment (UE) positioning in UTRAN, ETSI TS 125.305, 3GPP TS 25.305.*, ETSI.

[96] *LTE; Evolved Universal Terrestrial Radio Access (E-UTRA); Physical channels and modulation - 3GPP TS 36.211 version 9.1.0 Release 9*, ETSI, Apr 2010.

[97] C. Evrendilek and H. Akcan, "On the Complexity of Trilateration with Noisy Range Measurements," in *IEEE Communications Letters*, vol. 15, no. 10, Oct 2011, pp. 1097–1099.

[98] S.-H. Fang and T.-N. Lin, "A Novel Access Point Placement Approach for WLAN-Based Location Systems," in *Proc. of Wireless Communication and Networking Conference (WCNC)*, Apr 2010, pp. 1–4.

[99] ——, "Accurate Indoor Location Estimation by Incorporating the Importance of Access Points in Wireless Local Area Networks," in *Proc. of IEEE Global Telecommunications Conference (GLOBECOM)*, Miami, Florida, USA, 6-10 Dec 2010, pp. 1–5.

[100] ——, "A Dynamic Hybrid Projection Approach for Improved Wi-Fi Location Fingerprinting," in *IEEE Transactions on Vehicular Technology*, vol. 60, no. 3, 2011, pp. 1037 – 1044.

[101] ——, "Principal Component Localization in Indoor WLAN Environments," in *IEEE Transactions on Mobile Computing*, vol. 11, no. 1, 2012, pp. 100–110.

[102] S.-H. Fang, T.-N. Lin, and K.-C. Lee, "A Novel Algorithm for Multipath Fingerprinting in Indoor WLAN Environments," in *IEEE Transactions on Wireless Communications*, vol. 7, no. 9, Sep 2008.

[103] K. Farkas, A. Huszak, and G. Godor, "Optimization of Wi-Fi Access Point Placement for Indoor Localization," in *Informatics & IT Today (IIT)*, vol. 1, no. 1, Jul 2013.

[104] C. Feng, W. S. A. Au, S. Valaee, and Z. Tan, "Received Signal Strength based Indoor Positioning using Compressive Sensing," in *IEEE Transactions on Mobile Computing*, vol. 11, no. 12, Oct 2011, pp. 1983–1993.

[105] D. Fernandez, F. Barcelo-Arroyo, I. Martin-Escalona, M. Ciurana, M. Jofre, and E. Gutierrez, "Fusion of WLAN and GNSS observables for positioning in urban areas: the position ambiguity," in *Proc. of IEEE Symposium on Computers and Communications (ISCC)*, Jun 2011.

[106] J. A. Fernandez-Madrigal, E. Cruz-Martin, J. Gonzalez, C. Galindo, and J. L. Blanco, "Application of UWB and GPS technologies for vehicle localization in combined indoor-outdoor environments," in *Proc. of 9th International Symposium on Signal Processing and Its Applications (ISSPA)*, Feb 2007.

[107] G. Fettweis and S. Alamouti, "5G: Personal mobile internet beyond what cellular did to telephony," in *IEEE Communications Magazine*, vol. 52, no. 2, Feb 2014, pp. 140–145.

[108] P. M. Fishman and J. W. Betz, "Predicting Performance of Direct Acquisition for the M-Code Signal," in *Proc. of the 2000 National Technical Meeting of The Institute of Navigation*, Jan 2000, pp. 574–582.

[109] M. Foucras, B. Ekambi, F. Bacard, O. Julien, and C. Macabiau, "Assessing the Performance of GNSS Signal Acquisition - New Signals and GPS L1 C/A Code," in *Inside GNSS*, Jul/Aug 2014.

[110] S. B. Francescantonio Della Rosa, Helena Leppäkoski and J. Nurmi, "Ad-hoc Networks Aiding Indoor Calibrations of Heterogeneous Devices for Fingerprinting Applications," in *Proc. of International Conference on Indoor Positioning and Indoor Navigation (IPIN)*, Sep 2010.

[111] G. X. Gao, "DME/TACAN Interference and its Mitigation in L5/E5 Bands," in *Proc. of the 20th International Technical Meeting of the Satellite Division of The Institute of Navigation (ION GNSS)*, Sep 2007, pp. 1191–1200.

[112] C. Gernot, K. O'Keefe, and G. Lachapelle, "Comparison Of L1 C/A L2C Combined Acquisition Techniques," in *Proc. of European Navigation Conference (ENC-GNSS)*, 2008.

[113] S. Gezici, Z. Tian, G. B. Giannakis, H. Kobayashi, A. F. Molisch, H. V. Poor, and Z. Sahinoglu, "Localization via ultra-wideband radios: a look at positioning aspects for future sensor networks," in *IEEE Signal Processing Magazine*, vol. 22, no. 4, Jul 2005, pp. 70–84.

[114] G. Gibbons, "GNSS Interoperability - Not So Easy, After All," in *Inside GNSS*, 2011.

[115] R. Giuliano and F. Mazzenga, "On the coexistence of power-controlled ultrawide-band systems with UMTS, GPS, DCS1800, and fixed wireless systems," in *IEEE Transactions on Vehicular Technology*, vol. 54, no. 1, Jan 2005, pp. 62–81.

[116] S. Gleason and D. Gebre-Egziabher, *GNSS Applications and Methods*. Artech House, 2009.

[117] J. Goldhirsh and W. J. Vogel, "Handbook of Propagation Effects for Vehicular and Personal Mobile Satellite Systems - Overview of Experimental and Modeling Results," in *The John Hopkins University, The University of Texas at Austin*, 1998.

[118] J. Gonzalez, J. L. Blanco, C. Galindo, A. O. de Galisteo, J. A. Fernandez-Madrigal, F. A. Moreno, and J. L. Martinez, "Combination of UWB and GPS for indoor-outdoor vehicle localization," in *Proc. of International Symposium on Intelligent Signal Processing (WISP)*, Oct 2007.

[119] L. Görtschacher, J. Grosinger, H. N. Khan, D. Amschl, P. Priller, U. Muehlmann, and W. Bösch, "SDR based RFID reader for passive tag localization using phase difference of arrival techniques," in *Proc. of International Microwave Symposium (IMS)*, May 2016.

[120] Y. Gu, A. Lo, and I. Niemegeers, "A Survey of Indoor Positioning Systems for Wireless Personal Networks," in *IEEE Communications Surveys & Tutorials*, vol. 11, no. 1, 2009, pp. 13–32.

[121] J. Guo, X. Liu, and Z. Wang, "Optimized Indoor Positioning Based on WIFI in Mobile Classroom Project," in *Proc. of 11th International Conference on Natural Computation (ICNC)*, 2015, pp. 1208–1212.

[122] Z. Guowei, X. Zhan, and L. Dan, "Research and improvement on indoor localization based on RSSI fingerprint database and K-nearest neighbor points," in *Proc. of International Conference on Communications, Circuits and Systems*, 2013, pp. 68–71.

[123] F. Gustafsson and F. Gunnarsson, "Mobile positioning using wireless networks: Possibilities and fundamental limitations based on available wireless network measurements," in *IEEE Signal Processing Magazine*, vol. 22, no. 4, Jul 2005, pp. 41–53.

[124] A. Haeberlen, A. Rudys, E. Flannery, D. S. Wallach, A. M. Ladd, and L. E. Kavraki, "Practical robust localization over large-scale 802.11 wireless networks," in *Proc. of the 10th Annual International Conference on Mobile Computing and Networking (MOBICOM)*, 2004.

[125] M. Hämäläinen, V. Hovinen, R. Tesi, J. H. J. Iinatti, and M. Latva-aho, "On the UWB System Coexistence With GSM900, UMTS/WCDMA, and GPS," in *IEEE Journal on Selected Areas in Communications*, vol. 20, no. 9, Dec 2002, pp. 1712–1721.

[126] R. Hamila, E. S. Lohan, and M. Renfors, "Subchip multipath delay estimation for downlink WCDMA system based on Teager-Kaiser operator," in *IEEE Communications Letters*, vol. 7, no. 1, Jan 2003, pp. 1–3.

[127] Y. Han, H. Ma, and L. Zhang, "An Efficient RF Fingerprint Positioning Algorithm Based on Uneven Grid Layout," in *Proc. of 6th International Conference on Wireless, Mobile and Multi-Media (ICWMMN)*, Nov 2015.

[128] H. Hashemi, "The indoor radio propagation channel," in *Proc. of IEEE*, vol. 81, no. 7, Jul 1993.

[129] M. Hata, "Empirical formula for propagation loss in land mobile radio services," in *IEEE Transactions on Vehicular Technology*, vol. 29, no. 3, 1980, pp. 317–325.

[130] M. Hata and T. Nagatsu, "Mobile Location Using Signal Strength Measurements in a Cellular System," in *IEEE Transactions on Vehicular Technology*, vol. 29, no. 2, May 1980, pp. 245–252.

[131] S. He and S.-H. G. Chan, "Wi-Fi Fingerprint-Based Indoor Positioning: Recent Advances and Comparisons," in *IEEE Communications Surveys & Tutorials*, vol. 18, no. 1, 2016.

[132] C. Hegarty, M. Tran, and A. V. Dierendonck, "Acquisition algorithms for the GPS L5 signal," in *Proc. of the 16th International Technical Meeting of the Satellite Division of The Institute of Navigation (ION GPS/GNSS)*, Portland, OR, Sep 2003, pp. 165–177.

[133] G. W. Hein, J.-A. Avila-Rodriguez, S. Wallner, A. R. Pratt, J. I. R. Owen, J.-L. Issler, J. W. Betz, C. J. Hegarty, S. Lenahan, J. J. Rushanan, A. L. Kraay, and T. A. Stansell, "MBOC: The New Optimized Spreading Modulation Recommended for Galileo E1 OS and GPS L1C," in *Proc. of IEEE/ION Position, Location, And Navigation Symposium*, Apr 2006, pp. 883–892.

[134] G. W. Hein, J. Godet, J.-L. Issler, J.-C. Martin, P. Erhard, R. Lucas-Rodriguez, and T. Pratt, "Status of Galileo frequency and signal design," in *Proc. of the 15th International Technical Meeting of the Satellite Division of The Institute of Navigation (ION GPS)*, Sep 2002, pp. 266–277.

[135] G. W. Hein, M. Irsigler, J. A. Avila-Rodriguez, and T. Pany, "Performance of Galileo L1 signal candidates," in *Proc. of European Navigation Conference (ENC-GNSS)*, Rotterdam, Netherlands, May 2004.

[136] V. Heiries, J.-A. Avila-Rodrigues, M. Irsigler, G. W. Hein, E. Rebeyrol, and D. Roviras, "Acquisition Performance Analysis of Composite Signals for the L1 OS Optimized Signal," in *Proc. of the 18th International Technical Meeting of the Satellite Division of The Institute of Navigation (ION GNSS)*, Sep 2005, pp. 877–889.

[137] V. Heiries, D. Roviras, L. Ries, and V. Calmettes, "Analysis of Non Ambiguous BOC Signal Acquisition Performance ," in *Proc. of the 17th International Technical Meeting of the Satellite Division of The Institute of Navigation(ION GNSS)*, Sep 2004, pp. 2611–2622.

[138] S. Holm, "Ultrasound positioning based on time-of-flight and signal strength," in *Proc. of International Conference on Indoor Positioning and Indoor Navigation (IPIN)*, Npv 2012.

[139] V. Honkavirta, T. Perälä, S. Ali-Löytty, and R. Piché, "A Comparative Survey of WLAN Location Fingerprinting Methods," in *Proc. of the 6th Workshop on Positioning, Navigation and Communication (WPNC)*, Mar 2009, pp. 243–251.

[140] A. K. M. M. Hossain, Y. Jin, W.-S. Soh, and H. N. Van, "SSD: A Robust RF Location Fingerprint Addressing Mobile Devices' Heterogeneity," in *IEEE Transactions on Mobile Computing*, vol. 12, no. 1, Jan 2013, pp. 65–77.

[141] A. K. M. M. Hossain and W.-S. Soh, "Cramer-Rao Bound Analysis of Localization Using Signal Strength Difference as Location Fingerprint," in *Proc. of IEEE INFOCOM*, 2010, pp. 1–9.

[142] X. Hu, J. Shang, F. Gu, and Q. Han, "Improving Wi-Fi Indoor Positioning via AP Sets Similarity and Semi-Supervised affinity propagation Clustering," in *International Journal of Distributed Sensor Networks*, 2015.

[143] Z. Huang, J. Xia, H. Yu, Y. Guan, and J. Chen, "Clustering combined indoor localization algorithms for crowdsourcing devices: Mining RSSI relative relationship," in *Proc. of 6th International Conference on Wireless Communications and Signal Processing (WCSP)*, Hefei, China, Oct 2014.

[144] T. Huovinen, E. Pajala, and T. Ristaniemi, "On the analytic performance of differential spread spectrum code acquisition," in *Proc. of 10th International Conference on Communication Systems (ICCS 2006)*, Singapore, Nov 2006.

[145] *802.11-2012 IEEE Standard for Information technology - Telecommunications and information exchange between systems Local and metropolitan area networks - Specific requirements Part*

11: Wireless LAN Medium Access Control (MAC) and Physical Layer (PHY) Specifications, IEEE.

[146] *802.11ac-2013 IEEE Standard for Information technology - Telecommunications and information exchange between systems - Local and metropolitan area networks - Specific requirements - Part 11: Wireless LAN Medium Access Control (MAC) and Physical Layer (PHY) Specifications - Amendment 4: Enhancements for Very High Throughput for Operation in Bands below 6 GHz*, IEEE.

[147] *802.11ad-2012 IEEE Standard for Information technology - Telecommunications and information exchange between systems–Local and metropolitan area networks - Specific requirements- Part 11: Wireless LAN Medium Access Control (MAC) and Physical Layer (PHY) Specifications Amendment 3: Enhancements for Very High Throughput in the 60 GHz Band*, IEEE.

[148] *802.11af-2013 - IEEE Standard for Information technology - Telecommunications and information exchange between systems - Local and metropolitan area networks - Specific requirements - Part 11: Wireless LAN Medium Access Control (MAC) and Physical Layer (PHY) Specifications Amendment 5: Television White Spaces (TVWS) Operation*, IEEE.

[149] J. Iinatti and A. Pouttu, "Differentially coherent code acquisition in Doppler," in *Proc. of 50th IEEE Vehicular Technology Conference (VTC Fall)*, vol. 2, Sep 1999, pp. 703–707.

[150] J. Iinatti, "Comparison of threshold setting rules for the probability of acquisition in a DS spread spectrum receiver," in *Proc. of International Zurich Seminar on Broadband Communications*, 1998, pp. 23–28.

[151] ——, "On the threshold setting principles in code acquisition of DS-SS signals," in *IEEE Journal on Selected Areas in Communications*, vol. 18, no. 1, Jan 2000, pp. 62–72.

[152] N. Islam, E. S. Lohan, A. Lakhzouri, E. Pajala, H. Laitinen, and M. Renfors, "Indoor fading distributions for GPS-based pseudolite signals," in *Proc. of International Workshop on Satellite and Space Communications (IWSS)*, Salzburg, Austria, Sep 2007.

[153] D. Jiménez-Baños, N. Blanco-Delgado, G. López-Risueño, G. Seco-Granados, and A. Garcia-Rodriguez, "Innovative techniques for GPS indoor positioning using a snapshot receiver," in *Proc. of the 19th International Technical Meeting of the Satellite Division of The Institute of Navigation (ION GNSS)*, Fort Worth, TX, Sep 2006, pp. 2944–2955.

[154] J. Jung, "Implementation of Correlation Power Peak Ratio Based Signal Detection Method," in *Proc. of the 17th International Technical Meeting of the Satellite Division of The Institute of Navigation (ION GNSS)*, Long Beach, CA, Sep 2004, pp. 486–490.

[155] S. Jung, C. oh Lee, and D. Han, "Wi-Fi fingerprint-based approaches following log-distance path loss model for indoor positioning," in *Proc. of IEEE MTT-S International Microwave Workshop Series on Intelligent Radio for Future Personal Terminals (IMWS-IRFPT)*, Aug 2011.

[156] K. Kaemarungsi, "Efficient Design of Indoor Positioning Systems Based on Location Fingerprinting," in *Proc. of International Conference on Wireless Networks, Communications and Mobile Computing*, Jun 2005.

[157] ——, "Distribution of WLAN Received Signal Strength Indication for Indoor Location Determination," in *Proc. of 1st International Symposium on Wireless Pervasive Computing*, Jan 2006.

[158] K. Kaemarungsi and P. Krishnamurthy, "Modeling of Indoor Positioning Systems Based on Location Fingerprinting," in *Proc. of 23rd Annual Joint Conference of the IEEE Computer and Communications Societies (IEEE INFOCOM)*, vol. 2, Hong Kong, China, Mar 2004, pp. 1012–1022.

[159] B.-J. Kang and I.-K. Lee, "A Performance Comparison of Code Acquisition Techniques in DS-CDMA System," in *Wireless Personal Communications*, vol. 25, no. 2, May 2003, pp. 163–176.

[160] S. S. Kanhere, "Participatory Sensing: Crowdsourcing Data from Mobile Smartphones in Urban Spaces," in *Proc. of IEEE 12th International Conference on Mobile Data Management*, Jun 2011, pp. 2–6.

[161] E. D. Kaplan, *Understanding GPS - Principles and Applications*. Boston: Artech House, Inc., 1996.

[162] Karmeshu and R. Agrawal, "On efficacy of Rayleigh-inverse Gaussian distribution over K-distribution for wireless fading channels," in *Wireless Communications and Mobile Computing*, vol. 7, Jan 2007, pp. 1–7.

[163] S. M. Kay, *Fundamentals of Statistical Signal Processing: Estimation Theory*. Prentice Hall, 1993.

[164] ——, *Fundamentals of Statistical Signal Processing, Vol 2.: Detection Theory*. Prentice Hall, 1998.

[165] S. Kennedy, J. Hamilton, and H. Martell, "Architecture and System Performance of SPAN - NovAtel's GPS/INS Solution," in *Proc. of IEEE/ION PLANS 2006*, San Diego, USA, Apr 2006.

[166] B. Kim, M. Kwak, J. Lee, and T. T. Kwon, "A multi-pronged approach for indoor positioning with WiFi, magnetic and cellular signals," in *Proc. of International Conference on Indoor Positioning and Indoor Navigation (IPIN)*, Oct 2014.

[167] Y. Kim, Y. Chon, and H. Cha, "Smartphone-Based Collaborative and Autonomous Radio Fingerprinting," in *IEEE Transactions on Systems, Man, and Cybernetics, Part C (Applications and Reviews)*, vol. 42, no. 1, 2010, pp. 112–122.

[168] M. B. Kjaergaard, "Automatic Mitigation of Sensor Variations for Signal Strength Based Location Systems," in *Proc. of Second International Workshop on Location and Context Awareness*, 2006.

[169] M. B. Kjaergaard and C. V. Munk, "Hyberbolic Location Fingerprinting: A Calibration-Free Solution for Handling Differences in Signal Strength," in *Proc. of Sixth Annual International Conference on Pervasive Computing and Communications*, 2008, pp. 110–116.

[170] L. Klozar and J. Prokopec, "Propagation path loss models for mobile communication," in *Proc. of International Conference on Radioelektronika (RADIOELEKTRONIKA)*, Apr 2011.

[171] R. Klukas, G. Lachapelle, C. Ma, and G. Jee, "Gps signal fading model for urban centres," in *Proc. of IEE Proeedings on Microwaves, Antennas and Propagation*, vol. 150, no. 4, Aug 2003, pp. 245–252.

[172] K. R. Kolodziejski and J. W. Betz, "Effect of Non-white Gaussian Interference on GPS Code Tracking Accuracy," in *The MITRE Corporation Technical Report MTR99B21R1*, Jun 1999.

[173] L. Koski, T. Perälä, and R. Piché, "Indoor positioning using WLAN coverage area estimates," in *Proc. of Indoor Positioning and Indoor Navigation (IPIN)*, Zurich, Switzerland, Sep 2010.

[174] C. Koweerawong, K. Wipusitwarakun, and K. Kaemarungsi, "Indoor localization improvement via adaptive RSS fingerprinting database," in *Proc. of Information Networking*, Bangkok, Thailand, Jan 2013, pp. 412–416.

[175] S. P. Kuo, B. J. Wu, W. C. Peng, and Y. C. Tseng, "Cluster Enhanced Techniques for Pattern-Matching Localization Systems," in *Proc. of Mobile Adhoc and Sensor Systems (MASS)*, Pisa, Italy, Oct 2007, pp. 1–9.

[176] A. Kushki, K. N. Plataniotis, and A. N. Venetsanopoulos, "Kernel-based positioning in wireless local area networks," in *IEEE Transactions on Mobile Computing*, vol. 6, no. 6, 2007, pp. 689–705.

[177] ——, "Sensor Selection for Mitigation of RSS-based Attacks in Wireless Local Area Network Positioning," in *Proc. of IEEE International Conference on Acoustics, Speech and Signal Processing (ICASSP)*, Las Vegas, NV, USA, Mar 2008, pp. 2065 – 2068.

[178] G. Lachapelle, H. Kuusniemi, D. T. H. Dao, G. MacGougam, and M. E. Cannon, "HSGPS Signal Analysis and Performance under Various Indoor Conditions," in *Navigation: Journal of The Institute of Navigation*, vol. 51, no. 1, 2004, pp. 29–44.

[179] E. Laitinen and E. S. Lohan, "Are all the Access Points necessary in WLAN-based indoor positioning?" in *Proc. of International Conference on Localization and GNSS (ICL GNSS) 2015*, Gothenburg, Sweden, Jun 2015.

[180] ——, "Access Point topology evaluation and optimization based on Cramér-Rao Lower Bound for WLAN indoor positioning," in *Proc. of International Conference on Localization and GNSS (ICL GNSS) 2016*, Barcelona, Spain, Jun 2016.

[181] ——, "On the Choice of Access Point Selection Criterion and Other Position Estimation Characteristics for WLAN-Based Indoor Positioning," in *MDPI Sensors*, vol. 16, no. 5, May 2016.

[182] E. Laitinen, E. S. Lohan, J. Talvitie, and S. Shrestha, "Access Point Significance Measures in WLAN-based Location," in *Proc. of 9th Workshop on Positioning Navigation and Communication (WPNC)*, Dresden, Germany, Mar 2012, pp. 24–29.

[183] E. Laitinen, J. Talvitie, and E. S. Lohan, "On the RSS biases in WLAN-based indoor positioning," in *Proc. of IEEE International Communication Workshop (ICCW)*, London, UK, Jun 2015, pp. 797–802.

[184] E. Laitinen, J. Talvitie, E. S. Lohan, and M. Renfors, "Comparison of Positioning Accuracy of Grid and Path Loss-Based Mobile Positioning Methods Using Received Signal Strenghts," in *Proc. of Signal Processing and Applied Mathematics for Electronics and Communications (SPAMEC) 2011*, Cluj-Napoca, Romania, Aug 2011.

[185] A. Lakhzouri, E. S. Lohan, R. Hamila, and M. Renfors, "Extended Kalman Filter Channel Estimation for Line-of-Sight Detection in WCDMA Mobile Positioning," in *EURASIP Journal on Advances in Signal Processing*, vol. 13, Dec 2003, pp. 1268–1278.

[186] A. Lakhzouri, E. S. Lohan, I. Saastamoinen, and M. Renfors, "Interference and indoor channel propagation modeling based on gps satellite signal measurements," in *Proc. of the 18th International Technical Meeting of the Satellite Division of The Institute of Navigation (ION GNSS)*, Sep 2005, pp. 896–901.

[187] ——, "Measurement and characterization of satellite-to-indoor radio wave propagation channel," in *Proc. of the European Navigation Conference (ENC-GNSS)*, Jul 2005.

[188] ——, "On second order statistics of the satellite-to-indoor channel based on field measurements," in *Proc. of 16th International Symposium on Personal, Indoor and Mobile Radio Communications (PIMRC)*, vol. 4, Sep 2005, pp. 2632–2636.

[189] J. Lategahn, M. Muller, and C. Rohrig, "Extended Kalman filter for a low cost TDoA/IMU pedestrian localization system," in *Proc. of 11th Workshop on Positioning, Navigation and Communication (WPNC)*, Mar 2014.

[190] C. Laurendeau and M. Barbeau, "Centroid Localization of Uncooperative Nodes in Wireless Networks Using a Relative Span Weighting Method," in *EURASIP Journal on Wireless Communications and Networking*, Nov 2009.

[191] N. Lei, H. Zhu, and J. Cui, "Wavelet-based method for weak satellite signal acquisition," in *Proc. of International Conference on Transportation, Mechanical, and Electrical Engineering (TMEE)*, Dec 2011.

[192] B. Li, T. Gallagher, A. G. Dempster, and C. Rizos, "How feasible is the use of magnetic field alone for indoor positioning?" in *Proc. of International Conference on Indoor Positioning and Indoor Navigation (IPIN)*, Nov 2012.

[193] B. Li, I. J. Quader, and A. G. Dempster, "On outdoor positioning with Wi-Fi," in *Journal of Global Positioning Systems*, vol. 7, no. 1, 2008, pp. 18–26.

[194] D. Li, B. Zhang, and C. Li, "A Feature-Scaling-Based k-Nearest Neighbor Algorithm for Indoor Positioning Systems," in *IEEE Internet of Things Journal*, vol. 3, no. 4, Aug 2016.

[195] H. Li, X. Chen, L. Huang, and D. Yao, "A GPS/Wi-Fi Integrated System for Positioning in Cooperative Vehicle and Infrastructure System," in *Proc. of IEEE International Conference on Vehicular Electronics and Safety (ICVES)*, Jul 2012.

[196] J. Li, J. Zhang, B. Zhang, and B. Shen, "Operation and Development of BeiDou Navigation Satellite System," in *Proc. of International Association of Institutes of Navigation World Congress (IAIN)*, Prague, Czech Republic, Oct 2015.

[197] K. Li, J. Bigham, and L. Tokarchuk, "Validation of a Probabilistic Approach to Outdoor Localization," in *IEEE Wireless Communications Letters*, vol. 2, no. 2, Apr 2013, pp. 167–170.

[198] L. Li, J. Shen, C. Zhao, T. Moscibroda, J.-H. Lin, and F. Zhao, "Experiencing and Handling the Diversity in Data Density and Environmental Locality in an Indoor Positioning Service," in *Proc. of 20th Annual International Conference on Mobile Computing and Networking (MOBICOM)*, 2014.

[199] D. Liang, Z. Zhang, and M. Peng, "Access Point Reselection and Adaptive Cluster Splitting-Based Indoor Localization in Wireless Local Area Networks," in *IEEE Internet of Things Journal*, vol. 2, no. 6, Oct 2015, pp. 573–585.

[200] Y. Liu, X. Yi, and Y. He, "A Novel Centroid Localization for Wireless Sensor Networks," in *International Journal of Distributed Sensor Networks*, vol. 2012, 2011.

[201] E. S. Lohan, "Statistical analysis of BPSK-like techniques for the acquisition of Galileo signals," in *Journal of Aerospace Computing, Information, and Communication*, vol. 3, no. 5, 2006.

[202] E. S. Lohan and K. Borre, "Performance limits in multi-GNSS systems," in *In print IEEE Transactions on Aerospace*, Dec 2016.

[203] E. S. Lohan, A. Burian, and M. Renfors, "Low-Complexity Acquisition Methods for Split-Spectrum CDMA Signals," in *Wiley International Journal of Satellite Communications and Networking*, vol. 26, no. 6, 2008.

[204] E. S. Lohan, A. Lakhzouri, and M. Renfors, "Selection of the multiple-dwell hybrid-search strategy for the acquisition of Galileo signals in fading channels," in *Proc. of 15th IEEE International Symposium on Personal, Indoor and Mobile Radio Communications (PIMRC)*, vol. 4, Sep 2004.

[205] ——, "Binary-Offset-Carrier modulation techniques with applications in satellite navigation systems," in *Wireless Communications and Mobile Computing*, vol. 7, Jul 2006, pp. 767–779.

[206] ——, "Feedforward delay estimators in adverse multipath propagation for Galileo and modernized GPS signals," in *EURASIP Journal of Applied Signal Processing*, 2006, pp. 53–57.

[207] E. S. Lohan, J. L. Salcedo, and G. Seco-Granados, "Analysis of advanced post-detection integration techniques for the acquisition with pilot signals in High Sensitivity-Galileo receivers," in *4th International Colloquium Scientific and Fundamental Aspects of the Galileo Programme. ESA Proceedings WPP. European Space Agency, 2013.*, vol. 355, Prague, Czech Republic, Dec 2013.

[208] E. S. Lohan, J. Talvitie, P. Figueiredo e Silva, H. Nurminen, S. Ali-Löytty, and R. Piché, "Received signal strength models for WLAN and BLE-based indoor positioning in multi-floor buildings," in *Proc. of International Conference on Localization and GNSS (ICL-GNSS)*, Jun 2015, pp. 767–779.

[209] E. S. Lohan, J. Talvitie, and G. Seco-Granados, "Data fusion approaches for WiFi fingerprinting," in *Proc. of International Conference on Localization and GNSS (ICL-GNSS)*, Jun 2016.

[210] C. Loo, "A statistical model for a land mobile satellite link," in *IEEE Transaction on Vehicular Technology*, 1985, pp. 122–127.

[211] V. Lucas-Sabola, G. Seco-Granados, J. A. Lóopez-Salcedo, J. A. García-Molina, and M. Crisci, "Cloud GNSS receivers: New advanced applications made possible," in *Proc. of International Conference on Localization and GNSS (ICL-GNSS)*, Jun 2016.

[212] G. Lui, T. Gallagher, B. Li, A. G. Dempster, and C. Rizos, "Differences in RSSI readings made by different Wi-Fi chipsets: A limitation of WLAN localization," in *Proc. of International Conference on Localization and GNSS (ICL-GNSS)*, Tampere, Finland, Jun 2011, pp. 53–57.

[213] J. Ma, L. Miao, X. Zhang, and Z. Gao, "Weak signal acquisition algorithm of GPS software receiver aided by INS," in *Proc. of 6th International Symposium on Computational Intelligence and Design (ISCID)*, Oct 2013, pp. 321–325.

[214] J. Ma, X. Li, X. Tao, and J. Lu, "A novel clustering and KWNN-based strategy for Wi-Fi fingerprint indoor localization," in *Proc. of International Symposium on a World of Wireless, Mobile and Multimedia Networks (WoWMoM)*, 2008, pp. 1–8.

[215] J. Machaj and P. Brida, "Optimization of rank based fingerprinting localization algorithm," in *Proc. of International Conference on Indoor Positioning and Indoor Navigation (IPIN)*, Nov 2012.

[216] J. Machaj, P. Brida, and R. Piché, "Rank based fingerprinting algorithm for indoor positioning," in *Proc. of International Conference on Indoor Positioning and Indoor Navigation (IPIN)*, Sep 2011.

[217] K. Maneerat, K. Kaemarungsi, and C. Prommak, "Robust Floor Determination Algorithm for Indoor Wireless Localization Systems under Reference Node Failure," in *Mobile Information Systems*, vol. 2016, Sep 2016.

[218] K. Maneerat and C. Prommak, "An Enhanced Floor Estimation Algorithm for Indoor Wireless Localization Systems Using Confidence Interval Approach," in *International Journal of Computer, Electrical, Automation, Control and Information Engineering*, vol. 8, no. 7, 2014.

[219] D. E. Manolakis, "Efficient solution and performance analysis of 3-D position estimation by trilateration," in *IEEE Transactions on Aerospace and Electronic Systems*, vol. 32, no. 4, Oct 1996, pp. 1239–1248.

[220] W.-L. Mao and A.-B. Chen, "New code delay compensation algorithm for weak GPS signal acquisition," in *International Journal of Electronics and Communications*, vol. 63, no. 8, Aug 2009, pp. 665–677.

[221] A. Mariani, S. Kandeepan, A. Giorgetti, and M. Chiani, "Cooperative weighted centroid localization for cognitive radio networks," in *Proc. of International Symposium on Communications and Information Technologies (ISCIT)*, Oct 2012.

[222] N. Martin, V. Leblond, G. Guillotel, and V. Heiries, "BOC(x,y) signal acquisition techniques and performances," in *Proc. of the 16th International Technical Meeting of the Satellite Division of The Institute of Navigation (ION GPS/GNSS)*, Sep 2003, pp. 188–198.

[223] ——, "Acquisition of the Galileo OAS L1b/c signal for the mass-market receiver," in *Proc. of the 18th International Technical Meeting of the Satellite Division of The Institute of Navigation (ION GNSS)*, Long Beach, CA, USA, Sep 2005, pp. 1143–1152.

[224] R. K. Martin, A. S. King, J. R. Pennington, R. W. Thomas, R. Lenahan, and C. Lawyer, "Modeling and Mitigating Noise and Nuisance Parameters in Received Signal Strength Positioning," in *IEEE Transactions on Signal Processing*, vol. 60, no. 10, Oct 2012, pp. 5451–5463.

[225] S. Mazuelas, A. Bahillo, R. M. Lorenzo, P. Fernandez, F. A. Lago, E. Garcia, J. Blas, and E. J. Abril, "Robust Indoor Positioning Provided by Real-Time RSSI Values in Unmodified WLAN Networks," in *IEEE Journal of Selected Topics in Signal Processing*, vol. 3, no. 5, 2009, pp. 821–831.

[226] P. Mazumdar, V. J. Ribeiro, and S. Tewari, "Generating indoor maps by crowdsourcing positioning data from smartphones," in *Proc. of International Conference on Indoor Positioning and Indoor Navigation (IPIN)*, Oct 2014.

[227] C. Mensing and S. Sand, "Performance Enhancement of GNSS Positioning in Critical Scenarios by Wireless Communications Systems," in *Proc. of IEEE/ION Position, Location and Navigation Symposium*, May 2008.

[228] P. Mestre, C. Serodio, L. Coutinho, L. Reigoto, and J. Matias, "Hybrid technique for fingerprinting using IEEE802.11 wireless networks," in *Proc. of International Conference on Indoor Positioning and Indoor Navigation (IPIN)*, Sep 2011, pp. 1–7.

[229] H. Miao, Z. Wang, J. Wang, L. Zhang, and L. Zhengfeng, "A Novel Access Point Selection Strategy for Indoor Location with Wi-Fi," in *Proc. of Control and Decision Conference (CCDC)*, Changsha, China, May 2014, pp. 5260–5265.

[230] P. Mirowski, D. Milioris, P. Whiting, and T. K. Ho, "Probabilistic radio-frequency fingerprinting and localization on the run," in *Bell Labs Technical Journal*, vol. 18, no. 4, Mar 2014, pp. 111–133.

[231] A. F. Molisch, *Wireless Communications, Second Edition*. John Wiley & Sons, Inc., 2011.

[232] R. Mondal, J. Turkka, T. Ristaniemi, and T. Henttonen, "Performance Evaluation of MDT RF Fingerprinting Framework," in *Proc. of 7th international Conference on Mobile Computing and Ubiquitous Networking (ICMU2014)*, Jan 2014.

[233] L. D. Mundo, R. Ansay, C. Festin, and R. Ocampo, "A comparison of Wireless Fidelity (Wi-Fi) fingerprinting techniques," in *Proc. of Int. Conf. ICT Convergence*, 2011, pp. 20–25.

[234] M. Nakagami, "The *m*-distribution - A General Formula of Intensity Distribution of Rapid Fading," in *W. C. Hoffman: Statistical Methods of Radio Wave Propagation*, Oxford, England, 1960, pp. 3–36.

[235] "5G White Paper," Available via:
https://www.ngmn.org/, NGMN Alliance, Feb 2015.

[236] T. Nick, G. Smietanka, and J. Götze, "RSS-based channel measurements and their influence on localization in RFID applications," in *Proc. of 17th International Symposium on Consumer Electronics (ISCE)*, Hsinchu, Taiwan, 2013.

[237] H. Niedermeier, B. Eissfeller, J. Winkel, T. Pany, B. Riedl, T. Wörz, R. Schweikert, S. Lagrasta, G. Lopez-Risueno, and D. Jiminez-Banos, "DINGPOS: High Sensitivity GNSS platform for deep indoor scenarios," in *Proc. of International Conference on Indoor Positioning and Indoor Navigation (IPIN)*, Zürich, Switzerland, Sep 2010.

[238] J. Niu, B. Wang, L. Cheng, and J. J. P. C. Rodrigues, "WicLoc: An indoor localization system based on WiFi fingerprints and crowdsourcing," in *Proc. of IEEE International Conference on Communications (ICC)*, Jun 2015.

[239] A. S. Noh, W. J. Lee, and J. Y. Ye, "Comparison of the mechanisms of the Zigbee's indoor localization algorithm," in *Proc. of 9th ACIS International Conference on Software Engineering, Artificial Intelligence, Networking, and Parallel/Distributed Computing (SNPD)*, Phuket, Thailand, 2008, pp. 13–18.

[240] J. Nurmi, E. S. Lohan, S. Sand, and H. Hurskainen, *GALILEO Positioning Technology*. Springer, 2015.

[241] H. Nurminen, J. Talvitie, S. Ali-Löytty, and P. Müller, "Statistical Path Loss Parameter Estimation and Positioning Using RSS Measurements in Indoor Wireless Networks," in *Proc. of Indoor Positioning and Indoor Navigation (IPIN)*, Sydney, NSW, Australia, Nov 2012, pp. 1–9.

[242] T. Ohira, T. Hirai, S. Tomisato, and M. Hata, "A study of mobile path loss estimation models for a sloping terrain area in cellular systems," in *Proc. of 18th Asia-Pacific Conference on Communications (APCC)*, 2012, pp. 427–477.

[243] T. Ojanperä and R. Prasad, *Wideband CDMA for Third Generation Mobile Communications*. Artech House, Inc., 1998.

[244] Y. Okumura, E. Ohmori, T. Kawano, and K. Fukuda, "Field strength and its variability in VHF and UHF land-mobile radio service," in *Review of the Electrical Communications Laboratory*, vol. 16, no. 9-10, Sep 1968, pp. 825–873.

[245] A. Osseiran, F. Boccardi, V. Braun, K. Kusume, P. Marsch, M. Maternia, O. Queseth, M. Schellmann, H. Schotten, H. Taoka, H. Tullberg, M. A. Uusitalo, B. Timus, and M. Fallgren, "Scenarios for the 5G Mobile and Wireless Communications: the Vision of the METIS Project," in *IEEE Communications Magazine*, vol. 52, no. 5, May 2014, pp. 26–35.

[246] A. Osseiran, V. Braun, T. Hidekazu, P. Marsch, H. Schotten, H. Tullberg, M. A. Uusitalo, and M. Schellmann, "The foundation of the Mobile and Wireless Communications System for 2020 and beyond - Challenges, Enablers and Technology Solutions," in *Proc of. IEEE Vehicular Technology Conference (VTC Spring)*, 2013, pp. 1–5.

[247] V. Otsason, A. Varshavsky, A. LaMarca, and E. de Lara, "Accurate GSM indoor localization," in *Ubiquitous Computing (UbiComp), Lecture Notes in Computer Science*, vol. 3660, 2005, pp. 141–158.

[248] E. Pajala, "Code-Frequency Acquisition Algorithms for BOC Modulated CDMA Signals with Applications in Galileo and GPS Systems," Master's thesis, Institute of Communications Engineering, Tampere University of Technology, Tampere, Finland, 2005.

[249] E. Pajala, T. Huovinen, and T. Ristaniemi, "Enhanced differential correlation method for acquisition of Galileo signals," in *Proc. of 10th International Conference on Communication Systems (ICCS)*, Singapore, Nov 2006.

[250] E. Pajala, T. Isotalo, A. Lakhzouri, and E. S. Lohan, "An improved simulation model for Nakagami-m fading channels for satellite positioning applications," in *Proc. of 3rd Workshop on Positioning Navigation and Communication (WPNC)*, Hannover, Germany, Mar 2006, pp. 81–89.

[251] E. Pajala, E. S. Lohan, and M. Renfors, "On the choice of the parameters for fast hybrid-search acquisition architectures of GPS and Galileo signals," in *Proc. of Nordic Radio Symposium and Finnish Wireless Communication Workshop (NRS/FWCW)*, Oulu, Finland, Aug 2004.

[252] ——, "CFAR detectors for hybrid-search acquisition of Galileo signals," in *Proc. of European Navigation Conference (ENC-GNSS)*, Munich, Germany, Jul 2005.

[253] J. Pang, F. V. Graas, J. Starzyk, and Z. Zhu, "Fast Direct GPS P-code Acquisition," in *GPS Solutions*, vol. 7, no. 3, Dec 2003, pp. 168–175.

[254] J.-G. Park, D. Curtis, S. Teller, and J. Ledlie, "Implications of device diversity for organic localization," in *Proc. of IEEE INFOCOM*, 2011, pp. 3182–3190.

[255] V. Pasku, A. D. Angelis, M. Dionigi, G. D. Angelis, A. Moschitta, and P. Carbone, "A Positioning System Based on Low-Frequency Magnetic Fields," in *IEEE Transactions on Industrial Electronics*, vol. 63, no. 4, Apr 2016.

[256] N. Patwari, J. N. Ash, S. Kyperountas, A. O. Hero III, R. L. Moses, and N. S. Correal, "Locating the nodes: Cooperative localization in wireless sensor networks," in *IEEE Signal Processing Magazine*, vol. 22, no. 4, Jul 2005, pp. 54–69.

[257] N. Patwari, A. O. Hero III, M. Perkins, N. S. Correal, and R. J. O'Dea, "Relative Location Estimation in Wireless Sensor Networks," in *IEEE Transactions on Signal Processing*, vol. 51, no. 8, Aug 2003, pp. 2137–2148.

[258] V. Pawar and M. Zaveri, "Graph based K-nearest neighbor minutiae clustering for fingerprint recognition," in *Proc. of 10th International Conference on Natural Computation (ICNC)*, 2014, pp. 675–680.

[259] K. Pedersen, J. B. Andersen, J. P. Kermoal, and P. Mogensen, "A stochastic multiple-input-multiple-output radio channel model for evaluation of space-time coding algorithms," in *Proc. of Vehicular Technology Conference (VTC Fall)*, vol. 2, Boston, USA, Sep 2000, pp. 893–897.

[260] R. Pedone, M. Villanti, G. E. Corazza, and T. Mathiopolous, "Robust Frame Synchronization Design in the Presence of Frequency Errors," in *Proc. of 23rd International Communication Satellite Systems Conference (ICSSC) and 11th Ka and Broadband Communications Conference*, Rome, Italy, Sep 2005.

[261] L. Pei, R. Chen, Y. Chen, H. Leppäkoski, and A. Perttula, "Indoor/Outdoor Seamless Positioning Technologies Integrated on Smart Phone," in *Proc. of 1st International Conference on Advances in Satellite and Space Communications (SPACOMM)*, Jul 2009.

[262] I. Petrovski, K. Okano, M. Ishii, H. Torimoto, Y. Konishi, and R. Shibasaki, "Pseudolite Implementation for Social Infrastructure and Seamless Indoor/Outdoor Positioning," in *Proc. of the 15th International Technical Meeting of the Satellite Division of The Institute of Navigation (ION GPS)*, Sep 2002.

[263] A. Polydoros and C. L. Weber, "A Unified Approach to Serial Search Spread-Spectrum Code Acquisition - Parts I and II: A Matched-Filter Receiver," *IEEE Transactions on Communications*, vol. 32, no. 5, pp. 542–560, May 1984.

[264] D. Porcino, "Performance of a OTDOA-IPDL positioning receiver for 3GPP-FDD mode," in *Proc. of 2nd International Conference on 3G Mobile Communication Technologies*, London, UK, 2001, pp. 221–225.

[265] P. Prasithsangaree, P. Krishnamurthy, and P. Chrysanthis, "On indoor position location with wireless LANs," in *Proc. of 13th IEEE International Symposium on Personal, Indoor and Mobile Radio Communications*, Sep 2002.

[266] J. G. Proakis, *Digital Communications*. McGraw-Hill, 2004.

[267] M. L. Psiaki, "Block Acquisition of Weak GPS Signals in a Software Receiver," in *Proc. of Institute of Navigation GPS Conference (ION GPS)*, Salt Lake City, UT, Sep 2001, pp. 2838–2850.

[268] T. S. Rappaport, J. H. Reed, and B. D. Woerner, "Position location using wireless communications on highways of the future," in *IEEE Communications Magazine*, vol. 34, no. 10, 1996, pp. 33–41.

[269] A. Razavi, M. Valkama, and E. S. Lohan, "K-Means Fingerprint Clustering for Low-Complexity Floor Estimation in Indoor Mobile Localization," in *Proc. of Globecom Workshop on Localization and Tracking: Indoors, Outdoors and Emerging Networks*, San Diego, CA, USA, Dec 2015, pp. 1–7.

[270] A. E. C. Redondi and E. Amaldi, "Optimizing the placement of anchor nodes in RSS-based indoor localization systems," in *Proc. of 12th Annual Mediterranean Ad Hoc Networking Workshop (MED-HOC-NET)*, Jun 2013, p. 8.13.

[271] P. Richter, "Design and Implementation of an Ubiquitous Positioning System Based on GNSS Pseudoranges and Assisted With WLAN-RSSI," Ph.D. dissertation, Universidad Autónoma de Querétaro Facultad de Ingeniería, Santiago de Querétaro, Mexico, Sep 2016.

[272] M. E. Rida, F. Liu, Y. Jadi, A. A. A. Algawhari, and A. Askourih, "Indoor location position based on Bluetooth Signal Strength," in *Proc. of 2nd International Conference on Information Science and Control Engineering (ICISCE)*, Apr 2015.

[273] T. Ristaniemi and J. Joutsensalo, "Code timing acquisition for DS-CDMA in fading channels by differential correlations," in *IEEE Transactions on Communications*, vol. 49, no. 5, May 2001, pp. 899–910.

[274] Rohde and Schwarz, "LTE Location Based Services Technology Introduction, White Paper," Apr 2013, pp. 1–22.

[275] T. Roos, P. Myllymäki, H. Tirri, P. Misikangas, and J. Sievänen, "A Probabilistic Approach to WLAN User Location Estimation," in *International Journal of Wireless Information Networks*, vol. 9, no. 3, Jul 2002, pp. 155–163.

[276] A. Roxin, J. Gaber, M. Wack, and A. Nait-Sidi-Moh, "Survey of Wireless Geolocation Techniques," in *Proc. of IEEE Global Communications Conference (Globecom) Workshops*, Washington, DC, Nov 2007, pp. 1–9.

[277] A. Rusu-Casandra, E. S. Lohan, G. Seco-Granados, and I. Marghescu, "Investigation of Narrowband Interference Filtering Algorithms for Galileo CBOC Signals," in *Proc. of the 3rd European Conference of Circuits Technology and Devices - Recent Advances in Communications, Circuits & Technological Innovation*, Paris, France, Dec 2012.

[278] N. Samama, *Global Positioning - Technologies and performance*. John Wiley & Sons, Inc., 2008.

[279] D. A. Sanou and R. J. Landry, "Analysis of GNSS Interference Impact on Society and Evaluation of Spectrum Protection Strategies," in *Positioning*, vol. 4, 2013, pp. 169–182.

[280] C. Sapumohotti, M. Y. Alias, and T. S. Wei, "Spatial Aware Signal Space Clustering Algorithm for Optimal Calibration Point Locations in Location Fingerprinting," in *Proc. of 19th Asia-Pacific Conference on Communications (APCC)*, 2013, pp. 661–665.

[281] L. Schauer, F. Dorfmeister, and M. Maier, "Potentials and limitations of WIFI-positioning using Time-of-Flight," in *Proc. of Indoor Positioning and Indoor Navigation (IPIN)*, Montbeliard-Belfort, France, Oct 2013, pp. 1–9.

[282] A. Schmid and A. Neubauer, "Perfomance Evaluation of Differential Correlation for Single Shot Measurement Positioning," in *Proc. of the 17th International Technical Meeting of the Satellite Division of The Institute of Navigation (ION GNSS)*, Long Beach, CA, USA, Sep 2004, pp. 1998–2009.

[283] L. Schumacher, J. P. Kermoal, F. Frederiksen, K. I. Pedersen, A. Algans, and P. Mogensen, *MIMO Channel Characterisation*, IST Project IST-1999-11729 METRA Deliverable D2, Feb 2001.

[284] L. Schumacher, K. I. Pedersen, and P. E. Mogensen, "From antenna spacings to theoretical capacities - guidelines for simulating MIMO systems," in *proc. of 13th IEEE International Symposium on Personal, Indoor and Mobile Radio Communications*, vol. 2, Sep 2002, pp. 587–592.

[285] G. Seco-Granados, J. A. Lopez-Salcedo, D. Jimenez-Banos, and G. Lopez-Risueno, "Challenges in Indoor GNSS: Unveiling its core features in signal processing," in *IEEE Signal Processing Magazine*, vol. 29, no. 2, 2012, pp. 108–131.

[286] B. Selim, O. Alhussein, S. Muhaidat, G. K. Karagiannidis, and J. Liang, "Modeling and Analysis of Wireless Channels via the Mixture of Gaussian Distribution," in *IEEE Transactions on Vehicular Technology*, vol. 65, no. 10, Oct 2016.

[287] "GNSS Interference," Available via: http://www.insidegnss.com/, Septentrio nv, 2012.

[288] S. Sesia, I. Toufik, and M. Baker, *LTE - The UMTS Long Term Evolution: From Theory to Practice. 2nd edition.* John Wiley & Sons, Inc., 2011.

[289] Z. Shi, Y. Sun, L. Xiong, Y. Hu, and B. Yin, "A Multisource Heterogeneous Data Fusion Method for Pedestrian Tracking," in *Mathematical Problems in Engineering*, vol. 2015, 2015.

[290] S. Shrestha, E. Laitinen, J. Talvitie, and E. S. Lohan, "RSSI Channel Effects in Cellular and WLAN positioning," in *Proc. of 9th Workshop on Positioning Navigation and Communication (WPNC)*, Dresden, Germany, Mar 2012, pp. 187–192.

[291] S. Shrestha, J. Talvitie, and E. S. Lohan, "Deconvolution-based indoor localization with WLAN signals and unknown access point locations," in *Proc. of Localization and GNSS (ICL-GNSS)*, Turin, Italy, Jun 2013, pp. 1–6.

[292] Y. Shu, Y. Huang, J. Zhang, P. Coué, P. Cheng, J. Chen, and K. G. Shin, "Gradient-Based Fingerprinting for Indoor Localization and Tracking," in *IEEE Transactions on Industrial Electronics*, vol. 63, no. 4, 2015, pp. 2424–2433.

[293] M. K. Simon and M. S. Alouini, *Digital Communications over Fading Channels: A Unified Approach to Performance Analysis*. Wiley InterScience, Sep 2000.

[294] M. K. Simon, J. K. Omura, R. A. Scholtz, and B. K. Levitt, *Spread spectrum communications handbook: revised edition.* McGraw-Hill Inc., 1994.

[295] Y. Singh, "Comparison of Okumura, Hata and COST-231 Models on the Basis of Path Loss and Signal Strength," in *International Journal of Computer Applications*, vol. 59, Dec 2012.

[296] R. D. Soriano and J. J. S. Marciano, "Investigating received signal characteristics upon on-axis rotation of an embedded antenna in a mobile device," in *IEEE Region 10 Conference (TENCON)*, Nov 2016.

[297] E. A. Sourour and S. C. Gupta, "Direct-Sequence Spread-Spectrum Parallel Acquisition in a Fading Mobile Channel," in *IEEE Transactions on Communications*, vol. 38, no. 7, Jul 1990, pp. 992–998.

[298] M. R. Spiegel, *Theory and Problems of Probability and Statistics. Third Edition.* McGraw-Hill, 1998.

[299] J. J. Spilker, Jr., *Digital communications by satellite*. Prentice Hall, 1977.

[300] Spirent, "An Overview of LTE Positioning, White Paper," Feb 2012.

[301] M. A. Spirito and A. G. Mattioli, "Preliminary experimental results of a gsm mobile phones positioning system based on timing advance," in *Proc. of IEEE Vehicular Technology Conference*, vol. 4, Sep 1999, pp. 2072–2076.

[302] M. A. Spirito, S. Pöykkö, and O. Knuuttila, "Experimental performance of methods to estimate the location of legacy handsets in gsm," in *Proc. of IEEE Vehicular Technology Conference*, vol. 4, 2001, pp. 2716–2720.

[303] M. Stella, M. Russo, and D. Begusic, "RF Localization in Indoor Environment," in *Radioengineering*, vol. 21, no. 2, 2012, pp. 557–567.

[304] S. Subedi, G.-R. Kwon, S. Shin, S. seung Hwang, and J.-Y. Pyun, "Beacon Based Indoor Positioning System Using Weighted Centroid Localization Approach," in *Proc. of 8th International Conference on Ubiquitous and Future Networks (ICUFN)*, Jul 2016.

[305] A. Sulyman, A. Nassar, M. Samimi, G. MacCartney, T. Rappaport, and A. Alsanie, "Radio propagation path loss models for 5G cellular networks in the 28 GHZ and 38 GHZ millimeter-wave bands," in *IEEE Commununications Magazine*, vol. 52, no. 9, Sep 2014, pp. 78–86.

[306] G. Sun, J. Chen, W. Guo, and K. J. R. Liu, "Signal processing techniques in network-aided positioning: A survey of state-of-the-art positioning designs," in *IEEE Signal Processing Magazine*, vol. 22, no. 4, Jul 2005, pp. 12–23.

[307] L. Sun, Z. Zheng, T. He, and F. Li, "Multifloor Wi-Fi Localization System with Floor Identification," in *International Journal of Distributed Sensor Networks*, vol. 2015, Jun 2015.

[308] T. H. Ta, F. Dovis, D. Margaria, and L. L. Presti, "Comparative Study on Joint Data/Pilot Strategies for High Sensitivity Galileo E1 Open Service Signal Acquisition," in *IET Radar, Sonar & Navigation*, vol. 4, no. 6, Dec 2010, pp. 764–779.

[309] J. Talvitie, "Algorithms and Methods for Received Signal Strength Based Wireless Localization," Ph.D. dissertation, Department of Electronics and Communications Engineering, Tampere University of Technology, Tampere, Finland, Jan 2016.

[310] J. Talvitie, E. S. Lohan, and M. Renfors, "The effect of coverage gaps and measurement inaccuracies in fingerprinting based indoor localization," in *International Conference on Localization and GNSS 2014 (ICL-GNSS 2014)*, Helsinki, Finland, Jun 2014.

[311] J. Talvitie, M. Renfors, and E. S. Lohan, "Novel Indoor Positioning Mechanism Via Spectral Compression," in *IEEE Communications Letters*, vol. 20, no. 2, 2015, pp. 352–355.

[312] R. D. Taranto, S. Muppirisetty, R. Raulefs, D. T. Slock, T. Svensson, and H. Wymeersch, "Location-Aware Communications for 5G Networks - How location information can improve

scalability, latency, and robustness of 5G," in *IEEE Signal Processing Magazine*, Nov 2014, pp. 102–112.

[313] J. Torres-Sospedra, G. M. Mendoza-Silva, R. Montoliu, Ó. Belmonte, F. Benitez, and J. Huerta, "Ensembles of indoor positioning systems based on fingerprinting: Simplifying parameter selection and obtaining robust systems," in *Proc. of International Conference on Indoor Positioning and Indoor Navigation (IPIN)*, Oct 2016.

[314] J. Torres-Sospedra, R. Montoliu, G. M. Mendoza-Silva, Ó. Belmonte, D. Rambla, and J. Huerta, "Providing Databases for Different Indoor Positioning Technologies: Pros and Cons of Magnetic Field and Wi-Fi Based Positioning," in *Mobile Information Systems*, vol. 2016, 2016.

[315] J. Torres-Sospedra, R. Montoliu, S. Trilles, Ó. Belmonte, and J. Huerta, "Comprehensive Analysis of Distance and Similarity Measures for Wi-Fi Fingerprinting," in *Expert Systems with Applications*, vol. 42, no. 23, Dec 2015, pp. 9263–9278.

[316] P. Torteeka and X. Chundi, "Indoor positioning based on Wi-Fi Fingerprint Technique using Fuzzy K-Nearest Neighbor," in *Proc. of 11th International Bhurban Conference on Applied Sciences and Technology (IBCAST)*, Jan 2014, pp. 461–465.

[317] E. Trevisani and A. Vitaletti, "Cell-ID location technique, limits and benefits: an experimental study," in *Proc. of 6th IEEE Workshop on Mobile Computing Systems and Applications (WMCSA 2004)*, Dec 2004, pp. 51–60.

[318] J. B.-Y. Tsui, *Fundamentals of Global Positioning System Receivers - A Software Approach*. John Wiley & Sons, Inc., 2005.

[319] F. van Diggelen, "Indoor GPS Theory & Implementation," in *Proc. of IEEE Position, Location & Navigation Symposium 2002*, 2002, pp. 240–247.

[320] T. Vaupel, J. Seitz, F. Kiefer, S. Haimerl, and J. Thielecke, "Wi-Fi positioning: System considerations and device calibration," in *Proc. of Indoor Positioning and Indoor Navigation (IPIN)*, Sep 2010.

[321] S. Viswanathan and S. Srinivasan, "Improved path loss prediction model for short range indoor positioning using bluetooth low energy," in *Proc. of IEEE Sensors*, Nov 2015.

[322] Q. D. Vo and P. De, "A Survey of Fingerprint-Based Outdoor Localization," in *IEEE Communications Surveys & Tutorials*, vol. 18, no. 1, 2015, pp. 491–506.

[323] M. Vuckovic, I. Petrovic, D. Vidovic, Z. Kostovic, S. Pletl, and D. Kukolj, "Space grid resolution impact on accuracy of the indoor localization fingerprinting," in *Proc. of 19th Telecommunications Forum (TELFOR)*, Belgrade, Serbia, Nov 2011, pp. 321–324.

[324] J. J. Wang, "Modeling and Geometry Design for Pseudolite Augmented Airborne DGPS," in *Proc. of the 18th International Technical Meeting of the Satellite Division of The Institute of Navigation (ION GNSS)*, Sep 2005.

[325] L. Wang and W.-C. Wong, "A Novel RSS Model and Power-bias Mitigation Algorithm in fingerprinting-based Indoor Localization in Wireless Local Area Networks," in *Proc. of 20th European Wireless Conference*, Barcelona, Spain, May 2014.

[326] Z. Wang and Y. Zheng, "The Study of the Weighted Centroid Localization Algorithm based on RSSI," in *Proc. of International Conference on Wireless Communication and Sensor Network (WCSN)*, Dec 2014.

[327] P. W. Ward, "Performance Comparisons Between FLL, PLL and a Novel FLL-Assisted-PLL Carrier Tracking Loop Under RF Interference Conditions," in *Proc. of the 11th International Technical Meeting of the Satellite Division of The Institute of Navigation (ION GPS)*, Sep 1998, pp. 783–795.

[328] G. I. Wassi, C. Despins, D. Grenier, and C. Nerguizian, "Indoor location using received signal strength of IEEE 802.11b access point," in *Proc. of Canadian Conference on Electrical and Computer Engineering*, May 2005.

[329] J. R. Watson, "High-sensitivity gps l1 signal analysis for indoor channel modelling," Master's thesis, Department of Geomatics Engineering, University of Calgary, Calgary, Alberta, 2005.

[330] J. Werner, M. Costa, A. Hakkarainen, K. Leppänen, and M. Valkama, "Joint User Node Positioning and Clock Offset Estimation in 5G Ultra-Dense Networks," in *Proc. of IEEE Global Communications Conference (GLOBECOM)*, San Diego, CA, 2015.

[331] J. Werner, J. Wang, A. Hakkarainen, N. Gulati, D. Patron, D. Pfeil, K. Dandekar, D. Cabric, and M. Valkama, "Sectorized Antenna-based DoA Estimation and Localization: Advanced Algorithms and Measurements," in *IEEE Journal on Selected Areas in Communications*, vol. 33, no. 11, May 2015.

[332] M. Z. Win, A. Conti, S. Mazuelas, Y. Shen, W. M. Gifford, D. Dardari, and M. Chiani, "Network localization and navigation via cooperation," in *IEEE Communications Magazine*, vol. 49, no. 5, May 2011, pp. 56–62.

[333] H. Wymeersch, J. Lien, and M. Z. Win, "Cooperative Localization in Wireless Networks," in *Proc. of the IEEE*, vol. 97, no. 2, Feb 2009, pp. 427–450.

[334] L. Xin-Di, H. Wei, and T. Zeng-Shan, "The Improvement of RSS-based Location Fingerprint Technology for Cellular Networks," in *Proc. of Computer Science & Service System (CSSS)*, Nanjing, China, Aug 2012, pp. 1267–1270.

[335] D. Xu, J. Zhang, X. Gao, P. Zhang, and Y. Wu, "Indoor Office Propagation Measurements and Path Loss Models at 5.25 GHz," in *Proc. of Vehicular Technology Conference (VTC Fall)*, Oct 2007.

[336] R. Yamamoto, H. Matsutani, H. Matsuki, T. Oono, and H. Ohtsuka, "Position location technologies using signal strength in cellular systems," in *Proc. of Vehicular Technology Conference (VTC Spring)*, May 2001.

[337] D. Yang, G. Xue, X. Fang, and J. Tang, "Incentive Mechanisms for Crowdsensing: Crowdsourcing With Smartphones," in *IEEE/ACM Transactions on Networking*, May 2015, pp. 1–13.

[338] Z. Yang and Y. Liu, "Quality of Trilateration: Confidence-Based Iterative Localization," in *IEEE Transactions on Parallel and Distributed Systems*, vol. 21, no. 5, May 2010, pp. 631–640.

[339] K. Yedavalli, B. Krishnamachari, S. Ravula, and B. Srinivasan, "Ecolocation: A sequence based technique for RF localization in wireless sensor networks," in *Proc. of 4th International Symposium on Information Processing in Sensor Networks (IPSN)*, Apr 2005.

[340] Y. Yelkovan, H. Guneren, A. Akgoz, F. Eybek, A. Turk, I. Gol, and O. Cetin, "Infrared beacon based sub-meter indoor localization," in *Proc. of Signal Processing and Communications Applications Conference (SIU)*, Apr 2014.

[341] R. W. Yeung, *A First Course in Information Theory*. Springer US, 2002.

[342] J. Yin, Q. Yang, and L. M. Ni, "Learning adaptive temporal radio maps for signal-strength-based location estimation," in *IEEE Transactions on Mobile Computing*, vol. 7, no. 7, Jul 2008, pp. 869 – 883.

[343] K. W. Yip and T. S. Ng, "A simulation model for Nakagami-m fading channels, $m < 1$," in *IEEE Transactions on Communications*, vol. 48, no. 2, Feb 2000, pp. 214–221.

[344] M. A. Youssef, A. Agrawala, and A. U. Shankar, "WLAN location determination via clustering and probability distributions," in *Proc. of Pervasive Computing and Communications*, Fort Worth, TX, USA, 2003, pp. 143–150.

[345] N. Youssef, T. Munakata, and M. Takeda, "Fade statistics in Nakagami fading environments," in *Proc. of 4th International Symposium on Spread Spectrum Techniques and Applications*, Sep 1996, pp. 1244–1247.

[346] Y. Yu, "Indoor GPS clock," US Patent Application Publication 6725157 B1, Apr 2004.

[347] S. Yun, Z. Yao, T. Wang, and M. Lu, "High Accuracy and Fast Acquisition Algorithm for Pseudolites-based Indoor Positioning Systems," in *Proc. of 4th International Conference on Ubiquitous Positioning, Indoor Navigation and Location Based Services (UPINLBS)*, Nov 2016.

[348] L. Yunxiao and Q. Sujuan, "An Improved Indoor Positioning Method Based on Received Signal Strengths," in *Proc. of International Conference on Intelligent Transportation, Big Data and Smart City (ICITBS)*, Dec 2015.

[349] P. A. Zandbergen, "Accuracy of iPhone Locations: A Comparison of Assisted GPS, WiFi and Cellular Positioning," in *Transactions in GIS*, vol. 3, no. 1, Jun 2009, pp. 5–25.

[350] M. H. Zarrabizadeh and E. S. Sousa, "A Differentially Coherent PN Code Acquisition Receiver for CDMA Systems," in *IEEE Transactions on Communications*, vol. 45, no. 11, Nov 1997, pp. 1456–1465.

[351] M. B. Zeytinci, V. Sari, F. K. Harmanci, E. Anarim, and M. Akar, "Location estimation using RSS measurements with unknown path loss exponents," in *EURASIP Journal on Wireless Comm. and Networking*, Jun 2013.

[352] J. Zhang and E. S. Lohan, "Effect and Mitigation of Narrowband Interference on Galileo E1 signal Acquisition and Tracking Accuracy," in *Proc. of International Conference on Localization and GNSS (ICL-GNSS)*, Tampere, Finland, Jun 2011, pp. 36–41.

[353] ——, "Effect of narrowband interference on Galileo E1 signal receiver performance," in *International Journal of Navigation and Observation*, vol. 2011, 2011.

[354] W. Zhang, X. Chen, J. Wan, and J. Zhang, "GPS/Cellular network hybrid positioning method based on two scatter model," in *Proc. of International Conference on Computer Science and Electronics Engineering (ICCSEE)*, Mar 2012.

[355] X. Zhang and J. G. Andrews, "Downlink Cellular Network Analysis With Multi-Slope Path Loss Models," in *IEEE Transactions on Communications*, vol. 63, no. 5, May 2015, pp. 1881–1894.

[356] Q. Zhao, S. Zhang, J. Quan, and X. Lin, "A novel approach for WLAN-based outdoor fingerprinting localization," in *Proc. of IEEE 3rd International Conference on Communication Software and Networks (ICCSN)*, May 2011, pp. 432 – 436.

[357] Y. Zhao, "Standardization of mobile phone positioning for 3G systems," in *IEEE Communications Magazine*, vol. 40, no. 7, Jul 2002, pp. 108–116.

[358] S. Zhou, B. Wang, Y. Mo, and W. Liu, "Indoor Multi-Resolution Subarea Localization Based on Received Signal Strength Fingerprint," in *Proc. of International Conference on Wireless Communications & Signal Processing (WCSP)*, Oct 2012.

[359] Y. Zhou, X. Chen, S. Zeng, J. Liu, and D. A. Liang, "AP Selection Algorithm in WLAN Indoor Localization," in *Information Technology Journal*, vol. 12, 2013, pp. 3773–3776.

[360] Y. Zhuang, Z. Syed, Y. Li, and N. El-Sheimy, "Evaluation of Two WiFi Positioning Systems Based on Autonomous Crowd Sourcing on Handheld Devices for Indoor Navigation," in *IEEE Transactions on Mobile Computing*, Sep 2015.

[361] Y. Zhuang, B. Wright, Z. Syed, Z. Shen, and N. El-Sheimy, "Fast WiFi access point localization and autonomous crowdsourcing," in *Proc. of Ubiquitous Positioning Indoor Navigation and Location Based Service (UPINLBS)*, Nov 2014.

[362] S. Zirazi, P. Canalda, H. Mabed, and F. Spies, "WiFi GPS based combined positioning algorithm," in *Proc. of International Conference on Wireless Communications, Networking and Information Security (WCNIS)*, Jun 2010.

[363] ——, "Wi-Fi Access Point Placement within Stand-alone, Hybrid and Combined Wireless Positioning System," in *Proc. of 4th International Conference on Communications and Electronics (ICCE)*, Aug 2012, pp. 1–5.

[364] G. Zou, L. Ma, Z. Zhang, and Y. Mo, "An indoor positioning algorithm using joint information entropy based on WLAN fingerprint," in *Proc. of International Conference on Computing, Communication and Networking Technologies (ICCCNT)*, 2014, pp. 1–6.

[365] H. Zou, Y. Luo, X. Lu, H. Jiang, and L. Xie, "A Mutual Information Based Online Access Point Selection Strategy for WiFi Indoor Localization," in *Proc. of International Conference on Automation Science and Engineering (CASE)*, Gothenburg, Sweden, Aug 2015, pp. 180–185.

[366] J. Zyren, "White Paper: Overview of the 3GPP Long Term Evolution Physical Layer," 2007.

Tampereen teknillinen yliopisto
PL 527
33101 Tampere

Tampere University of Technology
P.O.B. 527
FI-33101 Tampere, Finland

ISBN 978-952-15-3937-4
ISSN 1459-2045